UNIVERSITY OF CALIFORNIA
RIVERSIDE

Self-Assembly of Functionalized Supramolecular Structures

A Dissertation submitted in partial satisfaction
of the requirements for the degree of

Doctor of Philosophy

in

Chemistry

by

Michael Christopher Young

August 2014

Dissertation Committee:
Dr. Richard J. Hooley, Chairperson
Dr. Christopher Switzer
Dr. Michael J. Marsella

The Dissertation of Michael Christopher Young is approved:

_____

_____

_____

Committee Chairperson

University of California, Riverside

Acknowledgements

It is difficult to decide whom to thank first, but I think it has to start with my parents Tim and Vivian Young, and my grandmother Janette Young. The support you have given me over the years with regard to my education has been invaluable. I am especially grateful for the sacrifices with regard to time you have made, such as coming to visit me since I could so rarely pull myself away from my studies to come visit. A special thanks goes to my grandmother, who is almost single-handedly to blame for my decision to be a scientist. Being exposed to so many books about science as a child is what lead to the curiosity which currently drives my research, and for that I am eternally grateful.

I wouldn't have made it to graduate school if it were not for many wonderful teachers throughout the years. I must thank Mr. Mike Shaw and Mr. Alan Chadbourne for endulging my never ending deluge of questions in high school. I am forever indebted to Prof. Brian Dinkelmeyer for his training at Western Carolina University, which really helped shape my interests as well as gave me a chance to figure out how to think about chemistry. Also, I must thank Brian for "lying" on my recommendation letter: I hope I have more than met the expectations you set for me in graduate school.

My time at UC-Riverside has been primarily shaped by my advisor, Prof. Richard Hooley, and I have to thank him for his continued support, both financially and intellectually. I'm sure I made the job difficult with my constant questions, misunderstandings, and desire to try out things that were not directly

relevant to my research to better myself as a scientist. I have had the opportunity to learn so much, and I am very thankful for that.

Working for five years in the same place, I appreciate the rest of the group for their support and their ability to help make 12+ hour days seem much more managible. I'm indebted to Dr. Amber Johnson and Dr. Ana Gamboa for all of their help on our mutually-investigated work, and I appreciate the arrival to the group of Ms. Lauren Holloway, who I hope can pick up where I left off on some pretty exciting projects. I must also thank my undergraduate researchers, Ms. Erica Liew and Ms. Mi La, for their help over the years. A special thanks goes to Dr. Jonathan Ashby, Mr. Dan Orr, and the Morton lab, including Mr. Jar-Ar Bendo, Mr. Hou Ung, and Mr. Erik Romero, for helping me to make the most of the precious few moments spent outside of lab. There are many analytical methods I have benefited from in graduate school, and I am indebted to Mr. Yi Ming, Dr. Dan Borchardt, Dr. Rich Kondrat, Mr. Ron New, and Dr. Fook Tham for all of their assistance with analysis over the past five years.

Finally, acknowledgement is made to the National Science Foundation, UC-Riverside, and the American Chemical Society who funded my adviser's proposals, allowing me to devote more time in lab. I must personally thank UC-Riverside for funding that allowed me to have a little more flexibility in what I was researching, both through a Dissertation Research Grant and a Dissertation Year Fellowship.

ABSTRACT OF THE DISSERTATION

Self-Assembly of Functionalized Supramolecular Structures

by

Michael Christopher Young

Doctor of Philosophy, Graduate Program in Chemistry
University of California, Riverside, August 2014
Dr. Richard J. Hooley, Chairperson

Enzymes are capable of exquisite selectivity in catalysis chemical reactions because of a well-evolved mechanism that binds substrates in internal active sites based on size and shape complementarity. The cavities of these enzymes are decorated with organic or inorganic groups which can promote reactivity once the substrate is non-covalently bound. Synthetic molecular hosts to date have been able to bind to substrates in a similar, biomimetic fashion, but *functionalized* molecular hosts are still virtually unknown.

One convenient way to prepare molecular hosts is by the self-assembly of organic coordinating ligands with suitable metal salts. The reversible dative bonds holding these cage structures together allow incorrect products to break apart and reform, favoring creation of the most thermodynamically stable product. This leads to discrete, solution phase cages that can function as cavity-

containing hosts. Some of these hosts have shown efficacy as catalysts for pericyclic reactions due to favorable transition states of the bound substrates. These cages, however, fail to orient reactive functional groups into their interiors. Truly biomimetic cages will require modifying traditional self-assembled targets to incorporate these reactive functionalities.

This work explores the self-assembly of metal-organic cages displaying covalent modifications on their interior. Incorporation of unreactive and poorly reactive groups was found to have a significant impact on the outcome of the self-assembly process. Cages with endohedral alcoholic functionality were found to have different binding properties than unfunctionalized analogs. Cages with introverted alcohol groups were also exploited for their ability to self-catalyze reactions *on the interior* of the hosts. The metal vertices themselves could also be used as functional groups, and showed the ability to sense neutral analytes in hybrid dative/hydrogen bonded self-assemblies.

Table of Contents

Table of Figures

Chapter 1 – Introduction to Supramolecular Chemistry

Chapter 2 – Towards Self-Assembled Transition Metal Cages Incorporating "Dynamic" Introverted Functionality

Chapter 8 – Self-Assembly and Guest Binding Properties of Cages Containing Lanthanides and Actinides

Table of Tables

Chapter 4 – Self-Assembly and Functionalization of Fe(II)-Iminopyridine Complexes with Hydrogen Bonding Groups

Chapter 8 – Experimental

Table of Equations

Chapter 4 – Self-Assembly and Functionalization of Fe(II)-Iminopyridine Complexes with Hydrogen Bonding Groups

Chapter 7 – Assembly via Mixed Hydrogen and Dative Bonding

Chapter 1 – Introduction to Supramolecular Chemistry

1.1 History

Supramolecular chemistry has been broadly defined as the "chemistry beyond the molecule."[1] The field is primarily concerned with intermolecular and intramolecular association through non-covalent interactions.[2] Interest in supramolecular chemistry has grown considerably since the 1987 Nobel Prize in Chemistry recognized early achievements leading to popularization of macrocycles capable of binding other atoms and molecules.[3] Since then, work in this field has made use of principles such as the hydrogen bond, pi-pi interactions, and London dispersion forces to assemble molecules together in solution or the solid state. In addition, the formation of metal-ligand complexes, or Werner complexes, is now regarded as an important foundation in supramolecular chemistry.[4]

One of the reasons supramolecular chemistry has become so prominent is because of its overlap with other fields. The principles behind non-covalent molecular interactions are of importance to the field of biology. The so-called "lock and key" concept devised over a century ago is now generally understood to be not only the size and shape-based complementarity between an enzyme and its substrate, but also a complementarity of intermolecular forces such as hydrogen bonds and π-stacking.[5] These can often be thought of as host:guest systems where the guest is the substrate which binds to the enzyme, or host.

The current scope of supramolecular chemistry is quite broad, with implications for all branches of chemistry. Crown ethers have seen use as phase transfer agents in organic synthesis[6] and sensors in analytical chemistry.[7] Self-assembled species held

together by hydrogen bonds have been used to prepare various materials[8] as well as molecular machines.[9] Recent work using organic host molecules shows promise for the construction of membrane-based receptors and transporters.[10]

Supramolecular chemists have also found ways to apply non-covalent interactions towards synthetic challenges. Researchers have recently had success using chiral thiourea-based catalysts which help to activate their substrates through mild Lewis acid catalysis while also leading to enantioselectivity.[11] These catalysts work because of hydrogen bond-driven self-assembly.[12] Other catalysts have shown novel reactivity[13] or enhanced rates of reaction[14] through encapsulation inside macromolecular structures. The binding event is often a simple implementation of the hydrophobic effect: non-polar guests fill the non-polar cavity of aromatic[15] or aliphatic[16] species dissolved in water.

1.2 Biological Inspiration

Supramolecular chemistry takes a number of cues from nature. Many supramolecular systems utilize species derived from pyrimidine and purine bases, the same nitrogenous molecules that hold the two strands of DNA together.[17] These bases display a linear combination of hydrogen bond donor groups (alcohols, amines and amides) as well as hydrogen bond acceptor groups (carbonyls and imines).[18] This is a useful strategy for creating molecules that can assemble in solution. While nature assembles only two or three donor-acceptor pairs in a row, chemists have made molecules with significantly more pairs in tandem, and have observed markedly stronger binding affinity as a result (Figure 1).[19]

Although the hydrogen bond is a vital component of many supramolecular systems, synthetic hydrogen bonding systems are not as complex as those found in nature. Enzyme active sites are highly decorated with different organic[20] and occasionally inorganic[21] functional groups. This leads to enzymes that are highly selective for particular substrates.[22] The combination of numerous, weakly favored hydrogen bonds at the precise locations for a given substrate can be responsible for selective binding, as well as contributing the necessary amount of activation for enzymatic catalysis.[23]

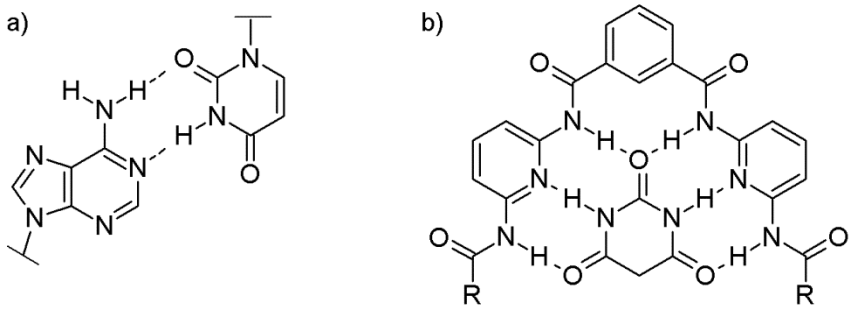

Figure 1.1: Comparison of natural versus synthetic hydrogen-bound dimers: a) Adenine-uracil dimer based on two-point hydrogen bonding; b) Hamilton-type receptor bound to barbituric acid through six complementary hydrogen bonds.

An example of a protein that displays a complex binding pocket is the VDR nuclear receptor. This protein is responsible for a variety of cellular functions, including differentiation and cell growth.[24] The receptor has the ability, depending on its binding state with other receptors and ligands, to interact with transcription cofactors and thus up-regulate or deregulate transcription of the genes to which it is attached. One ligand to which it binds is the active form of vitamin D, 1α,25-dihydroxyvitamin D_3. Figure 1.2 shows a portion of the crystal structure of the vitamin D species bound inside of a VDR construct. In addition to favorable placement of hydrophobic side chains along the interior, non-polar portion of the molecule, there are also a number of favorable

hydrogen bonding interactions. The acidic guanidinium on residue Arg274A donates a proton to one alcohol, which in turn donates a hydrogen bond to the alcohol of Ser237A. A similar arrangement exists with the other alcohol on vitamin D, where the marginally acidic Tyr143A donates a hydrogen bond to the hydroxyl group. This OH in turn hydrogen bonds with Ser278A, while two histidine residues interact with the final hydroxide of the substrate.

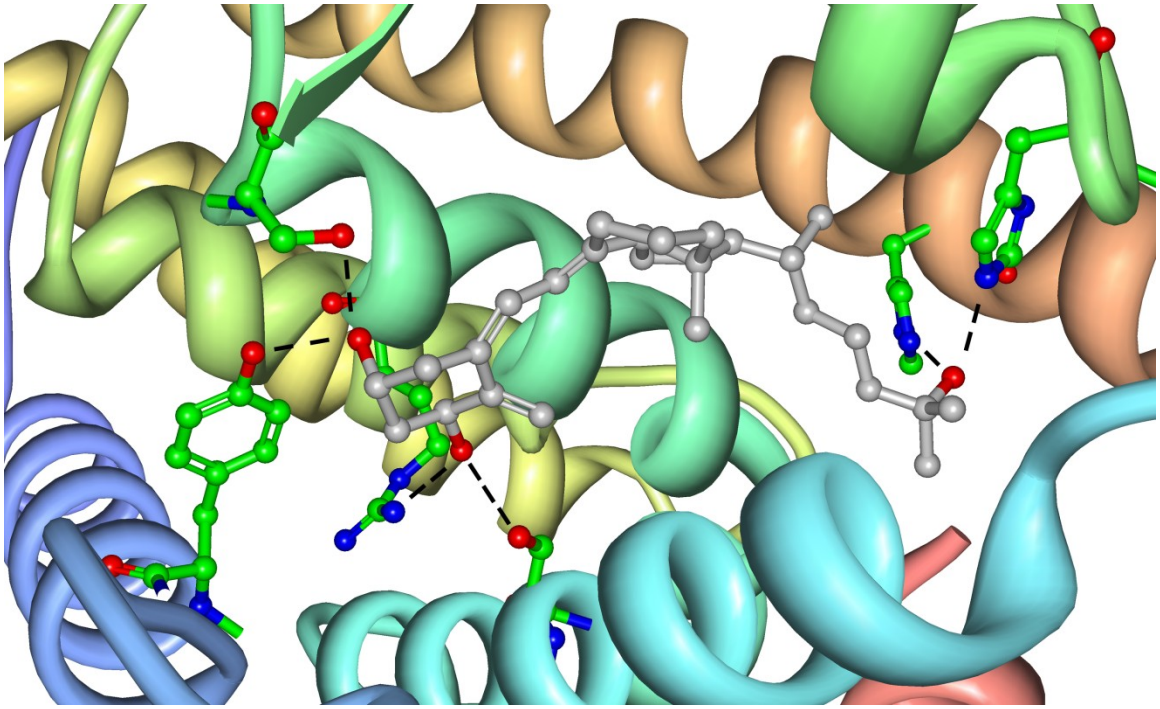

Figure 1.2: Active site of a VDR construct showing the intermolecular interactions responsible for high binding affinity for 1α,25-dihydroxyvitamin D_3 (vitamin D).

1.3 Dative Bond-Driven Self-Assembly

Many molecules capable of size-based recognition of substrates are macrocylic structures. Traditional synthesis of covalently-prepared macrocyclic hosts poor yield. When the molecules become larger and more flexible, undesirable side reactions can

dominate.[25] The average hydrogen bond, however, is significantly lower in energy than a covalent bond, meaning that hydrogen bonds can break and reform more easily.[26] This allows kinetically deleterious products in local minima to break apart, giving rise to solely thermodynamic products. The benefit of this self-assembly strategy is that components organize based on intrinsic electronic information and pairing of substituents, leading to fewer byproducts.

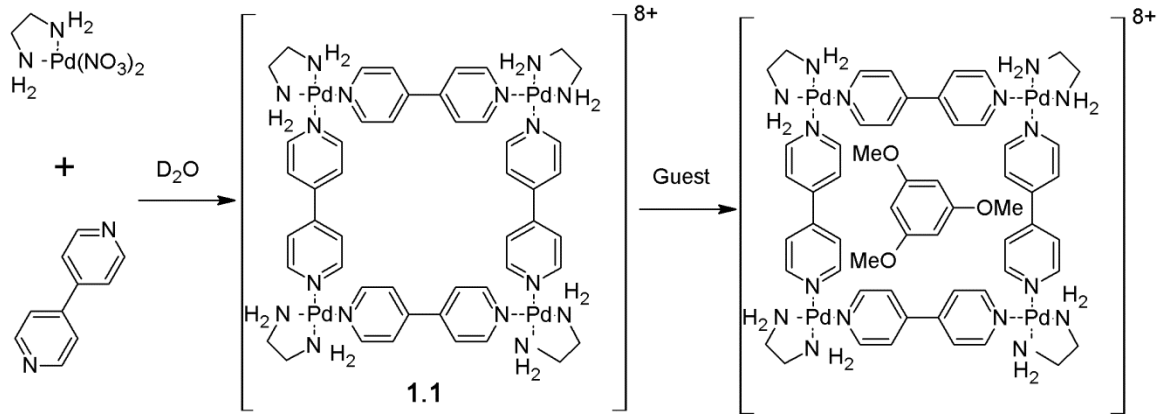

Figure 1.3: Self-assembly of M_4L_4 square **1.1** in deuterium oxide from $[Pd(en)(NO_3)_2]$ and 4,4'-bipyridine, followed by subsequent aromatic guest encapsulation driven by the hydrophobic effect.

Dative bonds (also known as coordinate covalent, dipolar, or dative covalent bonds) are useful for self-assembly for the same reason as hydrogen bonds.[27] Dative bond formation occurs when a lone pair donor gives its electrons to an empty orbital of a metal.[28] Although stronger than hydrogen bonds, these dative bonds are still weak enough to be reversibly formed. This strategy was first used to make supramolecular helices, that were prepared by the enthalpically-driven formation of dative bonds between copper and polypyridine ligands.[29] This strategy was also applied to synthesize a discrete self-assembled molecular square (Figure 1.3),[30] prepared by combining two relatively simple components. Heating 4,4'-bipyridine and $Pd(en)(NO_3)_2$ gave a

tetranuclear square in solution in water. $Pd(en)(NO_3)_2$ has two free coordination sites oriented cis to each other by the presence of ethylene diamine at the Pd center.

As the palladium in this square contains two open coordination sites, it is enthalpically favorable to coordinate to two pyridine ligands to fully occupy the Pd coordination sphere. This requires the use of two different ligands, however, because 4,4'-bipyridine is too rigid to wrap around to saturate the palladium. Despite the potential to form complex oligomers from this stategy, the discrete complex was obtained as the only product. The discovery of this square led to the preparation of similar polygonal complexes[31] and polyhedra,[32] and a variety of different chelating groups were later used to direct the self-assembly of metal-organic cages with transition metals. These include monodentate groups such as pyridines (**1.2**)[33] and phosphines (**1.3**),[34] bidentate groups such as bipyridines (**1.4**)[35] and salicylidinimines (**1.5**),[36] as well as even larger groups such as pyridylacylhydrazones (**1.6**).[37]

These self-assembled cages were all prepared using transition metals. The benefit of using transition metals as structural vertices is their well-defined coordination chemistry, which is easily exploited in the rational design of self-assembled cages.[38] Other metals, such as lanthanides (**1.7**),[39] actinides (**1.8**),[40] main group metals (**1.9**),[41] metalloids (**1.10**),[42] and even some non-metals (**1.11**)[43] have been applied following similar strategies. One benefit to replacing transition metals is that lanthanides display a stable +3 oxidation state, and are much less susceptible to redox chemistry. Many transition metals are paramagnetic, making NMR analysis difficult. In contrast, most main group metals and some lanthanides are diamagnetic. This is important because NMR spectroscopy is a powerful tool for analyzing host-guest chemistry in solution.

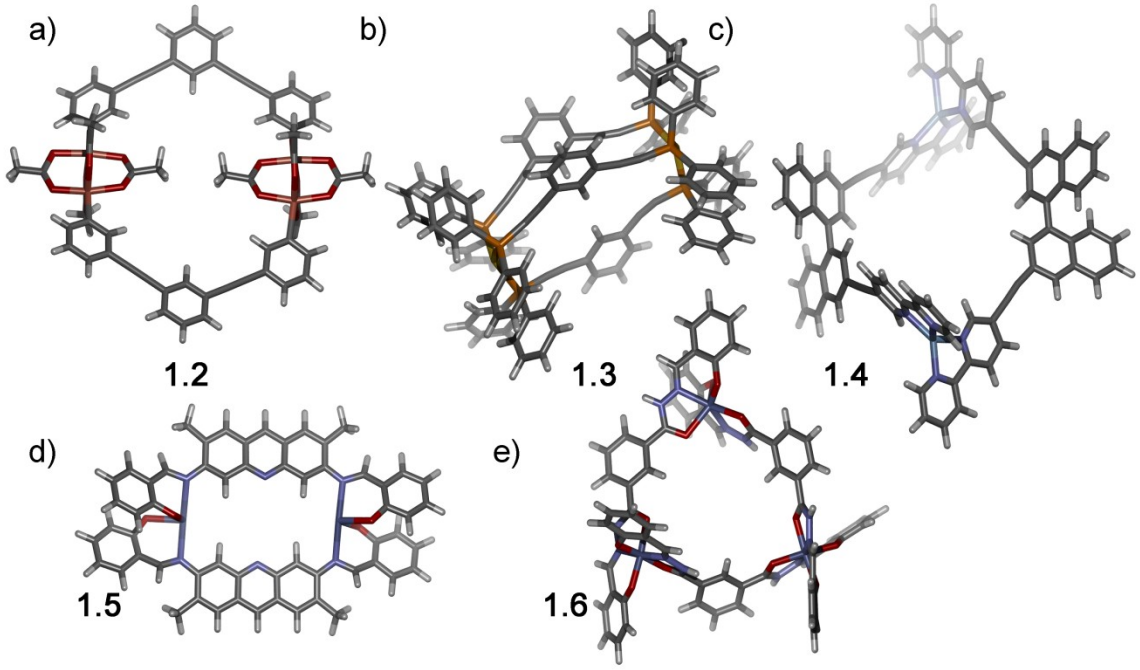

Figure 1.4: Self-assembled polynuclear transition metal complexes using different coordinating ligands: a) acetate-bridged Cu(II)-pyridine **1.2**; b) Au(III)-phosphine **1.3**; c) Ag(I)-2,2'-bipyridyl **1.4**; d) Co(II)-salicylidinimine **1.5**; e) Co(II)-pyridylacylhydrazone **1.6**.

Although many cage structures have been successfully characterized, it is not a trivial task to prepare them. Self-assembled systems are governed by the thermodynamics of multiple weak interactions. Small changes in steric or electronic effects can lead to significant changes in obtained product, as seen in analogues of **1.1**. While 4,4'-bipyridine selectively forms a square, longer linear bipyridines do not.[44] Longer ligands instead form a mixture of the expected M_4L_4 square and a discrete M_3L_3 triangle. In some cases, there is also evidence for the formation of non-discrete oligomers. Increasing the size of ancillary ligands on Pd(II)-based assemblies also disfavors the self-assembly of a square.[45] Use of either 2,2'-bipyridine or N,N,N',N'-tetramethyl-ethylenediamine led to similar equilibria between self-assembled triangles

and squares. Rhenium[46] and manganese[47] species bearing carbonyl ligands are amenable to the selective formation of squares with larger ligands.

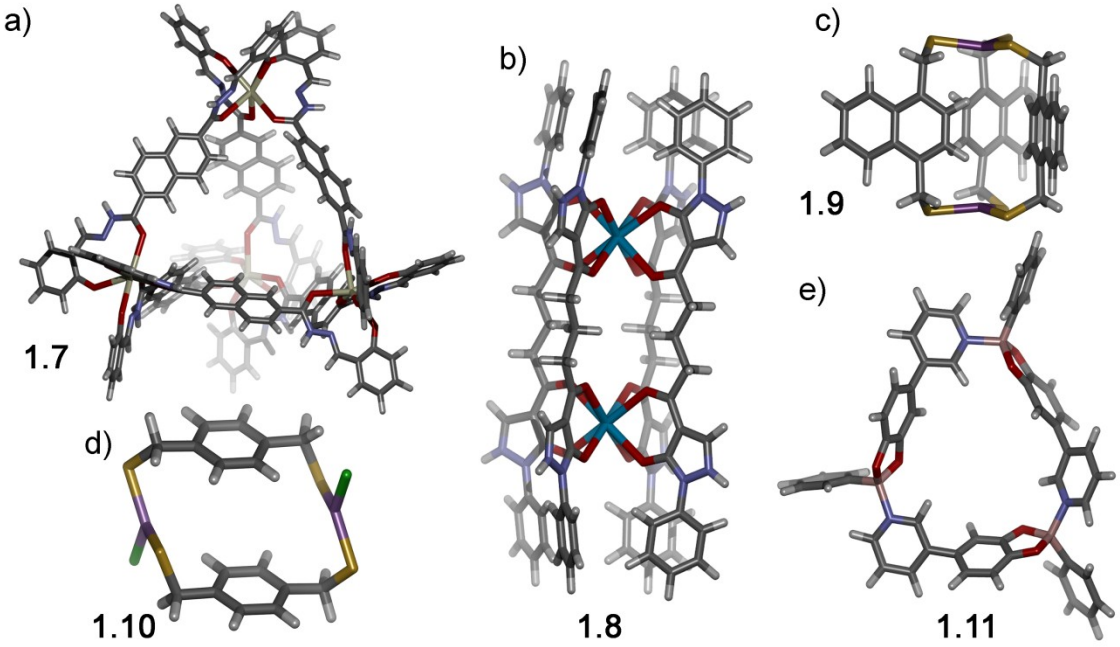

Figure 1.5: Self-assembled cages using non-transition metal vertices: a) Ce(III)-(2-phenoxy)acylhydrazone **1.7**; b) Th(IV)-hydroxyketone **1.8**; c) Bi(III)-thiolate **1.9**; d) chloro As(III)-thiolate **1.10**; e) phenyl B(III)-pyridylcatecholate **1.11**.

There are also challenges in preparing complexes with larger, bidentate chelators. The most problematic is the presence of stereoisomers. For example, $[Ru(bipy)_3]Cl_2$ contains an octahedral metal, but the symmetry of the ligand prevents the formation of stereoisomers. If one of the rings were to be derivatized, there are now four stereochemical possibilities. The substituted rings can all be 90° from each other (the *fac* conformation), but the adjacent rings could either twist clockwise or counterclockwise (Figure 1.6a) to give the *fac*-Δ or the *fac*-Λ isomers. In the event that the substituted rings were all in the same plane (the *mer* conformation), there exist two more stereoisomers depending on whether the adjacent rings twist to give the *mer*-Δ or *mer*-Λ

conformer (Figure 1.6b). In polynuclear complexes, this isomerism leads to even more stereochemical possibilities.

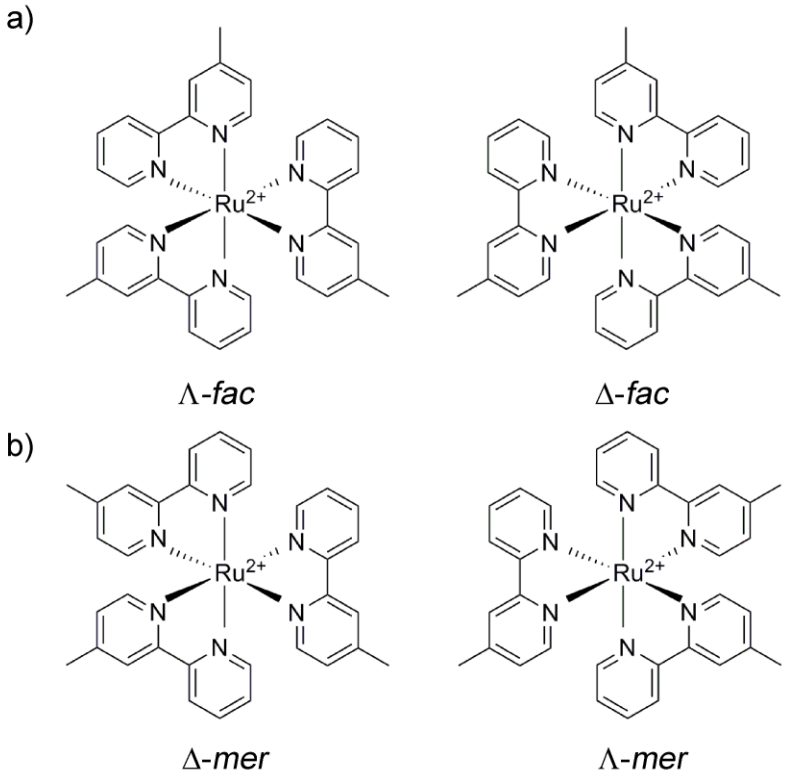

Figure 1.6: Stereochemical orientations around a saturated octahedral metal.

Research on Ga(III)-catecholates has shown that the stereochemistry of these cages can be controlled in different ways. The use of rigid ligands promotes stereochemical communication between the metals.[48] Mixing of stereocenters in a polynuclear complex leads to added strain, and if the ligands are rigid enough this strain allows selection of a single diastereomer. Another strategy is to incorporate chiral groups near the chelator.[49] These chiral groups can lead to complete enantioselectivity in the product assembly. Stereocontrol can also be obtained by templation: use of a chiral

guest can lead to the formation of a chiral cage.[50] The favorable enthalpy of binding a guest drives formation of the cage which best encapsulates the chiral guest, allowing it to form selectively.

1.4 Guest Binding and Reactivity in Metal-Organic Cages

One highly desirable use of these cages is their ability to bind substrates and catalyze reactions on the bound guests. Numerous applications for this biomimicry have been devised. These cages typically have pockets that keep their cavities protected from forces outside of the cage. In one case, white phosphorus is bound inside a highly charged cage (**1.12**) decorated with sulfate groups (Figure 1.7).[51] The pyrophoric white phosphorus inside this cage is stable to air exposure for many months. Only when **1.12** is treated with a more favorable guest such as benzene is the white phosphorus released and able to react with air. A related iron-based M_4L_4 iminopyridine cage binds cyclohexane.[52] Without cyclohexane to serve as a template, a much larger $M_{12}L_{12}$ nanostructure is observed,[53] illustrating how small differences in energy can lead to different assemblies forming.

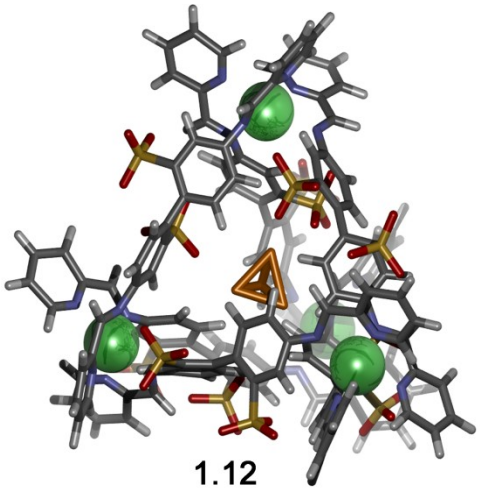

Figure 1.7: Fe(II)-iminopyridine biphenyl tetrahedron **1.12** with bound P_4.

A Pd-pyridine-based octahedron[54] (**1.13**, Figure 1.8) has shown the ability to bind organic species in aqueous solution. These cages contain multiple palladium(II) cations which confer water solubility on the product assembly, while the aromatic portions of the ligands provide hydrophobic surfaces to promote binding of organic guests. Due to the open structure, guests can actively diffuse in and out of the cage. A related Pd-pyridine coordination cage[55] can bind different guests in aqueous solution, even stabilizing the red fluorescence of azaphorphin which is typically lost in water.

Self-assembled cages can also be used to bind ionic species in solution. Polycationic Fe(II)-iminopyridine cages, are capable of binding a variety of suitably sized anions.[56] The presence of a suitably sized anion bound on the cage interior can be used to increase rigidity and confer diastereoselectivity in otherwise unselective self-assemblies.[57] Anionic Ga(III)-catecholate cages are able to bind a variety of cationic organometallic guests.[58] This allows the stabilization of otherwise reactive

organometallics in aqueous solution. Other unstable molecules, such as iminium ions, are also favorably encapsulated by these anionic cages.[59]

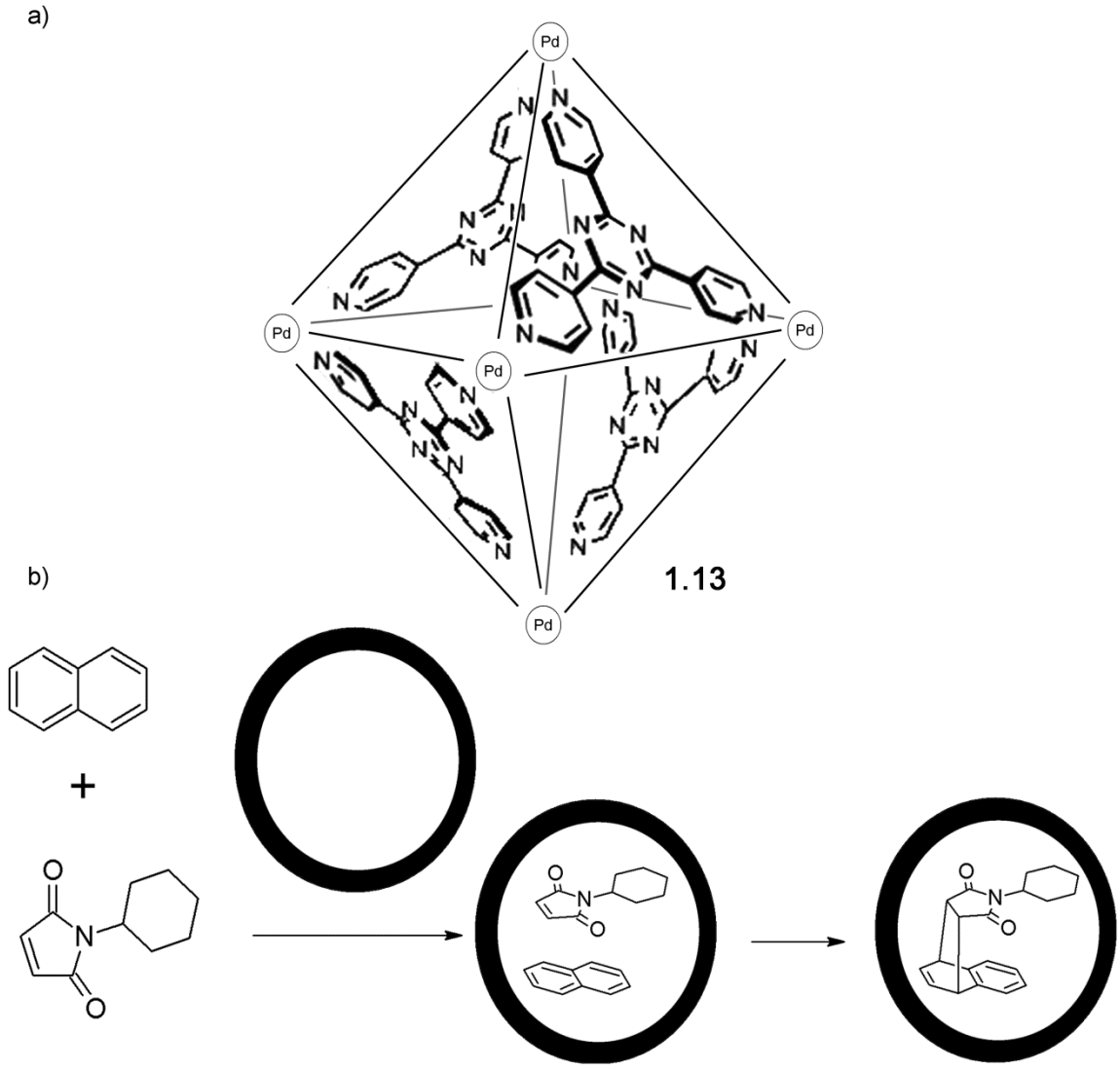

Figure 1.8: Favorable preorganization of reagents in Pd(II)-pyridyl octahedron **1.13**.

Ga(III)-catecholate cages are also known for promoting pericyclic reactions of bound guests. It is possible to perform aza-Cope rearrangements upon bound guests using an anionic cage.[60] In another example, Nazarov cyclization of a cationic intermediate occurs

with a rate increase of 2 x 10^6.[61] These cages have also shown the ability to modify the pKa of bound substrates, making amines[62] and orthoformates[63] more basic due to the favorable enthalpy of binding a cationic guest.

Pd(II)-pyridine octahedron **1.13** can also catalyze pericyclic reactions. Diels-Alder reactions of co-encapsulated substrates can occur, such as the reaction of naphthalene and N-substituted maleimides (Figure 1.8).[64] The components are favorably pre-organized in solution to promote these reactions. Acceleration of otherwise unobserved photo-induced [2+2] reactions can also occur.[65] An overcrowded chromic alkene formed from two planar aromatic systems can be encapsulated as its meta-stable twisted isomer.[66] While encapsulated this can be functionalized via electrophilic aromatic substitution to lock the compound as the less favorable isomer. Another example involves the acceleration of Knoevenagel condensations of naphthaldehydes in water.[67] In this case the cationic nature of the cage helps promote the formation of the reactive enolate nucleophiles.

1.5 Endohedral Functionalization of Metal-Organic Cages

Although there are numerous examples of reactivity in self-assembled cages, the reactions only make use of pre-organization. Enzymes typically perform catalysis through reactive functional groups displayed on their interior. Even those that do not, such as enzymes in the Cytochrome P450 family, orient specific substrates towards a reactive metal center bound inside of the protein.[68] In comparison, self-assembled cage are typically devoid of functional groups. Although plenty of ionic intermediates as well

as electrocyclic transition states can be stabilized to promote catalysis, true biomimicry requires targeting cages with endohedral reactive functionality.

One way of overcoming this limitation of traditional self-assembled cages is by co-encapsulating a catalyst with the target substrate. This is similar to enzymes that use co-factors to perform catalysis. A co-encapsulation strategy using anionic cages allowed the combination of a reactive organometallic complex with the desired substrate inside of a cage.[69]

The inclusion of functional groups directly on the self-assembly is still an under-utilized method of preparing functionalized hosts. Functionalization with even weakly reactive groups, such as ureas, can influence cage properties. A self-assembled Fe(II)-bipyridyl helix containing ureas was capable of reassembling to form an M_4L_6 tetrahedron **1.14** in which the six urea groups coordinate around suitable tetrahedral (*T*) symmetrical anions (Figure 1.9).[70] This occurs in part due to the favorable electrostatic interactions between the cationic cage and the anionic guests, yet the ability to hydrogen bond with the interior ureas seems vital. Anions that cannot engage in these hydrogen bonds do not serve to template the M_4L_6 tetrahedron.

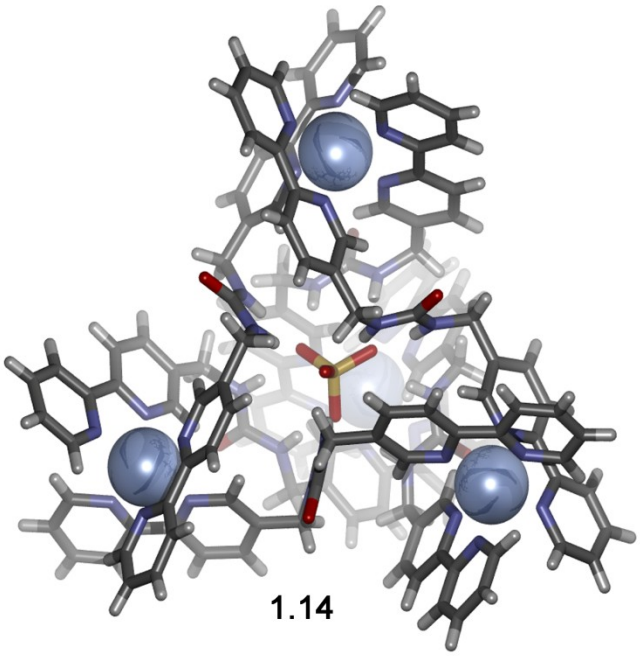

Figure 1.9: Recognition of sulfate in urea-functionalized self-assembled tetrahedron **1.14**.

Neutral guests can also be bound using a similar principle. Two related cages, a tetranuclear cerium-based tetrahedron and an octanuclear cerium-based triangular prism are capable of binding selectively to sucrose and lactose respectively.[71] This selectivity is imparted due to the arrangement of amides around the active site created by the ligands. The luminescence imparted by the lanthanide allows this binding to be easily measured by fluorescence spectroscopy. In addition, various nanocapsules have been constructed by combining bis-pyridine ligands containing a 120° bend with palladium(II) to form large $M_{12}L_{24}$ or $M_{24}L_{48}$ structures.[72] This angle allows a functional group to be pointed towards the interior of the cage structure. The functionality can be used to attach a protein to one of the ligands, giving a hetereocomplex that incorporates a single protein encapsulated in its cavity.[73] Incorporation of a saccharide helps direct

the formation of a TiO_2 nanoparticle on the interior of the assembly.[74] Calcination leads to the release of nanoparticles with relatively uniform size and shape.

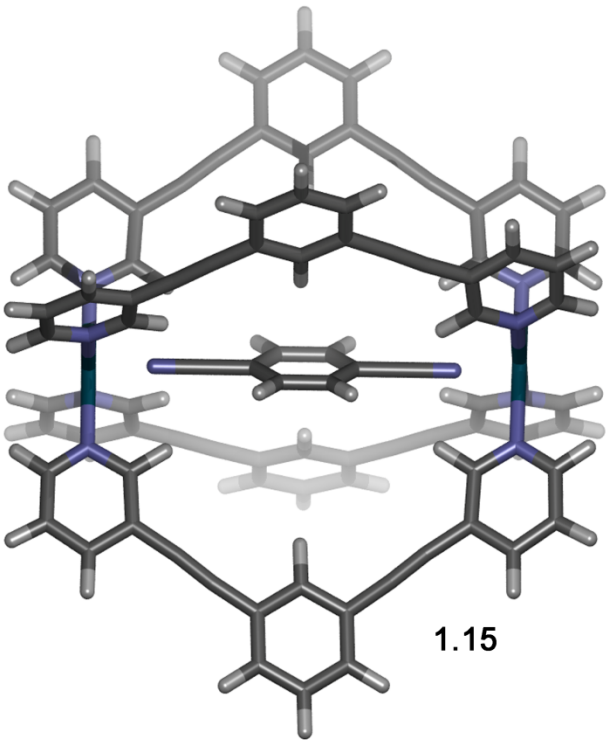

Figure 1.10: SPARTAN model of the recognition of terephthalate by dinuclear palladium(II) paddlewheel **1.15**.

Related but smaller palladium-paddlewheels display a unique form of functionalization.[75] The cages present an open coordination site on the metal vertices of the cage to the interior and these allow for recognition of select guests. Successfully bound guests must contain one or two groups with lone pairs, such as a nitrile or halide. Terephthalonitrile is a suitable guest containing two groups which can donate to the open coordination site of the palladium vertices (Figure 1.10). In addition, guests must be able to fit inside the cavity. Although terephthalonitrile is bound, dicyanoanthracene is too large and is not encapsulated. Even though 1,4-dicyanobutane or 1,6-dicyanobutane

could conceivably fill the cavity adequately, neither is bound, presumably due to disfavorable guest constraint upon encapsulation.

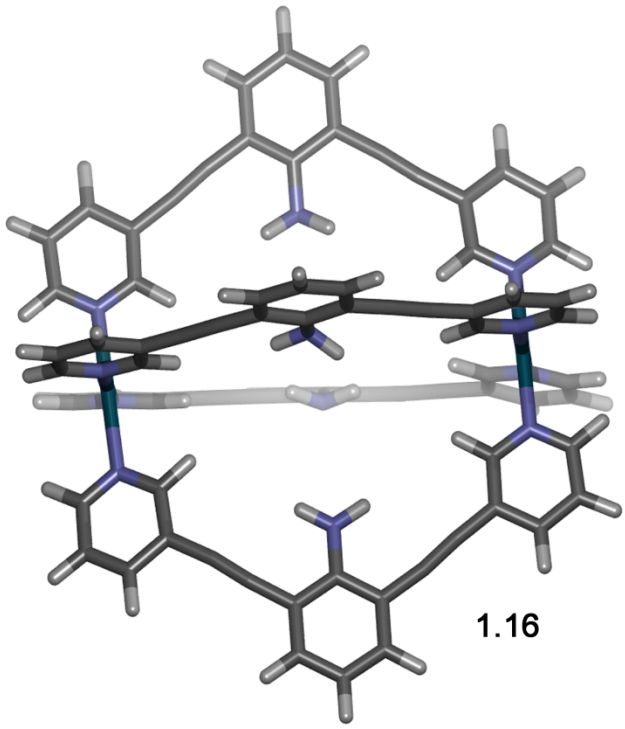

Figure 1.11: SPARTAN model of endohedral amine functionalized dinuclear palladium(II) paddlewheel **1.16**.

In addition to the metal center serving as a "functional group," these paddlewheel complexes were also capable of orienting organic functional groups (weakly reactive pyridine or aniline) into the interior of the self-assembly (Figure 1.11).[76]. Although these functional groups were essentially inert, crystallographic evidence showed that upon addition of the functional group, the space within the cavity became limited. This underscores a challenge in preparing functionalized cages: the cage must be large enough to accommodate both a functional group as well as the desired substrate. Future

cages must find ways to combine effective self-assembly with reactive functionality on the cage interiors while maintaining structures that can function as effective hosts.

1.6 References

1) Steed, J. W.; Atwood, J. L. "Concepts." *Supramolecular Chemistry*, 2nd Ed., Wiley & Sons: West Sussex, **2009**; Chapter 1.

2) Lehn, J.-M. "Supramolecular Chemistry." *Science*, **1993**, *260*, 1762-1763.

3) Schalley, C. A. "Thematic Series on Supramolecular Chemistry." *Beilstein J. Org. Chem.*, **2009**, *5*, 76.

4) Fabbrizzi, L. "From Simple to Complex Compounds" *Inorg. And Bio-Inorg. Chem., Vol I.*, Encylcopedia of Life Suppor Systems, **2009**; 40-87.

5) Hartkoorn, R. C.; Pojer, F.; Read, J. A.; Gingell, H.; Neres, J.; Horlacher, O. P.; Altmann, K.-H.; Cole, S. T. "Pyridomycin Bridges the $NADH^-$ and Substrate-Binding Pockets of the Enoyl Reductase InhA." *Nat. Chem. Bio.*, **2014**, *10*, 96-98.

6) Ooi, T.; Maruoka, K. "Recent Advances in Asymmetric Phase-Transfer Catalysis" *Angew. Chem. Int. Ed.*, **2007**, *46*, 4222-4266.

7) a) Ly, T.; Liu, Z.; Pujanauski, B. G.; Sarpong, R.; Julian, R. R. "Survey Ubiquitin Structure by Noncovalent Attachment of Distance Constrained Bis(crown) Ethers." *Anal. Chem.*, **2008**, *80*, 5059-5064; b) Suzuki, K.; Watanabe, K.; Matsumoto, Y.; Kobayashi, M.; Sato, S.; Siswanta, D.; Hisamoto, H. "Design and Synthesis of Calcium and Magnesium Ionophores Based on Double-Armed Diazacrown Ether Compounds and Their Application to an Ion Sensing Component for an Ion-Selective Electrode." *Anal. Chem.*, **1995**, *67*, 324-334.

8) a) Huo, Q.; Russell, K. C.; Leblanc, R. M. "Chromatic Studies of a Polymerizable Diacetylene Hydrogen Bonding Self-Assembly: A "Self-Folding" Process To Explain the Chromatic Changes of Polydiacetylenes." *Langmuir*, **1999**, *15*, 3972-3980; b) Choi, I. S.; Li, X.; Simanek, E. E.; Akaba, R.; Whitesides, G. M. "Self-Assembly of Hydrogen-Bonded Polymeric Rods Based on the Cyanuric Acid·Melamine Lattice." *Chem. Mater.*, **1999**, *11*, 684-690; c) Dinkelmeyer, B.; Lauher, J. W.; Fowler, F. W. "Designed 2-Substituted Butadiene Structures." *Mol. Cryst. Liq. Cryst. Sci. Technol., Sect. A.*, **1998**, *313*, 259-264.

9) a) Panman, M. R.; Bakker, B. H.; den Uyl, D.; Kay, E. R.; Leigh, D. A.; Buma, W. J.; Brouwer, A. M.; Geenevasen, J. A. J.; Woutersen, S. "Water Lubricates Hydrogen-Bonded Molecular Machines." *Nat. Chem.*, **2013**, *5*, 929-934; b) Kay, E. R.; Leigh, D. A. "Hydrogen Bond-Assembled Synthetic Molecular Motors and Machines." *Top. Curr. Chem.*, **2005**, *262*, 133-177.

10) a) Ghang, Y.-J.; Schramm, M. P.; Zhang, F.; Acey, R. A.; David, C. N.; Wilson, E. H.; Wang, Y.; Cheng, Q.; Hooley, R. J. "Selective Cavitand-Mediated Endocytosis of Targeted Imaging Agents into Live Cells." *J. Am. Chem. Soc.*, **2013**, *135*, 7090-7093; b) Liu, Y.; Young, M. C.; Moshe, O.; Cheng, Q.; Hooley, R. J. "A Membrane-Bound Synthetic Receptor Promotes Growth of a Polymeric Coating at the Bilayer–

Water Interface." *Angew. Chem. Int. Ed.*, **2012**, *51*, 7748-7751; c) Liu, T.; Taira, T.; Young, M. C.; Ajami, D.; Rebek, J., Jr.; Cheng, Q.; Hooley, R. J. "Protein Recognition by a Self-Assembled Deep Cavitand Monolayer on a Gold Substrate." *Langmuir*, **2012**, *28*, 1391-1398.

11) a) Brown, A. R.; Uyeda, C.; Brotherton, C. A.; Jacobsen, E. N. "Enantioselective Thiourea-Catalyzed Intramolecular Cope-Type Hydroamination." *J. Am. Chem. Soc.*, **2013**, *135*, 6747-6749; b) Lalonde, M. P.; McGowan, M. A.; Rajapaksa, N. S.; Jacobsen, E. N. "Enantioselective Formal Aza-Diels-Alder Reactions of Enones with Cyclic Imines Catalyzed by Primary Aminothioureas." *J. Am. Chem. Soc.*, **2013**, *135*, 1891-1894.

12) Zuend, S. J.; Jacobsen, E. N. "Mechanism of Amido-Thiourea Catalyzed Enantioselective Imine Hydrocyanation: Transition State Stabilization via Multiple Non-Covalent Interactions." *J. Am. Chem. Soc.*, **2013**, *131*, 15358-15374.

13) Yoshizawa, M.; Tamura, M.; Fujita, M. "Diels-Alder in Aqueous Molecular Hosts: Unusual Regioselectivity and Efficient Catalysis." *Science*, **2006**, *312*, 251-254.

14) Kang, J.; Rebek, J. Jr. "Acceleration of a Diels-Alder Reaction by a Self-Assembled Molecular Capsule" *Nature*, **1997**, *385*, 50-52.

15) a) Hooley, R. J.; Biros, S. M.; Rebek, J. Jr. "A Deep, Water-Soluble Cavitand Acts as a Phase-Transfer Catalyst for Hydrophobic Species." *Angew. Chem. Int. Ed.*, **2006**, *45*, 3517-3519; b) Ronson, T. K.; Giri, C.; Beyeh, N. K.; Minkkinen, A.; Topić, F.; Holstein, J. J.; Rissanen, K.; Nitschke, J. R. "Size-Selective Encapsulation of Hydrophobic Guests by Self-Assembled M_4L_6 Cobalt and Nickel Cages." *Chem.-Eur. J.*, **2013**, *19*, 3374-3382.

16) Breslow, R.; Zhang, B. "Cholesterol Recognition and Binding by Cyclodextrin Dimers." *J. Am. Chem. Soc.*, **1996**, *118*, 8495-8496.

17) a) Moehlig, A. R.; Djernes, K. E.; Krishnan, V. M.; Hooley, R. J. "Cytosine Derivatives Form Hemiprotonated Dimers in Solution and the Gas Phase." *Org. Lett.*, **2012**, *14*, 2560-2563; b) Beijer, F. H.; Kooijman, H.; Spek, A. L.; Sijbesma, R. P.; Meijer, E. W. "Self-Complementarity Achieved Through Quadruple Hydrogen Bonding" *Angew. Chem. Int. Ed.*, **1998**, *37*, 75-78.

18) Glowacki, E. D.; Irimia-Vladu, M.; Bauer, S.; Sariciftei, N. S. "Hydrogen-Bonds in Molecular Solids – From Biological Systems to Organic Electronics." *J. Mater. Chem. B*, **2013**, *1*, 3742-3753.

19) Dirksen, A.; Hahn, U., Schwanke, F.; Nieger, M.; Reek, J. N. H.; Vögtle, F.; De Cola, L. "Multiple Recognition of Barbiturate Guests by Hamilton-Receptor-Functionalized Dendrimers." *Chem.-Eur. J.*, **2004**, *10*, 2036-2047.

20) Kuhn, B.; Kollman, P. A. "QM-FE and Molecular Dynamics Calculations on Catechol *O*-Methyltransferase: Free Energy of Activation in the Enzyme and in Aqueous

Solution and Regioselectivity of the Enzyme-Catalyzed Reaction." *J. Am. Chem. Soc.*, **2000**, *122*, 2586-2596.

21) Costas, M.; Mehn, M. P.; Jensen, M. P.; Que, L. "Dioxygen Activation at Mononuclear Nonheme Iron Active Sites: Enzymes, Models, and Intermediates." *Chem. Rev.*, **2004**, *104*, 939-986.

22) Hedfors, C.; Hult, K.; Martinelle, M. "Lipase Chemoselectivity Towards Alcohol and Thiol Acyl Acceptors in a Transacylation Reaction." *J. Mol. Catal. B: Enzym.*, **2010**, *66*, 120-123.

23) DeVore, N. M.; Scott, E. E. "Structures of Cytochrome P450 17A1 with Prostate Cancer Drugs Abiraterone and TOK-001." *Nature*, **2012**, *482*, 116-119.

24) Rochel, N.; Wurtz, J. M.; Mitschler, A.; Klaholz, B.; Moras, D. "The Crystal Structure of the Nuclear Receptor for Vitamin D Bound to Its Natural Ligand." *Mol. Cell.*, **2000**, *5*, 173-179.

25) Field, K. W.; Glover, A. D.; Moroz, J. S.; Collander, D. J.; Kolb, K. E. ""Crown Ether" Synthesis: An Organic Laboratory Experiment." *J. Chem. Educ.*, **1979**, *56*, 269-270.

26) Desiraju, G. R. "A Bond by Any Other Name." *Angew. Chem. Int. Ed.*, **2011**, *50*, 52-59.

27) a) Djernes, K. E.; Padilla, M.; Mettry, M.; Young, M. C.; Hooley, R. J. "Hydrocarbon Oxidation Catalyzed by Self-Folded Metal-Coordinated Cavitands." *Chem. Commun.*, **2012**, *48*, 11576-11578; b) Holliday, B. J.; Mirkin, C. A. "Strategies for the Construction of Supramolecular Compounds Through Coordination Chemistry." *Angew. Chem. Int. Ed.*, **2001**, *40*, 2022-2043.

28) Miessler, G. L.; Tarr, D. A. "Coordination Chemistry I: Structures and Isomers." *Inorganic Chemistry*, 3rd Ed., Pearson Prentice Hall: New Jersey, **2004**; Chapter 9.

29) a) Kramer, R.; Lehn, J.-M.; Marquis-Rigault, A. "Self-Recognition in Helicate Self-Assembly: Spontaneous Formation of Helical Metal Complexes from Mixtures of Ligands and Metal Ions." *Proc. Natl. Acad. Sci. USA*, **1993**, *90*, 5394-5398; b) Lehn, J.-M.; Rigault, A.; Siegel, J.; Harrowfield, J.; Chevrier, B.; Moras, D. "Spontaneous Assembly of Double-Stranded Helicates from Oligobipyridine Ligands and Copper(I) Cations: Structure of an Inorganic Double Helix." *Proc. Natl. Acad. Sci. USA*, **1987**, *84*, 2565-2569.

30) Fujita, M.; Yazaki, J.; Ogura, K. "Preparation of a Macrocyclic Polynuclear Complex, $[(en)Pd(4,4'\text{-}bpy)]_4(NO_3)_8$, Which Recognizes an Organic Molecule in Aqueous Media." *J. Am. Chem. Soc.*, **1990**, *112*, 5645-5647.

31) Fujita, M.; Yazaki, J.; Kuramochi, T.; Ogura, K. "Self-Assembly of a Macrocyclic Dinuclear Pd(II)-Phosphine Complex." *Bull. Chem. Soc. Jpn.*, **1993**, *66*, 1837-1839.

32) a) Fujita, M.; Oguro, D.; Miyazawa, M.; Oka, H.; Yamaguchi, K.; Ogura, K. "Self-Assembly of Ten Molecules into Nanometre-Sized Organic Host Frameworks." *Nature*, **1995**, *378*, 469-471; b) Baxter, P.; Lehn, J.-M.; DeCian, A.; Fischer, J. "Multicomponent Self-Assembly: Spontaneous Formation of a Cylindrical Complex from Five Ligands and Six Metal Ions." *Angew. Chem. Int. Ed.*, **1993**, *32*, 69-72.

33) Schultheiss, N.; Ellsworth, J. M.; Bosch, E.; Barnes, C. L. "Formation of Hexagonal Coordination Complexes." *Eur. J. Inorg. Chem.*, **2005**, 45-46.

34) Lim, S. H.; Cohen, S. M. "Self-Assembled Supramolecular Clusters Based on Phosphines and Coinage Metals: Tetrahedra, Helicates, and Mesocates." *Inorg. Chem.*, **2013**, *52*, 7862-7872.

35) Lützen, A.; Hapke, M.; Griep-Raming, J.; Haase, D.; Saak, W. "Synthesis and Stereoselective Self-Assembly of Double- and Triple-Stranded Helicates." *Angew. Chem. Int. Ed.*, **2002**, *41*, 2086-2089.

36) Mañeru, D. R.; Ojea, M. J. H.; Rosado, L.; Aromí, G.; Zuazo, J.; Castro, G.; Sañudo, E. C. "New Nanostructured Materials: Nanostructuration of a Fluorescent Magnet Based on Acridine Yellow." *Polyhedron*, **2013**, *66*, 136-141.

37) Wu, H.; He, C.; Lin, Z.; Liu, Y.; Duan, C. "Metallohelical Triangles for Selective Detection of Adenosine Triphosphate in Aqueous Media." *Inorg. Chem.*, **2009**, *48*, 408-410.

38) Chakrabarty, R.; Mukherjee, P. S.; Stang, P. J. "Supramolecular Coordination: Self-Assembly of Finite Two- and Three-Dimensional Ensembles." *Chem. Rev.*, **2011**, *111*, 6810-6918.

39) Liu, Y.; Wu, X.; He, C.; Jiao, Y.; Duan, C. "Self-Assembly of Cerium-Based Metal–Organic Tetrahedrons for Size-Selectively Luminescent Sensing Natural Saccharides." *Chem. Commun.*, **2009**, 7554-7556.

40) Xu, J.; Raymond, K. N. "Structurally Characterized Quadruple-Stranded Bisbidentate Helicates." *Angew. Chem. Int. Ed.*, **2006**, *45*, 6480-6485.

41) Cangelosi, V. M.; Zakharov, L. N.; Johnson, D. W. "Supramolecular "Transmetalation" Leads to an Unusual Self-Assembled P_2L_3 Cryptand." **2010**, *49*, 1248-1251.

42) Cangelosi, V. M.; Zakharov, L. N.; Fontenot, S. A.; Pitt, M. A.; Johnson, D. W. "Host-Guest Interactions in a Series of Self-Assembled $As_2L_2Cl_2$ Macrocycles." *Dalton Trans.*, **2008**, 3447-3453.

43) Sheepwash, E.; Zhou, K.; Scopelliti, R.; Severin, K. "Self-Assembly of Arylboronate Esters with Pyridyl Side Chains." *Eur. J. Inorg. Chem.*, **2013**, 2558-2563.

44) Fujita, M.; Sasaki, O.; Mitsuhashi, T.; Fujita, T.; Yazaki, J.; Yamaguchi, K.; Ogura, K. "On the Structure of Transition-Metal-Linked Molecular Squares." *Chem. Commun.*, **1996**, 1535-1536.

45) Uehara, K.; Kasai, K.; Mizuno, N. "Syntheses and Characterizations of Palladium-Based Molecular Triangle/Square Compounds and Hybrid Composites with Polyoxometalates." *Inorg. Chem.*, **2007**, *46*, 2563-2570.

46) Sun, S.-S.; Lees, A. J. "Self-Assembly Triangular and Square Rhenium(I) Tricarbonyl Complexes: A Comprehensive Study of Their Preparation, Electrochemistry, Photophysics, Photochemistry, and Host–Guest Properties." *J. Am. Chem. Soc.*, **2000**, *122*, 8956-8967.

47) Karthikeyan, S.; Velavan, K.; Sathishkumar, R.; Varghese, B.; Manimaran, B. "Self-Assembly of Manganese(I)-Based Molecular Squares: Synthesis and Spectroscopic and Structural Characterization." *Organometallics,* **2012**, *31*, 1953-1957.

48) Xu, J.; Parac, T. N.; Raymond, K. N. "Meso Myths: What Drives Assembly of Helical Versus Meso M_2L_3 Clusters?" *Angew. Chem. Int. Ed. Engl.*, **1999**, *38*, 2878-2882.

49) Enemark, E. J.; Stack, T. D. P. "Synthesis and Structural Characterization of a Stereospecific Dinuclear Gallium Triple Helix: Use of the *trans*-Influence in Metal-Assisted Self-Assembly." *Angew. Chem. Int. Ed. Engl.*, **1995**, *34*, 996-998.

50) Terpin, A. J.; Ziegler, M.; Johnson, D. W.; Raymond, K. N. "Resolution and Kinetic Stability of a Chiral Supramolecular Assembly Made of Labile Components." *Angew. Chem. Int. Ed.*, **2001**, *40*, 157-160.

51) Mal, P.; Breiner, B.; Rissanen, K.; Nitschke, J. R. "White Phosphorus is Air-Stable Within a Self-Assembled Tetrahedral Capsule." *Science*, **2009**, *324*, 1697-1699.

52) Bilbeisi, R. A.; Clegg, J. K.; Elgrishi, N.; de Hatten, X.; Devillard, M.; Breiner, B.; Mal, P.; Nitschke, J. R. "Subcomponent Self-Assembly and Guest-Binding Properties of Face-Capped $Fe_4L_4^{8+}$ Capsules. " *J. Am. Chem. Soc.*, **2012**, *134*, 5110-5119.

53) Bilbeisi, R. A.; Ronson, T. K.; Nitschke, J. R. "A Self-Assembled $[Fe^{III}_{12}L_{12}]$ Capsule with an Icosahedral Framework." *Angew. Chem. Int. Ed.*, **2013**, *52*, 9027-9030.

54) Kusukawa, T.; Fujita, M. "Self-Assembled M_6L_4-Type Coordination Nanocage with 2,2'-Bipyridine Ancillary Ligands. Facile Crystallization and X-ray Analysis of Shape-Selective Enclathration of Neutral Guests in the Cage." *J. Am. Chem. Soc.*, **2002**, *124*, 13576-13582.

55) a) Ono, K.; Klosterman, J. K.; Yoshizawa, M.; Sekiguchi, K.; Tahara, T.; Fujita, M. "ON/OFF Red Emission from Azaporphine in a Coordination Cage in Water." *J. Am. Chem. Soc.*, **2009**, *131*, 12526-12527; b) Umemoto, K.; Yamaguchi, K.; Fujita, M. "Molecular Paneling via Coordination: Guest-Controlled Assembly of Open Cone

and Tetrahedron Structures from Eight Metals and Four Ligands." *J. Am. Chem. Soc.*, **2000**, *122*, 7150-7151.

56) Riddell, I. A.; Smulders, M. M. J.; Clegg, J. K.; Hristova, Y. R.; Breiner, B.; Thoburn, J. D.; Nitschke, J. R. "Anion-Induced Reconstitution of a Self-Assembly System to Express a Chloride-Binding $Co_{10}L_{15}$ Pentagonal Prism." *Nature Chem.*, **2012**, *4*, 751-756.

57) Clegg, J. K.; Cremers, J.; Hogben, A. J.; Breiner, B.; Smulders, M. M. J.; Thoburn, J. D.; Nitschke, J. R. "A Stimuli Responsive System of Self-Assembled Anion-Binding $Fe_4L_6^{8+}$ Cages." *Chem. Sci.*, **2013**, *4*, 68-76.

58) Fiedler, D.; Bergman, R. G.; Raymond, K. N. "Stabilization of Reactive Organometallic Intermediates Inside a Self-Assembled Nanoscale Host." *Angew. Chem. Int. Ed.*, **2006**, *45*, 745-748.

59) Dong, V. M.; Fiedler, D.; Carl, B.; Bergman, R. G.; Raymond, K. N. "Molecular Recognition of Iminium Ions in Water." *J. Am. Chem. Soc.*, **2006**, *128*, 14464-14465.

60) Fiedler, D.; Bergman, R. G.; Raymond, K. N. "Supramolecular Catalysis of a Unimolecular Transformation: Aza-Cope Rearrangement Withing a Self-Assembled Host." *Angew. Chem. Int. Ed.*, **2004**, *43*, 6748-6751.

61) Hastings, C. J.; Berman, R. G.; Raymond, K. N. "Enzymelike Catalysis of the Nazarov Cyclization by Supramolecular Encapsulation." *J. Am. Chem. Soc.*, **2010**, *132*, 6938-6940.

62) Pluth, M. D.; Bergman, R. G.; Raymond, K. N. "Catalytic Deprotection of Acetals in Strongly Basic Solutions Using a Self-Assembled 'Nanozyme'." *Angew. Chem. Int. Ed.*, **2007**, *46*, 8587-8589.

63) Pluth, M. D.; Berman, R. G.; Raymond, K. N. "Acid Catalysis in Basic Solution: A Supramolecular Host Promotes Orthoformate Hydrolysis." *Science*, **2007**, *316*, 85-88.

64) Murase, T.; Horiuchi, S.; Fujita, M. "Naphthalene Diels-Alder in a Self-Assembled Molecular Flask." *J. Am. Chem. Soc.*, **2010**, *132*, 2866-2867.

65) Nishioka, Y.; Yamaguchi, T.; Kawano, M.; Fujita, M. "Asymmetric [2+2] Olefin Cross Photoaddition in a Self-Assembled Host with Remote Chiral Auxiliaries." *J. Am. Chem. Soc.*, **2008**, *130*, 8160-8161.

66) Takezawa, H.; Murase, T.; Fujita, M. "Temporary and Permanent Trapping of the Metastable Twisted Conformer of an Overcrowded Chromic Alkene via Encapsulation." *J. Am. Chem. Soc.*, **2012**, *134*, 17420-17423.

67) Murase, T.; Nishijima, Y.; Fujita, M. "Cage-Catalyzed Knoevenagel Condensation Under Neutral Conditions in Water." *J. Am. Chem. Soc.*, **2012**, *134*, 162-164.

68) a) Wang, Z. J.; Peck, N. E.; Renata, H.; Arnold, F. H. “Cytochrome P450-Catalyzed Insertion of Carbenoids into N-H Bonds.” *Chem. Sci.*, **2014**, *5*, 598-601; b) McIntosh, J. A.; Coelho, P. S.; Farwell, C. C.; Wang, Z. J.; Lewis, J. C.; Brown, T. R.; Arnold, F. H. “Enantioselective Intramolecular C-H Amination Catalzyed by Engineered Cytochrome P450 Enzymes *in vitro* and *in vivo*.” *Angew. Chem. Int. Ed.*, **2013**, *52*, 9209-9312.

69) Wang, Z. J.; Clary, K. N.; Bergman, R. G.; Raymond, K. N.; Toste, F. D. “A Supramolecular Approach to Combining Enzymatic and Transition Metal Catalysis.” *Nat. Chem.*, **2013**, *5*, 100-103.

70) Custelcean, R.; Bonnesen, P. V.; Duncan, N. C.; Zhang, X.; Watson, L. A.; Berkel, G. V.; Parson, W. B.; Hay, B. P. “Urea-Functionalized M_4L_6 Cage Receptors: Anion-Templated Self-Assembly and Selective Guest Exchange in Aqueous Solutions.” *J. Am. Chem. Soc.*, **2012**, *134*, 8525-8534.

71) Jiao, Y.; Zhang, J.; Zhang, L.; Lin, Z.; He, C.; Duan, C. “Metal-Organic Polyhedra Containing 36 and 24 Folds of Amide Groups for Selective Luminescent Recognition of Natural Disaccharides.” *Chem. Commun.*, **2012**, *48*, 6022-6024.

72) Bunzen, J.; Iwasa, J.; Bonakdarzadeh, P.; Numata, E.; Rissanen, K.; Sato, S.; Fujita, M. “Self-Assembly of $M_{24}L_{48}$ Polyhedra Based on Empirical Prediction.” *Angew. Chem. Int. Ed.*, **2012**, *51*, 3161-3163.

73) Fujita, D.; Suzuki, K.; Sato, S.; Yagi-Utsumi, M.; Yamaguchi, Y.; Mizuno, N.; Kumansaka, T.; Takata, M.; Noda, M.; Uchiyama, S.; Kato, K.; Fujita, M. “Protein Encapsulation Within Synthetic Molecular Hosts.” *Nat. Commun.*, **2012**, *3*, 1093-1099.

74) Ichijo, T.; Sato, S.; Fujita, M. “Size-,Mass-, and Density-Controlled Preparation of TiO_2 Nanoparticles in a Spherical Coordination Template.” *J. Am. Chem. Soc.*, **2013**, *135*, 6786-6789.

75) Liao, P.; Langloss, B. W.; Johnson, A. M.; Knudsen, E. R.; Tham, F. S.; Julian, R. R.; Hooley, R. J. “Two-Component Control of Guest Binding in a Self-Assembled Cage Molecule.” *Chem. Commun.*, **2010**, *46*, 4932-4934.

76) Johnson, A. M.; Moshe, O.; Gamboa, A. S.; Langloss, B. W.; Limtiaco, J. F. K.; Larive, C. K.; Hooley, R. J. “Synthesis and Properties of Metal-Ligand Complexes with Endohedral Amine Functionality.” *Inorg. Chem.*, **2011**, *50*, 9430-9442.

Chapter 2 – Towards Self-Assembled Transition Metal Cages Incorporating "Dynamic" Introverted Functionality

2.1 Stategies for Covalent Endohedral Functionalization

The design of self-assembled species bearing reactive functional groups on their interior is necessary to realize truly biomimetic catalysis. Most of the work making endohedrally functionalized cages has made use of one strategy for functionalization: forced or "static" endohedral functionalization. To achieve this, rigid ligands were targeted which force a functional group towards the center of the cage (Figure 2.1). There are definite benefits to this method of preparing endohedrally functionalized cages.

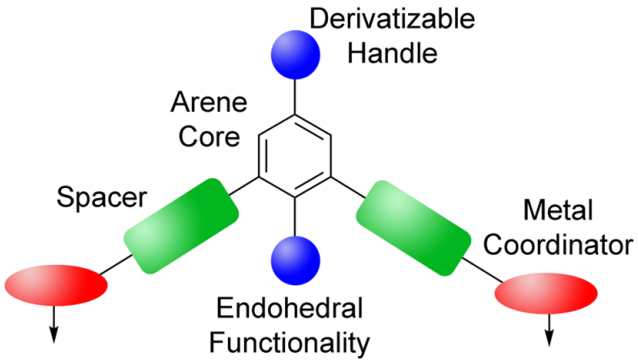

Figure 2.1: Static endohedral functionalization strategy.

The first benefit is that numerous functionalized 2,6-dihaloaromatics are commercially available, such as 2,6-dibromopyridine, 2,6-dibromoaniline, and 2,6-diiodo-4-nitrophenol. These halogenated reagents allow the rapid synthesis of functionalized ligands through Pd-catalyzed cross coupling reactions. The desired metal-chelating group can be attached in one step via Sonogashira coupling of the alkyne compound, or Suzuki coupling with a boronic acid. The coupling partner can also be a precursor to the desired chelator, allowing the preparation of a wide variety of metal-binding groups. This

modular approach has the benefit that it is compatible with many desired internal functionalities. In addition, the availability of 2,6-dibromoaniline should allow for other, less common functionalities to be targeted through conversion to the corresponding diazonium followed by a Sandmeyer reaction. This strategy also has some limitations. Although Pd cross coupling reactions typically give good to excellent yields,[1] steric crowding can lead to poor or no conversion.[2] Another limitation of this strategy is that many of the desired alkyne and boronic acid coupling partners are more expensive. The use of bent ligands also favors the formation of smaller complexes which cannot serve as supramolecular hosts.[3]

An alternate strategy involves the use of linear ligands to introduce endohedral functionality. Instead of forcing the functional group directly into the cavity, these ligands position the functional group "arms" around the open faces of the cage. As long as the core can freely rotate, either arm can rotate inside of the cage. This strategy alleviates some of the problems of the static strategy. Palladium cross-coupling reactions of p-dihalobenzenes proceed in greater yield than those of m-dihalobenzenes due to decreased steric impediment. There are also more p-dihaloarenes commercially available than m-dihaloarenes, and the selectivity of electrophilic aromatic substitutions on hydroquinone and p-xylene derivatives provides further opportunities to add functionality. Unless the chelating group positions the metal too far away from the ligand,[4] a lower order helical self-assembly will be sterically disfavored.

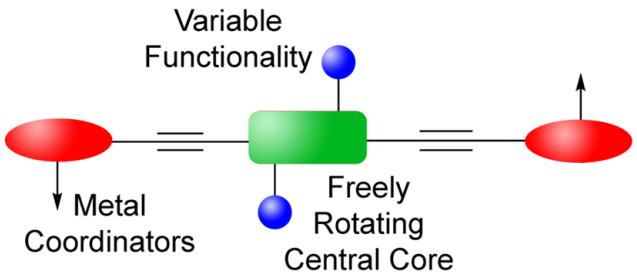

Figure 2.2: Dynamic endohedral functionalization strategy.

2.2 Self-Assembly of Functionalized 1,4-Bispyridylaromatics

As discussed in Chapter 1, few cages with endohedral functional groups are known, Understanding the role such groups would have on the self-assembly process was necessary, however, for the rational design of reactive hosts. Palladium-based paddlewheel complexes such as **1.15** and **1.16** are sensitive to the size of endohedral functional groups, leading to dramatic differences in self-assembly.[5] In these Pd(II)-paddlewheel complexes, small groups could be incorporated on the interior of cages. When two ligands with small functional groups were combined into cages, no selectivity of heterocluster formation was observed (Figure 2.3). When one of the groups became larger such as a trifluoroacetamide, a discrete cage did not form. The larger functional groups couldn't all fit inside of the cage, and a discrete homocluster was not observed. A single trifluoroacetamide could be accommodated, however, leading to mixed cages containing one functionalized ligand and three unfunctionalized selectively. When the endohedral group was made significantly larger, such as a phenylurea, neither a discrete homocluster nor heterocluster cage could be formed.

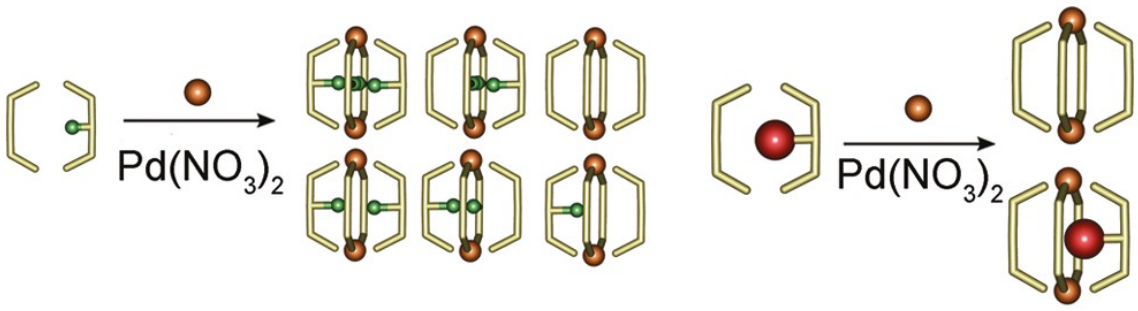

Figure 2.3: Steric bias of mixed ligand palladium-based paddlewheel complexes.

As discussed in Chapter 1, linear Pd(II)-bipyridyls larger than biphenyl are known to be inefficient for the formation of M_4L_4 squares due to the poor differentiation between square and triangle species during self-assembly. What was unknown was whether or not the equilibrium between M_4L_4 and M_3L_3 could instead be pushed towards the triangle by sterics. Terphenyl-based bipyridines represent a simple system to study the effects of steric bias on functionalized linear ligands. Ligand **2.1a** and **2.1b** provide small arms which should not significantly bias the formation of a triangle (Figure 2.4). Ligand **2.1c** provides flexible alkyl groups, and **2.1d** provides two inflexible rotor functions (Figure 2.4).

The synthesis of these compounds was relatively straightforward, and a modification of a known procedure was used.[6] The desired dihalocores could be combined in either DMF or a mixture of PhMe and EtOH, along with the mild base cesium carbonate or sodium carbonate and a slight excess of the 4-pyridylboronic acid coupling partner and a catalytic amount of a Pd(0) complex generated *in situ*.[7] Upon work-up the products could be isolated cleanly after simple recrystallization from absolute ethanol. The dihalide precursor to **2.1c**, **2.2**, was made by alkylating hydroquinone with butyl iodide in DMF in the presence of potassium hydroxide, followed by iodination with iodine monochloride in MeOH.

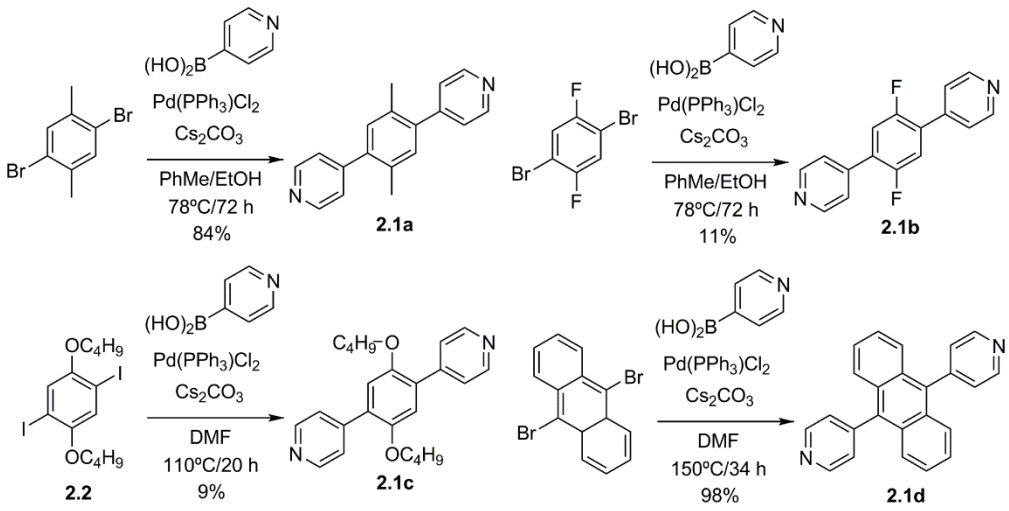

Figure 2.4: Synthesis of 1,4-bis(4-pyridyl)aromatic ligands through Suzuki cross-coupling reactions.

The use of palladium salts with two coordination sites blocked by a bulky ligand had previously been shown to give mixtures of square vs. triangular assemblies of 4,4'-bipyridines. With longer bipyridines, however, it might be possible for $[Pd(en)(NO_3)_2]$ to self-assemble with ligands **2.1a**-**2.1d** to give triangles selectively. Synthesis of this salt involved adding $[Pd(en)Cl_2]$ to deionized water with $AgNO_3$ and a catalytic amount of HNO_3.[8] After being allowed to sit for 12 h at room temperature the AgCl precipitate was filtered, and the water evaporated *in vacuo* to give the desired palladium salt. Complexation between **2.1a** and $[Pd(en)(NO_3)_2]$ in D_2O at 70°C, however, afforded a ^1H NMR spectrum that did not indicate a single product was formed (Figure 2.5). A cleaner spectrum was obtained when this experiment was reattempted in DMSO-d_6, however there were still multiple species observed.

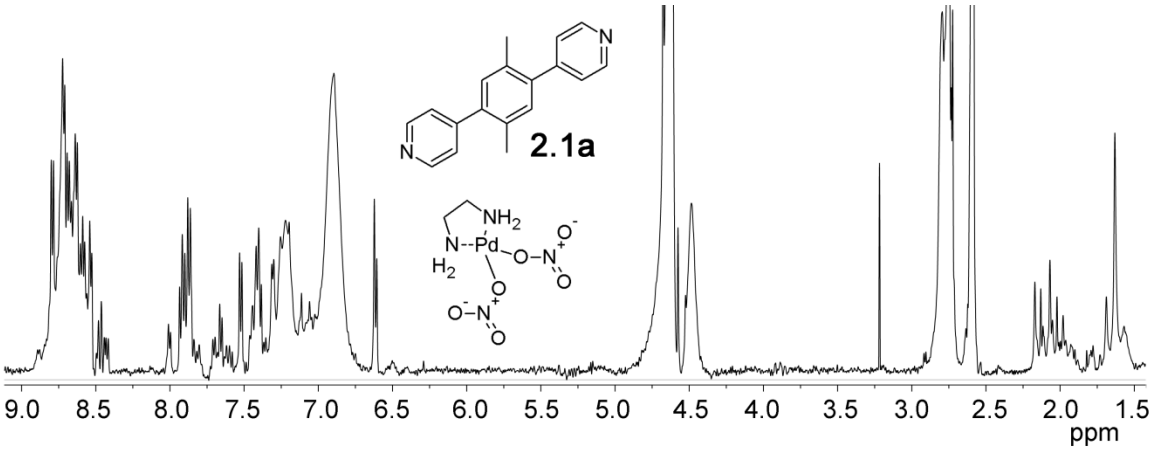

Figure 2.5: ^{1}H NMR of the mixture observed upon complexation of **2.1a** with [Pd(en)$(NO_3)_2$] (D_2O, 400 MHz, 298 K).

Although [Pd(en)]$(NO_3)_2$ did not force the formation of a self-assembled triangle with **2.1a**, a larger ligand in place of ethylene diamine had already been shown to destabilize the M_4L_4 assembly. As discuss in Chapter 1, this is because a larger ligand on the palladium would contribute greater bulk to the coordination environment. Coupled with a bulkier bipyridyl, this might completely disfavor the M_4L_4 species. Starting from the commercially available palladium complex [Pd(dppf)Cl_2] (dppf = 1,1'-bis(diphenylphosphino)ferrocene), a bulkier palladium species was prepared by halide abstraction using $AgBF_4$ to give the highly organic soluble **2.3** (Figure 2.6a). Unfortunately, this too failed to give a single, discrete species as determined by ^{31}P NMR (Figure 2.6b) and ^{1}H NMR (Figure 2.6c).

As the issues of making a single discrete palladium species could not easily be overcome, the analogous [Re$(CO)_3$Cl] based assembly was investigated.[9] These complexes were targeted by heating the bispyridyl ligands in toluene to replace two of the carbonyl groups in [Re$(CO)_5$Cl] with pyridines to give rise to a self-assembled

square. Unfortunately, these conditions did not give complete conversion to the desired discrete complexes of either **2.1a** or **2.1d**, nor could the products be cleanly isolated.

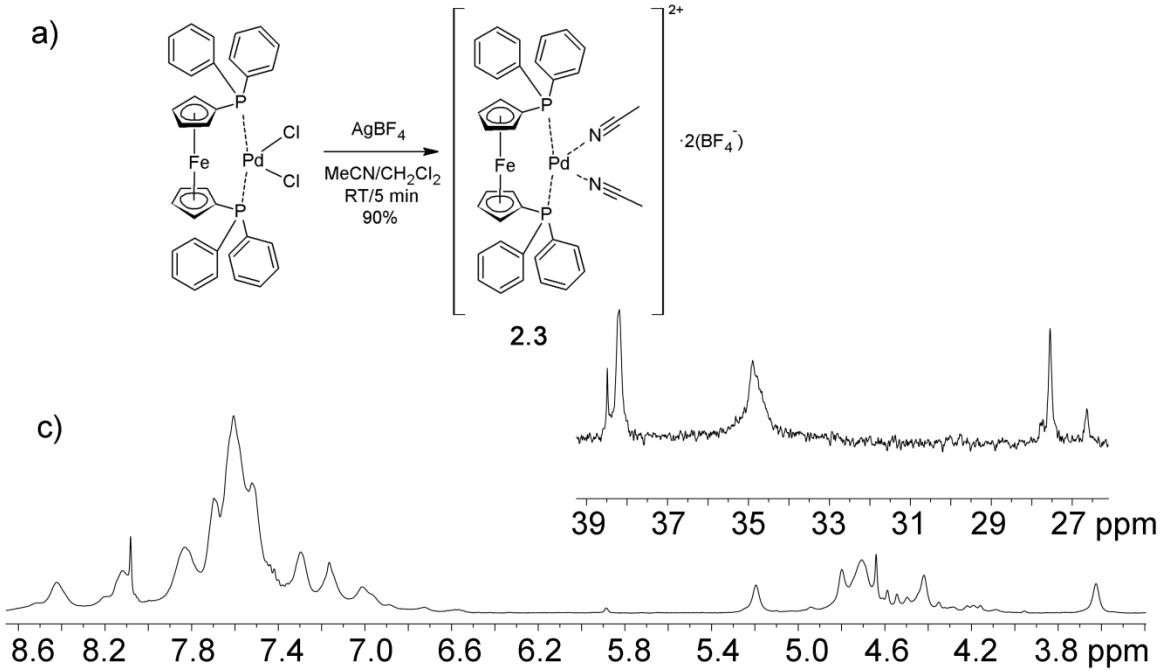

Figure 2.6: Synthesis of **2.3** and subsequent self-assembly: a) Synthesis of **2.3** from $[Pd(dppf)Cl_2]$; b) ^{31}P NMR spectrum (161.9 MHz, CD_3CN, 298K); c) ^{1}H NMR spectrum (CD_3CN, 400 MHz, 298 K).

The poor lability of CO ligands on $[Re(CO)_5Cl]$ necessitated a switch to the more labile $[Mn(CO)_5Br]$.[10] When **2.1a** was combined in acetone with $[Mn(CO)_5Br]$ and left at room temperature for 9 h, the ^{1}H NMR spectrum showed complete conversion to a new species containing predominately one new complex (Figure 2.7). This species was amenable to mass spectrometric analysis, and showed the presence of the M_4L_4 species **$[2.1a_4 \bullet Mn_4](CO)_{12}Br_4$**. Although this species should exist as a square in solution, no solid state analysis was possible. Attempts to grow crystals of **$[2.1a_4 \bullet Mn_4](CO)_{12}Br_4$** failed, with and without the addition of cyclic aliphatic and aromatic guests which might be able to stabilize the formation of a more favorable solid state complex. The presence of a

single species, however, suggested this would be a good system to study the effect of a bulkier ligand.

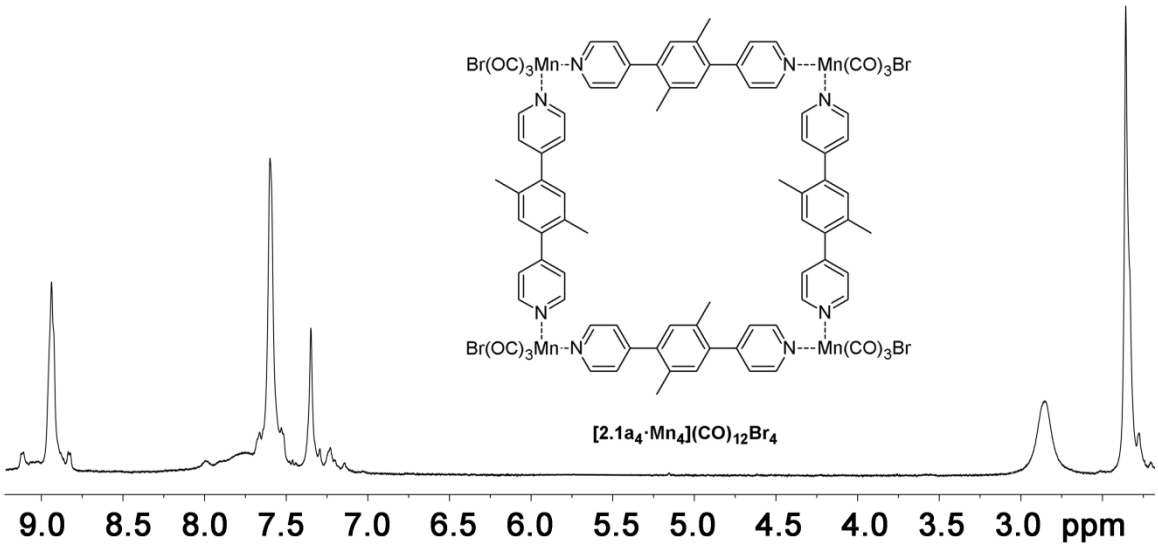

Figure 2.7: ^{1}H NMR spectrum of **[2.1a$_4$•Mn$_4$](CO)$_{12}$Br$_4$** (CD_3CN, 400 MHz, 298K).

When the anthracene ligand **2.1d** was then added to $[Mn(CO)_5Br]$ in acetone, discrete complex was not observed. A variety of conditions were screened, but in every case the complex was too insoluble to analyze. The best result was obtained by combining the components in DMSO-d_6 and heating for 5 h. After cooling a broad ^{1}H NMR spectrum was observed. In case the broadness was a consequence restricted rotation of the anthracene,[11] the sample was heated to 100°C without sign of any peaks coalescing. These results suggest that the complex forms a poorly soluble oligomer.[12]

Although linear 4,4”-bispyridyls did not seem to be a viable system for preparing larger discrete structures, their 3,3” analogues offered some unexplored opportunities. If a linear coordination motif could be combined with these ligands that only contained two open coordination sites 180° from each other, unsymmetrical hexagonal M_3L_3 polygons

could be prepared. Ligand **2.4** was synthesized through a Sonogashira coupling reaction (Figure 2.8). In this case, the dihalo core and 3-ethynyl pyridine could be combined in anhydrous solvents with Pd(II) and Cu(I) salts and then heated to give the desired product.

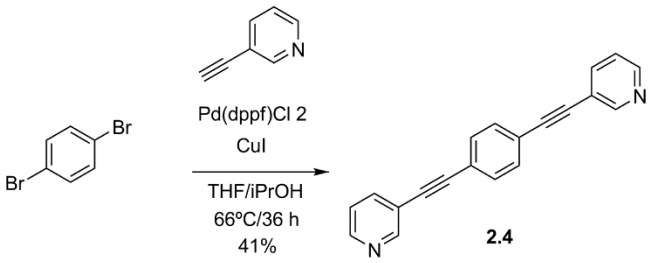

Figure 2.8: Synthesis of 1,4-bis(3-pyridylethynyl)aromatic ligand **2.4** through a Sonogashira cross-coupling reaction.

Au(I) salts are known to form linear complexes,[13] and a suitable, poorly ligated salt was freshly prepared *in situ* by halide abstraction of $[Au(Me_2S)Cl]$ with $AgBF_4$. Titration of this into an acetonitrile solution of **2.4** showed formation of a discrete assembly. The complexes, however, were not stable at room temperature. After preparation, they would slowly decompose back to the ligand and pink or purple solutions. This is indicative of the gold complexes decomposing to give gold nanoparticles.[14]

2.3 Self-Assembly of Functionalized Aminomethylpyridine Rotors

The Fe(II)-iminopyridine motif is popular for synthesizing molecular helices,[15] and more recently to prepare the water-soluble tetrahedron **1.12**.[16] The motif was anticipated to be more robust than any of the monodentate strategies targeted in Section 2.2. Access to ligands of this type would require appending an aniline to the end of the

dihaloarene core, followed by condensation with 2-formylpyridine. The first strategy involved treating p-dibromobenzene under Suzuki conditions with 4-aminophenyl boronic acid-pinacol ester. The aniline substrate however was too electron rich to undergo the required organometallic chemistry,[17] and conversion to the dianiline was unsuccessful.

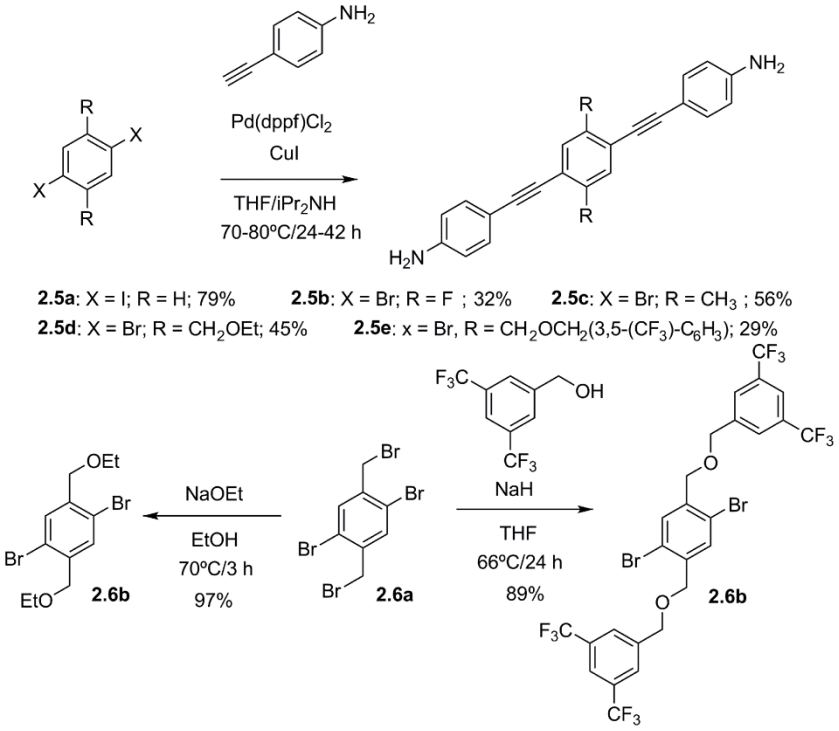

Figure 2.9: Synthesis of 1,4-bis[(4-aminophenyl)ethynyl]aromatic ligands **2.5a-2.5e** through Sonogashira cross-coupling reactions.

Dianilines can also be prepared using a Sonogashira coupling between dihaloarene cores and 4-ethynylaniline (Figure 2.9). Unlike the Suzuki procedure for making these dianilines, Sonogashira coupling with 4-ethynylaniline was capable of giving the desired products.[18] Dianilines **2.5a**, **2.5b**, and **2.5c** were all accessible from commercially available dibromoarenes. Compounds **2.5d** and **2.5e** were prepared from **2.6b** and **2.6c** respectively. These were conveniently prepared by NBS bromination of 2,5-dibromo-p-

xylene to give **2.6a**,[19] followed by subsequent reaction with either sodium ethoxide or sodium (3,5-bis(trifluoromethyl)phenyl)methoxide respectively. The yields of these Sonogashira cross-couplings, with the exception of **2.5b**, suggest the reaction is less tolerant to bulkier functional groups.

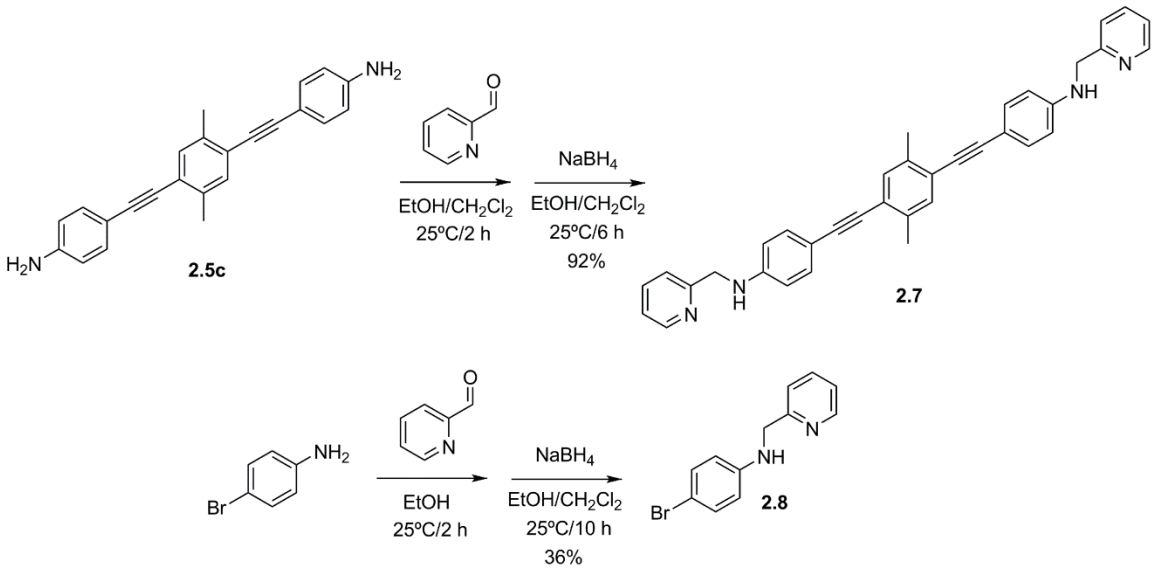

Figure 2.10: Reductive amination of dianiline **2.5c** and *p*-bromoaniline to give ligand **2.7** and test ligand **2.8**.

Initial attempts at condensing dianilines **2.5a**-**2.5e** with 2-formylpyridine proved unsuccessful. Although some conversion was observed in each case, the reactions failed to go to completion. Screening different solvents and temperatures, molecular sieves, and even Dean-Stark conditions failed to give full conversion on the reactions. It was also impossible to purify the imine product without further hydrolysis back to the starting materials. Although there was the potential to prepare cages *in situ*, it desirable to first isolate a ligand to study its metal coordination directly. The strategy was modified to prepare a series of more stable analogues of **2.5a**-**2.5e**. Reductive amination of **2.5c**

and **2.5d** using 2-formylpyridine and sodium borohydride (Figure 2.10) gives ligand **2.7** which is no longer susceptible to imine hydrolysis.

A test ligand, **2.8**, was also prepared using a reductive amination strategy. This ligand was accessible in one step from cheap reagents, making it better for screening metal-coordination than bi-functional **2.7**. A variety of transition metals (Cr(III), Mn(III), Fe(II), Fe(III), Co(II), Ni(II), Cu(I), Cu(II), Zn(II), Ru(III), Rh(III), Cd(II), and Hg(II)) were screened for complexation with **2.8** in DMSO-d_6 and followed by ^{1}H NMR spectroscopy. In addition the main group metal Ga(III) and lanthanides Sm(III) and Gd(III) were also screened for complexation with **2.8**.

It became apparent that any counterion that coordinated more tightly than a nitrate could not be displaced by **2.8**. This eliminated acetate, acetoacetonoates, halides, and sulfate as viable metal salts for complexation with the aminomethylpyridine ligands. More weakly coordinating salts, such as triflate, trifluroacetate, tetrafluoroborate, and nitrate could be displaced to give complexes. The best results were obtained when **2.8** was combined with $Cr(NO_3)_3 \bullet 9H_2O$.

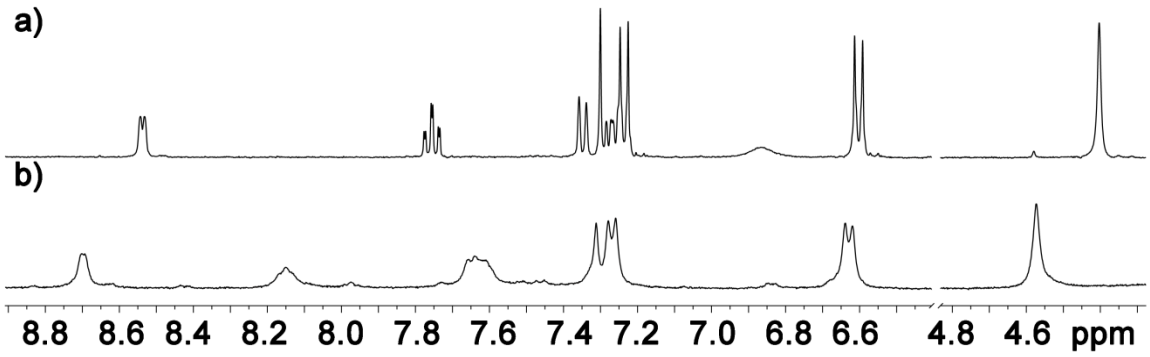

Figure 2.11: ^{1}H NMR analysis of **[2.7$_x$•Cr$_x$](NO$_3$)$_{3x}$** (DMSO-d_6, 400 MHz, 298K): a) **2.7**; b) 1 eq Cr(III).

A solution of Cr(III) was then titrated into a DMSO-d_6 solution of ligand **2.7** and the results followed by ^{1}H NMR spectroscopy. This data suggested that a 1:1 complex was being formed (Figure 2.11), implying that two of the bidentate ligands were coordinating to each metal. Although Cr(III) is a d^3 metal, only a slight broadening occurs in the ^{1}H NMR spectrum. Despite attempts to either crystallize or study this species by ESI-MS and MALDI-MS, no further elucidation of the structure was achieved. Diffusion NMR showed all of the peaks co-diffused, but without a reference the diffusion coefficient was not useful to predict the shape and size of the assembly.

2.4 Self-Assembly of Functionalized Iminopyridine Rotors

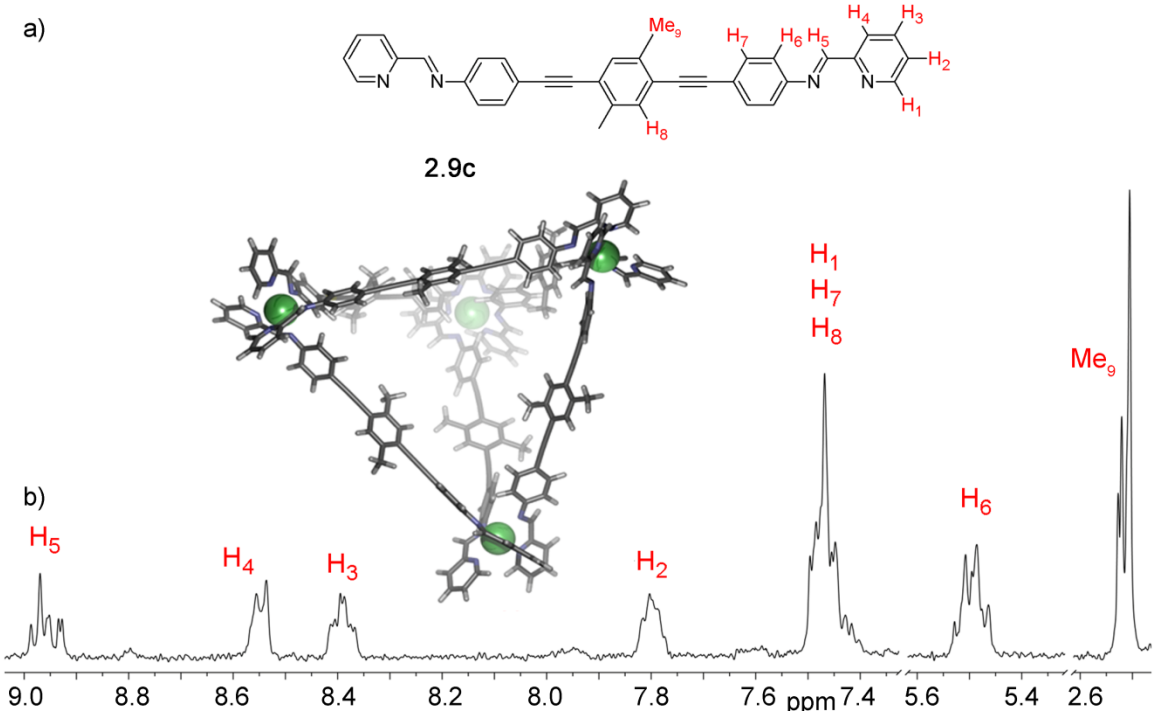

Figure 2.12. Structure and characterization of **[2.9c$_x$•Fe$_y$](ClO$_4$)$_{2y}$**: a) chemdraw and SPARTAN model of the expected M_4L_6 self-assembly (AM1 forcefield); b) ^{1}H NMR with the relative groups of resonances labeled (400 MHz, CD_3CN).

Although the bis-aminomethylpyridine ligand **2.7** was capable of forming complexes, these complexes were not robust, and condensation of **2.5a**-**2.5e** to give iminopyridines **2.9a**-**2.9e** was therefore revisited. Given the precedence for *in situ* condensation of 2-formylpyridine *en route* to copper(I) complexes,[20] screens were set-up to see if a similar iron(II) species could be achieved. Different Fe(II) salts were screened with dianiline **2.5c** and 2-formylpyridine in various solvents. Only the combination of **2.5c** with 2-formylpyridine and $Fe(ClO_4)_2 \cdot xH_2O$ in MeCN gave any sign of complexation. Although the successful screen was isolated by evaporating the solvent *in vacuo*, a more effective way to isolate the complex from MeCN was to precipitate it with Et_2O.

The Fe(II)-iminopyridine complex of **2.9a** gave a brilliant purple color due to a metal-to-ligand charge transfer band located between 500 and 600 nm similar to **1.12**.[21] The ^1H NMR spectrum of this species, however, did not suggest that a single species had formed. Whereas the ^1H NMR spectrum of **1.12** contained only one set of peaks, $\mathbf{[2.9c_x \cdot Fe_y](ClO_4)_{2y}}$ showed multiple resonances (Figure 2.12) for each proton. A general diagnostic resonance for these iminopyridine complexes is the proton labeled H_6. Although it should be much further downfield due to its electron deficient nature, the presence of shielding from adjacent aromatic rings causes the peak to shift approximately 2 ppm upfield. The presence of this supports formation of the desired product.

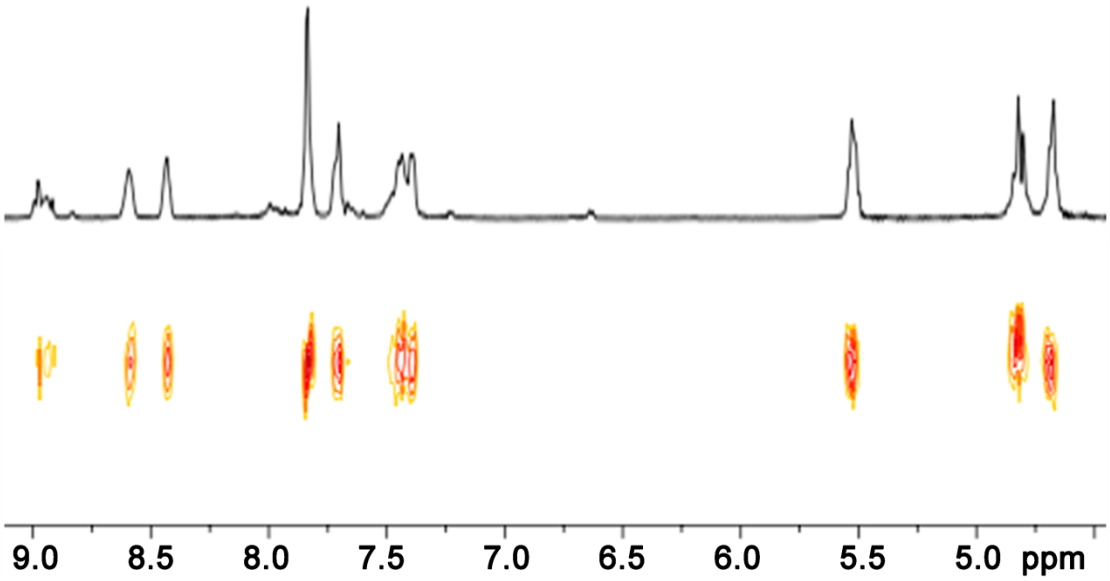

Figure 2.13. Diffusion NMR of **[2.9e$_6$•Fe$_4$](ClO$_4$)$_8$** (600 MHz, CD_3CN, 298K).

One potential reason for this is that the sample is a mixture of different species in solution. Although the ESI mass spectrum was able to show very small peaks which correspond to the M_4L_6 species in solution, this doesn't prove that either smaller or larger structures could not be present as well. Diffusion NMR was performed on the sample to determine if there were multiple stoichiometries present. As can be seen from Figure 2.13, all of the peaks present diffuse at the same rate, suggesting that all of the peaks derive from some form of M_4L_6 assembly.

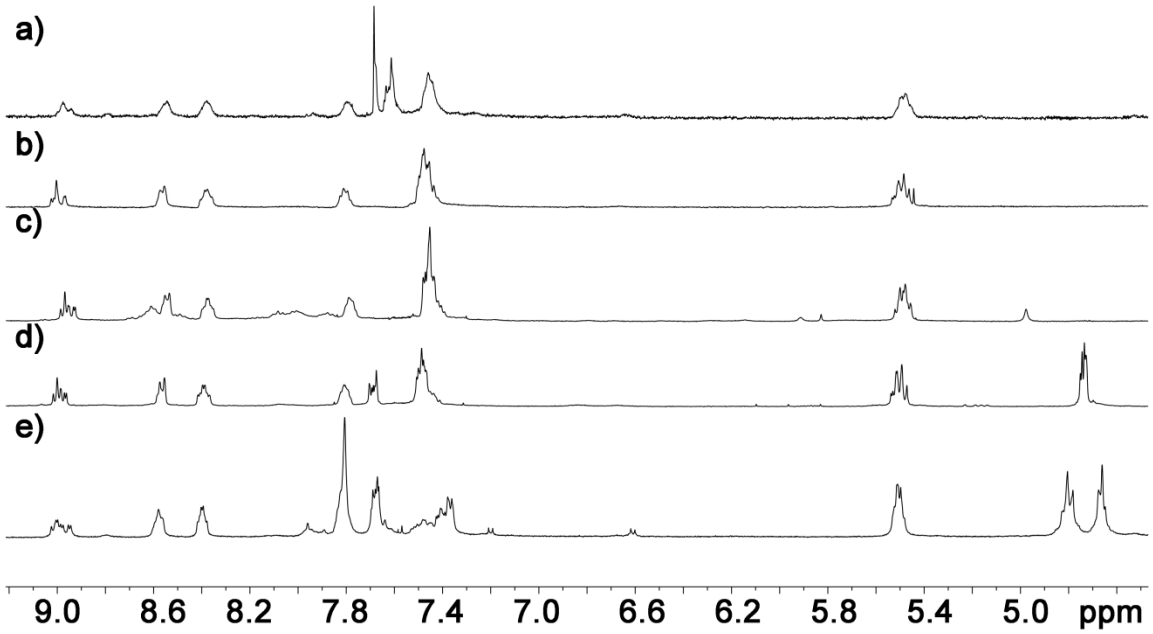

Figure 2.14. ^{1}H NMR of **[2.9a-e$_6$•Fe$_4$](ClO$_4$)$_8$**: a) **[2.9a$_6$•Fe$_4$](ClO$_4$)$_8$**; b) **[2.9b$_6$•Fe$_4$](ClO$_4$)$_8$**; c) **[2.9c$_6$•Fe$_4$](ClO$_4$)$_8$**; d) **[2.9d$_6$•Fe$_4$](ClO$_4$)$_8$**; e) **[2.9e$_6$•Fe$_4$](ClO$_4$)$_8$** (400 MHz, CD_3CN, 298K).

Another plausible explanation was that the complexes were simply desymmetrized due to restricted rotation. The methyl group of **2.9c**, though not large, could be responsible for this. To test this, the complexes of **2.9a** and **2.9b** were prepared containing the smaller H and F substituents (Figure 2.14 a and b), and gave similar desymmetrized ^{1}H NMR spectra to **[2.9a$_6$•Fe$_4$](ClO$_4$)$_8$** (Figure 2.14c). The larger ethoxymethyl **2.9d** and bis-trifluoromethylbenzyloxymethyl **2.9e** based cages were prepared (Figure 2.14 d and e) and also gave similar ^{1}H NMR spectra.

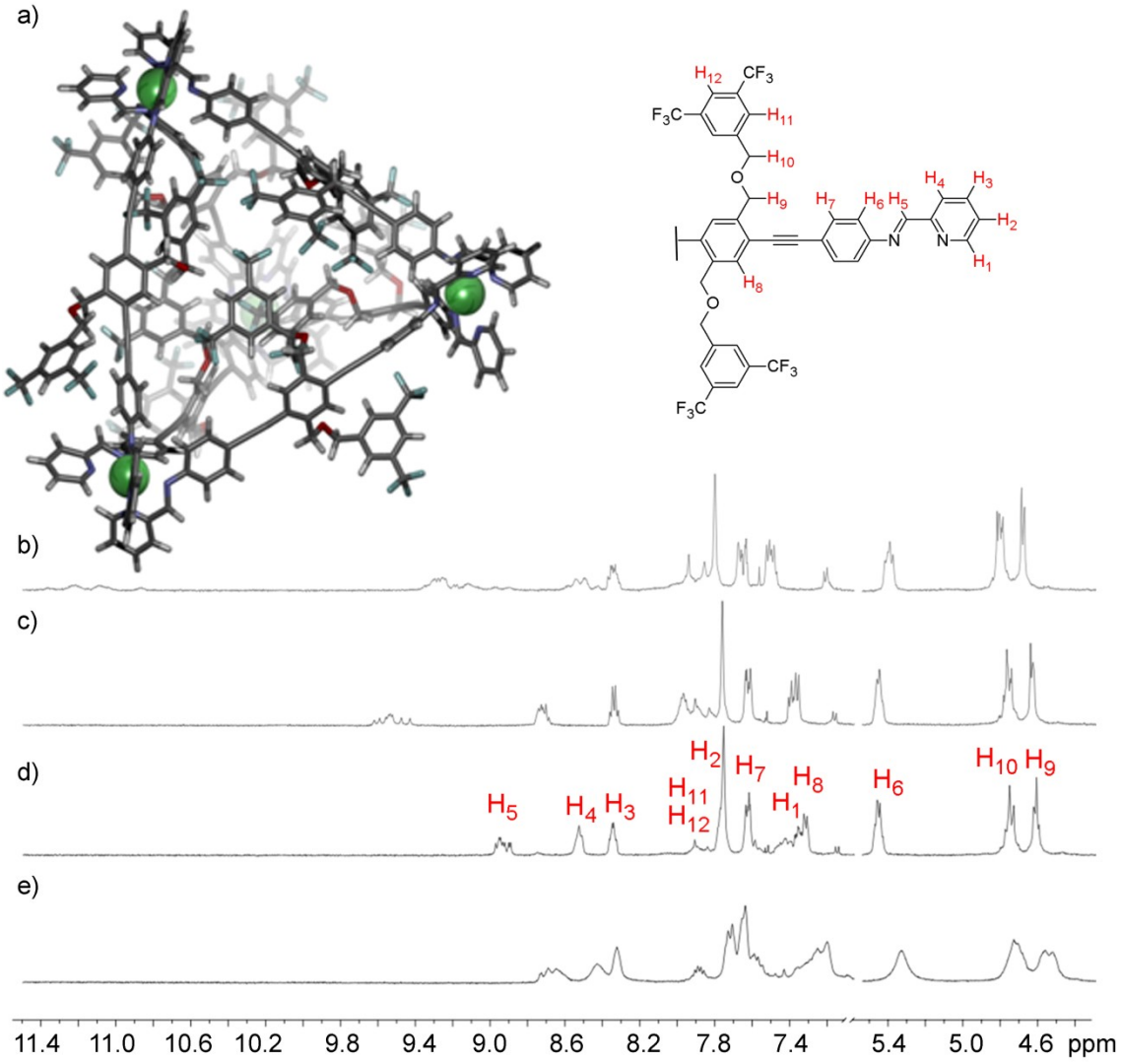

Figure 2.15. Variable temperature ^{1}H NMR spectra of **[2.9e$_6$•Fe$_4$](ClO$_4$)$_8$**: a) SPARTAN model and chemdraw of **[2.9e$_6$•Fe$_4$](ClO$_4$)$_8$** (AM1 forcefield); b) 75°C; c) 50°C; d) 25°C; e) -40°C (500 MHz, CD_3CN).

Although restricted rotation was unlikely across the full range of side chains sampled, the largest rotor complex **[2.9e$_6$•Fe$_4$](ClO$_4$)$_8$** was subjected to variable temperature (VT) NMR (Figure 2.15). Despite its large size, very little change was observed in the resonances attributed to the rotor arms as the temperature was

decreased. The peaks begin to broaden out close to -40°C, but this due to an increase in viscosity as the solvent approaches its melting point. The only significant change is in the protons close to the iron center. Resonances H_1 and H_5 each experience an approximately 2 ppm shift downfield between 25 and 75°C. The signals for H_2 and H_4 also shift downfield, albeit in more modest amounts.

The dianilines **2.5a**-**2.5e** lead to the M_4L_6 complexes **[2.9a-e$_6$•Fe$_4$](ClO$_4$)$_8$** only, and that there was no sign of restricted rotation in these complexes. The next likely cause of desymmetrization was diastereoisomerism at the metal centers, as had been observed in catecholate assemblies.[22] While this work on the self-assembled rotors was being pursued, a publication from another group showed that longer, less rigid Fe(II)-iminopyridine complexes such as **2.10** also show less diastereocontrol (Figure 2.16).[23]

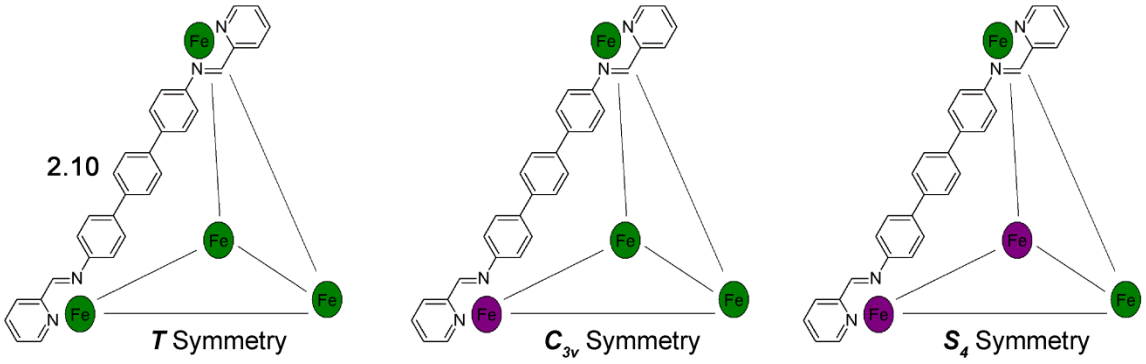

Figure 2.16. The three possible diastereomers observed in tetra-*fac* Fe(II)-iminopyridine cages.

The main isomer of **2.10** displayed tetrahedral (*T*) symmetry in which all four of the iron centers adopt the same stereoconfiguration, and every hydrogen was represented by a single resonance in the ^{1}H NMR spectrum. The less symmetrical C_3 cage was also observed, adding three different proton resonances. The final S_4 symmetric cage adds

four more signals per proton on the ligand: one between each of the matched stereocenters, and two on each ligand between mismatched stereocenters. The presence of seven different unique protons in such a mixture explains the spectra obtained for **[2.9a-e_6•Fe_4](ClO_4)$_8$**.

2.5 Conclusion

Self-assembly of linear ligands to form functionalized metal-organic cages presents easy synthetic targets. The need to use rigid ligands to direct assembly of discrete species requires sp^2 and sp linkages in the backbone of such molecules. In the case of terphenyl reagents, this can lead to decreased solubility. Extension of the backbone, however, can still lead to additional flexibility causing self-assembled ligands to lose stereochemical communication as evidenced by the Fe(II)-iminopyridine example. This loss of communication leads to more complex ^{1}H NMR spectra which are harder to analyze, and will make guest binding and reactivity studies more challenging.

2.6 References

1) Liu, S.-Y.; Choi, M. J.; Fu, G. C. “A Surprisingly Mild and Versatile Method for Palladium-Catalyzed Suzuki Cross-Couplings of Aryl Chlorides in the Presence of a Tri*aryl*phosphine.” *Chem. Commun.*, **2001**, 2408-2409.

2) Sasaki, S.; Ogawa, K.; Watanabe, M.; Yoshifuji, M. “Synthestis and Properties of Sterically Crowded Triarylphosphines Bearing Naphthoquinone Moieties.” *Organometallics*, **2010**, *29*, 757-766.

3) Kerckhoffs, J. M. C. A.; Peberdy, J. C.; Meistermann, I.; Childs, L. J.; Isaac, C. J.; Pearmund, C. R.; Reudegger, V.; Kahlid, S.; Alcock, N. W.; Hannon, M. J.; Rodger, A. “Enantiomeric Resolution of Supramolecular Helicates with Different Surface Topographies.” *Dalton Trans.*, **2007**, 734-742.

4) Caulder, D. L.; Raymond, K. N. “Supramolecular Self-Recognition and Self-Assembly in Gallium(III) Catecholamide Triple Helices.” *Angew. Chem. Int. Ed.*, **1997**, *36*, 1439-1442.

5) Johnson, A. M.; Hooley, R. J. “Steric Effects Control Self-Sorting in Self-Assembled Clusters.” *Inorg. Chem.*, **2011**, *50*, 4671-4673.

6) Knight, L. K.; Vukotic, V. N.; Viljoen, E.; Caputo, C. B.; Loeb, S. J. “Eliminating the Need for Independent Counterions in the Construction of Metal-Organic Rotaxane Frameworks (MORFs).” *Chem. Commun.*, **2009**,5585-5587.

7) Wei, C. S.; Davies, G. H. M.; Soltani, O.; Albrecht, J.; Gao, Q.; Pathirana, C.; Hsiao, Y.; Tummala, S.; Eastgate, M. D. “The Impact of Palladium(II) Reduction Pathways on the Structure and Activity of Palladium(0) Catalysts.” *Angew. Chem. Int. Ed.*, **2013**, *52*, 5822-5826.

8) Drew, H. D. K.; Pinkard, F. W.; Preston, G. H.; Wardlaw, W. “The Supposed Isomerism Among the Palladodiammines.” *J. Chem. Soc.*, **1932**, 1895-1909.

9) Sun, S.-S.; Lees, A. J. “New Self-Assembly Luminescent Molecular Triangle and Square Rhenium(I) Complexes.” *Inorg. Chem.*, **1999**, *38*, 4181-4182.

10) Crabtree, R. H. “General Properties of Organometallic Complexes.” O*rganometallic Chemistry of the Transition Metals*, 5th Ed., Wiley & Sons: West Sussex, **2009**; Chapter 2.

11) Kishi, N.; Li, Z.; Yoza, K.; Akita, M.; Yoshizawa, M. “An M_2L_4 Molecular Capsule with an Anthracene Shell: Encapsulation of Large Guests up to 1 nm.” *J. Am. Chem. Soc.*, **2011**, *133*, 11438-11441.

12) Qin, Z.; Jennings, M. C.; Puddephatt, R. J. “Self-Assembly in Palladium(II) and Platinum(II) Chemistry: The Biomimetic Approach.” *Inorg. Chem.*, **2003**, *42*, 1956-1965.

13) Lavallo, V.; Wright, J. H.; Tham, F. S.; Quinlivan, S. “Perhalogenated Carba-*closo*-dodecaborate Anions as Ligand Substituents: Applications in Gold Catalysis.” *Angew. Chem. Int. Ed.*, **2013**, *52*, 3172-3176.

14) Vekilov, P. G. “Grown in a Crystal.” *Nature Nanotech.*, **2011**, *6*, 82-83.

15) a) Kerchkhoffs, J. M. C. A.; Peberdy, J. C.; Meistermann, I.; Childs, L. J.; Isaac, C. J.; Pearmund, C. R.; Reudegger, V.; Khalid, S.; Alcock, N. W.; Hannon, M. J.; Rodger, A. “Enantiomeric Resolution of Supramolecular Helicates with Different Surface Topographies.” *Dalton Trans.*, **2007**, 734-742; b) Hannon, M. J.; Painting, C. L.; Jackson, A.; Hamblin, J.; Errington, W. “An Inexpensive Approach to Supramolecular Architecture.” *Chem. Commun.*, **1997**, 1807-1808.

16) Riddell, I. A.; Smulders, M. M. J.; Clegg, J. K.; Nitschke, J. R. “Encapsulation, Storage, and Controlled Release of Sulfur Hexafluoride from a Metal-Organic Capsule.” *Chem. Commun.*, **2011**, *47*, 457-459.

17) Barder, T. E.; Walker, S. D.; Martinelli, J. R.; Buchwald, S. L. “Catalysts for Suzuki-Miyaura Coupling Processes: Scope and Studies of the Effect of Ligand Structure.” *J. Am. Chem. Soc.*, **2005**, *127*, 4685-4696.

19) Lu, Q.; Liu, K.; Zhang, H.; Du, Z.; Wang, X.; Wang, F. “From Tunneling to Hopping: A Comprehensive Investigation of Charge Transport Mechanism in Molecular Junctions Based on Oligo(*p*-phenylene Ethylene)s.” *ACS Nano*, **2009**, *3*, 3861-3868.

20) Bonifacio, M. C.; Robertson, C. R.; Jung, J.-Y.; King, B. T. “Polycyclic Aromatic Hydrocarbons by Ring-Closing Metathesis.” *J. Org. Chem.*, **2005**, *70*, 8522-8526.

21) Nitschke, J. R. “Mutual Stabilization Between Imine Ligands and Copper(I) Ions in Aqueous Solution.” *Angew. Chem. Int. Ed.*, **2004**, *43*, 3073-3075.

22) Neelakandan, P. P.; Jimenez, A.; Nitschke, J. R. “Fluorophore Incorporation Allows Nanomolar Guest Sensing and White-Light Emission in M_4L_6 Cage Complexes.” *Chem. Sci.*, **2014**, *5*, 908-915.

23) Seeber, G.; Tiedemann, B.; Raymond, K. N. “Supramolecular Chirality in Coordination Chemistry.” *Top. Curr. Chem.*, **2006**, *265*, 147-183.

24) Meng, W.; Clegg, J. K.; Thoburn, J. D.; Nitschke, J. R. “Controlling the Transmission of Stereochemical Information Through Space in Terphenyl-Edged Fe_4L_6 Cages.” *J. Am. Chem. Soc.*, **2011**, *133*, 13652-13660.

Chapter 3 – Control of Self-Assembly Through Endohedral Functionalization of Fe(II)-Iminopyridine Cages

3.1 Rationale

One observation about the diastereoselectivity of **2.10** and its analogues was that while longer, less rigid iminopyridine ligands experienced decreased diastereoselectivity upon self-assembly with Fe(II), the inclusion of methyl groups to the ligand could enhance the otherwise diminished selectivity. This suggested that addition of endohedral groups could rigidify the resulting self-assembly. However, **[2.9e$_6$•Fe$_4$](ClO$_4$)$_8$** contained a significantly larger group that was still able to freely rotate and provided little steric benefit. This means that a larger and more rigid group such as anthracenylmethanol would have to be added to the rotor which could lead to a less soluble complex. In addition, the separation observed for isomers of **[2.9(a-e)$_6$•Fe$_4$](ClO$_4$)$_8$** by ^{1}H NMR spectroscopy was not enough to allow for facile identification of all the isomers, resulting in a challenging analysis.

A simple model system could be achieved by using the static functionalization strategy defined in Figure 2.1 combined with a M_2L_3 helix. The presence of two (as opposed to four) metal centers would limit the number of proton resonances in a ^{1}H NMR spectrum, simplifying analysis. Simple Fe(II)-iminopyridine helices have been known for many years (Figure 3.1),[1] and all show complete diastereoselectivity in a variety of solvents and with different counterions. They are also robust, having been investigated for their ability to bind to DNA in aqueous, concentrated salt environments.[2]

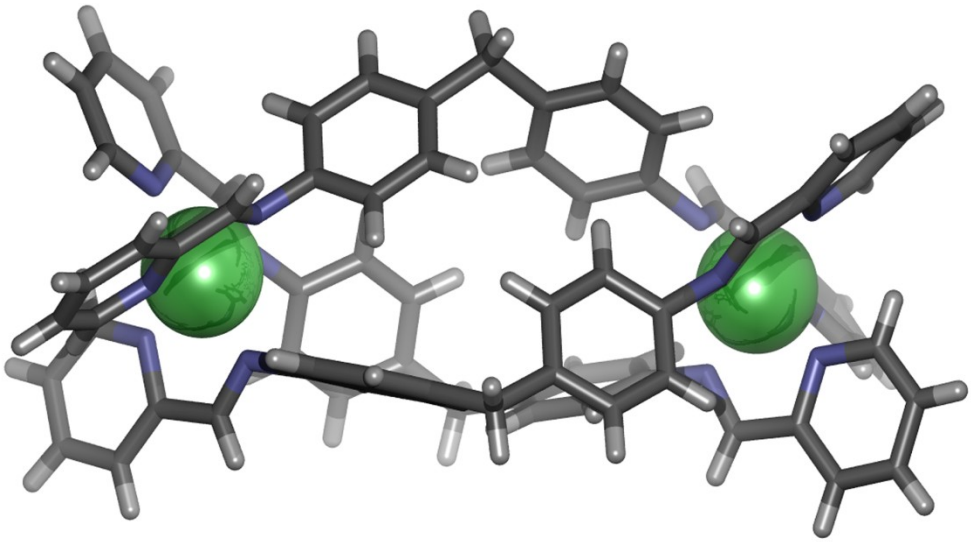

Figure 3.1: X-ray crystal structure of the first M_2L_3 Fe(II)-iminopyridine helix.

3.2 Ligand Design and Synthesis

The strategy for synthesizing ligands for this study focused on the Sonogashira coupling of 2,6-dihalobenzene cores with 4-ethynyl aniline (Figure 3.2). The simplest dianiline of this type was already known,[3] and the method was generally applicable to other substrates. Simple ligand **3.1a**, amine-functionalized **3.1b** and the exterior nitro analogue **3.1c** were synthesized with similar, albeit low yields.[4] These three species served as a control, as their lack of bulky internal functionality should provide a mixture of diastereomers upon multi-component self-assembly with Fe(II).

The addition of a bulkier group was achieved by reacting 2,6-dibromophenol with benzyl bromide in the presence of potassium carbonate to give the core **3.2a** (Figure 3.3). Sonogashira coupling of **3.2a** to give **3.1d** proceeded with lower conversion than previous iterations, conceivably due to the increased steric bulk of the side chain. Attempts to prepare an ester-functionalized core by reaction of 2,6-dibromophenol with

ethyl bromoacetate gave a significant amount of side product in addition to the desired **3.2b**, identified as the difunctionalized product **3.3**. Although clean **3.2b** could be obtained after purification, the Sonogashira coupling was problematic. The coupling product of **3.2b** was detected in the mixture by ^{1}H NMR spectroscopy and ESI-MS analysis, but it was not possible to separate it from the monoaniline side product.

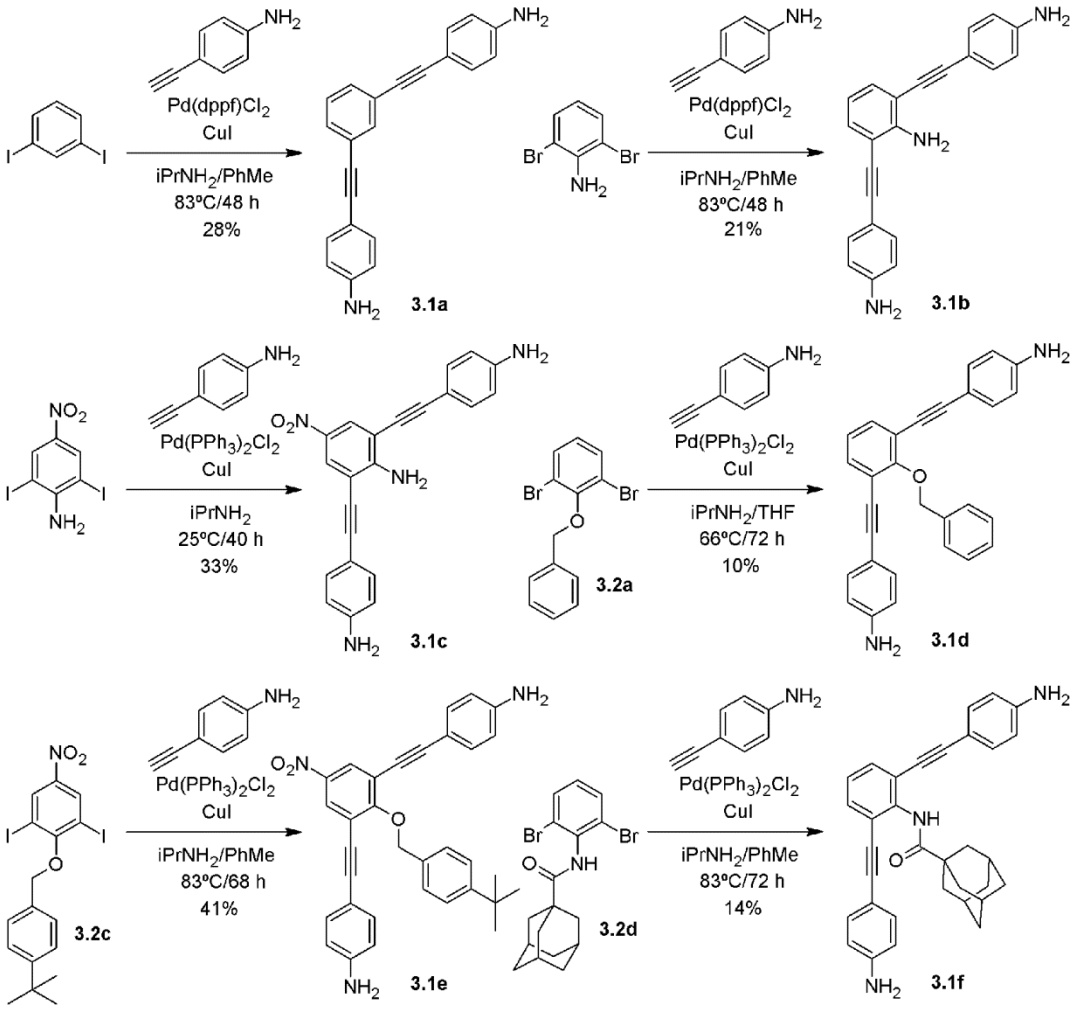

Figure 3.2: Synthesis of dianilines **3.1a**-**3.f** using the Sonogashira cross-coupling reaction.

Switching from 2,6-dibromophenol to 2,6-diiodo-4-nitrophenol limited side reactions in preparation of 4-(tert-butyl)benzyl core **3.2c**. In addition, the more reactive iodides were expected to increase the yield of the cross-coupling reaction. Sonogashira coupling of **3.2c** with 4-ethynyl aniline gave better conversion compared to dianilines **3.2a**-**d**.

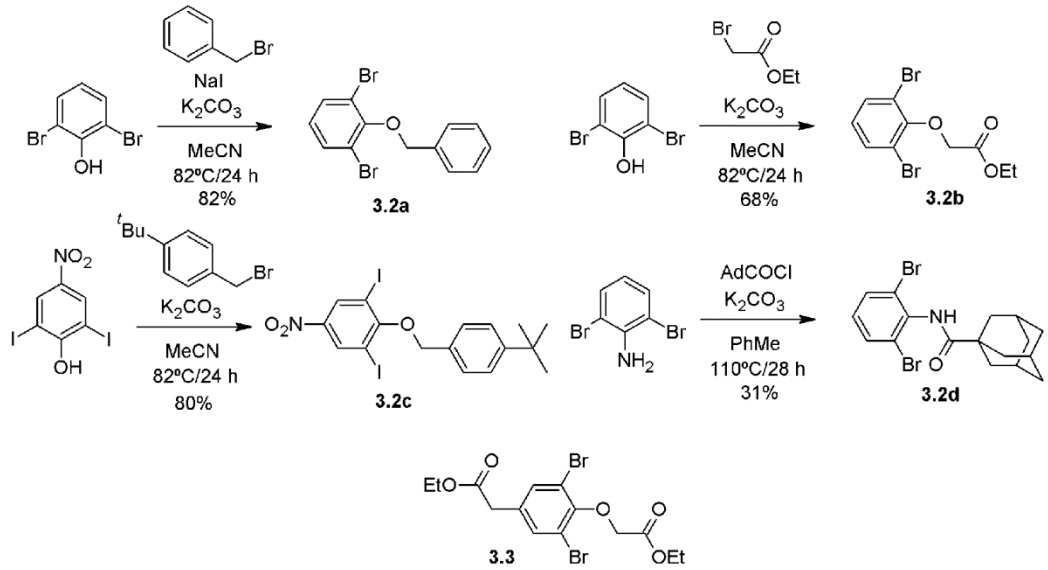

Figure 3.3: Synthesis of cores **3.2a**-**3.2d** and the side product **3.3**.

Dianilines **3.1d** and **3.1e** provided flexible but bulky internal groups. Dianiline **3.1e** contains a bulky tert-butyl group that could point outside of the cavity altogether. A bulky, less rigid ligand was also desirable. The bulky adamantanamide core **3.2d** was prepared by refluxing 2,6-dibromoaniline with 1-adamantanecarboxyl chloride in toluene. Although the Sonogashira coupling reaction for this proceeded in low yield, it could be performed on sufficiently high scale to provide enough dianiline **3.1f** to study.

3.3 Synthesis and Analysis of Complexes Derived From V-Shaped Iminopyridine Ligands

In addition to dianilines **3.1a**-**3.1f**, the commercially available 4,4'-methylenedianiline was also investigated as a spectral reference when analyzing the ^{1}H NMR spectra of the other complexes. In addition, iminopyridine **3.4** could be prepared, and allowed the comparison of *in situ* condensation and complexation with the more traditional two-step procedure (Figure 3.4).

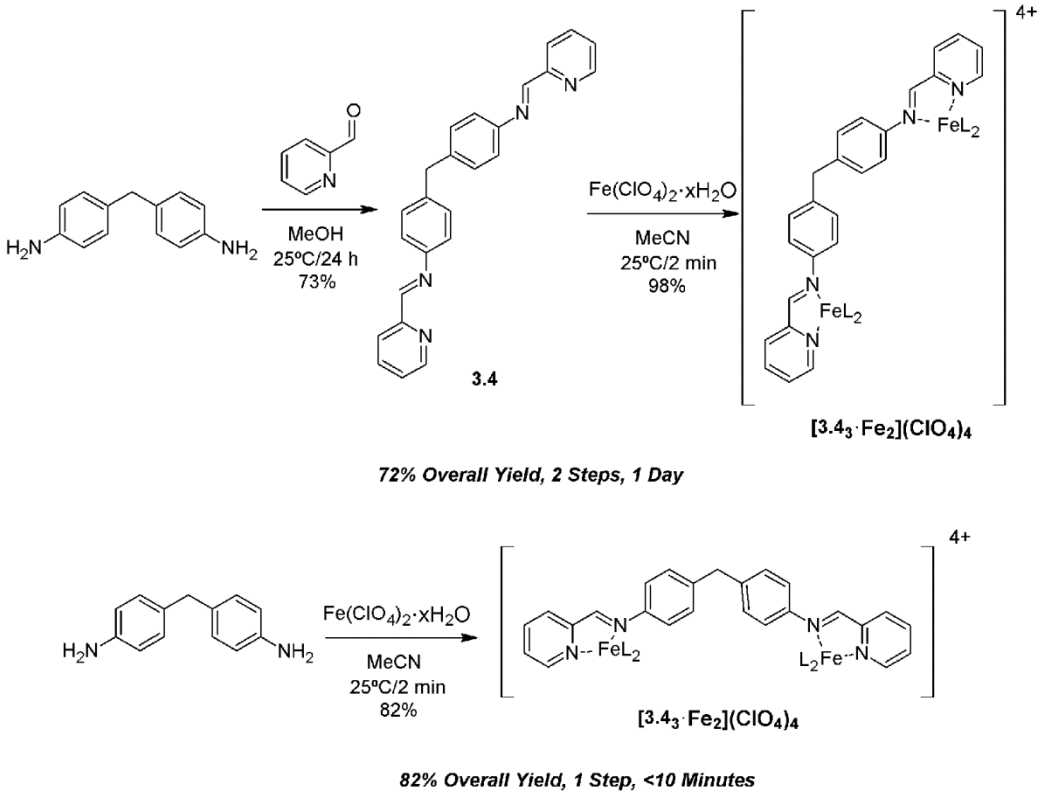

Figure 3.4: Synthesis of **3.4** and comparison of methods for preparing **[3.4$_3$•Fe$_2$](ClO$_4$)$_4$**.

Condensation of 4,4'-methylenedianiline with 2-formylpyridine in MeOH, followed by coordination of the ligand with $Fe(ClO_4)_2$•xH_2O and subsequent isolation of the complex proceeded in a 72% overall yield. The one pot procedure was then performed by *in situ*

condensation of the dianiline with 2-formylpyridine in the presence of the $Fe(ClO_4)_2 \bullet xH_2O$ salt. The rate of condensation was increased in the presence of the Lewis acidic iron(II).[5] The results showed that the one pot procedure was more efficient and gave a higher overall yield of complex.

3.1a was combined with 2-formylpyridine and $Fe(ClO_4)_2 \bullet xH_2O$ in acetonitrile to immediately give a deep purple colored solution of **$[3.5a_x \bullet Fe_y](ClO_4)_{2y}$** (Figure 3.5). The reaction was generally performed in an oxygen free atmosphere to prevent oxidation of the iron. Precipitation with diethyl ether gave the assembly as an air-stable purple solid.

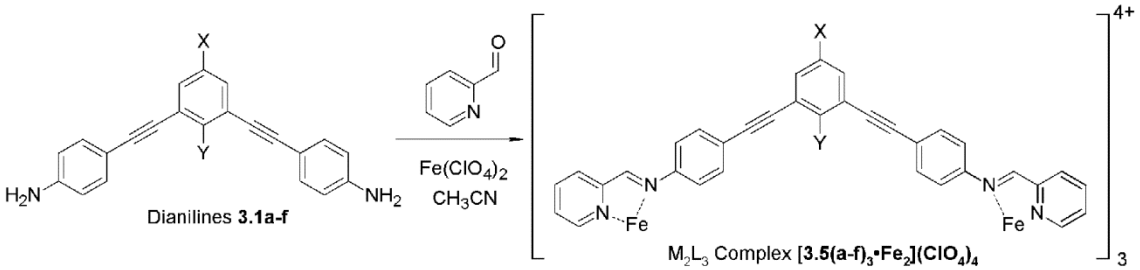

3.1a: X = H, Y = H; **3.1b:** X = H, Y = NH_2
3.1c: X = NO_2, Y = NH_2; **3.1d:** X = H, Y = OBn
3.1e: X = NO_2, Y = O-4-(tBu)Bn;
3.1f: X = H, Y = NHCOAd

3.5a: X = H, Y = H; **3.5b:** X = H, Y = NH_2
3.5c: X = NO_2, Y = NH_2; **3.5d:** X = H, Y = OBn
3.5e: X = NO_2, Y = O-4-(tBu)Bn;
3.5f: X = H, Y = NHCOAd

Figure 3.5: Synthesis of **$[3.5(a\text{-}f)_3 \bullet Fe_2](ClO_4)_4$** from the corresponding dianilines **3.1a**-**3.1f**.

Analysis of the self-assembly by ^{1}H NMR spectroscopy showed one major species corresponding to the matched helicate (Figure 3.6a), with a set of minor peaks that were expected to be from the mesocate. The peaks could be easily assigned by comparison with the ^{1}H NMR spectrum of **$[3.4_3 \bullet Fe_2](ClO_4)_4$** (Figure 3.6b). Analysis by diffusion ^{1}H NMR spectroscopy established that all of the peaks were from similarly sized species, consistent with a mixture of the matched ΔΔ/ΛΛ and mismatched ΔΛ species in solution

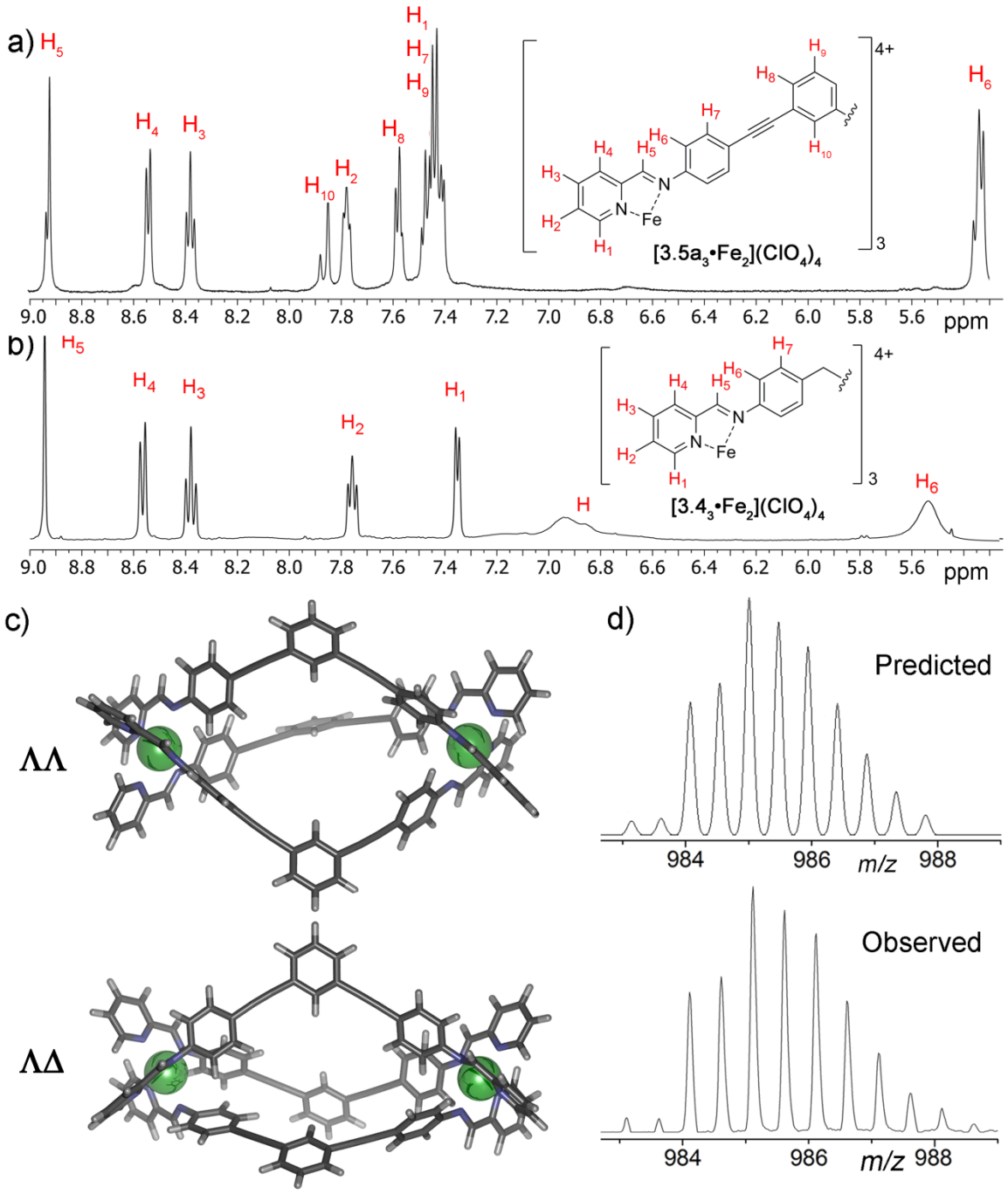

Figure 3.6: Analysis of **[3.5a$_3$•Fe$_2$](ClO$_4$)$_4$**: a) ^{1}H NMR spectrum of **[3.5a$_3$•Fe$_2$](ClO$_4$)$_4$** (CD_3CN, 500 MHz, 298 K) b) ^{1}H NMR spectrum of **[3.4$_3$•Fe$_2$](ClO$_4$)$_4$** for comparison (CD_3CN, 400 MHz, 298 K); c) SPARTAN models of ΛΛ and ΛΔ **[3.5a$_3$•Fe$_2$](ClO$_4$)$_4$** (AM1 forcefield); d) ESI-MS of M_2L_3.

(Figure 3.6c). ESI-MS confirmed the presence of only the desired M_2L_3 species **[3.5a$_3$•Fe$_2$](ClO$_4$)$_4$** (Figure 3.6d). Although no X-ray quality crystals could be grown of this species, the assignment of the matched helix as the major isomer consistent other observed Fe(II)-iminopyridine helices.[2]

Complexes prepared from the aniline **3.1b** and p-nitroaniline **3.1c** also formed M_2L_3 species **[3.5b$_3$•Fe$_2$]$^{4+}$** (Figure 3.7b) and **[3.5c$_3$•Fe$_2$]$^{4+}$** (Figure 3.7c). These contained a mixture of two separate species that ESI-MS and diffusion analysis showed were the matched helicate and the mismatched mesocate. While the internal aniline showed preference for the matched helicate (as did **[3.5a$_3$•Fe$_2$]$^{4+}$**), nitroaniline **[3.5c$_3$•Fe$_2$]$^{4+}$** showed a nearly identical mixture of the two diastereomers, although the reason is unclear.

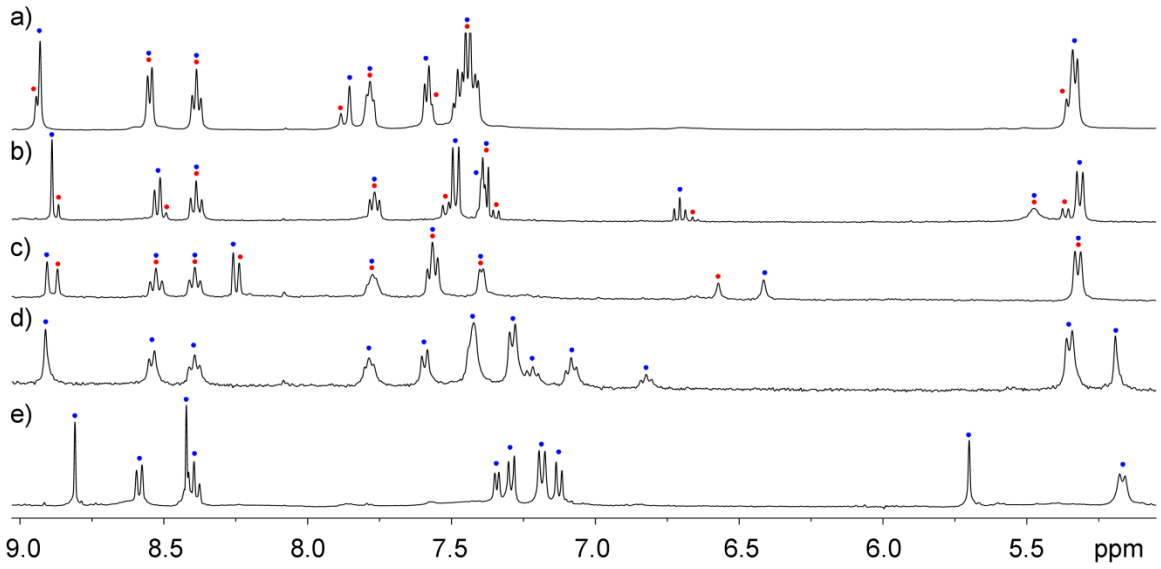

Figure 3.7: ^{1}H NMR spectra of **[3.5(a-e)$_3$•Fe$_2$](ClO$_4$)$_4$**, with helicate resonances labeled with a blue dot and mesocate resonances labeled with a red dot: a) **[3.5a$_3$•Fe$_2$](ClO$_4$)$_4$**; b) **[3.5b$_3$•Fe$_2$](ClO$_4$)$_4$**; c) **[3.5c$_3$•Fe$_2$](ClO$_4$)$_4$**; d) **[3.5d$_3$•Fe$_2$](ClO$_4$)$_4$**; e) **[3.5e$_3$•Fe$_2$](ClO$_4$)$_4$** (CD_3CN, 400 MHz, 298 K).

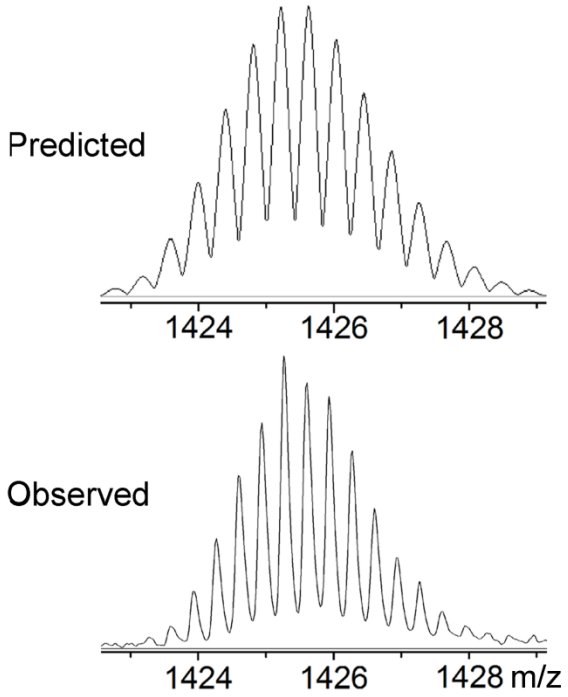

Figure 3.8: Predicted and observed ESI-MS spectra of **{[3.5d$_6$•Fe$_4$](ClO$_4$)$_5$}$^{3+}$**, showing evidence of rearrangement of **[3.5d$_3$•Fe$_2$]$^{4+}$** into **[3.5d$_6$•Fe$_4$]$^{8+}$** in the gas phase.

In comparison, the addition of a bulky benzyl group inside of **[3.5d$_3$•Fe$_2$]$^{4+}$** led to only one set of resonances by ^{1}H NMR spectroscopy (Figure 3.7d). This suggests that the benzyl group rigidified the complex. Guest binding has favored M_4L_6 tetrahedra in systems that prefer to assemble as M_2L_3 helices.[6] It is unclear what effect an endohedral benzyl group can have on the stoichiometry of the product assembly. The diffusion coefficient for **[3.5d$_3$•Fe$_2$]$^{4+}$** was similar to those observed for **[3.5(a-c)$_3$•Fe$_2$]$^{4+}$**, and it is likely that **[3.5d$_3$•Fe$_2$]$^{4+}$** is the correct identity of the assembly. ESI-MS analysis showed the presence of multiple fragments consistent with the M_2L_3 assembly in solution, along with a larger aggregate that corresponded to an M_4L_6 structure (Figure 3.8). Presumably, the increase in steric bulk on the interior of the cage led to the presence of larger

aggregates, as **[3.5(a-c)$_3$•Fe$_2$]$^{4+}$** showed no evidence of M_4L_6 structures in the gas phase.

SPARTAN models of **[3.5d$_3$•Fe$_2$]$^{4+}$** (Figure 3.9a) and **[3.5d$_6$•Fe$_4$]$^{8+}$** (Figure 3.9b) show that the benzyl groups fill the cavity of the M_2L_3 and confer the strain required for the observed diastereoselectivity. The M_2L_3 structure is too small to fit all three benzyl groups on the interior, but one or more flexible benzyl groups can easily move outside of the cavity. This does not cause enough strain to bias against the formation of the M_2L_3 helix in solution, although it does lead to the observed diastereoselectivity.

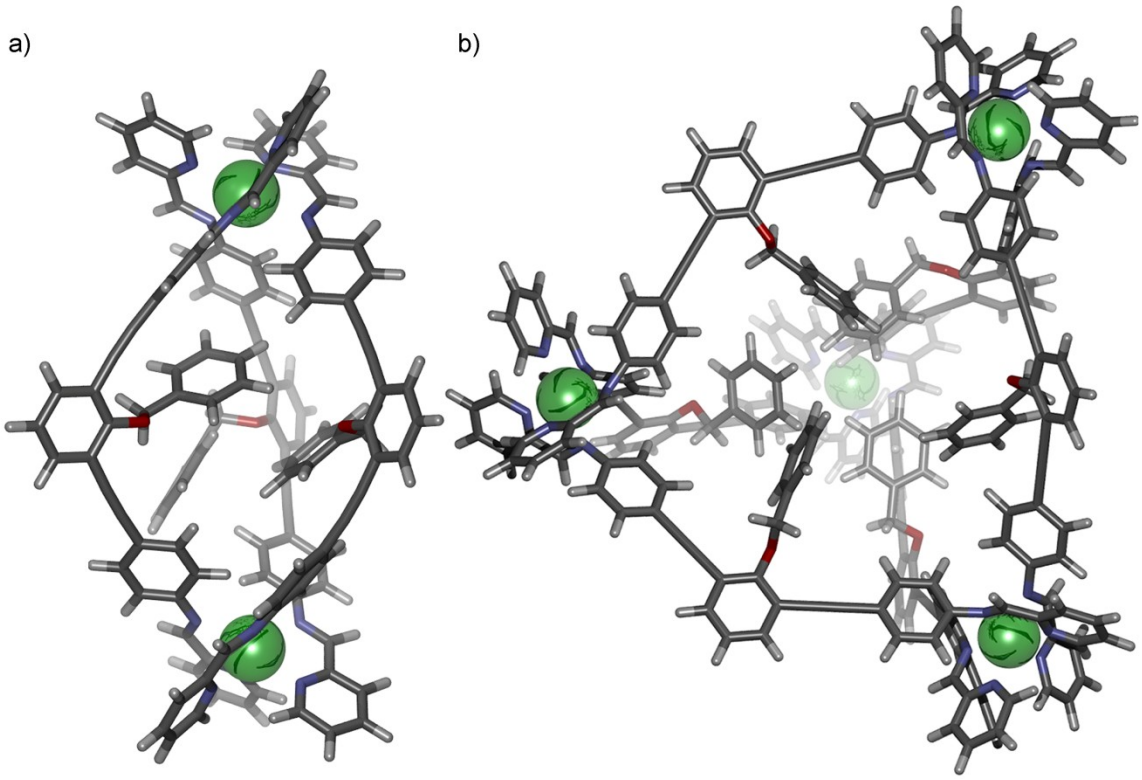

Figure 3.9: SPARTAN models of: a) **[3.5d$_3$•Fe$_2$]$^{4+}$**; b) **[3.5d$_6$•Fe$_4$]$^{8+}$** (AM1 forcefield).

The bulkier 4(tert-butyl)benzyl helix **[3.5e$_3$•Fe$_2$](ClO$_4$)$_4$** showed similar behavior to the benzyl-functionalized species (Figure 3.7e). The results were supported by SPARTAN modeling (Figure 3.10). Although **[3.5e$_3$•Fe$_2$](ClO$_4$)$_4$** contains tert-butyl groups, they are placed away from the cavity of the helix, and have little added steric contribution over that already contributed by the benzyl group.. As with the benzyl analogue, assembly of **[3.5e$_3$•Fe$_2$](ClO$_4$)$_4$** gives both an M_2L_3 as well as an M_4L_6 assembly in the gas phase.

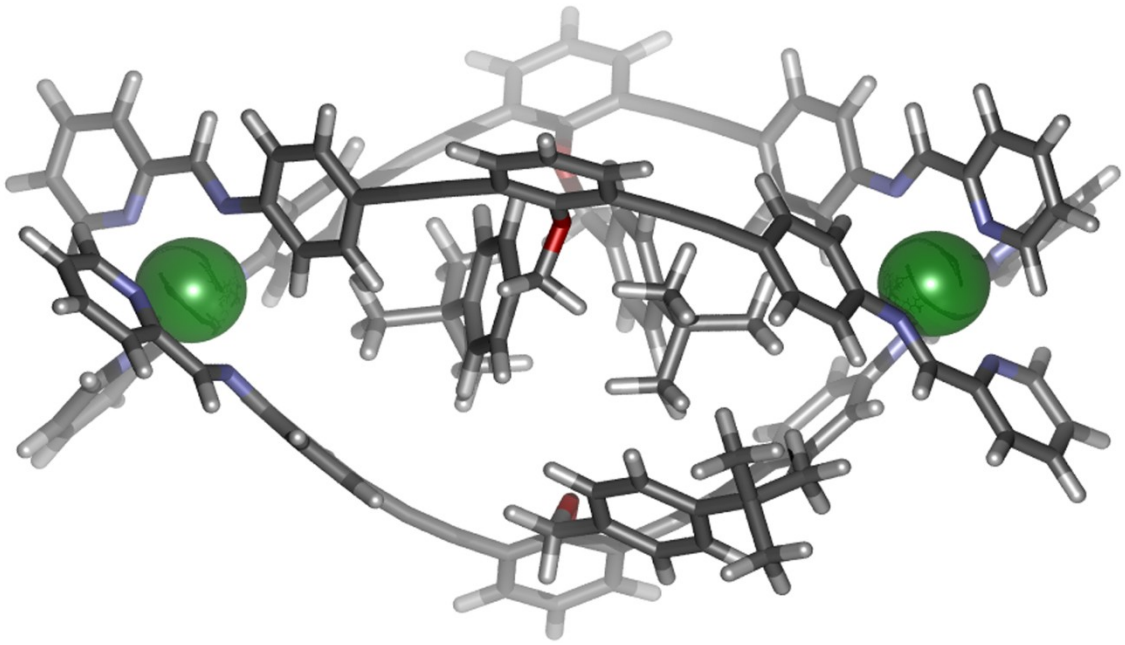

Figure 3.10: SPARTAN model of **[3.5e$_3$•Fe$_2$]$^{4+}$** (AM1 forcefield).

The two benzyl-functionalized species were capable of rigidifying the resulting complexes giving complete diastereoselectivity, showing that this is a valid strategy to control diastereoselectivity in self-assembled cages. The results of ESI-MS analysis of these two complexes suggested that it might be possible to prepare a functionalized cage that would be incapable of forming an M_2L_3 because of the bulk of the functionality,

but which could lead to a larger M_4L_6 aggregate. A more rigid group that could not rotate outside of the cavity was required to test this: the adamantane-functionalized **3.1f**. When **3.1f** was combined in acetonitrile with 2-formylpyridine and $Fe(ClO_4)_4 \bullet xH_2O$, a purple complex was observed. Precipitation by addition of Et_2O led to a purple solid as expected, but this solid was intractable. Only after extensive sonication could a small portion be redissolved. The complexation was reattempted directly in an NMR tube in CD_3CN, followed by sonication. The ^1H NMR spectrum suggested that a single discrete structure was not obtained (Figure 3.11).

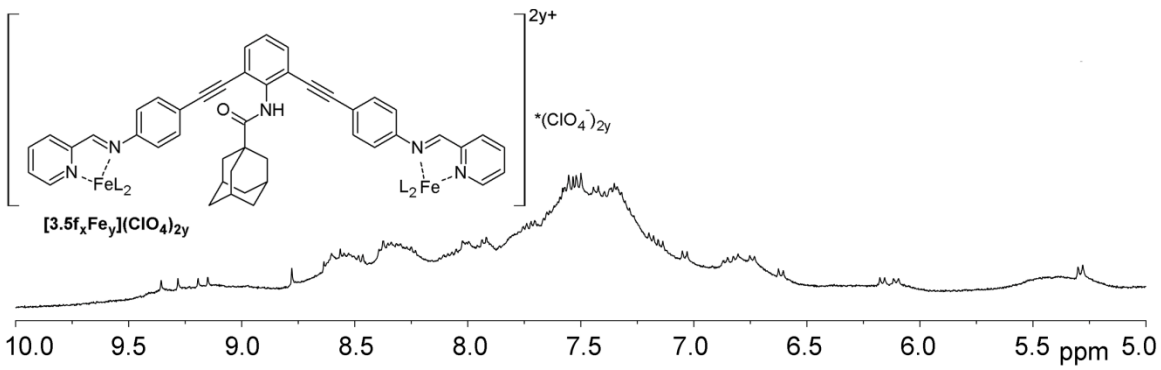

Figure 3.11: ^1H NMR spectrum of **$[3.5f_x \bullet Fe_y](ClO_4)_{2y}$** ($CD_3CN$, 400 MHz, 298 K).

Multi-component self-assembly of **3.1f** with 2-formylpyridine and Fe(II) results in the formation of an oligomeric aggregate, suggesting that the adamantyl species is too large to fit inside of the cavity of the M_2L_3 structure. This conclusion is supported by molecular modeling (Figure 3.12a). Formation of the larger M_4L_6 structure also fails to provide enough space to accommodate all of the adamantyl groups (Figure 3.12b) without distortion of the ligand. Upon precipitation, these oligomers likely give rise to even more complex coordination polymers, leading to their insolubility after precipitation.

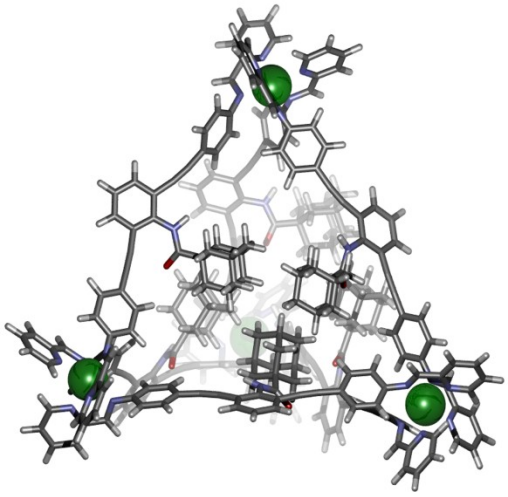

Figure 3.12: SPARTAN model of unobserved **[3.5f$_6$•Fe$_4$]$^{8+}$** (AM1 forcefield).

3.4 Mixed Ligand Assembly of V-Shaped Iron(II)-Iminopyridine Helices

Although the adamantyl species was too large to be accommodated in a single cage, it could conceivably be accommodated in a mixed ligand cage. When a mixture of **[3.5f$_x$•Fe$_y$](ClO$_4$)$_{2y}$** and **[3.5a$_3$•Fe$_2$](ClO$_4$)$_4$** were combined in an NMR tube, however, no change occurred upon heating. The soluble cage remained in solution while the coordination polymer remained at the bottom of the tube with no sign of ligand exchange or the formation of any mixed species. Combination of dianiline **3.1a** with the coordination polymer **[3.5f$_x$•Fe$_y$](ClO$_4$)$_{2y}$** followed by heating did show evidence of mixed species forming (Figure 3.13), however.

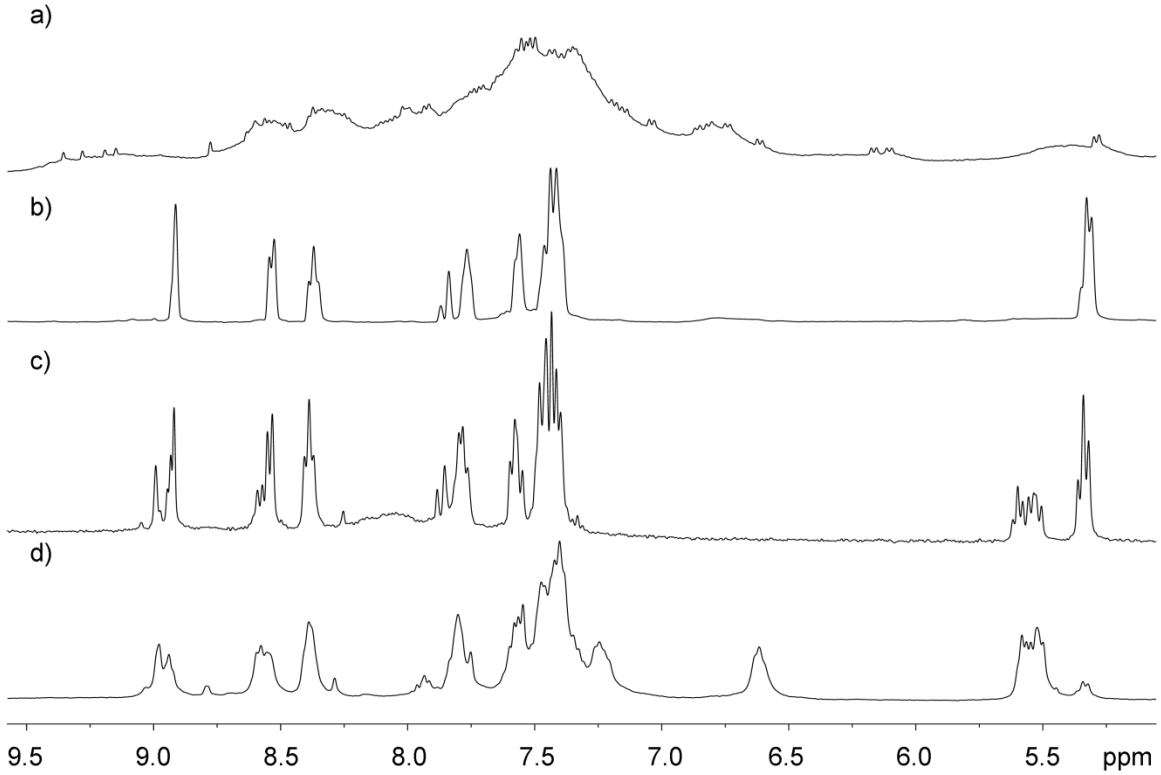

Figure 3.13: ^{1}H NMR spectra of mixed v-shaped iminopyridine helices: a) **[3.5f$_x$•Fe$_y$](ClO$_4$)$_{2y}$**; b) **[3.5a$_3$•Fe$_2$](ClO$_4$)$_4$**; c) **[3.5f$_x$•Fe$_y$](ClO$_4$)$_{2y}$** + 2 eq **3.1a**; d) **[3.5f$_x$•Fe$_y$](ClO$_4$)$_{2y}$** + 2 eq **3.1a** + 4 eq 2-pyridine carboxaldehyde + 1.33 eq Fe(ClO$_4$)$_4$•xH$_2$O (CD$_3$CN, 400 MHz, 298 K).

When **[3.5f$_x$•Fe$_y$](ClO$_4$)$_{2y}$** was combined with enough **3.1a**, 2-formylpyridine, and Fe(ClO$_4$)$_4$•xH$_2$O to allow formation of a 2:1 mixed species containing one equivalent of **3.5f**, a different ^{1}H NMR spectrum was obtained. While there is evidence of a small portion of unmixed **[3.5a$_3$•Fe$_2$](ClO$_4$)$_4$**, the majority of the peaks correspond to a new mixed species (Figure 3.13d). Although there was not enough resolution between the different resonances to assign whether individual peaks corresponded to **[3.5a$_2$•3.5f•Fe$_2$](ClO$_4$)$_4$** or **[3.5a•3.5f$_2$•Fe$_2$](ClO$_4$)$_4$**, it seems unlikely that only one of these two species is present in solution from integration. Comparison with the ^{1}H NMR spectra in Figure 3.13 suggests that **3.1a** preferentially displaces **3.5f** to give **3.1f** and

[3.5a$_2$•3.5f•Fe$_2$](ClO$_4$)$_4$. The formation of mixed helices only occurs with enough aldehyde and iron(II) to preserve the less favorable **3.5f**.

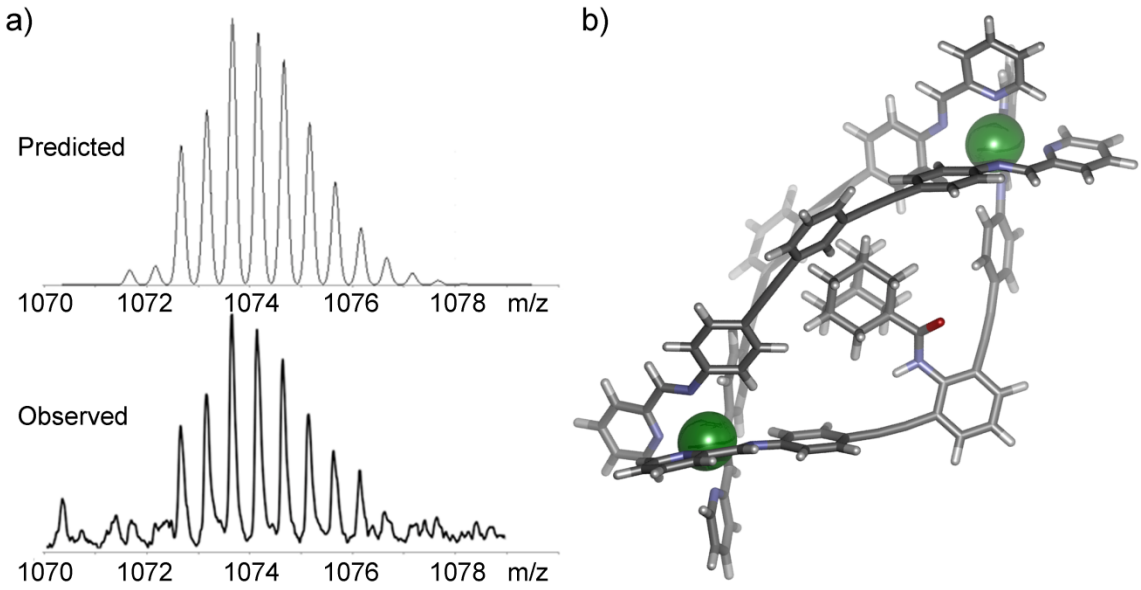

Figure 3.14: Justification for formation of mixed **[3.5a$_2$•3.5f•Fe$_2$](ClO$_4$)$_4$**: a) Predicted and observed ESI-MS of **{[3.5a$_2$•3.5f•Fe$_2$](ClO$_4$)$_4$+2H}$^{2+}$**; b) SPARTAN model of **[3.5a$_2$•3.5f•Fe$_2$]$^{4+}$** (AM1 forcefield).

ESI-MS was used to probe if monoadamantyl and diadamantyl mixed species were both present in solution. No sign of any species larger than ML_2 had been observed for the oligomer **[3.5f$_x$•Fe$_y$](ClO$_4$)$_{2y}$**, but a mixed species should be amenable to ESI-MS anaylsis. The mixed species **[3.5a$_2$•3.5f•Fe$_2$](ClO$_4$)$_4$** was the only polynuclear iron complex that could be identified in the mass spectrum (Figure 3.14a). The diadamantyl mixed helix **[3.5a•3.5f$_2$•Fe$_2$]$^{4+}$** may form in solution and be too unstable for ESI-MS analysis, but molecular modeling of **[3.5a$_2$•3.5f•Fe$_2$]$^{4+}$** suggests that there is only room in the cage for one of the bulky adamantyl groups (Figure 3.14b).

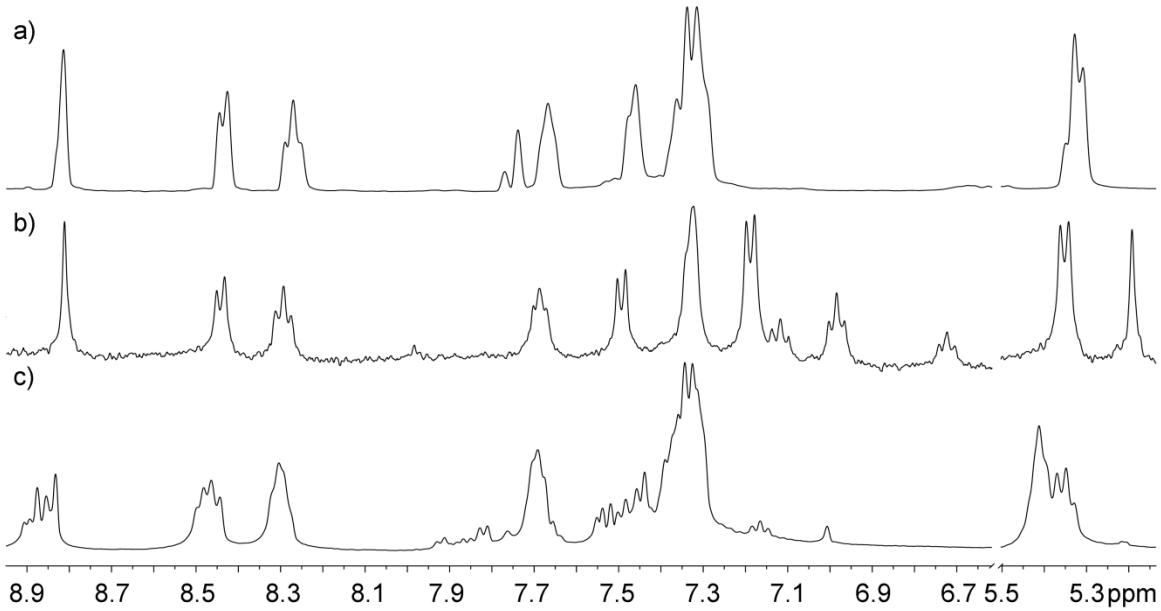

Figure 3.15: ^{1}H NMR spectra showing formation of mixed **[3.5a$_x$•3.5d$_y$•Fe$_2$](ClO$_4$)$_4$** assemblies: a) **[3.5a$_3$•Fe$_2$](ClO$_4$)$_4$**; b) **[3.5d$_3$•Fe$_2$](ClO$_4$)$_4$**; c) **[3.5a$_x$•3.5d$_y$•Fe$_2$](ClO$_4$)$_4$** (CD_3CN, 400 MHz, 298 K).

Only a single mixed species could be observed by ESI-MS of the CH-adamantanamide mixture **[3.5a•3.5f$_2$•Fe$_2$](ClO$_4$)$_4$**. To test the solution-phase behavior, a 1:1 mixture of both the CH complex **[3.5a$_3$•Fe$_2$](ClO$_4$)$_4$** (Figure 3.15a) and benzyl complex **[3.5d$_3$•Fe$_2$](ClO$_4$)$_4$** (Figure 3.15b) were combined in acetonitrile. There was some sign of mixing after 9 days at ambient temperature. After twenty one days there was complete conversion to a new species by ^{1}H NMR (Figure 3.15c).

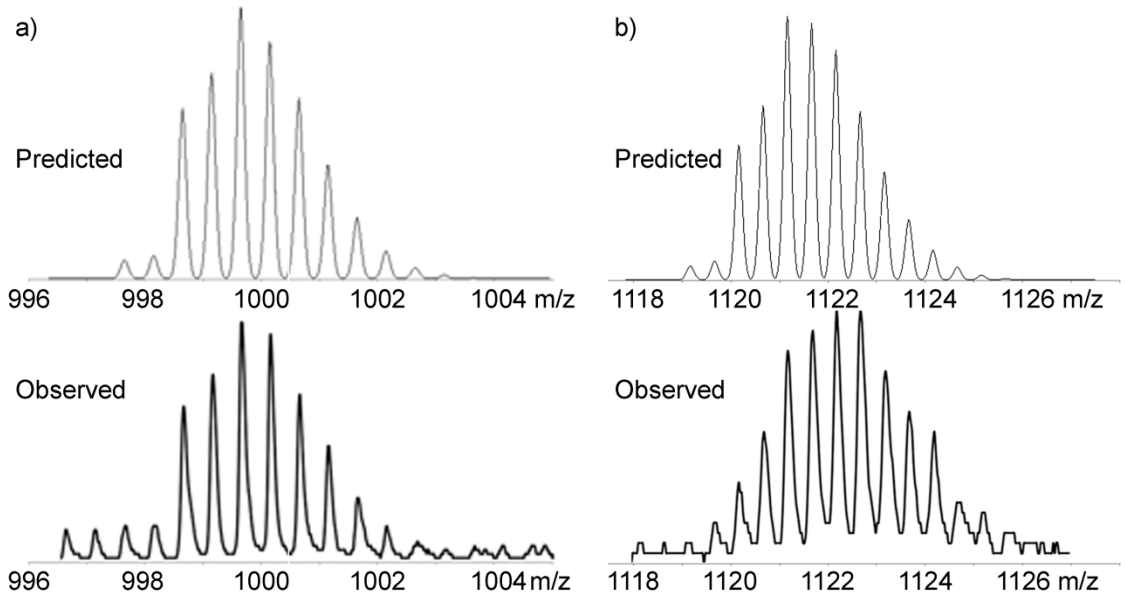

Figure 3.16: ESI-MS of **[3.5a$_x$•3.5d$_y$•Fe$_2$](ClO$_4$)$_4$** assemblies: a) **{[3.5a$_2$•3.5d•Fe$_2$](ClO$_4$)$_3$+Na}$^{2+}$**; b) **{[3.5a•3.5d$_2$•Fe$_2$](ClO$_4$)$_3$+H+2Na+2OAc}$^{2+}$** (MeCN).

Comparison of the ^{1}H NMR spectra (Figure 3.15) showed no sign of either homocomplex. Each complex was added in a 1:1 ratio, suggesting that both **[3.5a•3.5d$_2$•Fe$_2$](ClO$_4$)$_4$** and **[3.5a$_2$•3.5d•Fe$_2$](ClO$_4$)$_4$** were present in solution. This was confirmed by ESI-MS, whereby ions corresponding to both mixed species could be observed (Figure 3.16). The stable **[3.5a$_3$•Fe$_2$](ClO$_4$)$_4$** and **[3.5d$_3$•Fe$_2$](ClO$_4$)$_4$** helices show complete selectivity for the mixed helices **[3.5a•3.5d$_2$•Fe$_2$](ClO$_4$)$_4$** and **[3.5a$_2$•3.5d•Fe$_2$](ClO$_4$)$_4$** in solution. This shows just how subtle differences caused by even unreactive endohedral functional groups can alter the self-assembly of metal-organic structures.

3.5 Conclusions

Preparation of bent or “V-shaped” Fe(II)-iminopyridine complexes is subject to the same rules for diastereoselectivity as their linear analogues such as **2.10**. As the ligands become longer, the complexes lose the necessary rigidity for complete diastereoselectivity. The addition of bulky endohedral functional groups can be used to reverse this trend. These bulky groups pointed inside the cavity increase the strain of forming mismatched mesocates, allowing these complexes to form diastereoselectively as matched helicates. The subtle differences in energy even allow selectivity in the formation of heteroclusters, as mixed cages form to mitigate the strain of endohedral functionalization with bulky groups.

3.6 References

1) Hotze, A. C. G.; Hodges, N. J.; Hayden, R. E.; Sanchez-Can, C.; Paines, C.; Male, N.; Tse, M.-K.; Bunce, C. M.; Chipman, J. K.; Hannon, M. J. "Supramolecular Iron Cylinder with Unprecedented DNA Binding Is a Potent Cytostatic and Apoptotic Agent Without Exhibiting Genotoxicity." *Chem. Biol.*, **2008**, *15*, 1258-1267.

2) Bilbeisi, R. A.; Clegg, J. K.; Elgrishi, N.; de Hatten, X.; Devillard, M.; Breiner, B.; Mal, P.; Nitschke, J. R. "Subcomponent Self-Assembly and Guest-Binding Properties of Face-Capped $Fe_4L_4^{8+}$ Capsules." *J. Am. Chem. Soc.*, **2012**, *134*, 5110-5119.

3) Ide, T.; Takeuchi, D.; Osakada, K. "Columnar Self-Assembly of Rhomboid Macrocyclic Molecules *via* Step-Like Intermolecular Interaction. Crystal Formation and Gelation." *Chem. Commun.*, **2012**, *48*, 278-280.

4) Young, M. C.; Johnson, A. M.; Gamboa, A. S.; Hooley, R. J. "Achiral Endohedral Functionality Provides Stereochemical Control in Fe(II)-Based Self-Assemblies." *Chem. Comun.*, **2013**, *49*, 1627-1629.

5) Dragna, J. M.; Pescitelli, G.; Tran, L.; Lynch, V. M.; Anslyn, E. V.; Di Bari, L. "In Situ Assembly of Octahedral Fe(II) Complexes for the Enantiomeric Excess Determination of Chiral Amines Using Circular Dichroism Spectroscopy." *J. Am. Chem. Soc.*, **2012**, *134*, 4395-4397.

6) Scherer, M.; Caulder, D. L.; Johnson, D. W.; Raymond, K. N. "Triple Helicate—Tetrahedral Cluster Interconversion Controlled by Host-Guest Interactions." *Angew. Chem. Int. Ed. Engl.*, **1999**, *38*, 1587-1592.

Chapter 4 – Self-Assembly and Functionalization of Fe(II)-Iminopyridine Complexes with Hydrogen Bonding Groups

4.1 Rationale

The introduction of *reactive* functionality to a self-assembled system is extremely challenging. Strongly nucleophilic or electrophilic groups on the coordinating ligand can interfere with the metal-ligand interactions required for self-assembly. Most solution-phase self-assembled cages are formed reversibly and are sensitive to harsh reactive conditions. Subtle differences in energy can alter the selectivity of the assembly. Postsynthetic modification of the more robust solid state metal organic frameworks is a popular area of research,[1] allowing modification of the physical properties of the frameworks[2] and the inclusion of more reactive functional groups that are incompatible with the assembly process.[3] Only a few examples of postsynthetic modification of discrete, solution-phase self-assemblies, are known and are almost exclusively limited to bioorthogonal reactions on the exterior of the self-assemblies.[4] Biomimetic cages require functionalization with reactive groups on the interior of these cages, and the ability to undergo further reactivity is required to make truly biomimetic supramolecular catalysts. Although alcohols are not strongly nucleophilic, they are also not competitive with the self-assembly of Fe(II)-iminopyridine cages, and their reactions will be the focus of this chapter.

4.2 Synthesis and Multicomponent Self-Assembly of Dibenzosuberone-Based Ligands

Dibenzosuberone provides some advantages in preparing reactive self-assembled cages: amines can be introduced at the required positions using a two-step reductive

amination procedure to allow for functionalization to the desired iminopyridine ligand, while the internal ketone provides a handle for preparing a variety of other reactive internal functional groups, such as the desired alcohol. Dibenzosuberone can be nitrated using 90% HNO_3 to give the 3,7-dinitrodibenzosuberone **4.1a** (Figure 4.1).[5] Despite previous literature precedent, increasing the reaction time led to no improvement in the yield or nitration to tri- or tetranitrodibenzosuberones. The only side product observed by increasing the reaction time was the oxidized trione **4.1b**, which was isolated as an insoluble white powder.

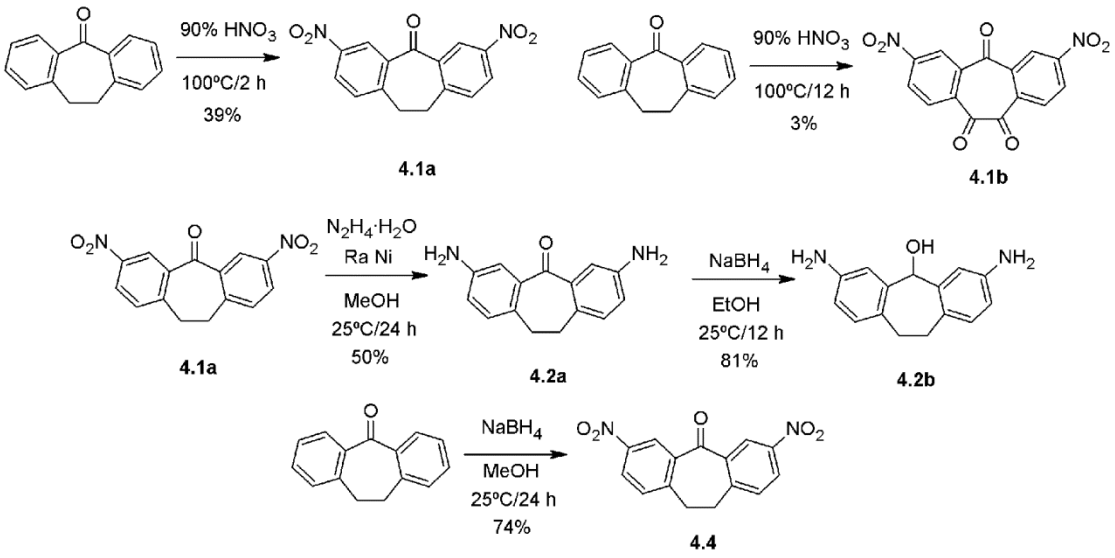

Figure 4.1: Synthesis of dibenzosuberone-based dianilines **4.2a** and **4.2b**.

The dinitro compound **4.1a** could be easily reduced to the dianiline **4.2a** by reduction using transfer hydrogenation of hydrazine monohydrate in methanol with Raney nickel as a catalyst. Ketone **4.2a** could then be reduced in ethanol using sodium borohydride to give the dibenzosuberol **4.2b**. Attempts to prepare Grignard-functionalized derivatives of **4.1a**[6] failed to give conversion to the desired alcohol

products, as the benzylic position is deprotonated, deactivating the ketone for nucleophilic addition.

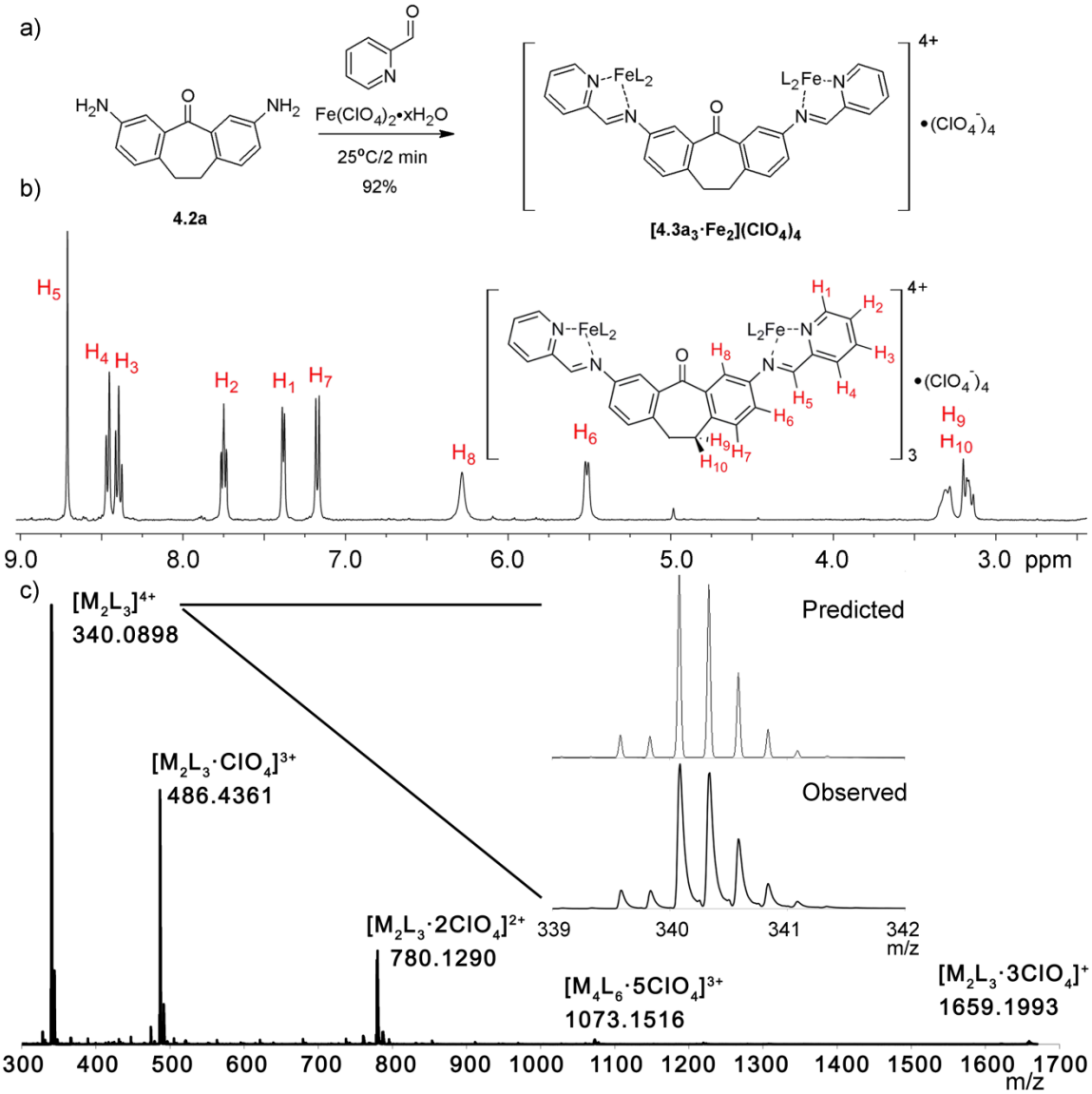

Figure 4.2: Synthesis and characterization of dibenzosuberone helix **[4.3a$_3$•Fe$_2$](ClO$_4$)$_4$**: a) Synthesis of **[4.3a$_3$•Fe$_2$](ClO$_4$)$_4$**; b) ^{1}H NMR of **[4.3a$_3$•Fe$_2$](ClO$_4$)$_4$** (CD_3CN, 400 MHz, 298 K); c) ESI-MS of **[4.3a$_3$•Fe$_2$](ClO$_4$)$_4$** (MeCN).

Multicomponent self-assembly of **4.2a** with 2-formyl pyridine and $Fe(ClO_4)_2$•xH_2O proceeded well at room temperature to give a purple complex of the ligand **4.3a**.[7]

Precipitation with diethyl ether afforded the complex as a purple solid in excellent yield and subsequent analysis by ^{1}H NMR spectroscopy (Figure 4.2b) showed that a single species was obtained. The added strain of the ethylene bridge allows the complex to display complete diastereoselectivity. The resonances corresponding to the iminopyridine ring are all downfield, with H_1 being the least shifted due to shielding from the adjacent pyridine rings in the self-assembly. The peaks corresponding to protons on the dibenzosuberone show that H_6 and H_8 both experience some shielding, although the external proton H_6 experiences more shielding. The ethylene peaks are desymmetrized in the assembly, suggesting the protons are diastereotopic and the seven-membered ring does not freely interconvert at room temperature. ESI-MS analysis confirmed the identity of the complex was the expected M_2L_3 helix (Figure 4.2c). There were minor peaks corresponding to the M_4L_6 in the ESI-MS analysis of **[4.3a$_3$•Fe$_2$](ClO$_4$)$_4$**, although the diffusion ^{1}H NMR supported formation of only the M_2L_3 species in solution.

Unlike the larger helices **[3.5(a-e)$_3$•Fe$_2$](ClO$_4$)$_4$**, **[4.3a$_3$•Fe$_2$](ClO$_4$)$_4$** afforded X-ray diffraction quality crystals by diffusion of benzene into a solution of acetonitrile. Analysis of this structure (Figure 4.3) shows that the complex does not exist as the diastereomerically pure ΔΔ/ΛΛ complex expected, but rather as the ΔΛ mesocate. There have been few reports of complexes that prefer a *meso* arrangement.[8] The ketone in **[4.3a$_3$•Fe$_2$](ClO$_4$)$_4$** is essentially planar, with the ethylene bridge bowing out of the plane to relieve strain. The X-ray structure also allows the chemical shifts of some proton resonances to be explained: proton H_6 experiences shielding due to its orientation towards a pyridine at the end of the ligand, while H_8 is much further away from other arene faces in the complex.

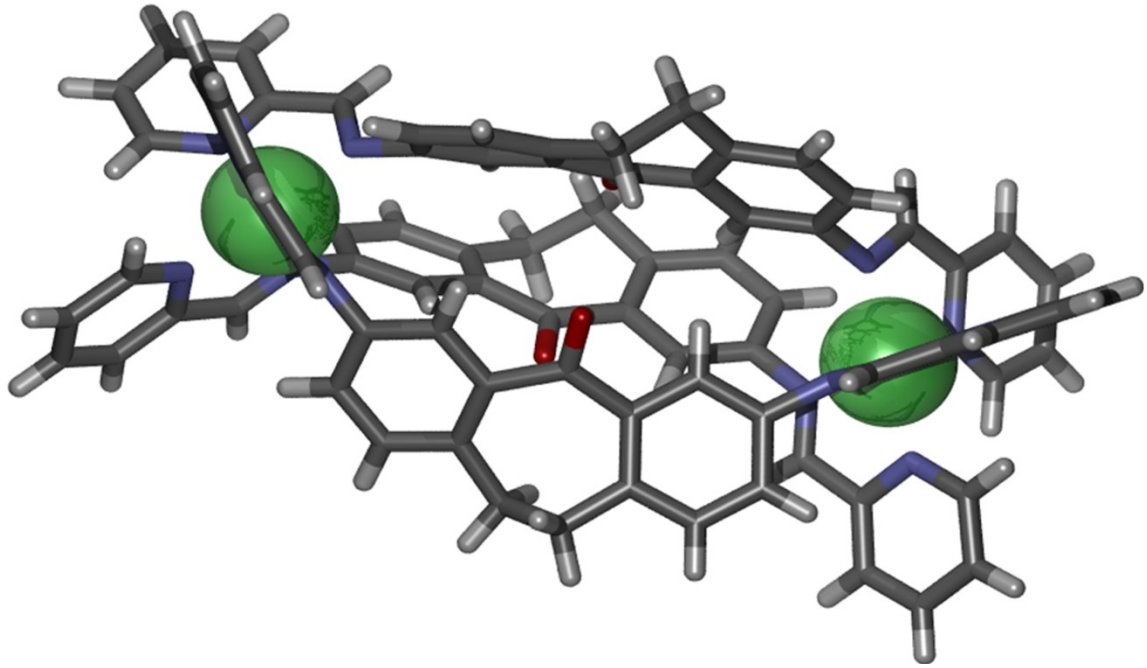

Figure 4.3: X-ray crystal structure of ketone **[4.3a$_3$•Fe$_2$](ClO$_4$)$_4$**.

A discrete complex was not observed when a similar synthesis was attempted using dianiline **4.2b**. A discrete species was only formed after application of heat. The dibenzosuberone scaffold is fairly rigid, but the sp^3 analogue is less so. The dibenzosuberol helix required heat to allow equilibration between kinetically-formed oligomers and the more thermodynamically-stable M_2L_3 (Figure 4.4a). Analysis of the observed complex by ESI-MS confirms that it too exists as an M_2L_3 helix. ^{1}H NMR analysis of **[4.3b$_3$•Fe$_2$](ClO$_4$)$_4$** (Figure 4.4b) shows that there is one major species present in solution, as well as other minor isomers. Diffusion NMR shows similar diffusion for the major and minor isomers of **[4.3b$_3$•Fe$_2$](ClO$_4$)$_4$**.

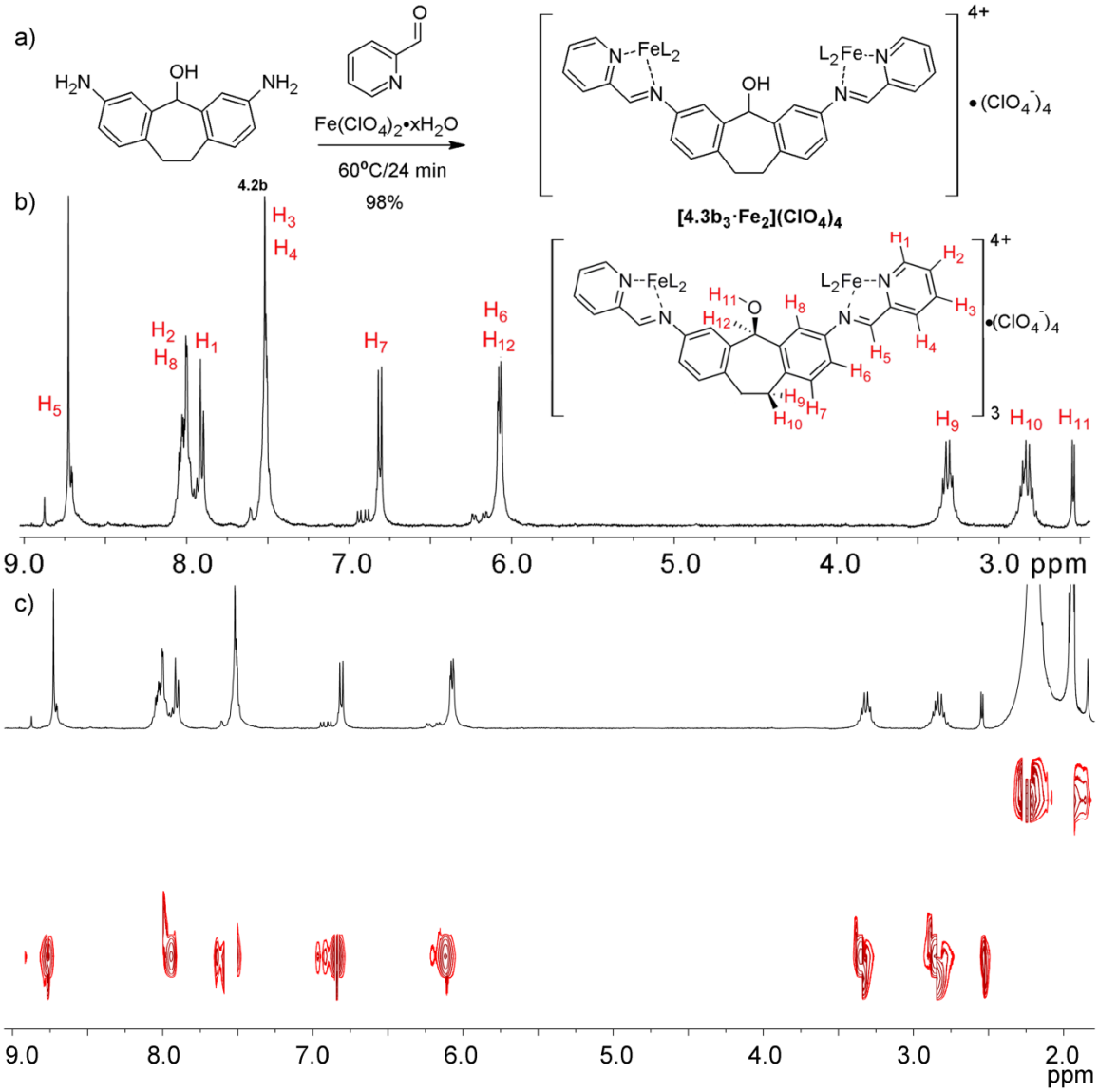

Figure 4.4: Synthesis and characterization of dibenzosuberol helix **[4.3b$_3$•Fe$_2$](ClO$_4$)$_4$**: a) Synthesis of **[4.3b$_3$•Fe$_2$](ClO$_4$)$_4$**; b) ^{1}H NMR of **[4.3b$_3$•Fe$_2$](ClO$_4$)$_4$** (CD_3CN, 400 MHz, 298 K); c) DOSY spectrum of **[4.3b$_3$•Fe$_2$](ClO$_4$)$_4$** (CD_3CN, 600 MHz, 298 K, Δ = 100 ms, δ = 2.6 μs, Diffusion Coefficient = 6.27 x 10^{-10} m^2/s vs. 3.95 x10^{-9} m^2/s for the solvent).

The extra resonances could represent decreased diastereoselectivity, as was seen with **2.10** and **[3.5(a-e)$_3$•Fe$_2$](ClO$_4$)$_4$**. Complex **[4.3b$_3$•Fe$_2$](ClO$_4$)$_4$** is much more flexible than ketone **[4.3a$_3$•Fe$_2$](ClO$_4$)$_4$**, and could have a small portion of the ΔΔ/ΛΛ isomer present. In the ^{1}H NMR spectra of **[3.5(a-c)$_3$•Fe$_2$](ClO$_4$)$_4$**, both ΔΔ/ΛΛ and ΔΛ isomers

each gave a single resonance due to symmetry. The spectrum for **[4.3b$_3$•Fe$_2$](ClO$_4$)$_4$** shows at least two peaks for the minor isomers, however, and this is inconsistent with them being the matched helicate. There is also potential for isomerism at the sp^3 center.

Vapor diffusion of diethyl ether into an acetonitrile solution of **[4.3b$_3$•Fe$_2$](ClO$_4$)$_4$** containing 1% mesitylene led to isolation of X-ray quality crystals (Figure 4.5a). Like its ketone analogue, **[4.3b$_3$•Fe$_2$](ClO$_4$)$_4$** forms a mesocate. Comparing the ^{1}H NMR spectrum with the solid state structure clarifies some of the analysis: H_8 is inside of the complex, but pointing away from the adjacent ligands, and subsequently shows up around 8 ppm in the ^{1}H NMR spectrum. H_6 is also not pointing directly at the adjacent pyridine rings, causing it to shift 0.5 ppm compared to **[4.3a$_3$•Fe$_2$](ClO$_4$)$_4$**. The crystal structure of the dibenzosuberol helix reveals that the ethylene bridge and the oxygen share a trans relationship on each ligand. All three of the alcohols point towards the inside of the cavity.

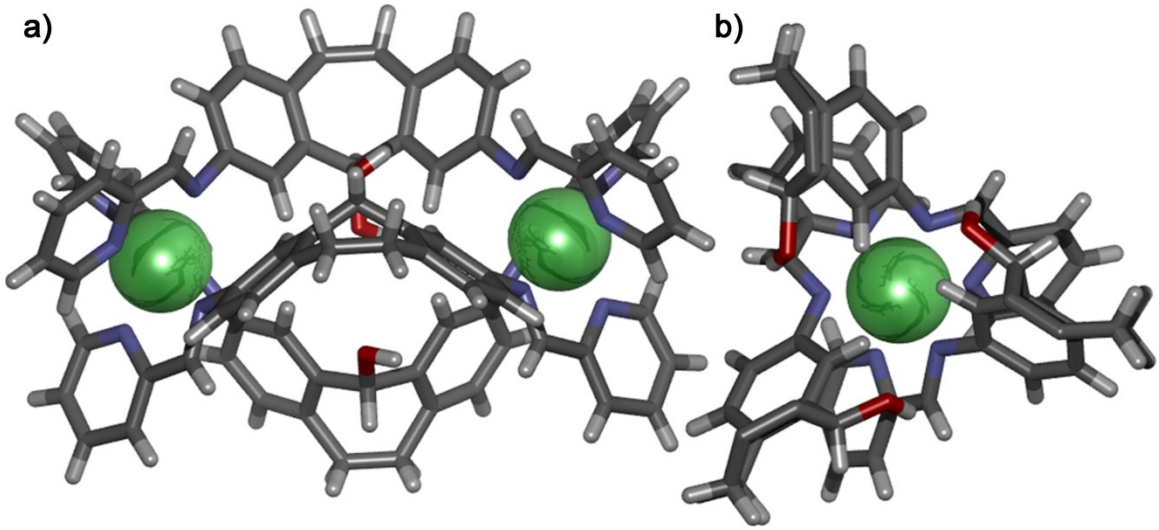

Figure 4.5: X-ray crystal structure of **[4.3b$_3$•Fe$_2$](ClO$_4$)$_4$**; a) Front view; b) Down Fe-Fe axis.

4.3 Postsynthetic Modification of Suberone-Based Helices

The preferential orientation of the ketone and alcohol groups inside the cavities of both mesocates suggested that **[4.3a$_3$•Fe$_2$](ClO$_4$)$_4$** and **[4.3b$_3$•Fe$_2$](ClO$_4$)$_4$** would be good candidates for studying further derivatization on the self-assembled species. Targeting postsynthetic modification of both would be challenging, as the reaction would have to target the internal function and not interrupt the iron chelation. The synthesis of **[4.3b$_3$•Fe$_2$](ClO$_4$)$_4$** by treating the ketone **[4.3a$_3$•Fe$_2$](ClO$_4$)$_4$** with a stoichiometric amount of sodium borohydride was attempted, but led to immediate decomposition of the helix.

An alternate scheme involved treating the ketone helix with an amine nucleophile to form an internal imine species. Unfortunately, unsymmetrical dimethyl ethylenediamine replaced the diamine **4.2a** in the complex, leading to mononuclear iron(II)-iminopyridine complexes based on the aliphatic ligand. The challenge of treating the ketone helix with nucleophiles is their higher affinity for the imine and iron than for the ketone. An alternate strategy is to use the alcohol in the alcohol helix **[4.3b$_3$•Fe$_2$](ClO$_4$)$_4$** as a nucleophile; the Fe(II)-iminopyridine motif should be inert in the presence of electrophilic reactants.

When acetyl chloride was added to a solution of **[4.3b$_3$•Fe$_2$](ClO$_4$)$_4$** almost immediate decomposition was observed. In acetonitrile, the halide leaving group outcompetes the iminopyridine ligand for coordination to the iron. The reaction was re-attempted in the presence of silver tetrafluoroborate. This strategy forces the halide to readily precipitate as insoluble AgCl, preventing the Fe(II)-iminopyridine complex from being disrupted. This too was met with very limited success, and clean conversion could not be achieved. Slow addition of the acid chloride also failed to give clean conversion to the functionalized helix.

The challenge of using a halide-containing electrophile could be circumvented using an electrophile such as trimethylsilyl triflate. The triflate ion is a poor ligand for Fe(II) and should not outcompete the iminopyridine coordinators. The reaction between **[4.3b$_3$•Fe$_2$](ClO$_4$)$_4$** and TMS-OTf was followed by ^{1}H NMR spectroscopy and showed conversion to a defined product. Stoichiometric quantities of trifluoromethanesulfonic acid were produced, however, leading to rapid decomposition of the **[4.3b$_3$•Fe$_2$](ClO$_4$)$_4$** helix. The addition of a base such as potassium carbonate led to decomposition of the helix similar to the addition of chloride ion. Small amounts of tertiary amines were tolerated, but the formation of the tertiary ammonium in the presence of the stoichiometric trifluoromethanesulfonic acid generated also led to decomposition.

A successful solution was to functionalize **[4.3b$_3$•Fe$_2$](ClO$_4$)$_4$** with an electrophile that produces no leaving group and could retain the acidic proton of the alcohol. When an alcohol reacts with an isocyanate, a carbamate (or urethane) is formed. There is no leaving group, and the hydrogen from the alcohol is incorporated into the product, preventing the formation of stoichiometric acid. Alcohols, however, are poor nucleophiles. The formation of a urethane requires one equivalent of alcohol to act as a Lewis acid to hydrogen bond with and activate the isocyanate for nucleophilic attack by a second equivalent of alcohol.[9] The bulky dibenzosuberol species might be too sterically inaccessible for this to occur. Combination of test reagent dibenzosuberol with butyl isocyanate in acetonitrile under reflux failed to give any conversion to product after 48 hours.

When the suberol cage **[4.3b$_3$•Fe$_2$](ClO$_4$)$_4$** was treated with stoichiometric butyl isocyanate in acetonitrile, however, there was evidence of product formation. This

product was the tris-carbamate species (as determined by ESI-MS analysis, Figure 4.6). This is impressive because the less sterically congested test reagent did not react but the more congested complex **[4.3b$_3$•Fe$_2$](ClO$_4$)$_4$** gave conversion to the tris-urethane. The enhanced reactivity can be explained by favorable activation inside the cage through cooperation of the multiple alcohols engaging in hydrogen bonds with the substrate. This was tested by following the reaction between **[4.3b$_3$•Fe$_2$](ClO$_4$)$_4$** and butyl isocyanate by ^{1}H NMR both with and without the competitive dimethylacetamide (DMA) added.

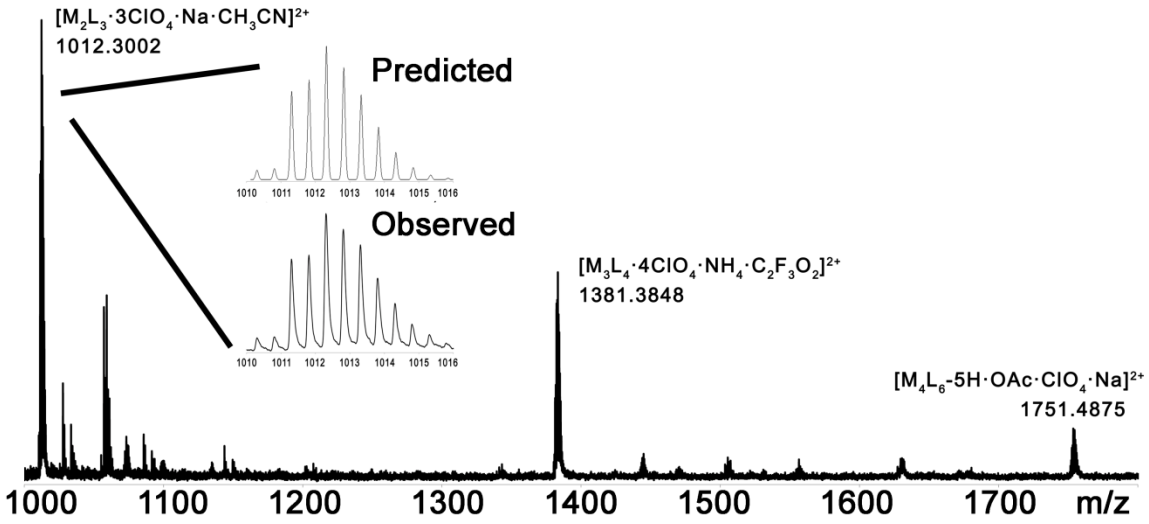

Figure 4.6: ESI-MS of tris-butyl urethane helix **[4.3c$_3$•Fe$_2$](ClO$_4$)$_4$** (MeCN).

DMA is a much stronger hydrogen bond acceptor than acetonitrile, and diluting the solution by adding 25% DMA should inhibit the reaction if it is promoted by internal hydrogen bonding. During the experiment the reaction between **[4.3b$_3$•Fe$_2$](ClO$_4$)$_4$** and butyl isocyanate had finished in approximately 6 h at 75°C using only acetonitrile, while performing the reaction with DMA led to only 70% conversion in the same time span. Since all of the alcohol functional groups are oriented on the interior of the cavity, they

are preorganized to form a biomimetic active site (Figure 4.7). As long as an isocyanate can fit on the inside it can be activated and react with a free alcohol. The tris-urethane was produced, suggesting the urethane product is also able to activate additional isocyanates, allowing the reaction to go to completion.

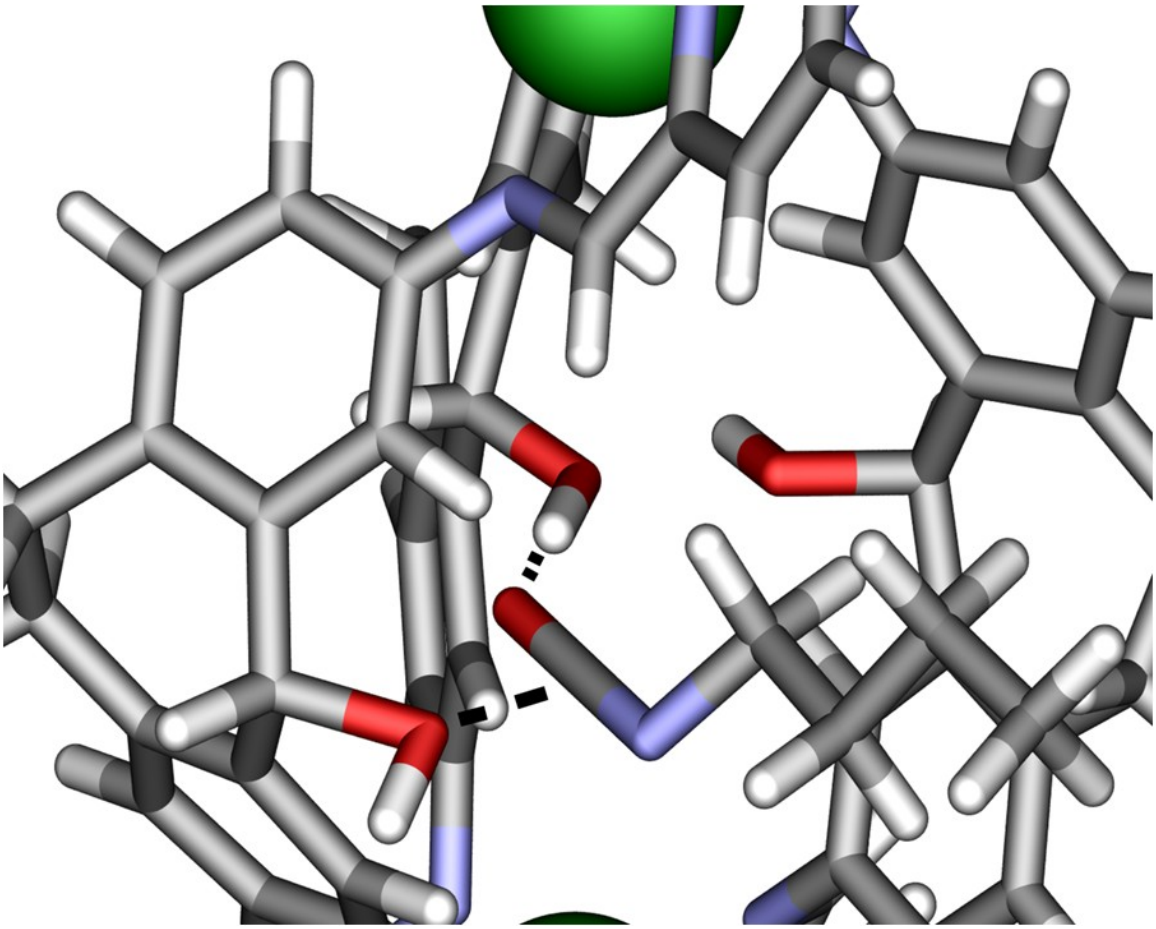

Figure 4.7: SPARTAN model detailing butyl isocyanate activation in the active site of helix **[4.3b$_3$•Fe$_2$](ClO$_4$)$_4$**.

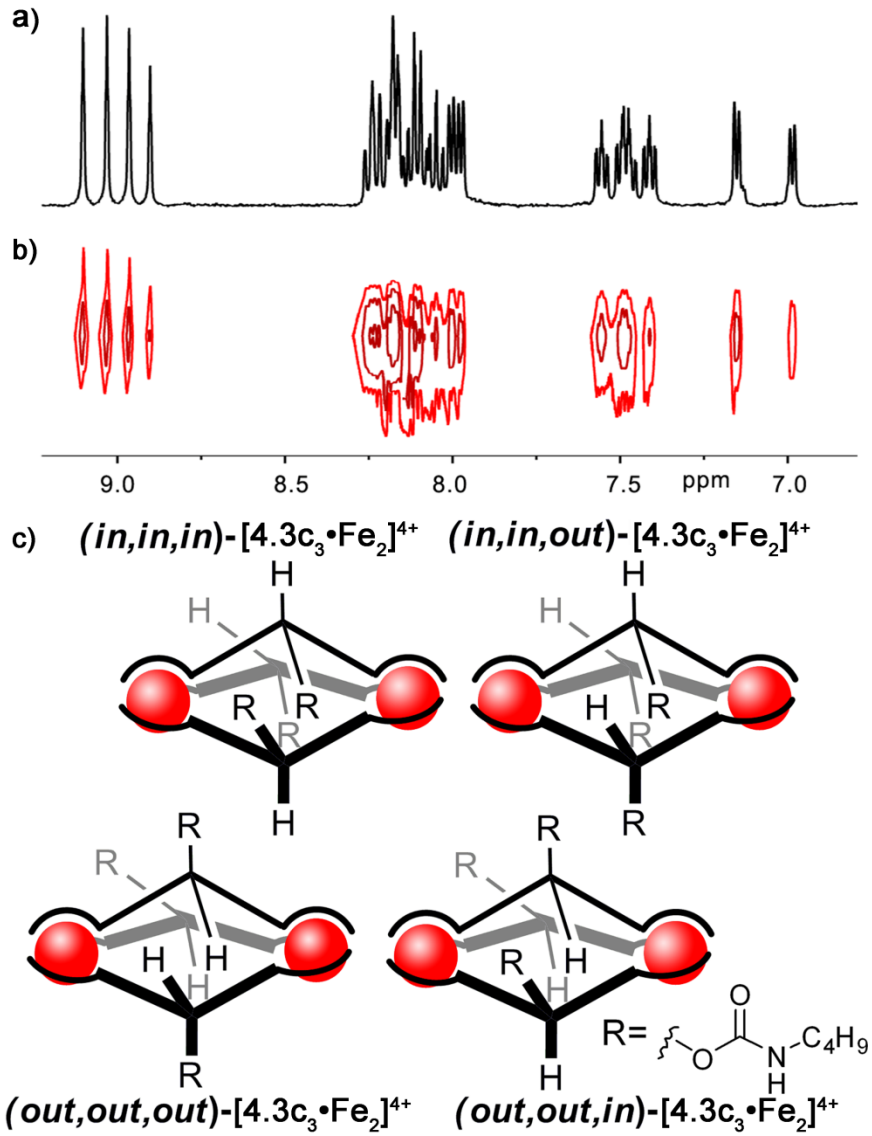

Figure 4.8: Characterization of **[4.3c$_3$•Fe$_2$](ClO$_4$)$_4$**: a) Downfield portion of ^{1}H NMR spectrum of **[4.3c$_3$•Fe$_2$](ClO$_4$)** (CD_3CN, 600 MHz, 298 K); b) Diffusion NMR signals showing co-diffusion (CD_3CN, 600 MHz, 298 K, Δ = 100 ms, δ = 2.6 μs, Diffusion Coefficient = 7.76 x10^{-10} m^2/s); c) Cartoon representation of the observed **[4.3c$_3$•Fe$_2$](ClO$_4$)$_4$** isomers in solution.

Although the formation of helix **[4.3c$_3$•Fe$_2$](ClO$_4$)$_4$** was successful based on ESI-MS analysis, the ^{1}H NMR spectrum showed more peaks than expected (Figure 4.8a). Diffusion NMR confirmed that all of these peaks corresponded to species of similar size (Figure 4.8b), and the agreement with the diffusion coefficients of **[4.3a$_3$•Fe$_2$](ClO$_4$)$_4$** and

[4.3b$_3$•Fe$_2$](ClO$_4$)$_4$ provided evidence these were all M_2L_3 species. One explanation is that the greater number of peaks in the ^{1}H NMR spectrum of **[4.3c$_3$•Fe$_2$](ClO$_4$)$_4$** were caused by isomerism at the sp^3 carbon. In the ^{1}H NMR spectrum there were at least four resonances located around 9.0 ppm. Analysis by COSY NMR confirmed these peaks represented the urethane NH protons. There are four potential isomers possible for **[4.3c$_3$•Fe$_2$](ClO$_4$)$_4$**: *in$_3$*, *in$_2$•out$_1$*, *in$_1$•out$_2$*, and *out$_3$* (Figure 4.8c). Variable temperature analysis of **[4.3c$_3$•Fe$_2$](ClO$_4$)$_4$** showed little change in the relative populations, suggesting they do not readily interconvert on the ^{1}H NMR timescale.

The scope of the reaction was tested by treating **[4.3b$_3$•Fe$_2$](ClO$_4$)** with a variety of commercially available isocyanates. All of these reactions proceeded to completion with minimal purification required, except for the reaction with isopropyl isocyanate. Isopropyl isocyanate was considerably more sensitive to water than the other isocyanates, requiring superstoichiometric amounts of the isocyanate to compensate for hydrolysis during the reaction and extensive purification to remove the isopropyl urea formed. The ^{1}H NMR spectra of **[4.3b$_3$•Fe$_2$](ClO$_4$)$_4$** (Figure 4.9a) and **[4.3c$_3$•Fe$_2$](ClO$_4$)$_4$** (Figure 4.9b), octyl urethane **[4.3d$_3$•Fe$_2$](ClO$_4$)$_4$** (Figure 4.9c), isopropyl urethane **[4.3e$_3$•Fe$_2$](ClO$_4$)$_4$** (Figure 4.9d), and both chiral α-methylbenzyl urethanes **[4.3f$_3$•Fe$_2$](ClO$_4$)$_4$** (Figure 4.9e-f) were then compared. the ^{1}H NMR spectra of octyl urethane **[4.3d$_3$•Fe$_2$](ClO$_4$)$_4$** and isopropyl urethane **[4.3e$_3$•Fe$_2$](ClO$_4$)$_4$** looked very similar to the butyl analogue **[4.3c$_3$•Fe$_2$](ClO$_4$)$_4$**, with numerous resonances for each proton consistent with the existence of different isomers in solution.

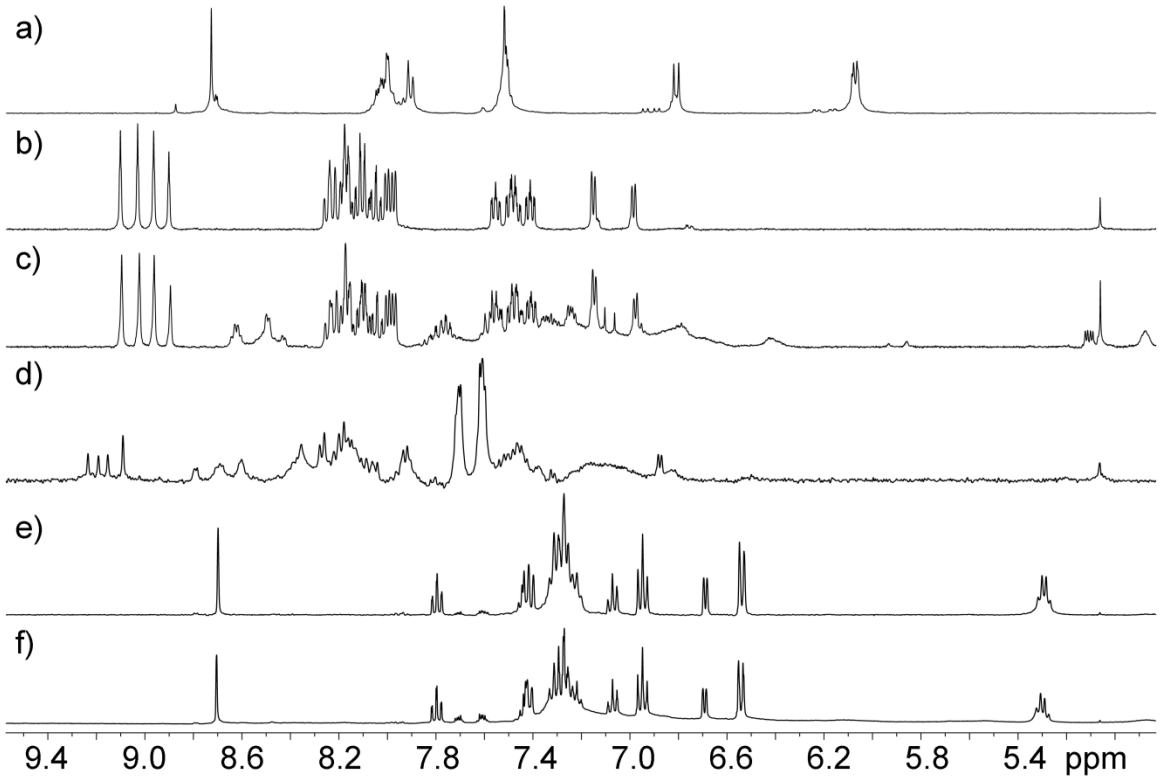

Figure 4.9: ^{1}H NMR spectra of functionalized **[4.3(b-f)$_3$•Fe$_2$](ClO$_4$)$_4$** assemblies (CD_3CN, 400 MHz, 298 K): a) **[4.3b$_3$•Fe$_2$](ClO$_4$)$_4$**; b) **[4.3c$_3$•Fe$_2$](ClO$_4$)$_4$**; c) **[4.3d$_3$•Fe$_2$](ClO$_4$)$_4$**; d) **[4.3e$_3$•Fe$_2$](ClO$_4$)$_4$**; e) **[(*S*)-4.3f$_3$•Fe$_2$](ClO$_4$)$_4$**; f) **[(*R*)-4.3f$_3$•Fe$_2$](ClO$_4$)$_4$**.

Although the aliphatic urethanes gave multiple isomers in solution, **[(*S*)-4.3f$_3$•Fe$_2$](ClO$_4$)$_4$** and **[(*R*)-4.3f$_3$•Fe$_2$](ClO$_4$)$_4$** showed only one species. This could be linked to stereoinduction by the functional group, which has been shown to have an effect even when the stereocenter is far removed from the metal chelator.[10] It is also possible that the less bulky groups in **[4.3(b-e)$_3$•Fe$_2$](ClO$_4$)$_4$** can occupy the interior of the cage, while the much larger α-methylbenzyl group is too large to point to the interior of the cavity. This can explain the complete selectivity for the *out$_3$* species (Figure 4.10).

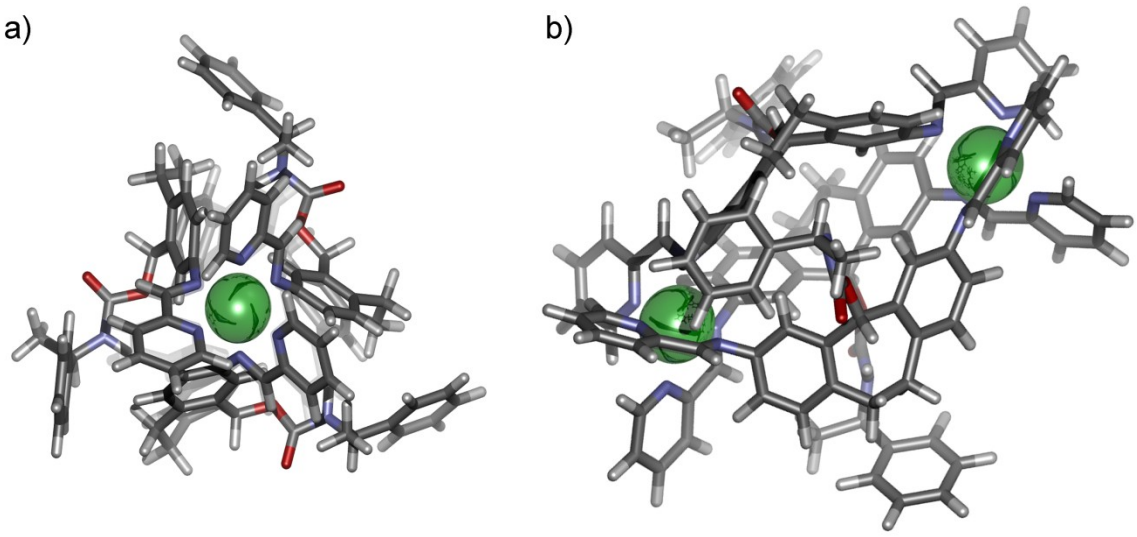

Figure 4.10: SPARTAN models detailing steric concerns giving rise to a single isomer of **[(*R*)-4.3f$_3$•Fe$_2$](ClO$_4$)$_4$**: a) View down the metal-metal axis; b) Side view.

The proposed active site suggests there would be a size-based limitation of isocyanates that could react with the mesocate. If a large, inflexible isocyanate that did not fit inside of the cavity was combined with **[4.3b$_3$•Fe$_2$](ClO$_4$)$_4$**, it would probably not react. The bulky phenyl isocyanate and 1-naphthyl isocyanate gave no conversion with the mesocate when heated under reflux in acetonitrile. To rule out electronic differences as an important factor in this selectivity, tert-butyl isocyanate was also added to the mesocate, and gave a similar lack of conversion. This shows how the catalysis is a supramolecular phenomenon: not only is the activation not seen outside of the supramolecular environment, only species that can enter the pocket are able to react.

Attempts to extend this postsynthetic modification strategy with allyl isothiocyanate proved unsuccessful. The donor ability of hydrogen bonding groups is insufficient to activate the less reactive isothiocyanate. The reaction also failed to occur in the presence of different Lewis acids including Fe(ClO$_4$)$_2$•xH$_2$O, La(OTf)$_3$, Sm(OTf)$_3$, and

$Bi(OTf)_3$. Treatment of **[4.3b$_3$•Fe$_2$](ClO$_4$)$_4$** with trans-2-methyl-3-phenyloxirane also gave no conversion with or without added Lewis acids. Other electrophiles, such as methyl vinyl ketone, sulfur pentaoxide, trimethyl borate, and butane boronic acid also failed to give conversion to functionalized complexes. Treatment of **[4.3b$_3$•Fe$_2$](ClO$_4$)$_4$** with sulfur trioxide-pyridine complex led to decomposition of the cage.

4.4 Self-Assembly and Reactivity of Diastereoselective Fluorenol-Based M_4L_6 Cages

The small size of **[4.3b$_3$•Fe$_2$](ClO$_4$)$_4$** limits the scope of reactions that the cage could promote. To include multiple reaction partners, a much larger cavity is required. A more linear scaffold was targeted that combined the ability to introvert a hydroxy group while forming a larger M_4L_6 structure. This was achieved by using fluorenone, which has the same reactivity as dibenzosuberone, but makes ligands with more linear geometry.

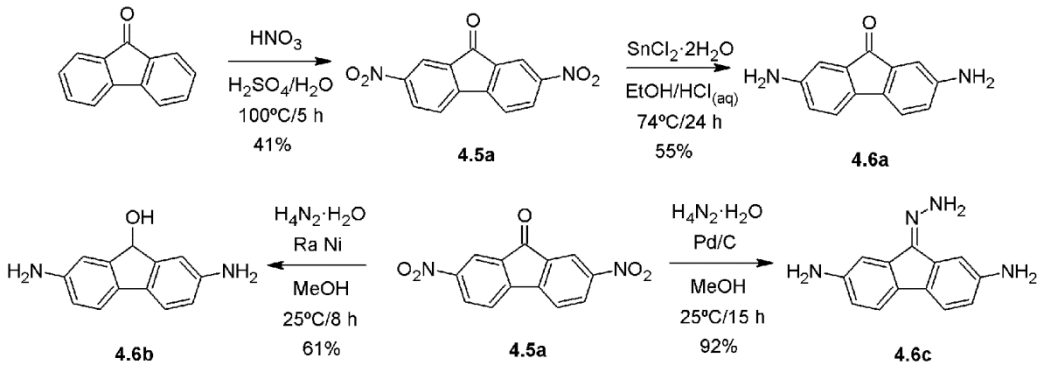

Figure 4.11: Synthesis of dianiline ligand precursors **4.6a**-**c**.

Fluorenone can be nitrated to give the dinitro compound **4.5a** that can then be reduced using Raney nickel (Figure 4.11). Fortuitously, **4.5a** is exhaustively reduced to the desired alcohol **4.6b** in one step. If the ketone **4.6a** is instead desired it can be

synthesized by tin dichloride reduction of **4.5a**. Attempts to prepare **4.6a** using Pd/C and hydrazine gave the hydrazone **4.6c** instead.

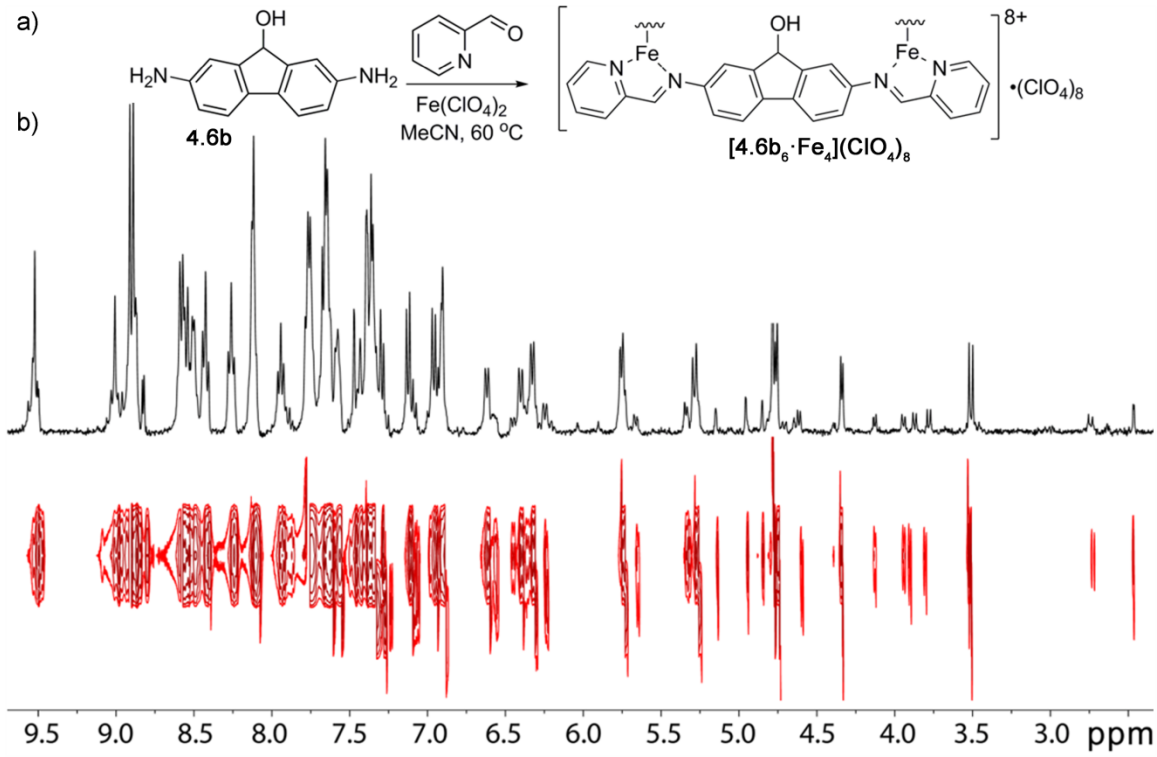

Figure 4.12: Synthesis and characterization of **[4.7b$_6$•Fe$_4$](ClO$_4$)$_8$**: a) Synthesis of **[4.7b$_6$•Fe$_4$](ClO$_4$)$_8$**; b) DOSY spectrum of **[4.7$_6$•Fe$_4$](ClO$_4$)$_8$** (CD_3CN, 600 MHz, 298K; Δ = 100 ms, δ = 2.6 μs, Diffusion Coefficient = 4.8 x 10^{-10} m^2/s).

Multicomponent self-assembly of dianiline **4.6b** gave the desired **[4.7b$_6$•Fe$_4$](ClO$_4$)$_8$** cage after heating (Figure 4.12a). ESI-MS analysis confirmed the presence of the M_4L_6 cage **[4.7b$_6$•Fe$_4$](ClO$_4$)$_8$** in solution. The ^{1}H spectrum, however, was complex (Figure 4.12b). Diffusion ^{1}H NMR showed that all of the peaks co-diffused, supporting the presence of only the M_4L_6 cage in solution. The fluorenol cage **[4.7b$_6$•Fe$_4$](ClO$_4$)$_8$** shows more resonances than the helix **[4.3b$_3$•Fe$_2$](ClO$_4$)$_4$**. The dibenzosuberol cage had two metals that formed a mesocate selectively, and gave rise to four different isomers at the alcohol position. Assuming three different metal-based tetrahedral diastereomers (*T*, C_3,

and S_4) for **[4.7b$_6$•Fe$_4$](ClO$_4$)$_8$** are possible,[11] there could be many more isomers based on the metal stereochemistry and directionality of the alcohols.

Crystals of **[4.7b$_6$•Fe$_4$](ClO$_4$)$_8$** were grown by slow evaporation from a saturated solution in CD_3CN. Analysis of this structure shows a number of unexpected features (Figure 4.13). The cage does not contain four-*fac* metal centers as is typically observed for linear Fe(II)-iminopyridine cages.[12] The **[4.7b$_6$•Fe$_4$](ClO$_4$)$_8$** cage contains pseudo-C_3 symmetry with three *mer* centers, more than previously encountered in Fe(II)-iminopyridine assemblies.[13] The structure is similar in shape to a wizard's hat, with a pointed top (the *fac* metal vertex), and a brim (made up of the three *mer* centers).

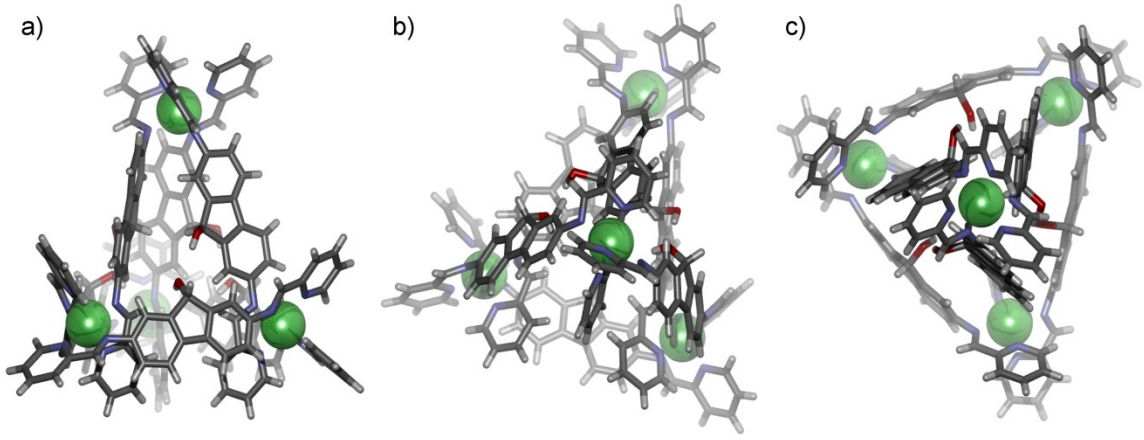

Figure 4.13: X-ray of analysis of **[4.7b$_6$•Fe$_4$](ClO$_4$)$_8$** (counterions removed for clarity): a) Side view of **[4.7b$_6$•Fe$_4$](ClO$_4$)$_8$**; b) View down one of the *mer* centers; c) View down the *fac* center.

This shape is adopted because the ligands on the peak of the hat-shaped structure have their hydroxide groups in a favorable position to engage in hydrogen bond-donation with the ligands on the brim (Figure 4.14). The brim hydroxides accept these hydrogen bonds, while themselves donating their protons towards a bound perchlorate anion. A

single major isomer is formed, rather than 118 different possible metal and OH-based isomers.

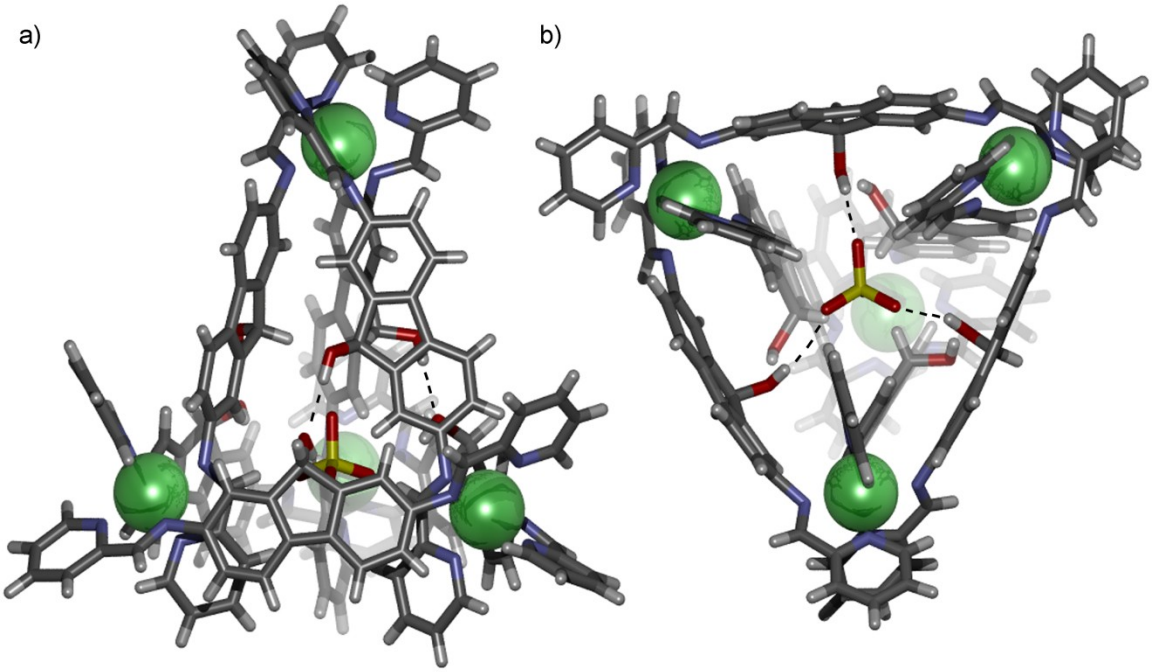

Figure 4.14: Hydrogen bonding in the crystal structure of **[(ClO_4)⊂4.7b_6•Fe_4](ClO_4)$_7$**: a) Hydrogen bonding between peak and brim alcohols; b) Hydrogen bonding between brim alcohols and bound perchlorate anion.

Although the solid state structure showed selectivity for a single isomer, it was not clear if this selectivity also occurred in solution. A suite of 2D NMR techniques were applied to the analysis of **[(ClO_4)⊂4.7b_6•Fe_4](ClO_4)$_7$** and confirmed that the pseudo-C_3 symmetric solid state structure represented the major isomer in solution (Figure 4.15). Key to this analysis are the NOE crosspeaks observed between the “axial” hydroxide peak and resonances of other protons around the cavity interior that facilitate the assignment of the remaining resonances. There are minor peaks in the ^{1}H NMR spectrum that correspond to between two and four other isomers. It is not possible to

determine if these minor isomers are different due to the position of the OH group alone or metal-based stereoisomerism.

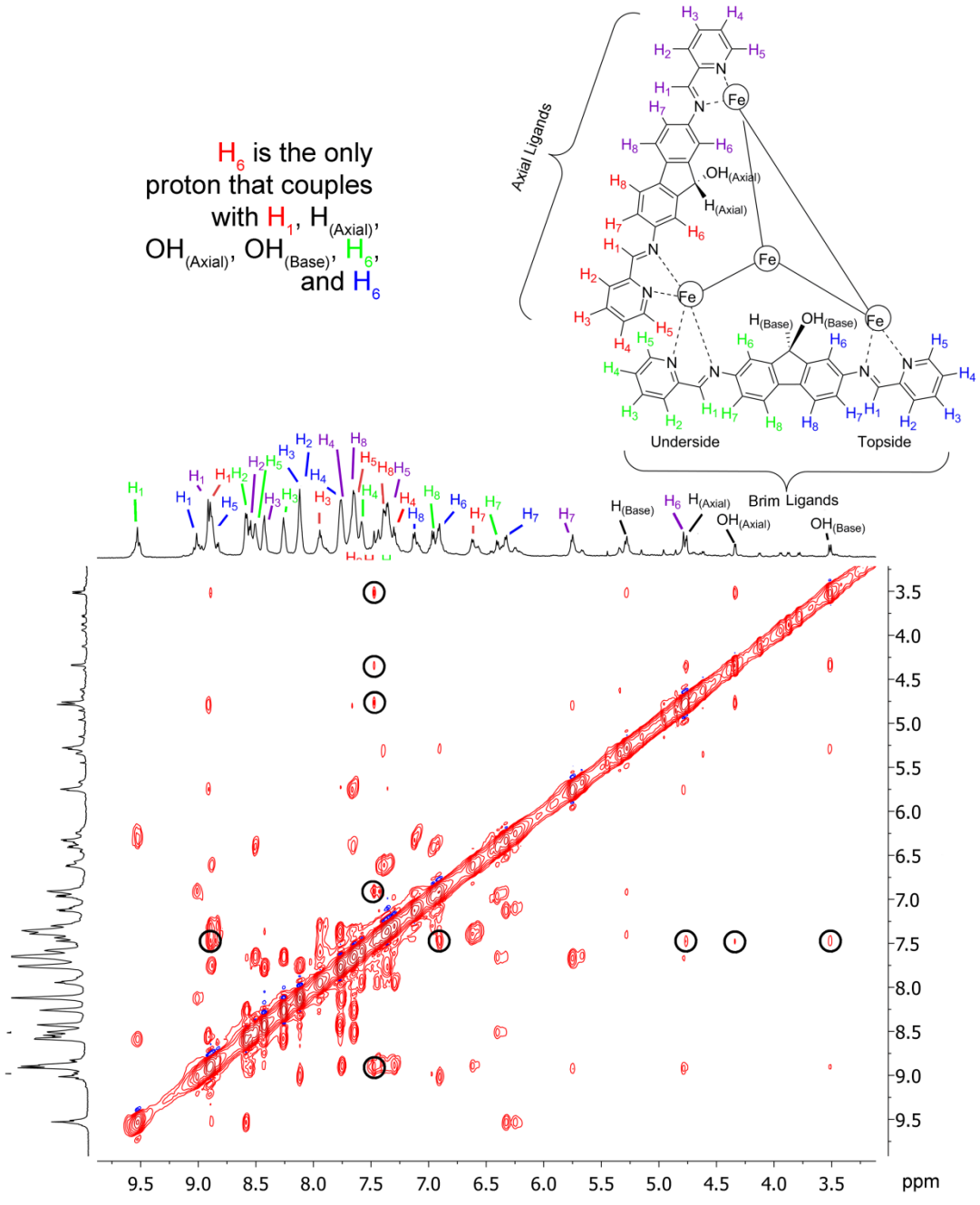

Figure 4.15: Labeled NOESY spectrum of **[(ClO_4)⊂4.7b_6•Fe_4]$(ClO_4)_7$** with some key crosspeaks circled to explain the assignment of H_6 (CD_3CN, 600 MHz, Mixing time = 70 ms, 298 K).

Multi-component self-assembly to form **[(ClO$_4$)⊂4.7b$_6$•Fe$_4$](ClO$_4$)$_7$** in ethanol led to formation of only the non-discrete assembly. If this mixture was then heated in acetonitrile, however, it was able to reform the discrete cage. Ethanol is a stronger hydrogen bond donor and acceptor than acetonitrile, and while complexation still occurs in ethanol as evidenced by a purple color, the discrete structure is not formed. This shows that the interligand hydrogen bonds are necessary for the assembly of **[(ClO$_4$)⊂4.7b$_6$•Fe$_4$](ClO$_4$)$_7$**.

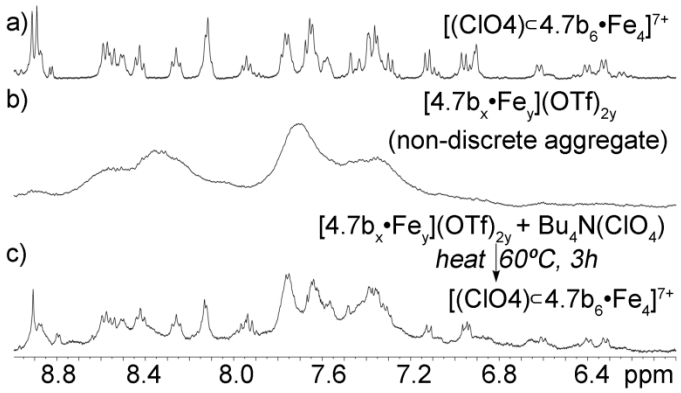

Figure 4.16: ^{1}H NMR spectra showing anion templation studies of **[4.7b$_6$•Fe$_4$]$^{8+}$** (CD_3CN, 400 MHz, 298K): a) **[(ClO$_4$)⊂4.7b$_6$•Fe$_4$](ClO$_4$)$_7$**; b) **[4.7b$_x$•Fe$_y$](OTf)$_{2y}$**; c) **[(ClO$_4$)⊂4.7b$_6$•Fe$_4$](OTf)$_7$**.

The presence of a bound anion in the solid state suggests that it is necessary for templation of the **[(ClO$_4$)⊂4.7b$_6$•Fe$_4$](ClO$_4$)$_7$** cage. This was tested by combination of **4.6b** with 2-formylpyridine and iron(II) triflate (prepared *in situ* by combining silver triflate with iron(II) chloride) in acetonitrile. Instead of giving a sharp ^{1}H NMR spectrum like **[(ClO$_4$)⊂4.7b$_6$•Fe$_4$](ClO$_4$)$_7$** (Figure 4.16a), this mixture showed only broad signals indicative of an undefined oligomeric assembly (Figure 4.16b). Treating this oligomer with tetrabutylammonium perchlorate also gave no discrete assembly, likely due to the fact that the Fe(II)-iminopyridine complex does not readily dissociate at room

temperature.[7] If the **[4.7b$_x$•Fe$_y$](OTf)$_{2y}$** mixture was heated in the presence of the perchlorate, the cage reassembled, and the obtained ^{1}H NMR spectrum looked almost identical to that of **[(ClO$_4$)⊂4.7b$_6$•Fe$_4$](ClO$_4$)$_7$** (Figure 4.16c).

The ability of **[4.7b$_x$•Fe$_y$](OTf)$_{2y}$** to "reassemble" when heated in the presence of a suitable template allowed other anions to be tested as templates. Table 4.1 lists the results of these screens. In addition to perchlorate, the fluorenol cage was templated in the presence of tetrafluoroborate, nitrate, and monobasic sulfate anions. In contrast, anions that were either too large to fit inside the cavity ($Ph_3F_2Si^-$) or too small to fill the cavity (Cl^-) were unable to template formation of the cage.

Table 4.1: Results of templating non-discrete **[4.7b$_x$•Fe$_y$](OTf)$_{2y}$** to give **[(X)⊂4.7b$_6$•Fe$_4$](OTf)$_7$**.

Anion	Bound	Anion	Bound	Anion	Bound	Anion	Bound
ClO_4^-	Yes	$Ph_3F_2Si^-$	No	SO_3^{2-}	No	Br^-	No
BF_4^-	Yes	$S_2O_4^{2-}$	No	$S_2O_3^{2-}$	No	I^-	No
HSO_4^-	Yes	SbF_6^-	No	IO_3^-	No	IO_4^-	Decomp
NO_3^-	Yes	PF_6^-	No	Cl^-	No	NO_2^-	Decomp

The complexity of the ^{1}H NMR spectrum of **[(ClO$_4$)⊂4.7b$_6$•Fe$_4$](ClO$_4$)$_7$** prevented the study of anion binding by titration of guest into a solution of cage and monitoring the shift of the proton resonances. ^{19}F NMR can overcome this by instead looking at the chemical shift of the anion (if it contains a fluorine atom), removing the complexity of the ^{1}H NMR spectrum. Titration of BF_4^- into preformed cage **[(BF$_4$)⊂4.7b$_6$•Fe$_4$](OTf)$_7$** led to shifts of the ^{19}F resonance, consistent with a fast exchange between bound and free BF_4^-. This shows that even though a template is required for cage formation, the bound anion can diffuse in and out of the cage. The cage is kinetically stable at room temperature, however, and this does not lead to the self-assembly decomposing or reassembling into oligomers.

Equation 4.1: Formula used in the Hill1 regression in OriginPro 8.

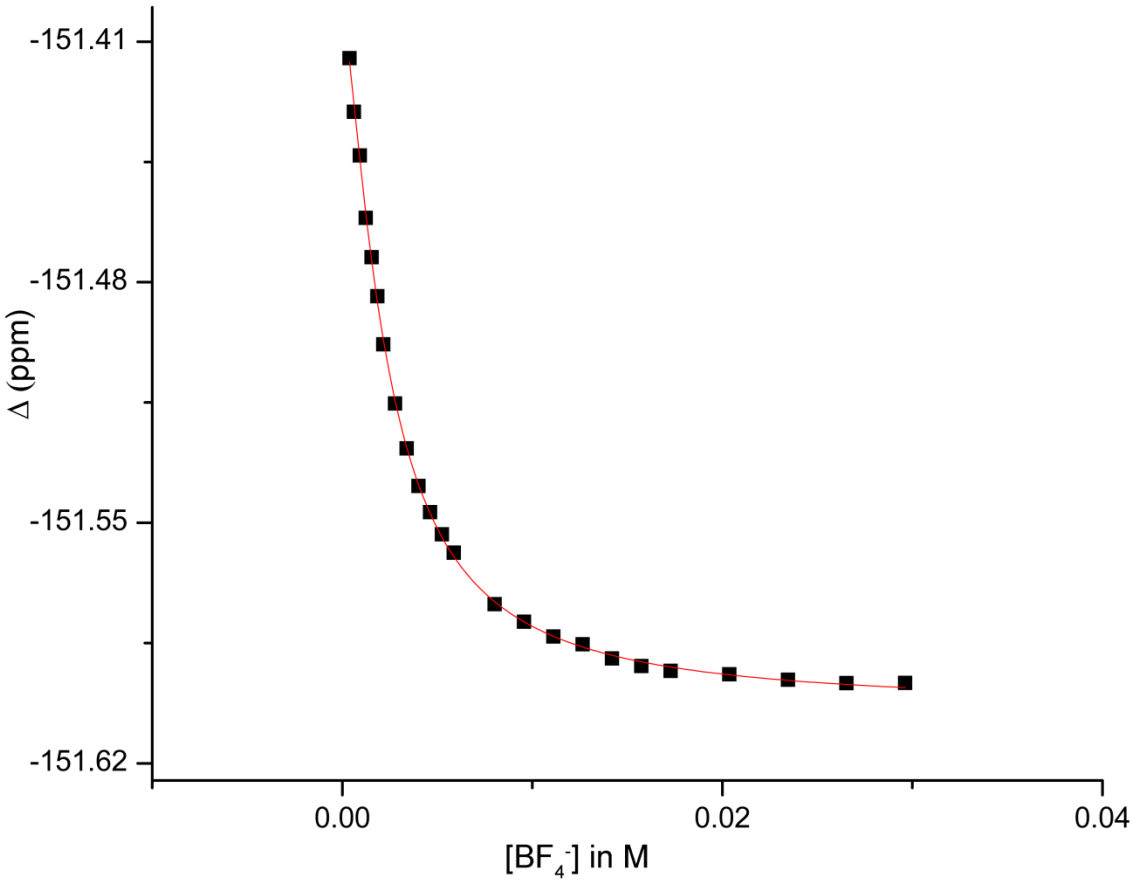

Figure 4.17: Fitting of ^{19}F shift upon titration of Bu_4NBF_4 into **[(BF$_4$)⊂4.7b$_6$•Fe$_4$](OTf)$_7$** (CD_3CN, 9.2 x 10^{-4} M).

When BF_4^- was titrated directly into **[(BF$_4$)⊂4.7b$_6$•Fe$_4$](OTf)$_7$**, the binding constant was determined to be 430±7 M^{-1} (Figure 4.17) using a Hill1 regression in Origin Pro 8 (Equation 4.1). When BF_4^- was titrated into **[(ClO$_4$)⊂4.7b$_6$•Fe$_4$](ClO$_4$)$_7$**, an even lower association constant of 15±2 M^{-1} was calculated. The decrease in tetrafluoroborate

binding in the presence of this anion indicates that perchlorate is more tightly bound inside the cage.

Treatment of **[(ClO$_4$)⊂4.7b$_6$•Fe$_4$](ClO$_4$)$_7$** with butyl isocyanate in refluxing acetonitrile also gave conversion to a functionalized complex (Figure 4.18). This butylurethane looked similar to the butylurethane **[4.3c$_6$•Fe$_4$](ClO$_4$)$_7$**, specifically the presence of four discernible urethane resonances. The fluorenol cage also contains a pocket decorated with alcohols, and can promote the reaction with encapsulated isocyanates. Control reactions with fluorenol confirmed that no conversion to urethane occurred in acetonitrile.

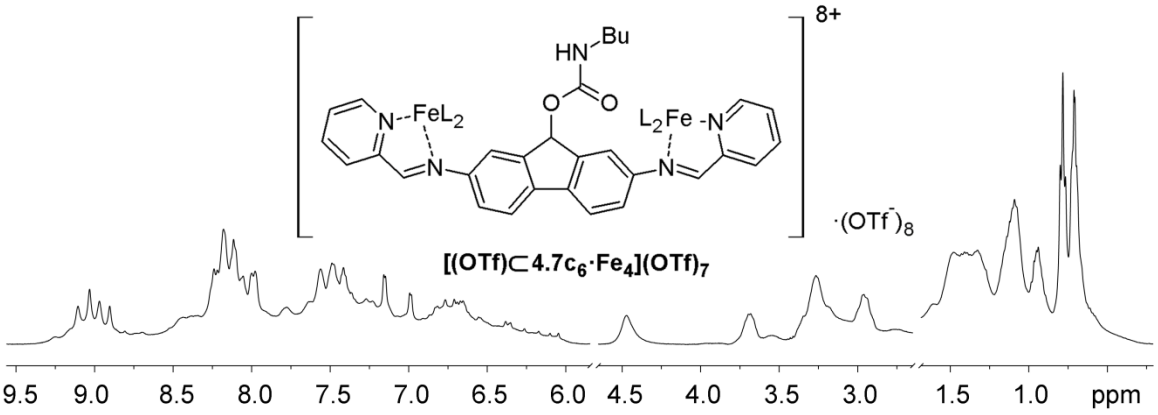

Figure 4.18: ^{1}H NMR spectrum of butylurethane-based fluorenol cage **[(OTf)⊂4.7c$_6$•Fe$_4$](OTf)$_7$** (CD_3CN, 400 MHz, 298 K).

Treatment of **[4.7b$_x$•Fe$_y$](OTf)$_{2y}$** with butyl isocyanate also leads to the formation of a discrete complex. Although a discrete pocket is not formed in the case of **[4.7b$_x$•Fe$_y$](OTf)$_{2y}$**, the aggregate does bring the alcohol groups into close proximity, allowing activation of the isocyanate and subsequent functionalization of the complex. Once the cage is functionalized the urethane oligomer **[4.7c$_x$•Fe$_y$](OTf)$_{2y}$** can reassemble. This is a consequence of either stronger interligand hydrogen bonds, or the

result of the more acidic urethanes hydrogen bonding with the less basic triflate anion inside of the cage. Titration of triflate into the cage caused shifts in the fluorine resonance, suggesting the triflate is bound inside of the urethane cage **[(OTf)⊂4.7c$_6$•Fe$_4$](OTf)$_7$**.

Treatment of **[(ClO$_4$)⊂4.7b$_6$•Fe$_4$](ClO$_4$)$_7$** with 2-(isocyanato)ethyl methacrylate provided access to the functionalized cage **[(ClO$_4$)⊂4.7d$_6$•Fe$_4$](ClO$_4$)$_7$** (Figure 4.19). The thiol-ene reaction was targeted as a mild reaction to perform on this complex.[14] The initial tests were promising: **[(ClO$_4$)⊂4.7d$_6$•Fe$_4$](ClO$_4$)$_7$** was tolerant to addition of excess propanethiol and stoichiometric azobisisobutyronitrile. When these were combined with the cage and heated to 50 °C, there was no sign of decomposition. Raising the temperature ultimately led to decomposition of the cage, suggesting this reaction is not mild enough for the Fe(II)-iminopyridine motif.

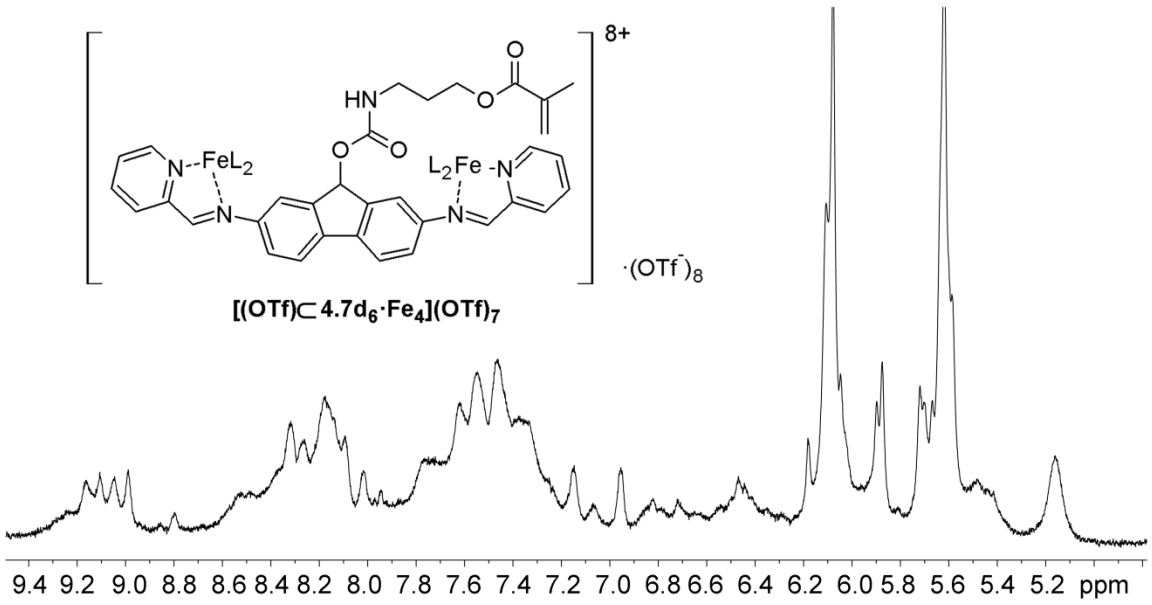

Figure 4.19: ^{1}H NMR spectrum of methacroylurethane-based fluorenol cage **[(OTf)⊂4.7d$_6$•Fe$_4$](OTf)$_7$** (CD_3CN, 400 MHz, 298 K).

Another way to perform reactions on the inside of a cage would be to target a more reactive amine, accessible from precursor **4.6c.** Multi-component self-assembly of **4.6c** with 2-formylpyridine and Fe(II) failed due to the competitive formation of imine at both the terminal amine as well as the reactive hydrazone. This gave rise to broad ^{1}H NMR spectra, indicative of an oligomeric aggregate. Changing the amount of aldehyde and the amount of metal to allow reaction at every position also failed to give a discrete assembly. This underscores the importance of selecting non-competitively coordinating functional groups for preparing endohedrally-functionalized self-assembled metal-organic cages.

4.5 Postsynthetic Modification for Stabilization of Complexes

There are many examples of narcissistic self-sorting complexes.[15] Most of these, however, require self-sorting between ligands of different shapes or sizes.[16] Self-sorting becomes more challenging when the ligands are the same shape. Pd(II)-paddlewheel complexes including **1.15** and **1.16** have demonstrated that self-sorting of ligands with the same overall shape can be biased by sterics. Complexes **[4.3a$_3$•Fe$_2$](ClO$_4$)$_4$**, **[4.3b$_3$•Fe$_2$](ClO$_4$)$_4$**, **[4.3c$_3$•Fe$_2$](ClO$_4$)$_4$** are similar, as are **[4.7b$_6$•Fe$_4$](ClO$_4$)$_8$** and **[4.7c$_6$•Fe$_4$](ClO$_4$)$_8$**, but it was unclear if the different endohedral functionalities would be able to also bias self-sorting.

Combination of **[4.3a$_3$•Fe$_2$](ClO$_4$)$_4$** and **[4.3b$_3$•Fe$_2$](ClO$_4$)$_4$** in acetonitrile followed by heating led to no change. These self-assemblies do not form any mixed aggregates. Mixing of **[4.3a$_3$•Fe$_2$](ClO$_4$)$_4$** with **[(*S*)-4.3f$_3$•Fe$_2$](ClO$_4$)$_4$** gave the same result. Heating a mixture of **[(*S*)-4.3f$_3$•Fe$_2$](ClO$_4$)$_4$** and **[(*R*)-4.3f$_3$•Fe$_2$](ClO$_4$)$_4$** also failed to show any

heterocluster formation by ^{1}H NMR. This suggests that the cages are either thermodynamically more stable as the homoclusters, or that they are kinetically incapable of interconverting. To test the kinetic stability of the cages, **[4.3a$_3$•Fe$_2$](ClO$_4$)$_4$** and **[(*S*)-4.3f$_3$•Fe$_2$](ClO$_4$)$_4$** were combined with a catalytic amount of isopropyl amine. There was no sign of interconversion after heating this mixture, suggesting the cages favor self-sorting for thermodynamic reasons.

The relative stability of the cages was determined by taking one complex and heating in the mixture of other anilines. This showed that **[4.3a$_3$•Fe$_2$](ClO$_4$)$_4$** did not exchange when treated with the alcohol **4.2b**, although the ketone **4.2a** was capable of displacing the alcohol, giving **4.2b** and **[4.3a$_3$•Fe$_2$](ClO$_4$)$_4$** in solution. The butylurethane dianiline could not be readily prepared for comparison, and the butylurethane cage showed no sign of displacement **[4.3c$_3$•Fe$_2$](ClO$_4$)$_4$** with either **4.2a** or **4.2b**. The cages **[4.3a$_3$•Fe$_2$](ClO$_4$)$_4$** and **[4.3b$_3$•Fe$_2$](ClO$_4$)$_4$** both showed exchange when treated with 4,4'-diaminodiphenylmethane, although urethane helix **[4.3c$_3$•Fe$_2$](ClO$_4$)$_4$** was still tolerated. This suggests that the postsynthetic modification of **[4.3b$_3$•Fe$_2$](ClO$_4$)$_4$** to give **[4.3c$_3$•Fe$_2$](ClO$_4$)$_4$** makes the complex more stable to displacement.

If the postsynthetic modification stabilizes the suberol helix, it should also stabilize the fluorenol cage. Treatment of the fluorenol cage **[4.7b$_6$•Fe$_4$](ClO$_4$)$_8$** with **4.2a** or **4.2b** led to the helices **[4.3a$_3$•Fe$_2$](ClO$_4$)$_4$** and **[4.3b$_3$•Fe$_2$](ClO$_4$)$_4$** respectively. When **[4.7b$_6$•Fe$_4$](ClO$_4$)$_8$** was treated with **4.2a** or **4.2b**, however, there was no sign of exchange. This suggests that postsynthetic modification can be used to prepare more robust self-assembled structures.

4.6 Conclusion

Preparing metal-organic cages functionalized with reactive groups requires the careful tuning of nucleophilicity. Groups that are poor nucleophiles will confer modest reactivity to the self-assembly, while nucleophiles that are too strong will interrupt the assembly process. Poor nucleophiles may not be able to react with the desired variety of substrates, but because the self-assembly process is dominated by weak interactions, weakly donating nucleophiles can have significant impact on the outcome of self-assembly.

4.7 References

1) a) Tanabe, K. K.; Cohen, S. M. “Postsynthetic Modification of Metal-Organic Frameworks – A Progress Report.” *Chem. Soc. Rev.*, **2011**, *40*, 498-519; b) Wang, Z.; Cohen, S. M. “Postsynthetic Modification of Metal-Organic Frameworks.” *Chem. Soc. Rev.*, **2009**, *38*, 1315-1329.

2) a) Nguyen, J. G.; Cohen, S. M. “Moisture-Resistant and Superhydrophobic Metal-Organic Frameworks Obtained via Postsynthetic Modification.” *J. Am. Chem. Soc.*, **2010**, *132*, 4560-4561; b) Wang, Z.; Tanabe, K. K.; Cohen, S. M. “Tuning Hydrogen Sorption Properties of Metal-Organic Frameworks by Postsynthetic Covalent Modification.” *Chem.-Eur. J.*, **2010**, *16*, 212-217; c) Wang, Z.; Cohen, S. M. “Modulating Metal-Organic Frameworks To Breathe: A Postsynthetic Covalent Modification Approach.” *J. Am. Chem. Soc.*, **2009**, *131*, 16675-16677.

3) Doonan, C. J.; Morris, W.; Furukawa, H.; Yaghi, O. M. “Isoreticular Metalation of Metal—Organic Frameworks.” *J. Am. Chem. Soc.*, **2009**, *131*, 9492-9493.

4) a) Han, Y-F.; Jin, G-X.; Hahn, F. E. “Postsynthetic Modification of Dicarbene-Derived Metallacycles via Photochemical [2 + 2] Cycloaddition.” *J. Am. Chem. Soc.*, **2013**, *135*, 9263-9266; b) Chakrabarty, R.; Stang, P. J. “Post-Assembly Functionalization of Organoplatinum(II) Metallacycles via Copper-Free Click Chemistry.” *J. Am. Chem. Soc.*, **2012**, *134*, 14738-14741; c) Wang, M.; Lan, W-J.; Zheng, Y-R.; Cook, T. R.; White, H. S.; Stang, P. J. “Designed Post-Self-Assembly Structural and Functional Modifications of a Truncated Tetrahedron.” *J. Am. Chem. Soc.*, **2011**, *133*, 10752-10755; d) Frank, M.; Hey, J.; Balcioglu, I.; Chen, Y.-S.; Stalke, D.; Suenobu, T.; Fukuzumi, S.; Frauendorf, H.; Clever, G. H. “Assembly and Stepwise Oxidation of Interpenetrated Coordination Cages Based on Phenothiazine.” *Angew. Chem., Int. Ed.*, **2013**, *52*, 10102-10106.

5) Ślusarczyk, M.; De Borggraeve, W. M.; Hoornaert, G.; Deroose, F.; Linders, J. T. M. “Synthesis and Biological Evaluation of Methylene-Bridged Analogs of the Potent Cannabinoid Receptor Antagonist Rimonabant.” *Eur. J. Org. Chem.*, **2008**, 1350-1357.

6) Freye, S.; Michel, R.; Stalke, D.; Pawliczek, M.; Frauendorf, H.; Clever, G. H. “Template Control over Dimerization and Guest Selectivity of Interpenetrated Coordination Cages.” *J. Am. Chem. Soc.*, **2013**, *135*, 8476-8479.

7) Young, M. C.; Johnson, A. M.; Hooley, R. J. “Self-Promoted Post-Synthetic Modification of Metal-Ligand M_2L_3 Mesocates.” *Chem. Commun.*, **2014**, *50*, 1378-1380.

8) Cooke, D. J.; Cross, J. M.; Fennessy, R. V.; Harding, L. P.; Rice, C. R.; Slater, C. “Steric Control of the Formation of Dinuclear Double Helicate and Dinuclear *meso*-Helicate Assemblies.” *Chem. Commun.*, **2013**, *49*, 7785-7787.

9) Ephraim, S.; Woodward, A. E.; Mesrobian, R. B. “Kinetic Studies of the Reaction of Phenyl Isocyanate with Alcohols in Various Solvents.” *J. Am. Chem. Soc.*, **1958**, *80*, 1326-1328.

10) Bolliger, J. L., Belenguer, A. M.; Nitschke, J. R. “Enantiopure Water-Soluble [Fe_4L_6] Cage: Host-Guest Chemistry and Catalytic Activity.” *Angew. Chem. Int. Ed.*, **2013**, *52*, 7958-7962.

11) Paul, R. L.; Argent, S. P.; Jeffery, J. C.; Harding, L. P.; Lynam, J. M.; Ward, M. D. “Structures and Anion-Binding Properties of M_4L_6 Tetrahedral Cage Complexes with Large Central Cavities.” *Dalton Trans.*, **2004**, 3453-3458.

12) Smulders, M. M. J.; Zarra, S.; Nitschke, J. R. “Qualitative Understanding of Guest Binding Enables the Design of Complex Host-Guest Behavior.” *J. Am. Chem. Soc.*, **2013**, *135*, 7039-7046.

13) Riddell, I. A.; Hristova, Y. R.; Clegg, J. K.; Wood, C. S.; Breiner, B.; Nitschke, J. R. “Five Discrete Multinuclear Metal-Organic Assemblies from One Ligand: Deciphering the Effects of Different Templates.” *J. Am. Chem. Soc.*, **2013**, *135*, 2723-2733.

14) Lowe, A. B. “Thiol-ene “Click” Reactions and Recent Applications in Polymer and Materials Synthesis.” *Polym. Chem.*, **2010**, *1*, 17-36.

15) Safont-Sempere, M. M.; Fernández, G.; Würthner, F. “Self-Sorting Phenomena in Complex Supramolecular Systems.” *Chem. Rev.*, **2011**, *111*, 5784-5814.

16) Sarma, R. J.; Nitschke, J. R. “Self-Assembly in Systems of Subcomponents: Simple Rules, Subtle Consequences.” *Angew. Chem. Int. Ed.*, **2007**, *47*, 377-380.

Chapter 5 – Reversible Self-Assembly of Metal-Organic Cages Containing Bismuth Salts

5.1 Rationale

Although iron(II)-iminopyridine cages provided a useful system for studying effects such as sterics on self-assembly, they did not display the stability or robustness that had been expected. The complexes had to be formed in acetonitrile, and they displayed varying levels of stability in solution. Another option is to explore the self-assembly of the main group metals. Group 13 metals, such as gallium and aluminum, are redox stable as +3 ions. Gallium(III) is useful for preparing diamagnetic self-assembled cages where the more paramagnetic iron(III) had previously been used.[1] These metals have small ionic radii and their coordination chemistry is similar to iron(III) or titanium(IV), especially their preference for charged oxygen-containing ligands. The synthesis of group 14-based self-assemblies using germanium,[2] tin,[3] and lead[4] is also possible. Although there is some potential for redox chemistry with tin[5] as well as for lead,[6] both of the common oxidation states for both metals are diamagnetic.

The group 15 elements are also capable of forming self-assembled structures.[7] The effect of size discrimination between electronically similar thiolate-pnictogen based self-assemblies has been explored using phosphorus, arsenic, antimony, and bismuth.[8] All of these cages form trivalent complexes, even the larger metal bismuth. Larger complexes with higher coordination number are also known,[9] ranging from 3 to 9-coordinate bismuth. This variability provides an interesting challenge: can supramolecular assembly be used to control the coordination number of Bi(III) complexes?

5.2 Coordination of Bismuth by Bidentate Chelators

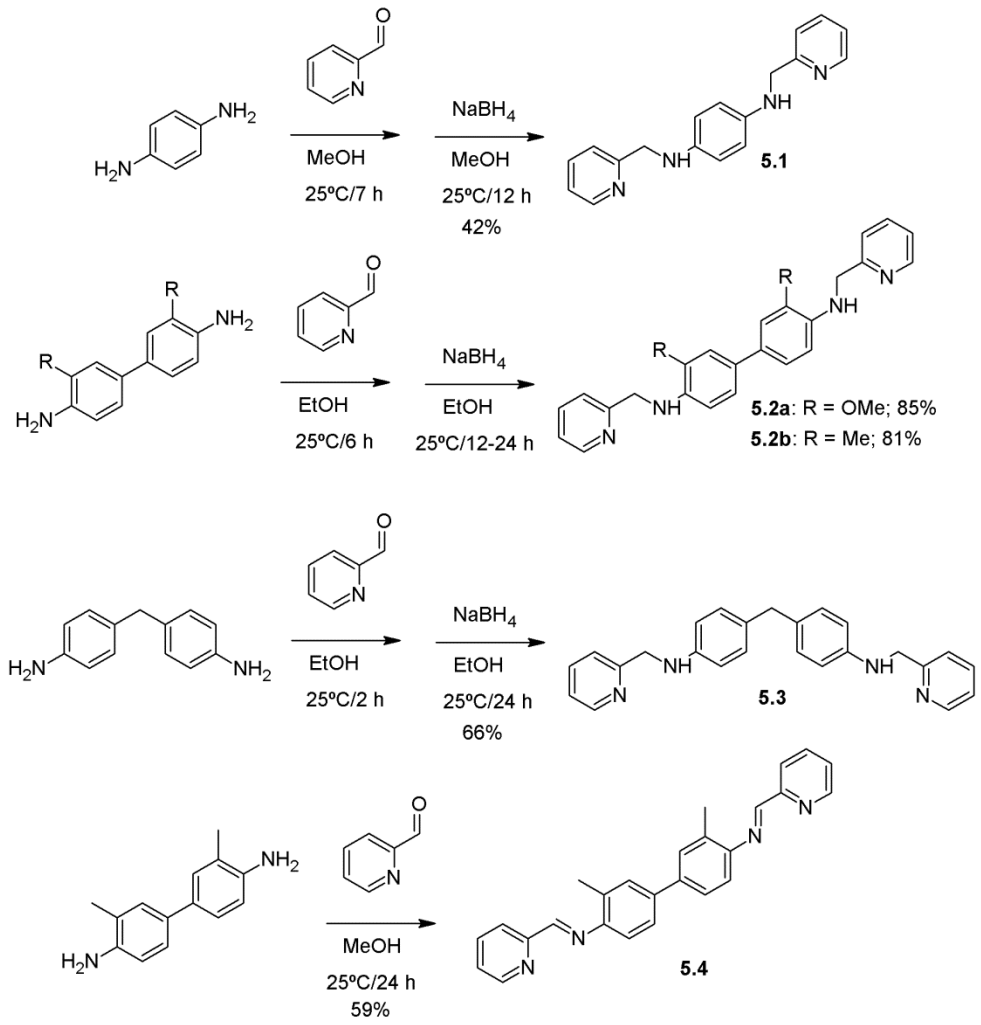

Figure 5.1: Synthesis of bis-aminomethylpyridine ligands **5.1**, **5.2a**, **5.2b**, and **5.3** and iminopyridine ligand **5.4**.

Aminomethylpyridine ligands **5.1**, **5.2a**, **5.2b**, and **5.3** were prepared directly from their commercially available dianiline precursors by *in situ* condensation followed by reduction using sodium borohydride in alcoholic solvents (Figure 5.1). There was evidence that similar diimine ligands formed six-coordinate complexes with bismuth(III) perchlorate, with additional sites filled with anions making the coordination number 9.[10] $Bi(OTf)_3$ was titrated into a solution of **5.1** in an NMR tube, and the titration was

monitored by ^{1}H NMR spectroscopy (Figure 5.2). Addition of the bismuth salt initially causes the peaks to shift downfield, consistent with a fast exchange between bound and unbound ligand. The resonance corresponding to the interior phenyl ring as well as those of the aniline and methylene protons broaden as bismuth is added.

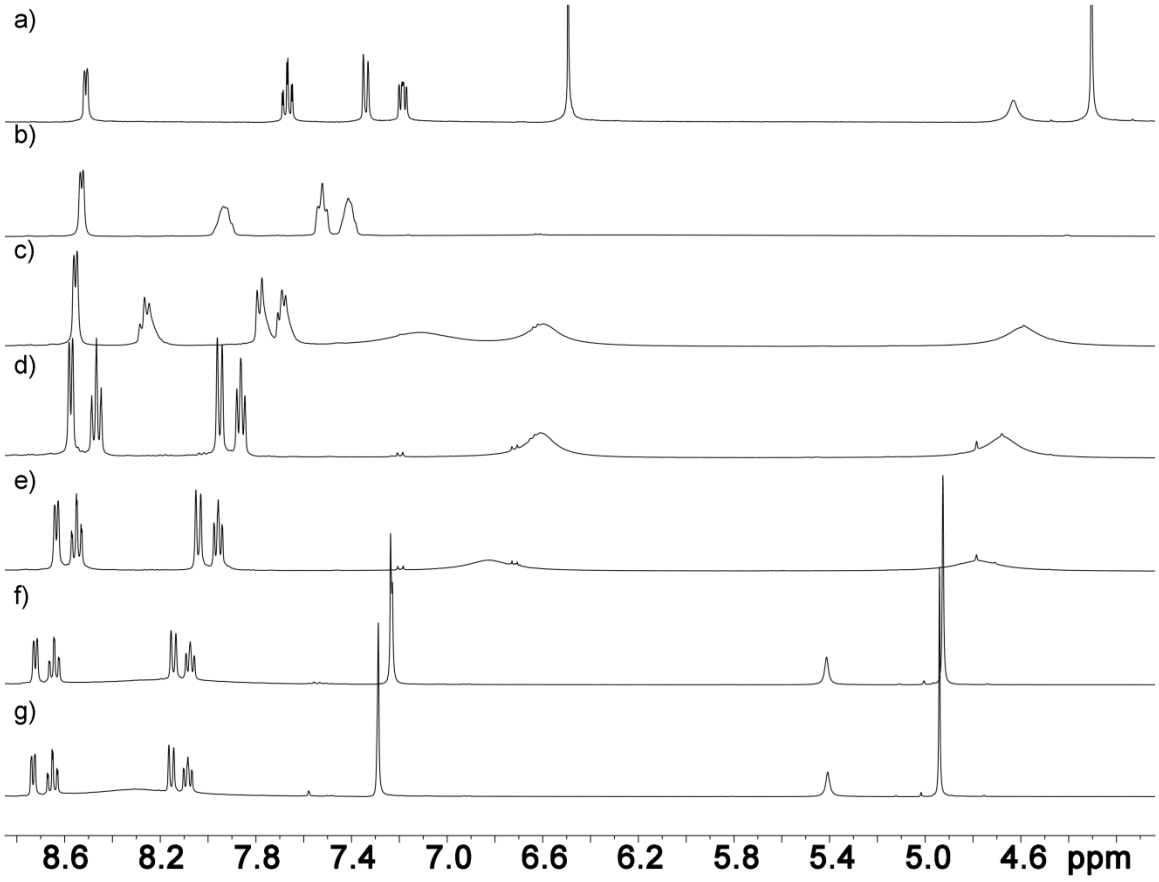

Figure 5.2: ^{1}H NMR titration of $Bi(OTf)_3$ into a solution of **5.1** (CD_3CN, 400 MHz, 298 K); a) 0 eq Bi(III); b) 0.125 eq Bi(III); c) 0.25 eq Bi(III); d) 0.38 eq Bi(III); e) 0.5 eq Bi(III); f) 1 eq Bi(III); g) 1.5 eq Bi(III).

Bi(III) is large, and although coordinated to the aminomethylpyridine it could also engage in cation-π association with the arene face of the ligand core, broadening out the signal.[11] The system could also form a self-assembly that brings the rings into close

proximity such as an M_2L_4 (Figure 5.3). This would cause gearing that slows the rotation of the rings. Addition of more $Bi(OTf)_3$ causes the peaks to sharpen up. Attempts to characterize this assembly by ESI-MS analysis were unsuccessful, and attempts to access X-ray quality crystals led only to the formation of a red, glassy substance.

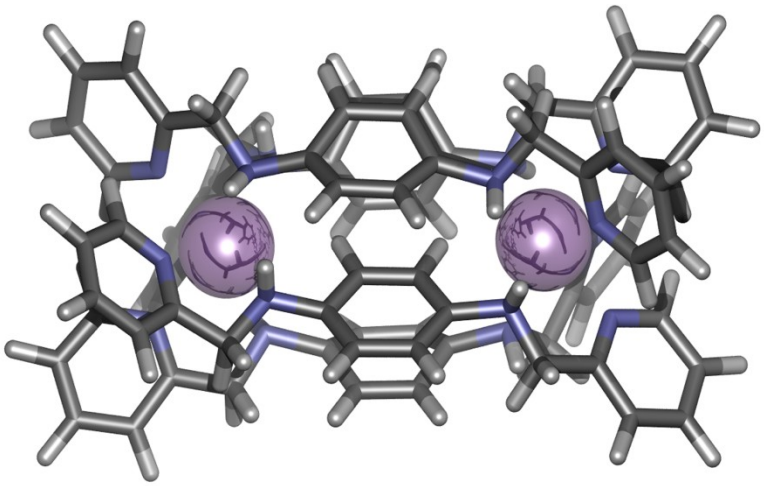

Figure 5.3: SPARTAN model of $\mathbf{[5.1_4 \bullet Bi_2]^{6+}}$ (AM1 forcefield).

Unlike **5.1**, ligand **5.2a** contains two pendant methoxy groups that may coordinate with the metal. Titration of $Bi(OTf)_3$ into an acetonitrile solution of **5.2a** again showed fast exchange between bound and unbound species. The resonances, however, stopped shifting after reaching a 1:1 ratio of ligand to metal (Figure 5.4a), suggesting some M_xL_x assembly with equal ratios of metal and ligand. The resonances for the biphenyl are also broadened in the titration. X-ray quality crystals were not forthcoming, although the presence of $\mathbf{[5.2a_4 \bullet Bi_4](OTf)_{12}}$ was confirmed by ESI-MS analysis. This species should exist as a molecular square with each ligand coordinating in a tridentate fashion to each bismuth center (Figure 5.4b).

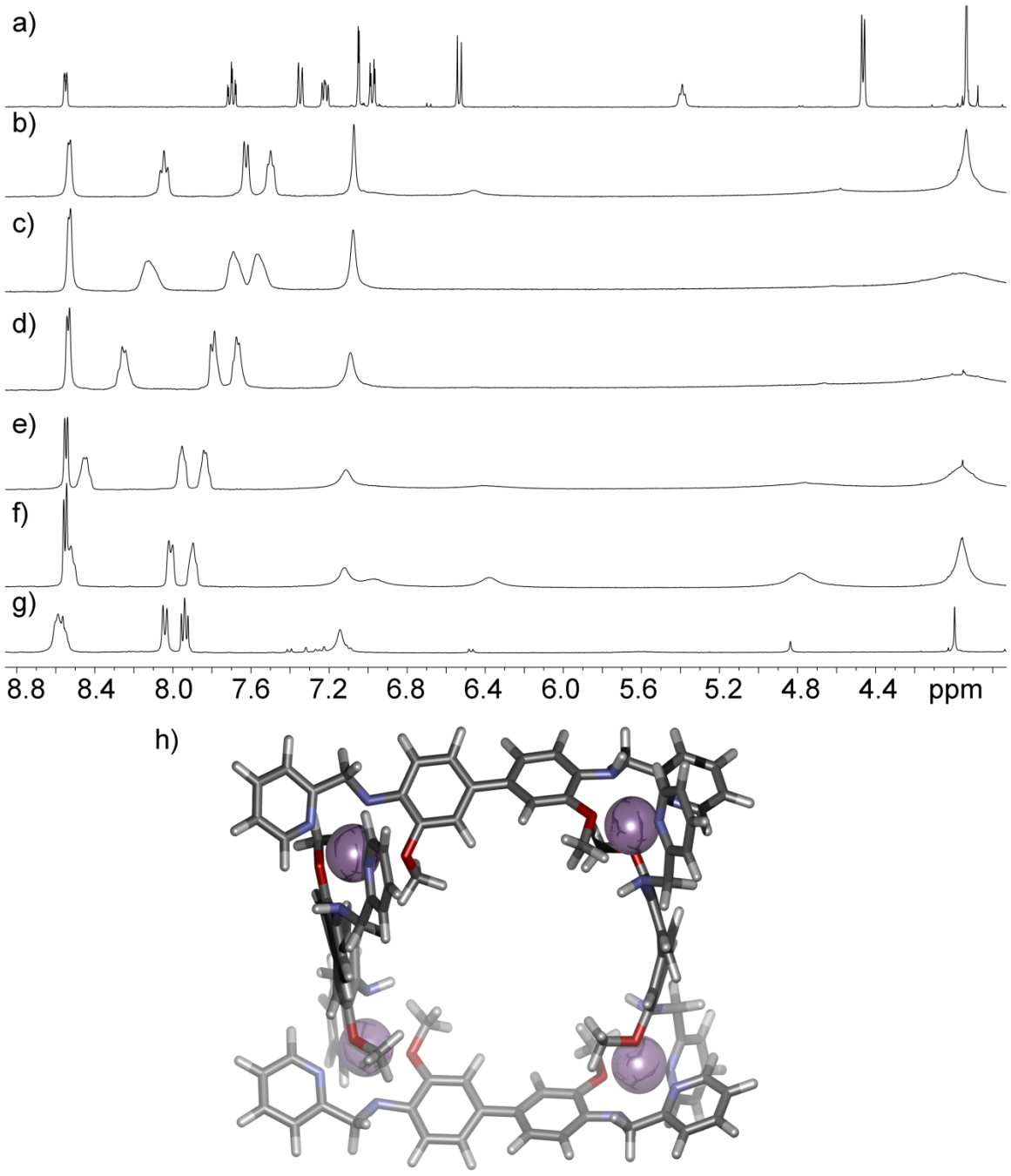

Figure 5.4: ^{1}H NMR titration of $Bi(OTf)_3$ into a solution of **5.2** (CD_3CN, 400 MHz, 298 K); a) 0 eq Bi(III); b) 0.25 eq Bi(III); c) 0.33 eq Bi(III); d) 0.5 eq Bi(III); e) 0.66 eq Bi(III); f) 0.75 eq Bi(III); g) 1 eq Bi(III); h) SPARTAN model of **[5.2$_4$•Bi$_4$]**$^{12+}$ (AM1 forcefield).

When ligand **5.2b**, was treated with $Bi(OTf)_3$, the result was very similar to that observed for **5.1** (Figure 5.5). Addition of ~10 eq. $Bi(OTf)_3$ caused the peaks to shift downfield. Attempts to verify the assembly by ESI-MS, crystallography, and even screening the binding of neutral guests proved ineffective. Titration experiments with both **5.1** and **5.2a** showed that the resonances stopped shifting downfield after addition of a single equivalent of bismuth(III). Ligand **5.2b**, however, required considerably more bismuth to reach the end point, suggesting the addition of the bulky methyl groups hinders complex formation.

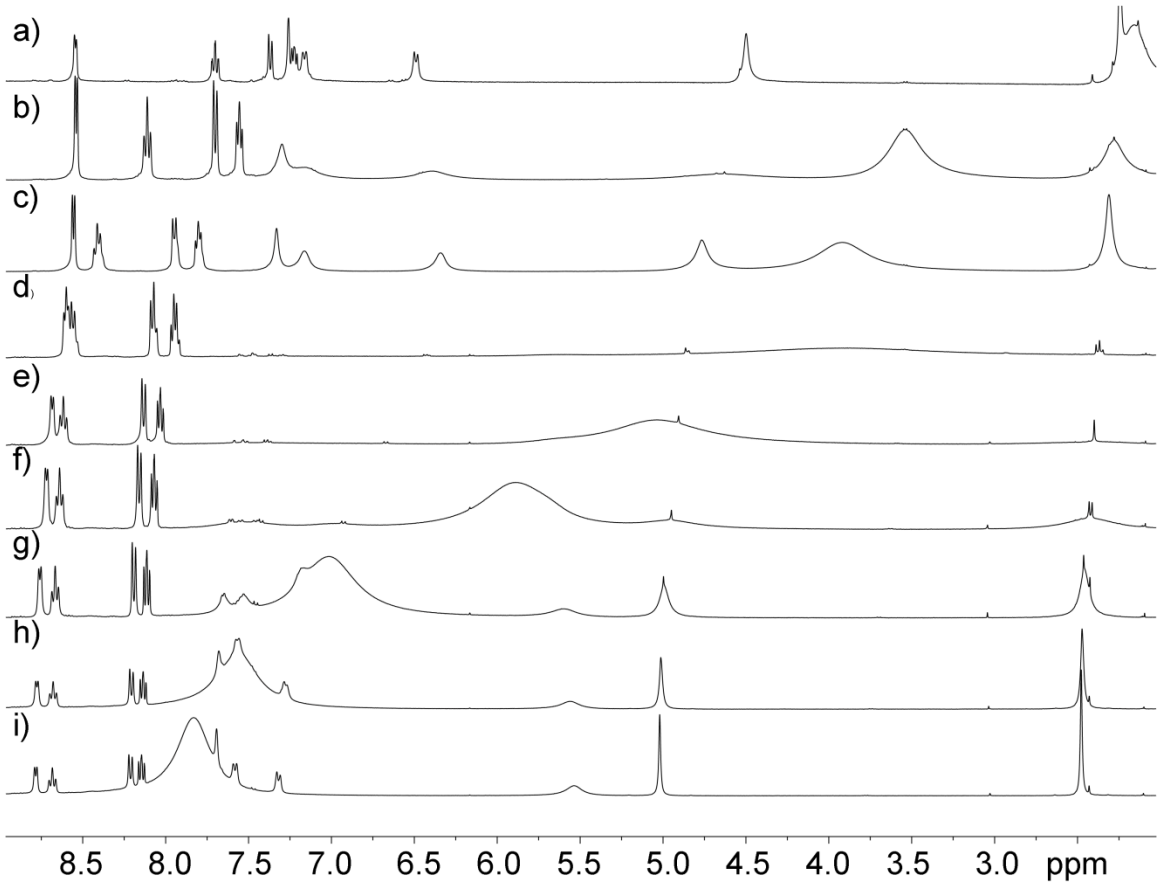

Figure 5.5: ^{1}H NMR spectra of **5.2b** titrated with $Bi(OTf)_3$ (CD_3CN, 400 MHz, 298 K: a) **5.2b**; b) 0.33 eq Bi(III); c) 0.66 eq Bi(III); d) 1.0 eq Bi(III); e) 2.0 eq Bi(III); f) 4.0 eq Bi(III); g) 6.0 eq Bi(III); h) 8.0 eq Bi(III); i) 10.0 eq Bi(III).

Aminomethylpyridines **5.1**, **5.2a**, and **5.2b** were ineffective chelators, suggesting a more robust motif was necessary. Ligand **5.4** was prepared by condensation of *o*-tolidine with 2-formylpyridine. When $Bi(OTf)_3$ was titrated into an acetonitrile solution of **5.4** there was evidence of coordination, as well as the presence of2-formylpyridine. This suggests the Lewis acidic bismuth(III) promotes hydrolysis of the ligand due to adventitious water present in the acetonitrile. Rather than regenerating both aldehyde and aniline, the aniline becomes at least partially oxidized as evidenced by the downfield shift of the corresponding resonances.

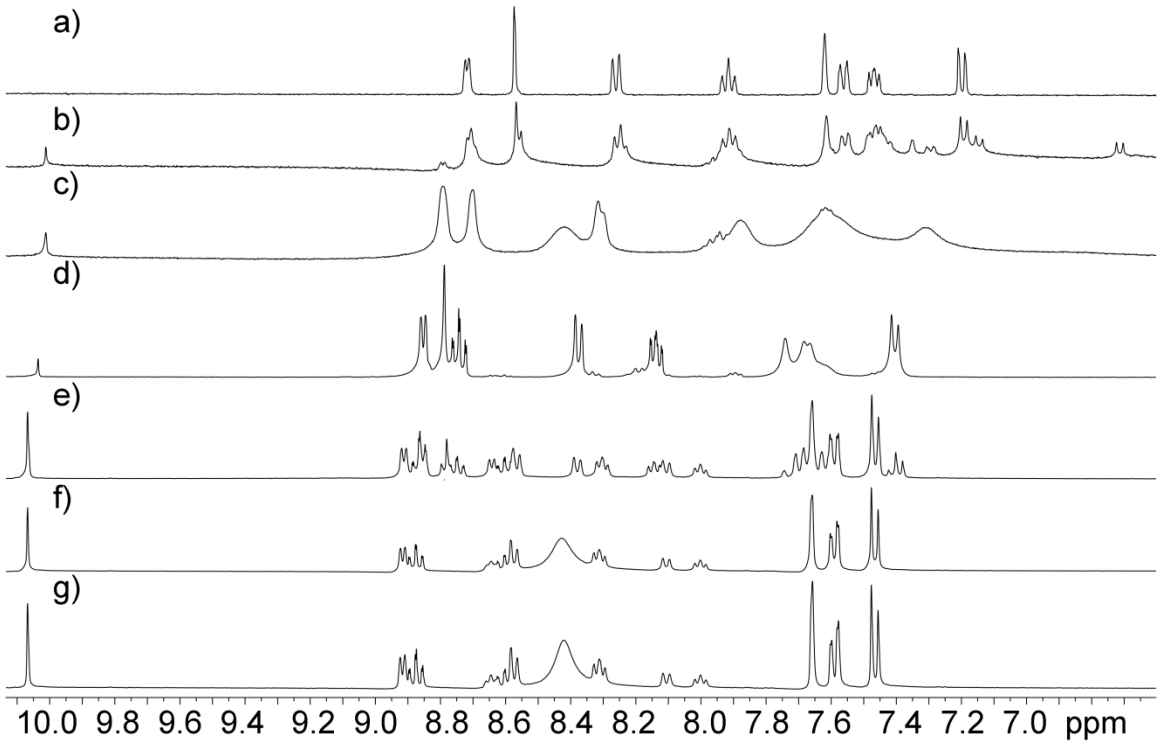

Figure 5.6: ^1H NMR spectra of **5.4** titrated with $Bi(OTf)_3$ (CD_3CN, 400 MHz, 298 K: a) **5.4**; b) 0.25 eq Bi(III); c) 0.33 eq Bi(III); d) 0.5 eq Bi(III); e) 0.66 eq Bi(III); f) 0.75 eq Bi(III); g) 1.0 eq Bi(III); h) 8.0 eq Bi(III); i) 10.0 eq Bi(III).

5.3 Tridentate Ligands for Preparing Self-Assemblies with Bismuth

One challenge of preparing complexes between Bi(III) and bidentate ligands was that the binding was weak. This binding could be maximized by an additional contact contributed by a tridentate chelator. The new chelator was based on an extended form of the iminopyridine ligands. The compound 4,4-biphenyl dicarboxylic acid was treated with *O*-(1H-6-Chlorobenzotriazole-1-yl)-1,1,3,3-tetramethylaminium hexafluorophosphate (HCTU) in the presence of triethylamine to afford an activated ester that could then be treated with hydrazine to afford bis-hydrazide **5.5** in good yield (Figure 5.7).[12] Condensation of this compound with salicylaldehyde afforded the desired ligand **H_2•5.6** in excellent yield.

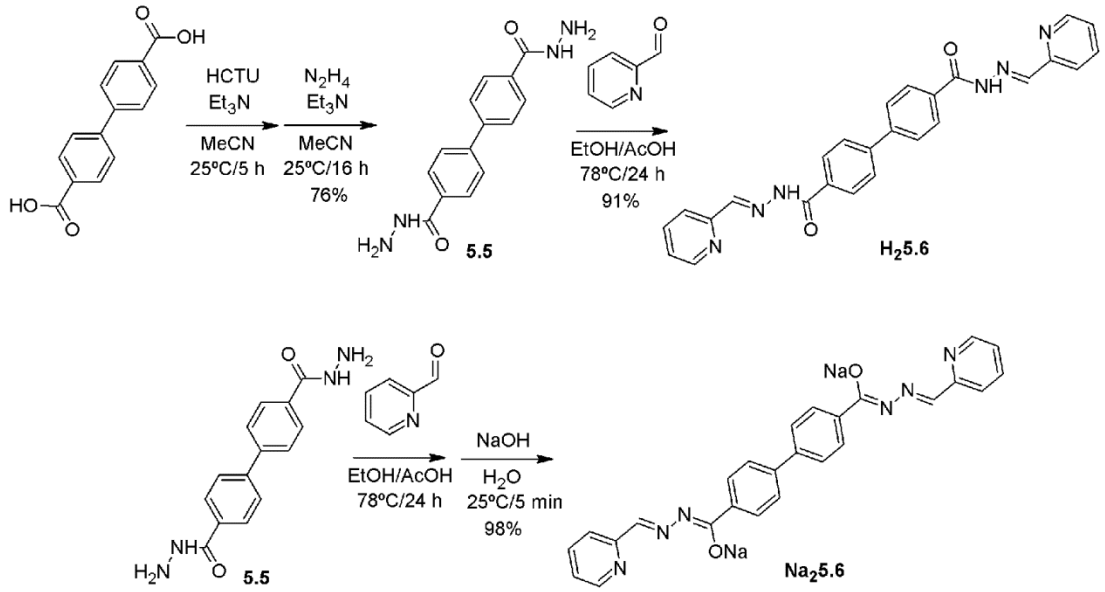

Figure 5.7: Synthesis of bis-(2-pyridyl)acylhydrazone ligands **H_2•5.6** and **Na_2•5.6**.

Complexation of $Bi(OTf)_3$ by **H_2•5.6** was initially studied in DMSO-d_6 due to the insolubility of the ligand in other solvents. The ligand was unable to outcompete the

solvent, and no complexation was observed. The sodium salt **Na_2•5.6** was prepared by washing the protonated ligand with aqueous sodium hydroxide to give a yellow solid (Figure 5.7). When 0.25 equivalents of $Bi(OTf)_3$ were added to a DMSO solution of **Na_2•5.6**, a new set of low intensity peaks appeared in the ^{1}H NMR spectrum. Addition of more bismuth led to formation of a second species that did not shift after approximately 0.66 equivalents of $Bi(OTf)_3$. As $Bi(OTf)_3$ was added to the solution, a peak just above 12 ppm appeared, followed by a second. Comparison with the ^{1}H NMR spectrum of **H_2•5.6** suggests these peaks are the result of partial protonation of the ligand in wet DMSO.

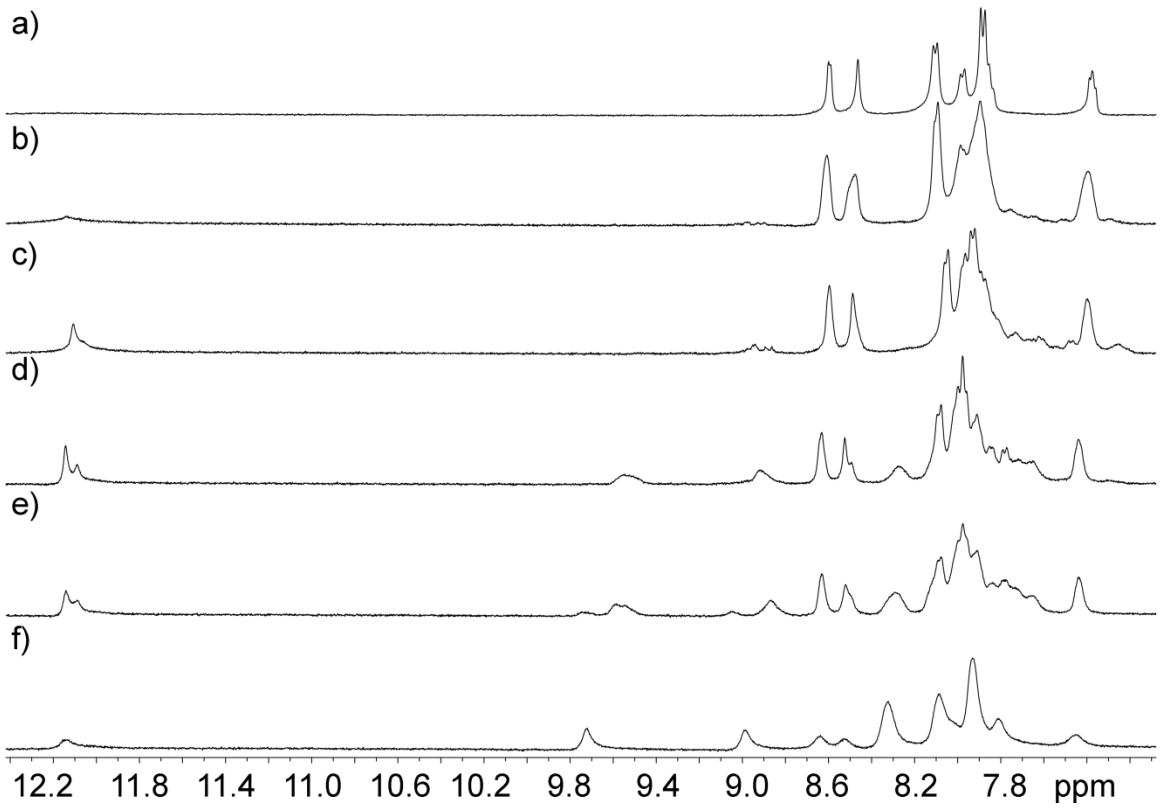

Figure 5.8: ^{1}H NMR spectra of **Na_2•5.6** titrated with $Bi(OTf)_3$ (DMSO-d_6; 400 MHz, 298 K): a) **Na_2•5.6**; b) 0.25 eq Bi(III); c) 0.33 eq Bi(III); d) 0.5 eq Bi(III); e) 0.66 eq Bi(III); f) 0.75 eq Bi(III); g) 1.0 eq Bi(III); h) 8.0 eq Bi(III); i) 10.0 eq Bi(III).

The titration experiment suggested that **[5.6$_6$•Bi$_4$]** was formed, and this began to precipitate from solution after complexation. Attempts to characterize this species by X-ray crystallography were unsuccessful. Crystals could be grown, but these were of the fully protonated ligand **H$_2$•5.6**. The acyl hydrazone is not strongly acidic, and once protonated can crystallize through a combination of favorable π-stacking and hydrogen bonding between neighboring acyl hydrazones.

Attempts to characterize this structure by ESI-MS were also challenging because of its poor solubility, although the complex was sparingly soluble in acetonitrile as determined by fluorescence spectroscopy. ESI-MS analysis did not show the anticipated M_4L_6 structure, and the largest species that could be detected was an M_3L_3 species.

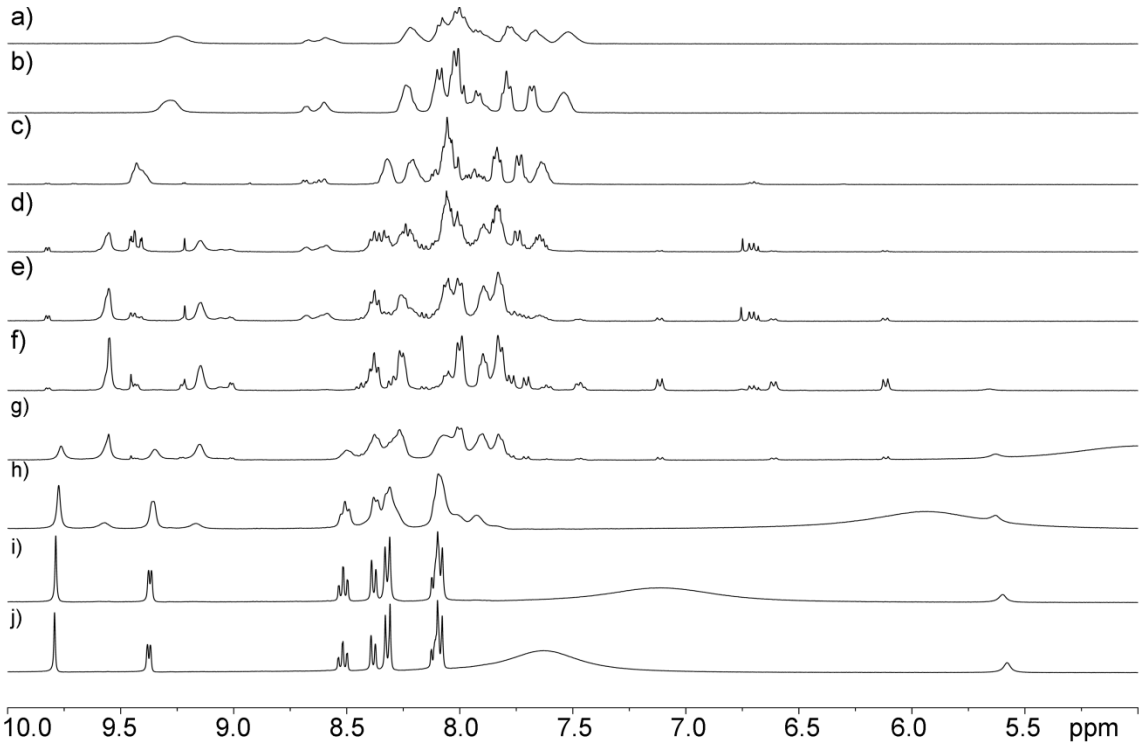

Figure 5.9: ^{1}H NMR spectra of **H$_2$•5.6** titrated with Bi(OTf)$_3$ (CD_3CN; 400 MHz, 298 K: a) 0.25 eq Bi(III); b) 0.33 eq Bi(III); c) 0.5 eq Bi(III); d) 0.66 eq Bi(III); e) 0.75 eq Bi(III); f) 1.0 eq Bi(III); g) 1.5 eq Bi(III); h) 2.0 eq Bi(III); i) 3.0 eq Bi(III); j) 4.0 eq Bi(III).

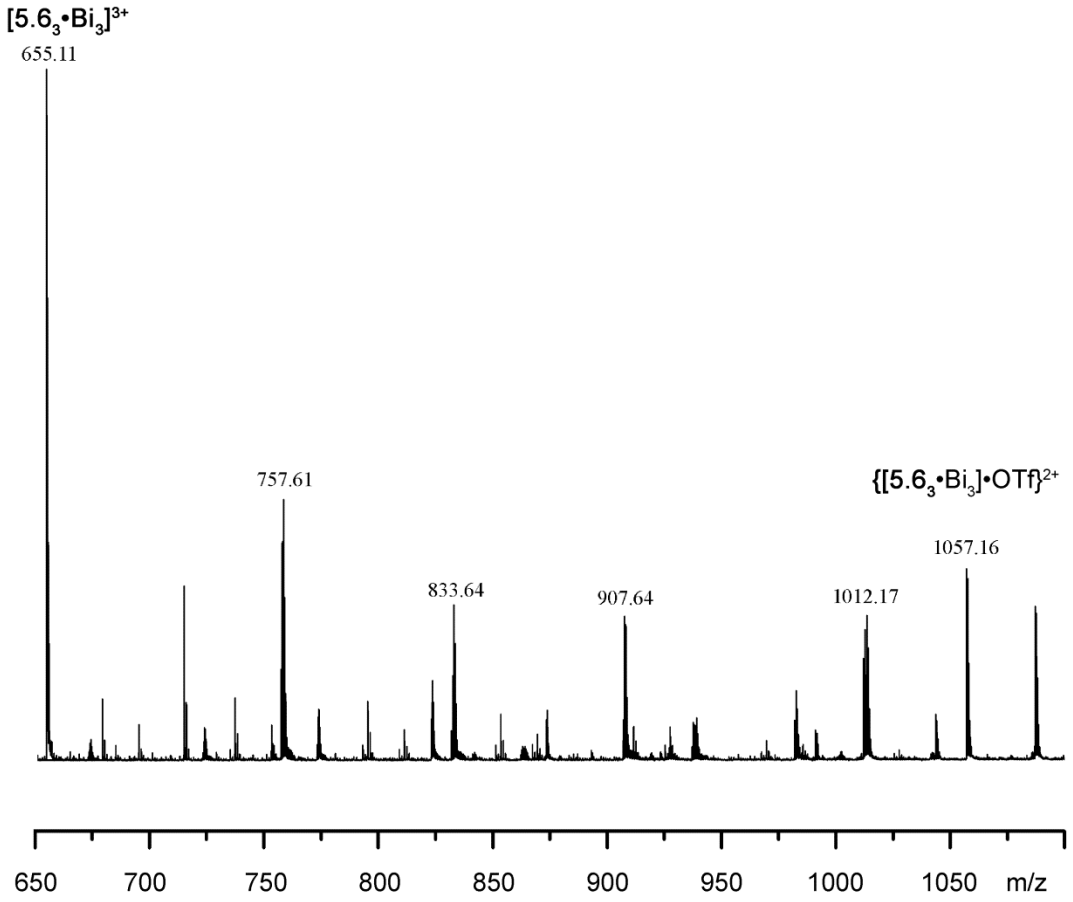

Figure 5.10. ESI-MS spectrum of **[(H_2•5.6)$_3$•Bi_3](OTf)$_9$** (MeCN).

As DMSO was too strongly coordinating for **H_2•5.6** to competitively bind bismuth, the less competitive solvent acetonitrile was used. Although **H_2•5.6** was not soluble in CD_3CN, addition of $Bi(OTf)_3$ to a suspension of the protonated ligand led to dissolution (Figure 5.9). At first the peaks were broad, but as additional $Bi(OTf)_3$ was added these gave way to new, sharper peaks further downfield. This indicates that there are different species in slow exchange with each other depending on the bismuth concentration. Increasing the $Bi(OTf)_3$ concentration to above two mol.-eq. gave rise to a single

species. ESI-MS analysis showed the presence of the M_3L_3 species (Figure 5.10), just as it had for the deprotonated ligand. The species formed at lower concentrations of bismuth could not be characterized by ESI-MS analysis, and attempts to grow crystals by either vapor diffusion or slow evaporation from acetonitrile failed to give these or the M_3L_3 species.

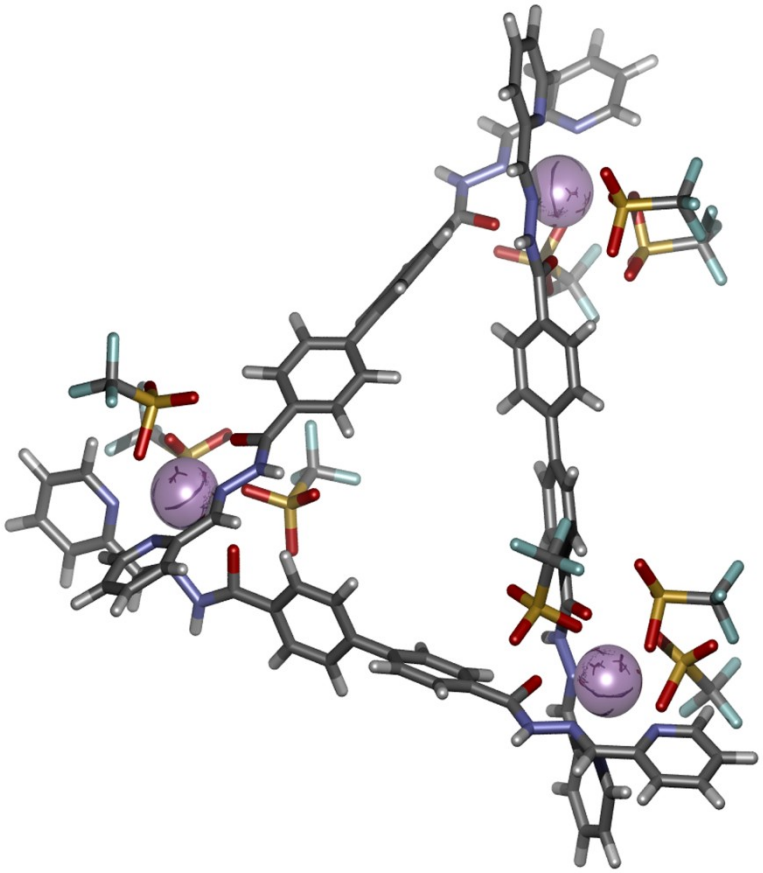

Figure 5.11. SPARTAN model of **$[(H_2 \bullet 5.6)_3 \bullet Bi_3](OTf)_9$**.

The exact nature of the other self-assemblies could not be directly determined, but data obtained for a "V-shaped" analogue suggested these structures are cages with higher coordination number for bismuth.[12] In the proposed M_3L_3 complex, the bismuth ion would only form six coordinate bonds with the organic ligands, while the rest of the

coordination sphere would be filled by triflate ions or solvent molecules. The bent analogue showed evidence that an M_2L_4 complex formed first. Increasing the bismuth concentration led to an M_2L_3 and finally an M_2L_2 assembly. For **H_2•5.6**, these other structures may include the M_4L_6, as well as some larger but entropically disfavored M_xL_x structures. A molecular triangle for **$[(H_2•5.6)_3•Bi_3](OTf)_9$** was modeled in which each metal is bound to two organic ligands and three triflates (Figure 5.11).

Molecular modeling with SPARTAN suggested that if **$[(H_2•5.6)_6•Bi_4](OTf)_{12}$** formed, it might be able to bind a complementary-shaped guest such as adamantane (Figure 5.12a). **H_2•5.6** was added to an NMR tube with one equivalent of adamantane (Figure 5.12b-h). As $Bi(OTf)_3$ was added, the adamantane peaks, that were initially distinct, began to broaden out and shift slightly upfield as formation of complex occurred. The ^1H NMR spectra of the assemblies looked different than they had in the absence of adamantane, although he identity of the host:guest complex could not be determined by ESI-MS analysis, nor could crystals be grown.

Terphenyl ligands **H_2•5.7** and **H_2•5.8** were prepared (Figure 5.13) to determine if extension of the backbone was accommodated in these complexes. The diester precursors were prepared by Suzuki-cross coupling between *p*-dibromide reagents and 4-ethoxycarbonylphenyl boronic acid. These proceeded in moderate yield to give the diesters **5.9** and **5.10**, which were then treated with hydrazine to give the desired dihydrazides **5.11** and **5.12** respectively. Synthesis of **5.12** required a co-solvent due to the low solubility of **5.10** in hot hydrazine. These hydrazides were then converted into ligands **H_2•5.7** and **H_2•5.8** through condensation with 2-formylpyridine, similar to the synthesis of **H_2•5.6**.

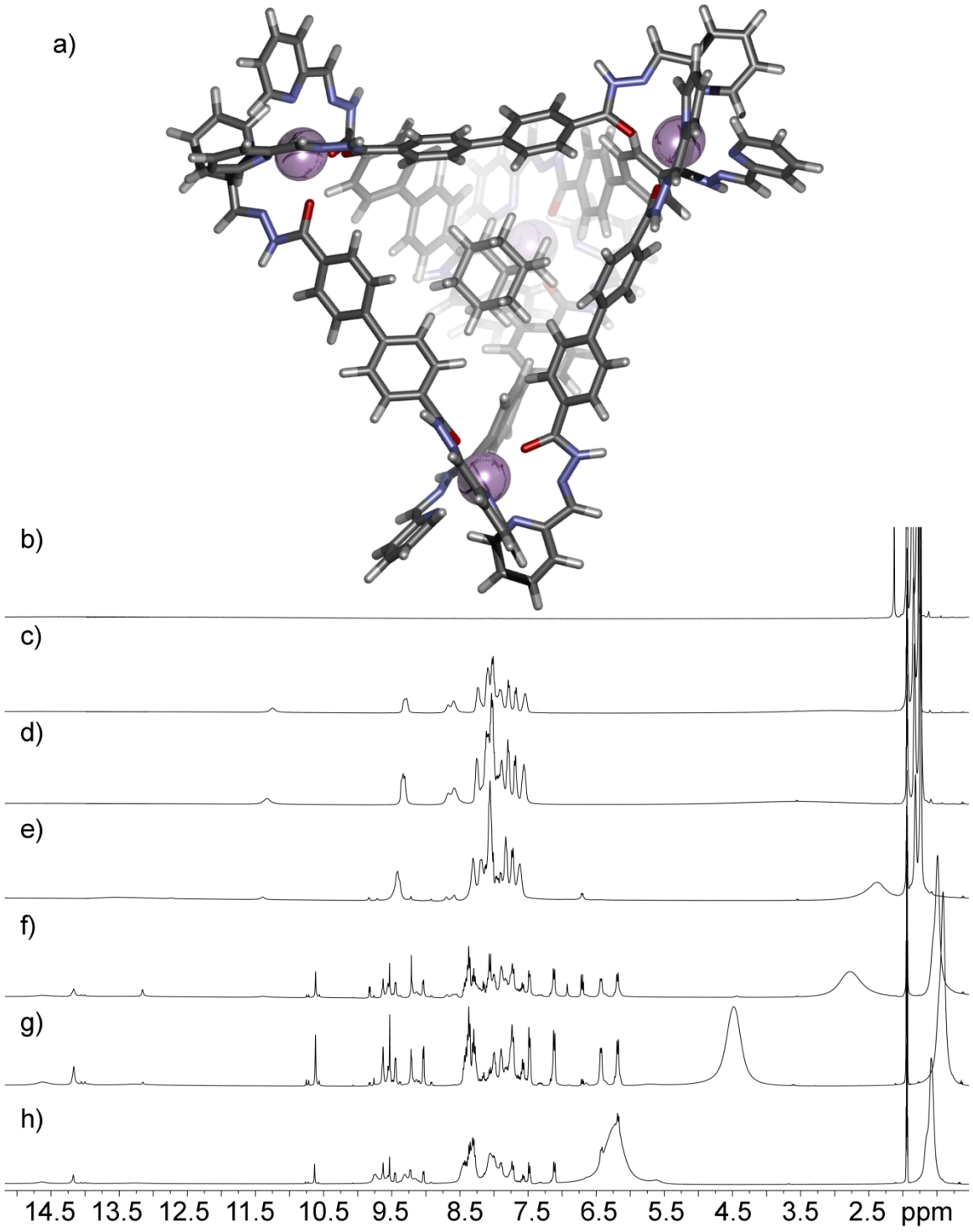

Figure 5.12: Guest-templation study of bismuth cages: a) SPARTAN model of **[adamantane⊂(H_2•5.6)$_6$•Bi_4]$^{12+}$**; b) ^{1}H NMR spectra of **H_2•5.6** titrated with Bi(OTf)$_3$ (CD_3CN; 400 MHz, 298 K): b) adamantane; c) 0.33 eq Bi(III); d) 0.66 eq Bi(III); e) 1.0 eq Bi(III); f) 1.5 eq Bi(III); g) 2.0 eq Bi(III); h) 3.0 eq Bi(III).

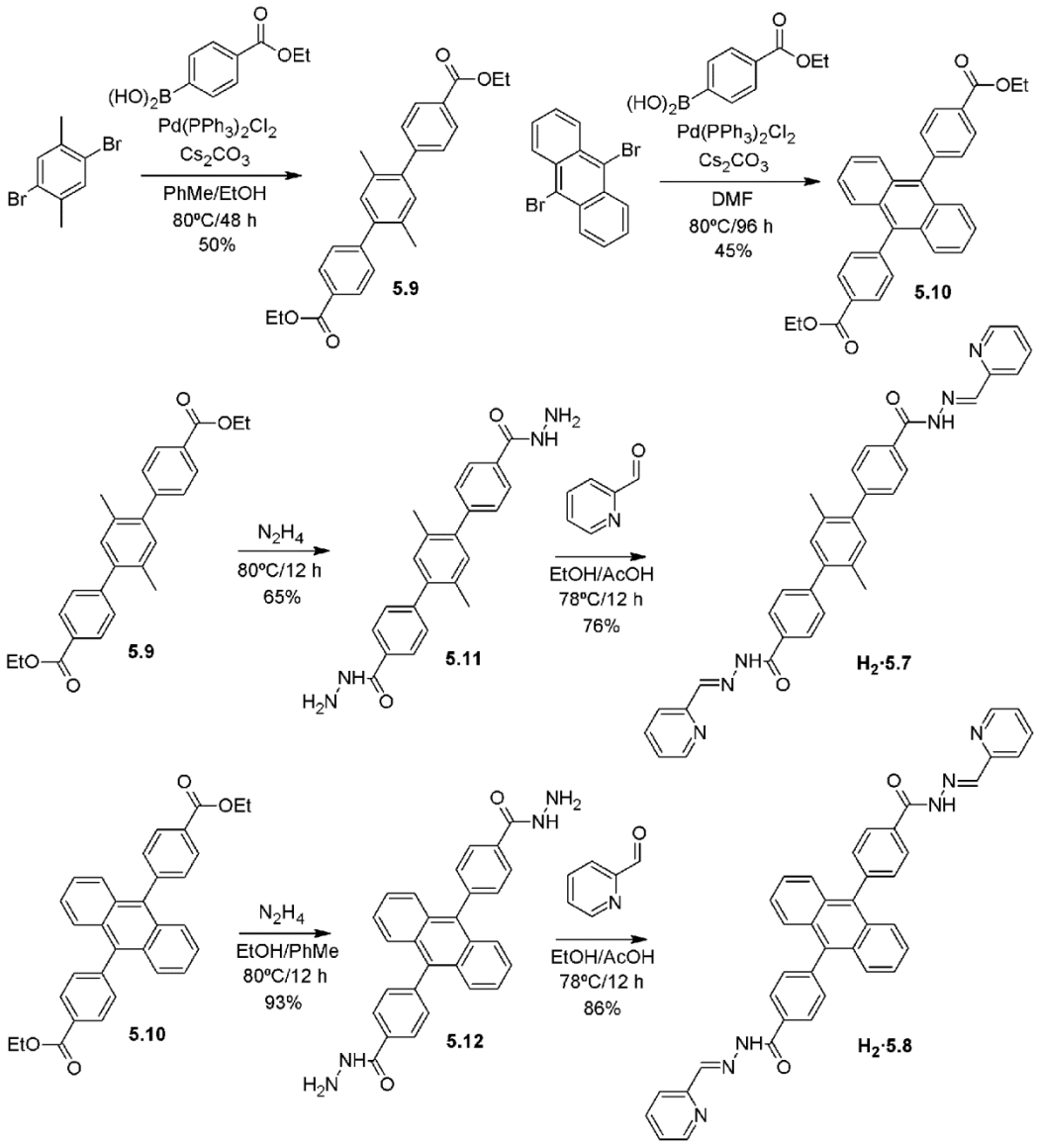

Figure 5.13: Synthesis of 2-pyridylhydrazone ligands **H_2•5.7 and H_2•5.8**.

Titration of $Bi(OTf)_3$ into a suspension of **H_2•5.7** in deuterated acetonitrile led to the formation of a complex that looked similar to that observed by titrating $Bi(OTf)_3$ into **H_2•5.6**. Analysis of the complex by ESI-MS confirmed the existence of **$[(H_2•5.7)_3•Bi_3](OTf)_9$**. There was no evidence of diastereomers in solution, suggesting

this self-assembly motif is less sensitive than the Fe(II)-iminopyridine scaffold to decreased diastereoselectivity.

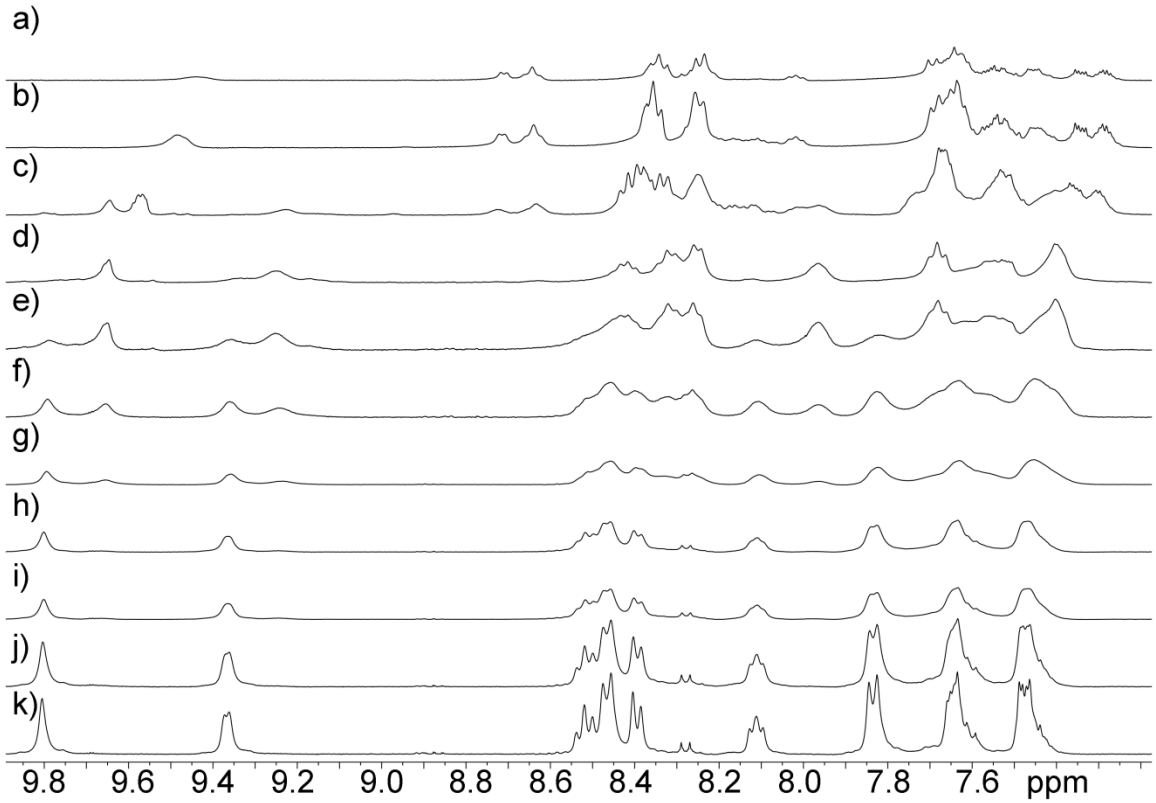

Figure 5.14: ^{1}H NMR spectra of **H_2•5.8** titrated with $Bi(OTf)_3$ (CD_3CN; 400 MHz, 298 K): a) 0.33 eq Bi(III); b) 0.66 eq Bi(III); c) 1.0 eq Bi(III); d) 1.5 eq Bi(III); e) 2.0 eq Bi(III); f) 3.0 eq Bi(III); g) 4.0 eq Bi(III); h) 5.0 eq Bi(III); i) 6.0 eq Bi(III); j) 8.0 eq Bi(III); k) 10.0 eq Bi(III).

Treatment of the anthracene ligand **H_2•5.8** with $Bi(OTf)_3$ showed a similar trend (Figure 5.14), although the formation of a single species required more bismuth than either **H_2•5.6** or **H_2•5.7**. Almost six full equivalents of bismuth were required to reach the endpoint of the titration. ESI-MS showed only the M_3L_3 species **$[(H_2•5.7)_3•Bi_3](OTf)_9$**. This implies that even a small amount of steric bulk, as in the case of **$[5.4_x•Bi_y](OTf)_{3y}$**, can negative impact the self-assembly process.

5.4 Conclusions

Self-assembly of bismuth(III) salts can be used to form supramolecular assemblies. The complexes all display weak binding, and this leads to variable coordination of the bismuth. These complexes exist in equilibrium with each other, and the interconversion is controlled as a function of bismuth concentration. The results suggest that smaller species are favored due to entropy, allowing the coordination number of to be controlled. Unlike transition metal-based complexes, these bismuth supramolecular cages show complete diastereoselectivity across different chelators and ligand sizes.

5.5 References

1) a) Caulder, D. L.; Brückner, C.; Powers, R. E.; König, S.; Parac, T. N.; Leary, J. A.; Raymond, K. N. "Design, Formation and Properties of Tetrahedral M_4L_4 and M_4L_6 Supramolecular Clusters." *J. Am. Chem. Soc.*, **2001**, *123*, 8923-8938; b) Sun, X.; Johnson, D. W.; Caulder, D. L.; Powers, R. E.; Raymond, K. N.; Wong, E. H. "Exploiting Incommensurate Symmetry Numbers: Rational Design and Assembly of $M_2M'_3$, L_6 Supramolecular Clusters with C_{3h} Symmetry." *Angew. Chem. Int. Ed. Engl.*, **1999**, *38*, 1303-1307.

2) Mugridge, J. S.; Fiedler, D.; Raymond, K. N. "A Ferrocene-Based Catecholamide Ligand: The Consequences of Ligand Swivel for Directed Supramolecular Self-Assembly." *J. Coord. Chem.*, **2010**, *63*, 2779-2789.

3) García-Zarracino, R.; Höpfl, H. "Self-Assembly of Diorganotin(IV) Oxides (R = Me, *n*Bu, Ph) and 2,5-Pyridinedicarboxylic Acid to Polymeric and Trinuclear Macrocyclic Hybrids with Porous Solid-State Structures: Influence of Substituents and Solvent on the Supramolecular Structure." *J. Am. Chem. Soc.*, **2005**, *127*, 3120-3130.

4) Onions, S. T.; Frankin, A. M.; Horton, P. N.; Hursthouse, M. B.; Matthews, C. J. "Self-Assembly of a Unique Hexadecanuclear [4 x (2 x 2)]-Pb_{16} 'Grid of Grids' Type Structure." *Chem. Commun.*, **2003**, *23*, 2864-2865.

5) Bellamy, F. D.; Ou, K. "Selective Reduction of Aromatic Nitro Compounds with Stannous Chloride in non Acidic and non Aqueous Medium." *Tetrahedron Lett.*, **1984**, *25*, 839-842.

6) Baumgarten, H. E.; Smith, H. L.; Staklis, A. "Reactions of Amines. XVIII. Oxidative Rearrangement of Amides with Lead Tetraacetate." *J. Org. Chem.*, **1975**, *40*, 3554-3561.

7) Pitt, M. A.; Johnson, D. W. "Main Group Supramolecular Chemistry." *Chem. Soc. Rev.*, **2007**, *36*, 1441-1453.

8) Cangelosi, V. M.; Zakharov, L. N.; Johnson, D. W. "Supramolecular Transmetallation Leads to an Unusual Self-Assembled P_2L_3 Cryptand." *Angew. Chem. Int. Ed.*, **2010**, *49*, 1248-1251.

9) a) Mendoza-Espinosa, D.; Rheingold, A. L.; Hanna, T. A. "Synthesis of Bismuth and Antimony Complexes of the "Larger" Calix[*n*]arenes (*n* = 6-8); from Mononuclear to Tetranuclear Complexes." *Dalton Trans.*, **2009**, 5226-5238; b) Roggan, S.; Limberg, C.; Ziemer, B.; Brandt, M. "Intramolecular C-H Activation in Complexes with Mo-Bi Metal Bonds." *Angew. Chem. Int. Ed.*, **2004**, *43*, 2846-2849; c) Summers, S. P.; Abboud, K. A.; Farrah, S. R.; Palenik. G. J. "Syntheses and Structures of Bismuth(III) Complexes with Nitrilotriacetic Acid, Ethylenediaminetetraacetic Acid, and Diethylenetriaminepentaacetic Acid." *Inorg. Chem.*, **1994**, *33*, 88-92; d) Stewart, C. A.; Calabrese, J. C.; Arduengo, A. J., III "Synthesis and Structure of the First 20-

Bi-9 System: a Discrete Nine-Coordinate 20-Electron Bismuth." *J. Am. Chem. Soc.*, **1985**, *107*, 3397-3398.

10) Schilt, A. A.; Taylor, R. C. "Infra-red Spectra of 1:10-Phenanthroline Metal Complexes in the Rock Salt Region Below 2000 cm^{-1}." *J. Inorg. Nuc. Chem.*, **1959**, *9*, 211-221.

11) Watt, M. M.; Collins, M. S.; Johnson, D. W. "Ion-π Interactions in Ligand Design for Anions and Main Group Cations." *Acc. Chem. Res.*, **2013**, *46*, 955-966.

12) Johnson, A. M.; Young, M. C.; Hooley, R. J. "Reversible Multicomponent Self-Assembly Mediated by Bismuth Ions." *Dalton Trans.*, **2013**, *42*, 8394-8401.

Chapter 6 – Self-Assembly and Guest Binding Properties of Cages Containing Lanthanides and Actinides

6.1 Rationale

The limitation in the use of bismuth (III) for self-assembly was its weak association with simple ligands, but the concept of using non-transition metals for making self-assembled cages is still valid. There has been recent interest in the preparation of lanthanide[1] and actinide[2] cages using similar strategies to those designed for transition metals. Lanthanides, which are most commonly encountered in the +3 oxidation state, provide a useful platform for studying self-assembly. They are redox stable, and are known to be oxophilic.[3] Examples of lanthanide-based cages have also not shown the stereochemical challenges that plague many bidentate transition metal-based cages.

The differences in size across the lanthanide series, coupled with their similar electronic properties, make them well suited for tuning the properties of cages by adjusting the size of the metal vertices and studying the subtle effects of metal size on the self-assembly process.[4] In addition, many Ln(III) complexes are luminescent,[5] which allows other analysis techniques to study the binding of weak or poorly soluble guests that cannot be studied adequately by NMR spectroscopy.

6.2 Exploration of Salicylaldehyde-Derivatized Acylhydrazones for Supramolecular Self-Assembly

The tridentate ligands from Chapter 5, **H_2•5.6**, **H_2•5.7**, and **H_2•5.8**, share an N,N,O-based chelator that has been used in the synthesis of cages with Ce(III).[6] These lanthanide-based cages promote reactions using open coordination sites on their

cationic metal centers, but were limited to the solid state. More robust assemblies were achieved, however, when the pyridine group was exchanged for a phenol.[7] This chelator formed stable solution-phase Ce(III) and Ce(IV) cages, suggesting it would be robust for preparing functionalized cages. Ligand **H_4•6.1** was synthesized in one step by condensation of the dihydrazide with salicylaldehyde in ethanol (Figure 6.1) to study the assembly of lanthanides with this (2-phenoxy)acylhydrazone ligand.

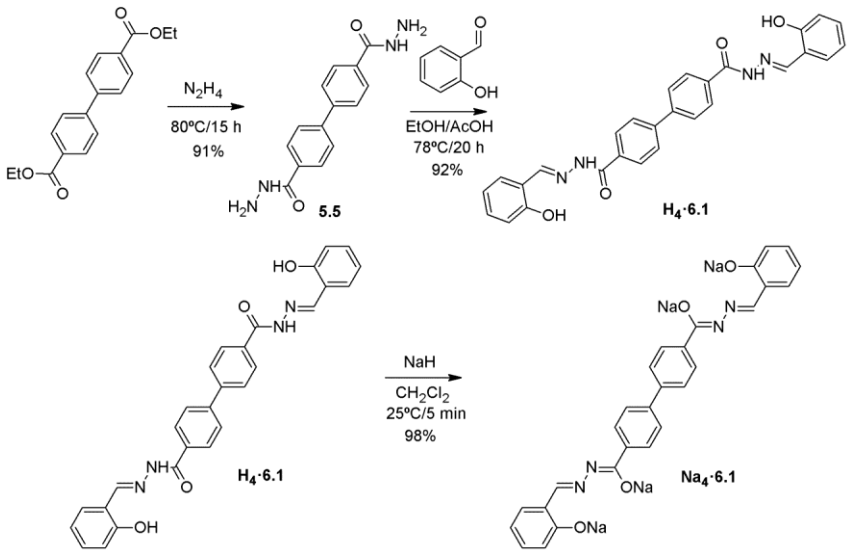

Figure 6.1: Synthesis of bis-(2-phenoxy)acylhydrazone ligand **H_4•6.1** and tetrasodium **Na_4•6.1**.

Literature precedent for the formation of lanthanide cages based on this (2-phenoxy)acylhydrazone chelator required combining the ligand and metal in a biphasic solvent mixture in the presence of an alkoxide base and crystallization of the assembly.[8] Attempts to replicate this procedure with **H_4•6.1**, however, were unsuccessful. In the presence of sodium methoxide or sodium hydroxide, the protonated ligand was found to preferentially crystallize. The formation of cage required deprotonation of the phenol proton, and so this was performed before attempting crystallization. Deprotonation of **H_4•6.1** was achieved by sonication of the ligand and sodium hydride in an anhydrous

solvent such as dichloromethane. The tetrasodium **Na_4•6.1** also preferentially crystallized after reprotonating, giving crystals of **H_4•6.1**.

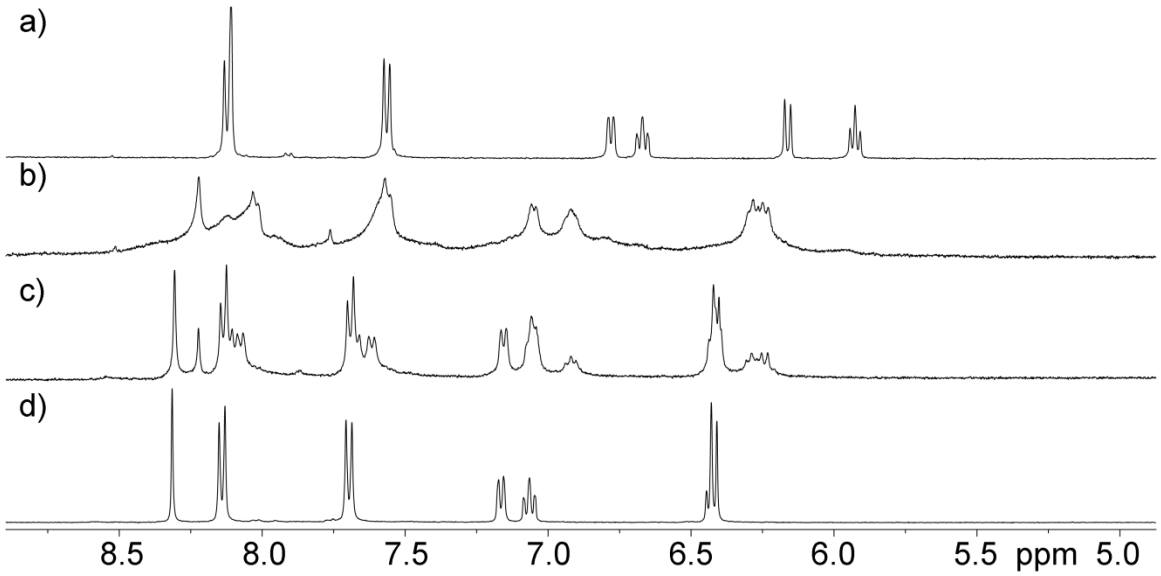

Figure 6.2: ^{1}H NMR titration of **Na_4•6.1** with La(OTf)$_3$ (DMSO-d_6, 400 MHz, 298 K): a) **Na_4•6.1**; b) 0.33 eq La(III); c) 0.50 eq La(III); d) 0.66 eq La(III).

Analysis by ^{1}H NMR spectroscopy showed that the peaks for ligand shifted downfield occurred when lanthanum(III) was added to a DMSO solution of the tetrasodium salt **Na_4•6.1**. The titration of La(OTf)$_3$ into solution of ligand confirmed that self-assembly occurred readily, and the end point suggests that the product assembly forms with a 3:2 ratio of ligand to metal. The shape of this ligand, similar to the iminopyridine motif discussed in Chapters 2, 3, and 4, prevents formation of the M_2L_3, suggesting formation of the tetrahedral M_4L_6.

Other lanthanides could also form complexes with **Na_4•6.1** (Figure 6.3). The lanthanide-surrogate yttrium and some lanthanides (Figure 6.3a-c) gave non-paramagnetically shifted spectra. Praeseodymium triflate, however, caused a dramatic

downfield shift for many of the proton resonances (Figure 6.3d). Ytterbium(III) led to a fairly significant upfield shift of many of the proton resonances instead (Figure 6.3e). In addition to lanthanum triflates, **Na_4•6.1** could also form these complexes with lanthanum nitrates and lanthanum chlorides.

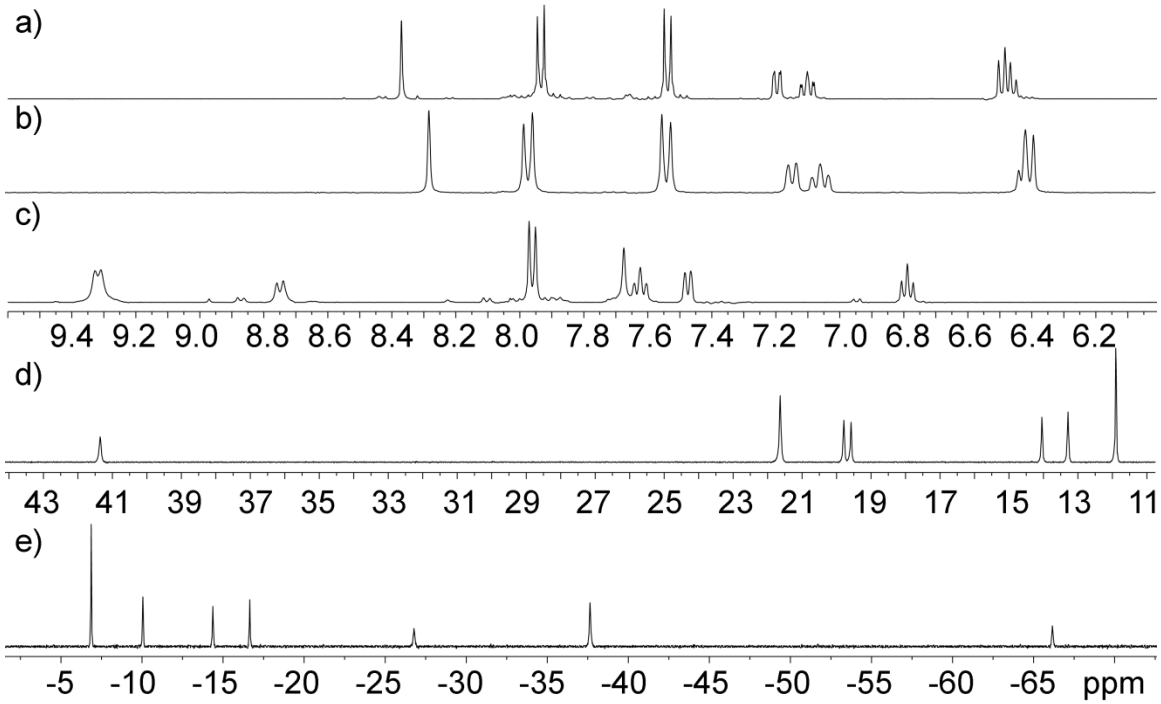

Figure 6.3: ^{1}H NMR spectra of various **$[6.1_x$•$Ln_y]^{z-}$** complexes (DMSO-d_6, 400 MHz, 298 K): a) **Na_4•6.1** + $Y(OTf)_3$; b) **Na_4•6.1** + $La(OTf)_3$; c) **Na_4•6.1** + $Sm(OTf)_3$; d) **Na_4•6.1** + $Pr(OTf)_3$; e) **Na_4•6.1** + $Yb(OTf)_3$.

These complexes were insoluble in solvents other than DMSO and DMF. Despite literature precedent for ESI-MS analysis of similar cages from mixtures of DMF and MeOH, only ligand was observed when any of the **$[6.1_x$•$Ln_y]^{z-}$** complexes were subjected to ESI-MS analysis. Although **H_4•6.1** added to THF with potassium t-butoxide and $La(OTf)_3$ led to a dilute solution of cage, this also failed to show any ions other than those from ligand. Analysis of these lanthanide complexes by UV/Vis spectroscopy

showed significant changes in the UV/Vis absorbance upon addition of metal. When the complexes were analyzed by fluorescence emission spectroscopy, the only emission was determined to be ligand-based, with very little shift from the emission of the free ligand. The addition of metal actually decreased the amount of fluorescence. There was an inverse relationship between the molecular weight of the metal and the fluorescence emission.

The poor solubility of these complexes and their inability to crystallize without extrusion of the metal ions necessitated investigation of modified end-pieces. Many functionalized salicylaldehyde derivatives are available commercially, allowing many related hydrazone ligands to be prepared (Figure 6.4). Ligands **H_4•6.2** and **H_4•6.5** were targeted for improved water solubility. Ligands **H_4•6.3** and **H_4•6.4** were expected to give greater solubility in volatile organic solvents.

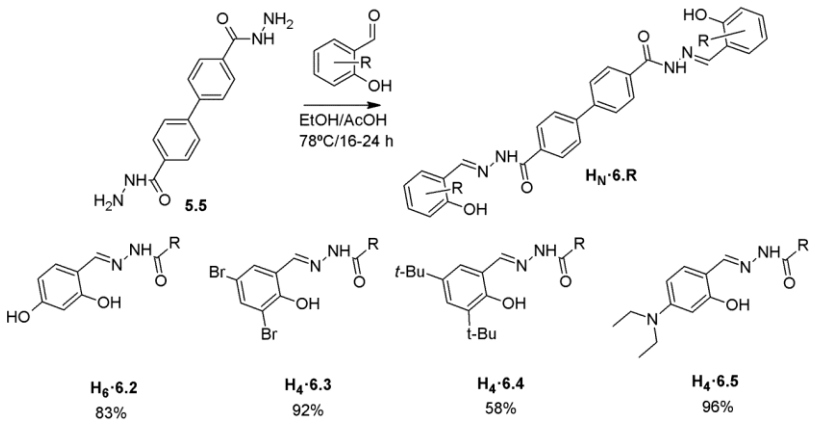

Figure 6.4: Synthesis of bis-(2-phenoxy)acylhydrazone ligands **H_6•6.2** - **H_4•6.5**.

Ligand **H_6•6.2** was ineffective for preparing lanthanide assemblies, as there was no clear sign of discrete complex formation during ^{1}H NMR titration of La(III) or Y(III) into solutions of the hexasodium salt **Na_6•6.2**. Complexation with **Na_4•6.4** occurred as metal

was added, but the tert-butyl groups result in dramatically decreased solubility, and the complex readily precipitated out of solution. This complex was not obviously more soluble in dichloromethane, chloroform, or acetonitrile than the complexes of **Na_4•6.4**. Both **H_4•6.3** and **H_4•6.5** gave similar conversion to self-assembled species upon titration of lanthanum triflate, but did not yield any crystalline complexes with $La(OTf)_3$ or $Y(OTf)_3$.

When **Na_4•6.1** was treated with $Th(NO_3)_4$•$4H_2O$ in DMSO (Figure 6.6), the ^{1}H NMR spectra were reminiscent of the variable coordination seen with Bi(III) in Chapter 5. No crystals were obtained using a variety of crystallization techniques. Although thorium nitrate is a poor alpha emitter, it was challenging to find facilities willing to analyze these species by ESI-MS, preventing analysis of the thorium adducts by mass spectrometry.

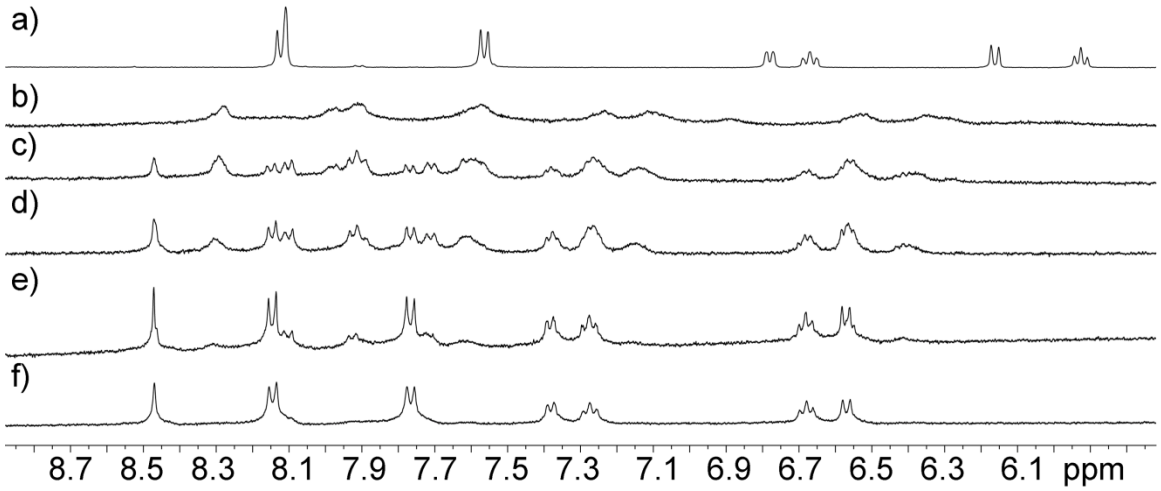

Figure 6.5: NMR titration of **Na_4•6.1** with $Th(NO_3)_4$•$4H_2O$ (DMSO-d_6, 400 MHz, 298 K): a) **Na_4•6.1**; b) 0.33 eq Th(IV); c) 0.66 eq Th(IV); d) 1.0 eq Th(IV); e) 2.0 eq Th(IV); f) 3.0 eq Th(IV).

Although the uranyl cation can accommodate as many as six ligands, it only forms planar complexes. This defined coordination sphere makes it more like a transition metal.[8] Combination of **H_4•6.1** with UO_2^{2+} should form an M_3L_3 structure, similar to that observed for **$[(H_2$•5.6$)_3$•$Bi_3](OTf)_9$**. Treatment of the protonated ligand **H_4•6.1** with

$UO_2(OAc)_2$•$2H_2O$ showed evidence of complexation, although it took over four equivalents of uranyl acetate to drive this to completion. When the tetrasodium **Na_4•6.1** was used instead, one equivalent of U(VI) was led to a single species in solution (Figure 6.6).

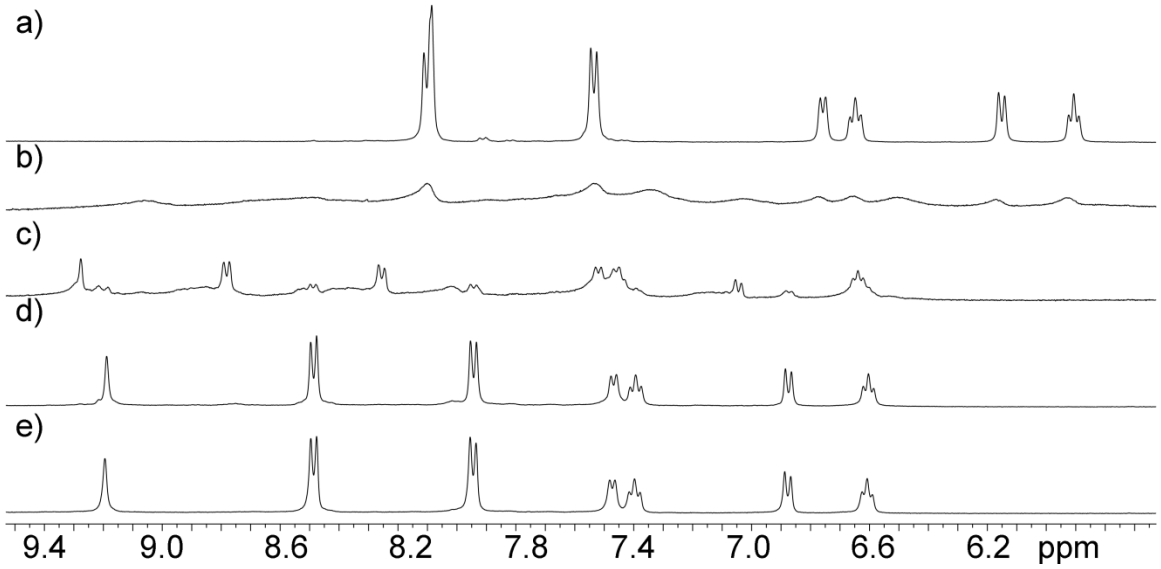

Figure 6.6: NMR titration of **Na_4•6.1** with $UO_2(OAc)_2$•$2H_2O$ (DMSO-d_6, 400 MHz, 298 K): a) **Na_4•6.1**; b) 0.33 eq U(VI); c) 0.66 eq U(VI); d) 1.0 eq U(VI); e) 2.0 eq U(VI).

Attempts to grow crystals of this complex through vapor diffusion of chloroform into DMSO gave rise to red-orange crystals. X-ray diffraction showed that instead of crystallizing as the 1:1 self-assembly observed during the ^{1}H NMR titration, the crystal contained the dinuclear **[H_2•6.1•$(UO_2)_2$•(Me_2SO)]$(OAc)_2$** (Figure 6.7). Although the closed structure forms in solution, in the solid state the M_2L is preferred.

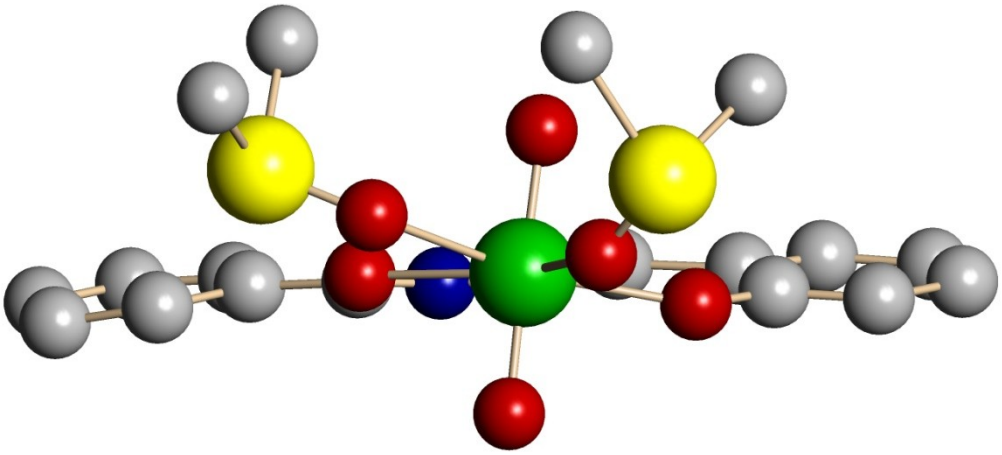

Figure 6.7: Expansion of the crystal structure of mononuclear portion of **[6.1•$(UO_2)_2$•$(Me_2SO)_4$]$(OAc)_2$**.

6.3 Terphenyl-Based Lanthanide Cages

Ligand **H_4•6.6** could be prepared by condensation of the terphenyl bis-hydrazide **5.11** with salicylaldehyde (Figure 6.9), and **H_4•6.7** could be accessed in a similar manner using bis-hydrazide **5.12**. Deprotonation also proceeded cleanly with sodium hydride to give **Na_4•6.6** and **Na_4•6.7**. Both ligands showed 3:2 adducts with lanthanide (III) salts. No crystals were observed for **Na_4•6.6** treated with $La(OTf)_3$, while **Na_4•6.7** combined with $La(OTf)_3$ led to crystallization of the protonated ligand **H_4•6.7**. The strong fluorescence emission of **[6.7_6•La_4]$^{12-}$** suggested it would be suitable to study guest binding. In DMSO, however, there was no sign of guest binding for a variety of aliphatic and aromatics.

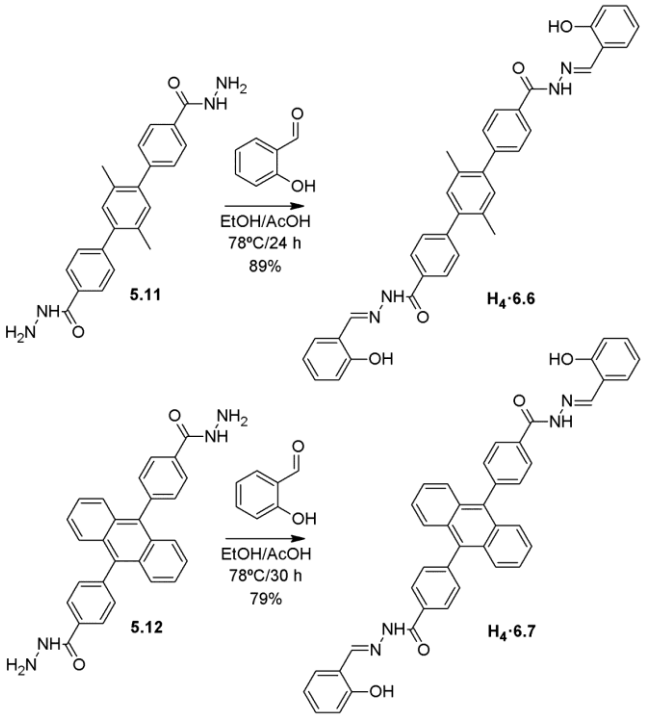

Figure 6.8: Synthesis of **H_4•6.6** and **H_4•6.7** from dihydrazide precursors.

6.4 Water-Soluble Lanthanide Cages

Most hosts capable of binding neutral guests do so by use of the hydrophobic effect.[9] This requires that the host be water soluble, or at least stable to an aqueous environment. To prepare a water soluble complex, the biphenyl ligand **Na_4•6.1** can be functionalized with water soluble sulfate groups. Attempts to do this directly by treating the aldehyde in concentrated sulfuric acid gave rise to purple-pink mixtures that contained many products. A survey of the literature proposed converting salicylaldehyde into an imine, followed by sulfonation, and finally hydrolyzing the imine to give the 5-sulfonosalicylaldehyde.[10]

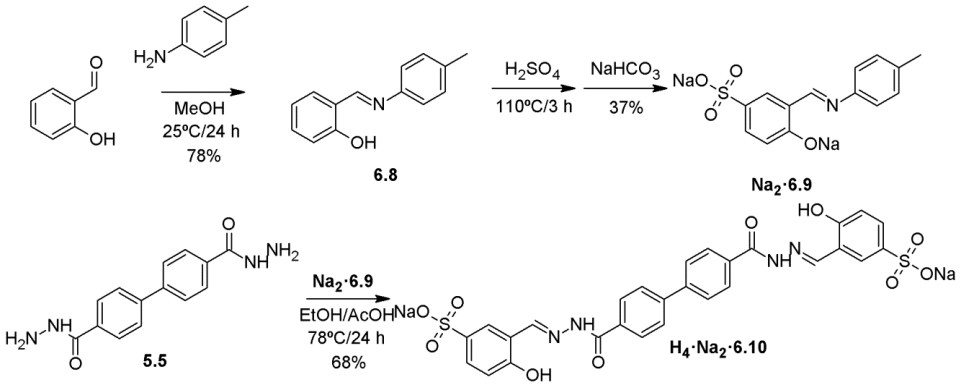

Figure 6.9: Synthesis of **Na_2•6.9** and **H_4•Na_2•6.10**.

This procedure was unsuccessful due to the challenge of cleanly hydrolyzing the aniline-derived imine and isolating the product aldehyde. A modification was used where salicylaldehyde was condensed with *p*-toluidine to give **6.8** (Figure 6.9). Imine **6.8** could then be sulfonated in conc. H_2SO_4 and precipitated as the disodium salt **Na_2•6.9**. Rather than try to hydrolyze this, however, it was possible to displace the imine with the more reactive hydrazide **5.5**, giving rise to **H_4•Na_2•6.10**. The ligand could be sonicated in anhydrous dichloromethane with sodium hydride to give **Na_6•6.10**. The ligand would readily protonate if exposed to air or wet solvent, making ^{1}H NMR analysis more difficult.

Despite this, titration of $Sm(OTf)_3$ into a solution of **Na_6•6.10** in DMSO-d_6 (Figure 6.10) showed downfield shifts of the resonances, consistent with complex formation. The partial protonation of the cage in wet DMSO leads to an overall charge state that is likely between 24^- and 12^-. The partial protonation also leads to extra resonances in the ^{1}H NMR spectrum, which were confirmed to be part of the complex based on similar DOSY NMR diffusion coefficients. When **Na_6•6.10** was added to D_2O, however, an insignificant amount of ligand dissolved. Addition of $Y(OTf)_3$ did not appreciably increase the

solubility, and there was not enough signal to study the complex by ^{1}H NMR spectroscopy.

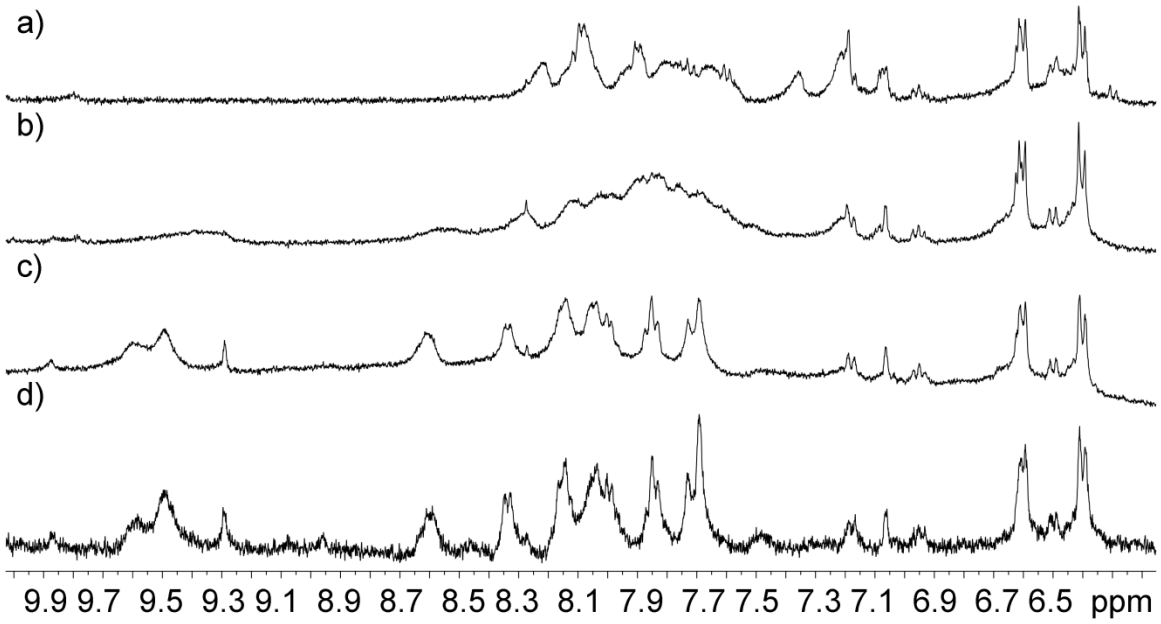

Figure 6.10: NMR titration of **Na_6•6.10** with $Sm(OTf)_3$ (DMSO-d_6, 400 MHz, 298 K): a) **Na_4•6.10**; b) 0.33 eq Sm(III); c) 0.66 eq S(III); d) 1.0 eq Sm(III).

Although the sulfonate cage was not soluble enough in water for ^{1}H NMR analysis, it did display great enough solubility for UV/Vis and fluorescence emission spectroscopic analysis. When the cage **$[6.10_6$•$Y_4]^{x-}$** was prepared in H_2O, there was a noticeable red shift in the UV/Vis spectrum compared to the free ligand (Figure 6.11). This is consistent with a significant change in the electronics upon coordination of the metal. Addition of metal also caused a decrease in the ligand-based fluorescence.

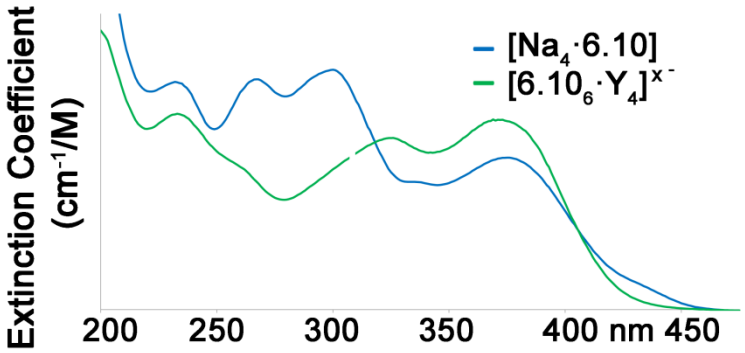

Figure 6.11: UV/Vis spectra of **Na_6•6.10** and **$[6.10_6•Y]^{x-}$** (18μM, H_2O).

The sparingly water soluble **$[6.10_6•Y]^{x-}$** was tested to see if it had better guest binding properties than the anthracene complex **$[6.7_6•Y_4]^{12-}$**. The water soluble cage should favor encapsulation of guests through the hydrophobic effect. Addition of a variety of organics showed evidence of guest binding in water. The two UV absorption bands at 322 and 376 nm shifted dramatically upon addition of metal, and they also shifted upon addition of adamantane, naphthalene, and benzene (Figure 6.12). The change in absorbance suggests shape of the cage flexes to better accommodate the bound guests.[10] The absorbance of these two peaks increased when anthracene, perylene and fluorescein were added, even though they do not absorb in the same region of the spectrum. There was no change upon treatment with C_{60} and fluorenone.

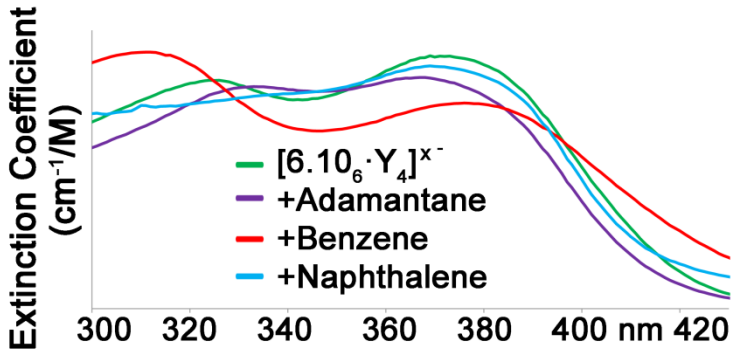

Figure 6.12: UV/Vis spectra of **$[6.10_6•Y]^{x-}$** with various guests (18μM, H_2O).

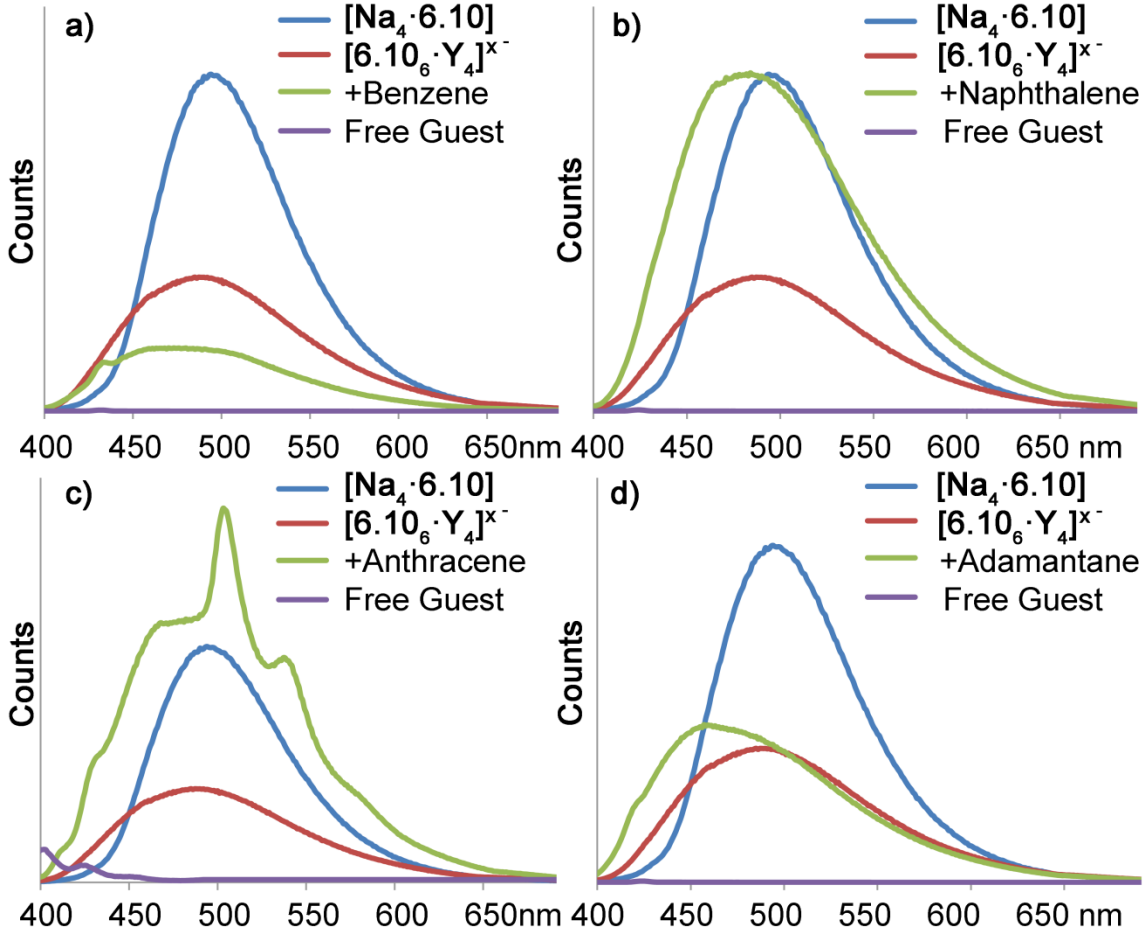

Figure 6.13: Fluorescence spectra showing guest binding properties of **[6.10$_6$•Y]$^{x-}$** (18μM, H_2O): a) **[6.10$_6$•Y]$^{x-}$** treated with benzene; b) **[6.10$_6$•Y]$^{x-}$** treated with naphthalene; c) **[6.10$_6$•Y]$^{x-}$** treated with anthracene; d) **[6.10$_6$•Y]$^{x-}$** treated with adamantane.

Similar experiments were performed using **[6.10$_6$•Y]$^{x-}$** and guest binding was monitored by fluorescence spectroscopy. Adding benzene to the aqueous mixture caused the ligand-based fluorescence to decrease further (Figure 6.13a). Naphthalene caused the fluorescence intensity to increase to the same level as it was for free ligand (Figure 6.13b). Anthracene causes an increase in the fluorescence intensity with a red shift of approximately 120 nm from the emission of anthracene in water. Mixing the free ligand with adamantane in water cause no red shift of the guest fluorescence,

suggesting this effect is only observed inside of the cage. The non-emissive guest adamantane was also studied (Figure 6.13d), showing a slight blue shift of the cage's emission band.

6.5 Conclusions

Synthesis of supramolecular cages based on lanthanide vertices do not present the same diastereocontrol issues observed with their transition metal counterparts. They do present other challenges, such as the need to use anionic ligands that makes them more sensitive to acidic environments. It is possible to prepare water soluble cages by addition of polar sulfate groups. The guest binding properties of these cages are improved in aqueous solution.

6.6 References

1) Wang, B.; Zang, Z.; Wang, H.; Dou, W.; Tang, X.; Liu, W.; Shao, Y.; Ma, J.; Li, Y.; Zhou, J. “Multiple Lanthanide Helicate Clusters and the Effects of Anions on Their Configuration.” *Angew. Chem. Int. Ed.*, **2013**, *52*, 3756-2759.

2) Xu, J.; Raymond, K. N. “Structurally Characterized Quadruple Stranded Bis-Bidentate Helicates.” *Angew. Chem. Int. Ed.*, **2006**, *45*, 6480-6485.

3) Jocher, C. J.; Moore, E. G.; Xu, J.; Avedano, S.; Botta, M.; Aime, S.; Raymond, K. N. “1,2-Hydroxypyridonates as Contrast Agents for Magnetic Resonance Imaging: TREN-1,2-HOPO.” *Inorg. Chem.*, **2007**, *46*, 9182-9191.

4) Johnson, A. M.; Young, M. C.; Zhang, X.; Julian, R. R.; Hooley, R. J. “Cooperative Thermodynamic Control of Selectivity in the Self-Assembly of Rare Earth Metal-Ligand Helices.” *J. Am. Chem. Soc.*, **2013**, *135*, 17723-17726.

5) Petoud, S.; Muller, G.; Moore, E. G.; Xu, J.; Sokolnicki, J.; Riehl, J. P.; Le, Y.; Cohen, S. M.; Raymond, K. N. “Brilliant Sm, Eu, Tb and Dy Chiral Lanthanide Complexes with Strong Circularly Polarized Luminescence.” *J. Am. Chem. Soc.*, **2007**, *129*, 77-83.

6) Wu, X.; Lin, Z.; He, C.; Duan, C. “Catalytic Performance of Lanthanide Molecular Solids Containing Well-Modified Metal-Organic Octahedra.” *New. J. Chem.*, **2012**, *36*, 161-167.

7) a) Wang, J.; He, C.; Wu, P.; Wang, J.; Duan, C. “An Amide-Containing Metal-Organic Tetrahedron Responding to a Spin-Trapping Reaction in a Fluorescent Enhancement Manner for Biological Imaging of NO in Living Cells.” *J. Am. Chem. Soc.*, **2011**, *133*, 12402-12405; b) Zhu, X.; He, C.; Dong, D.; Liu, Y.; Duan, C. “Cerium-Based Triple-Stranded Helicates as Luminescent Chemosensors for the Selective Sensing of Magnesium Ions.” *Dalton Trans.*, **2010**, *39*, 10051-10055.

8) Hagberg, D.; Karlström, G.; Roos, B. O.; Gagliardi, L. “The Coordination of Uranyl in Water: A Combined Quantum Chemical and Molecular Simulation Study.” *J. Am. Chem. Soc.*, **2005**, *127*, 14250-14256.

9) a) Snyder, P. W.; Mecinović, J.; Moustakas, D. T.; Thomas III, S. W.; Harder, M.; Mack. E. T.; Lockett, M. R.; Héroux, A.; Sherman, W.; Whitesides, G. M. “Mechanism of the Hydrophobic Effect in the Biomolecular Recognition of Arylsulfonamides by Carbonic Anhydrase.” *Proc. Natl. Acad. Sci. USA*, **2011**, *108*, 17889-17894; b) Hooley, R. J.; Van Anda, H. J.; Rebek Jr., J. “Extraction of Hydrophobic Species into a Water-Soluble Synthetic Receptor.” *J. Am. Chem. Soc.*, **2007**, *129*, 13464-13473; c) Biros, S. M.; Bergman, R. G.; Raymond, K. N. “The Hydrophobic Effect Drives the Recognition of Hydrocarbons by an Anionic Metal-Ligand Cluster.” *J. Am. Chem. Soc.*, **2007**, *129*, 12094-12095.

10) Berry, K. J.; Moya, F.; Murray, K. S.; van den Bergen, A. M. B.; West, B. O. "Water-Soluble Cobalt(II) Complexes of *N,N'*-Substituted Bis(salicylaldimine-5-sulphonic acids). Oxygen-Carrying Porperties and Conversion into Cobalt(III) Organometallic Compounds." *J. Chem. Soc., Dalton Trans.*, **1982**, 109-116.

11) Szlay, L.; Farkas, V.; Vass, E.; Hollósi, M.; Móczár, I.; Pintér, Á.; Huszthy, P. "Synthesis and Selective Lead(II) Binding of Achiral and Enantiomerically Pure Chiral Acridono-18-Crown-6 Ether Type Ligands." *Tetrahedron Asymmetry*, **2004**, *15*, 1487-1493.

Chapter 7 – Assembly via Mixed Hydrogen and Dative Bonding

7.1 Rationale

Although there are numerous examples of metal-ligand driven self-assembly, and as many examples of hydrogen bonded assemblies, very few examples combine these two strategies. This is because of the poor solubility of many inorganic complexes in the non-polar solvents required to stabilize hydrogen bonds. Polar solvents such as DMSO and methanol will typically disrupt hydrogen bonding, but these are commonly used to dissolve inorganic complexes.[1] These hybrid self-assemblies can be prepared in the solid state, negating the need for a disruptive solvent.[2] Another strategy is to add lipophilic counterions and append aliphatic groups to the ligands to help solubilize these complexes in non-competitively hydrogen bonding organic solvents.

7.2 Bipyridyl-Based Hybrid Assembled Switches

Hydrogen-bonded self-assembly has been used for controlled gelation,[3] and it should be possible to control gelation with a hybrid self-assembly as well. A convenient motif to use for molecular switches is the 2,2'-bipyridine unit.[4] The ligand 2,2'-bipyridine prefers a rotational conformer where the torsion angle between the two nitrogen atoms is 180°. In the presence of a metal ion, these nitrogen atoms rotate to give a 0° torsion angle so both can participate in dative bonding. A 2,2'-bipyridyl with attached hydrogen bonding groups would form a linear, oligomeric structure (Figure 7.1). Addition of metal would flip this conformation, allowing the formation of a discrete, closed structure.

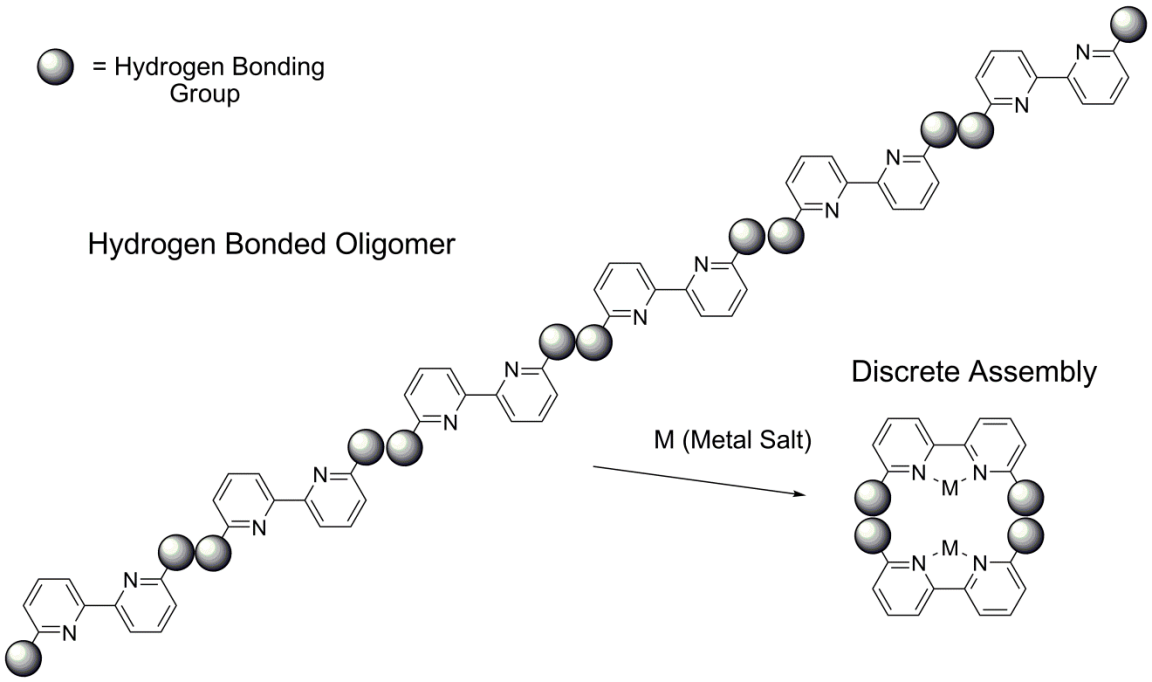

Figure 7.1: Function of a 2,2'-bipyridyl-based hybrid self-assembly.

Addition of 2,6-dibromopyridine to anhydrous diethyl ether, followed by treatment with n-butyl lithium gave 2-bromo-6-lithiopyridine *in situ* (Figure 7.2).[5] This was added to copper(II) chloride, followed by air oxidation to give the desired dibromide **7.1**. The coupling reaction between **7.1** and 5-ethynyluracil was known, however the Sonogashira cross coupling with precursors 5-iodouracil and trimethylsilylacetylene to prepare 5-ethynyluracil was unsuccessful.[6] Attempts to convert the alkyne to **7.1** to yield bis-alkyne **7.2** were successful, but this also failed to successfully undergo cross coupling with 5-iodouracil.

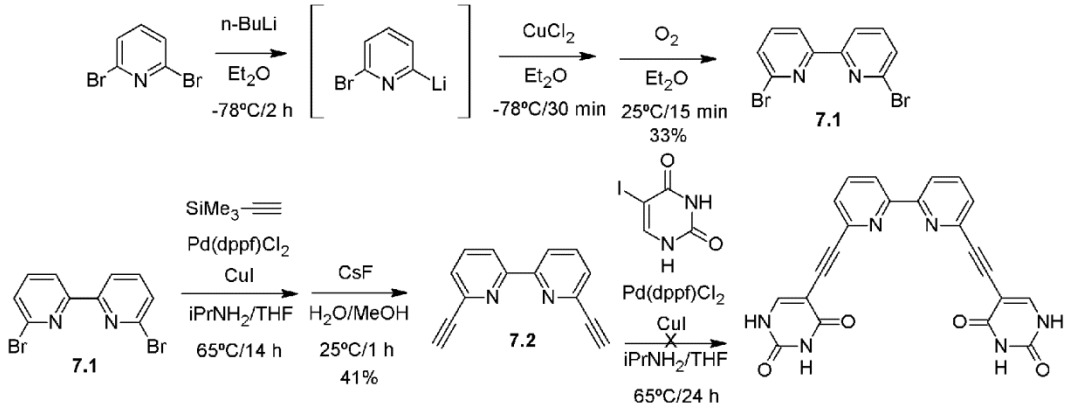

Figure 7.2: Synthesis of **7.1** from 2,6-dibromopyridine and the diethynyl derivative **7.2**.

It was known that melamine analogues that function as donor-acceptor-donor pairs could readily self-assemble in organic solvents with complementary hydrogen bonders such as barbituric acid derivatives,[7] so this motif was targeted. A suitable melamine analogue was prepared from 2,2'-bipyridine (Figure 7.3). Oxidation of 2,2'-bipyridine to the di-N-oxide **7.3** was achieved using hydrogen peroxide in acetic acid. The N-oxide could then be converted into the dinitrile **7.4** by activation of the N-oxides using benzoyl chloride followed by trimethylsilyl cyanide. The dinitrile was subjected to a cyclization reaction with dicyandiamide in the presence of KOH to give **7.5** in good yield.

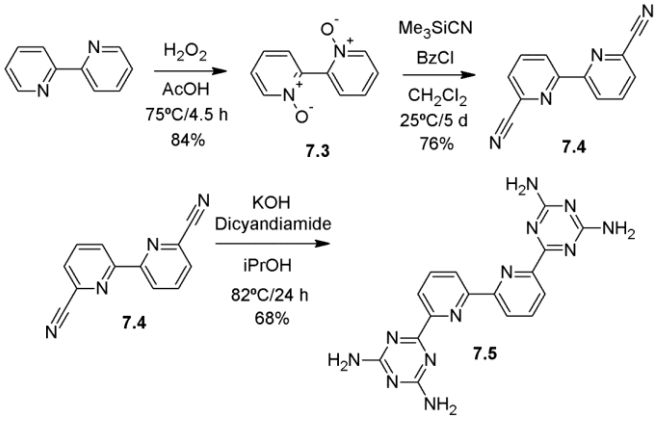

Figure 7.3: Synthesis of hydrogen bonder **7.5** and precursors from 2,2'-bipyridine.

Ligand **7.5** was only soluble in DMSO, however, an unsuitable solvent for studying hydrogen bonding self-assembly. Reaction of **7.5** with isocyanates and acid chlorides was attempted to confer organic solubility. These reactions failed to give conversion to the product, and only **7.5** was recovered. Another way to increase the solubility of the triazine was to alkylate the parent bipyridine. Treatment of 2,2'-bipyridine with butyl lithium, followed by oxidation with manganese dioxide, led to alkylated bipyridyl **7.6** (Figure 7.4). Oxidation of this to the di-N-oxide **7.7** was possible, however, the subsequent 4,4'-dinitrile could not be obtained using either benzoyl chloride or dimethylsulfate as an activating agent.

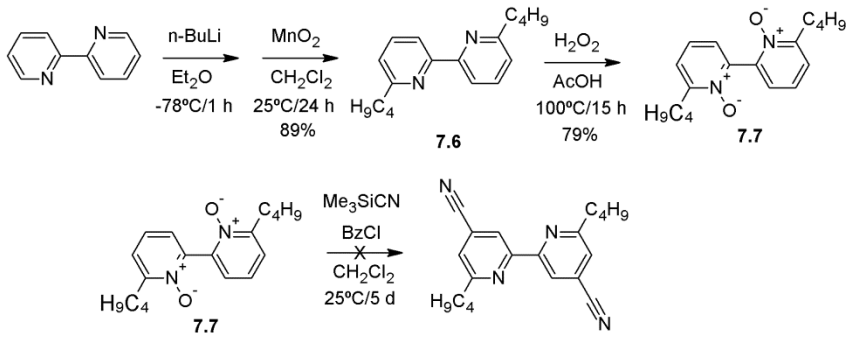

Figure 7.4: Attempted synthesis of alkylated bipyridyl hydrogen bonders.

7.3 Towards Triazine-Barbiturate Hybrid Self-Assemblies

The insolubility of **7.5** meant that an alternative metal chelator was required that was amenable to the triazine-barbiturate assembly strategy. The ligand 4-pyridyl diaminotriazine **7.8** (Figure 7.5) was prepared in one step from 4-cyanopyridine in excellent yield. Dioctylbarbituric acid[8] **7.9a** was also synthesized, as its long alkyl chains were expected to aid solubility in organic solvents. Acetonitrile was chosen as a solvent to study these assemblies because it is polar, but less disruptive of hydrogen bonds.

When **7.8** and **7.9a** were combined with the palladium salt **2.3** in acetonitrile, however, very little sign of complexation was observed. Ligand **7.8** was poorly soluble, and the solubility was not increased upon complex formation as was observed for **$[(H_2 \bullet 5.6)_3 \bullet Bi_3](OTf)_9$**.

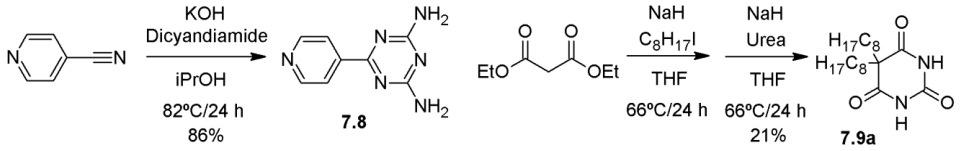

Figure 7.5: Synthesis of triazine **7.8** and barbiturate **7.9a**.

The 3-pyridyl analogue **7.10** was also prepared (Figure 7.6a) with the expectation that it could form a structure similar to **1.15** upon addition of a complementary hydrogen bonder (Figure 7.6b). Addition of $[Pd(MeCN)_4](BF_4)_2$ to **7.10** in acetonitrile showed new peaks, consistent with complex formation (Figure 7.6c and d). The number of peaks suggests a mixture of different orientations of the ligand at the metal center. Addition of **7.9a** followed by heating of the sample led to a single pyridyl species in solution, but this could not be crystallized. Further characterization by ESI-MS also failed to show any complexes larger than the $[ML]^{2+}$ in the gas phase.

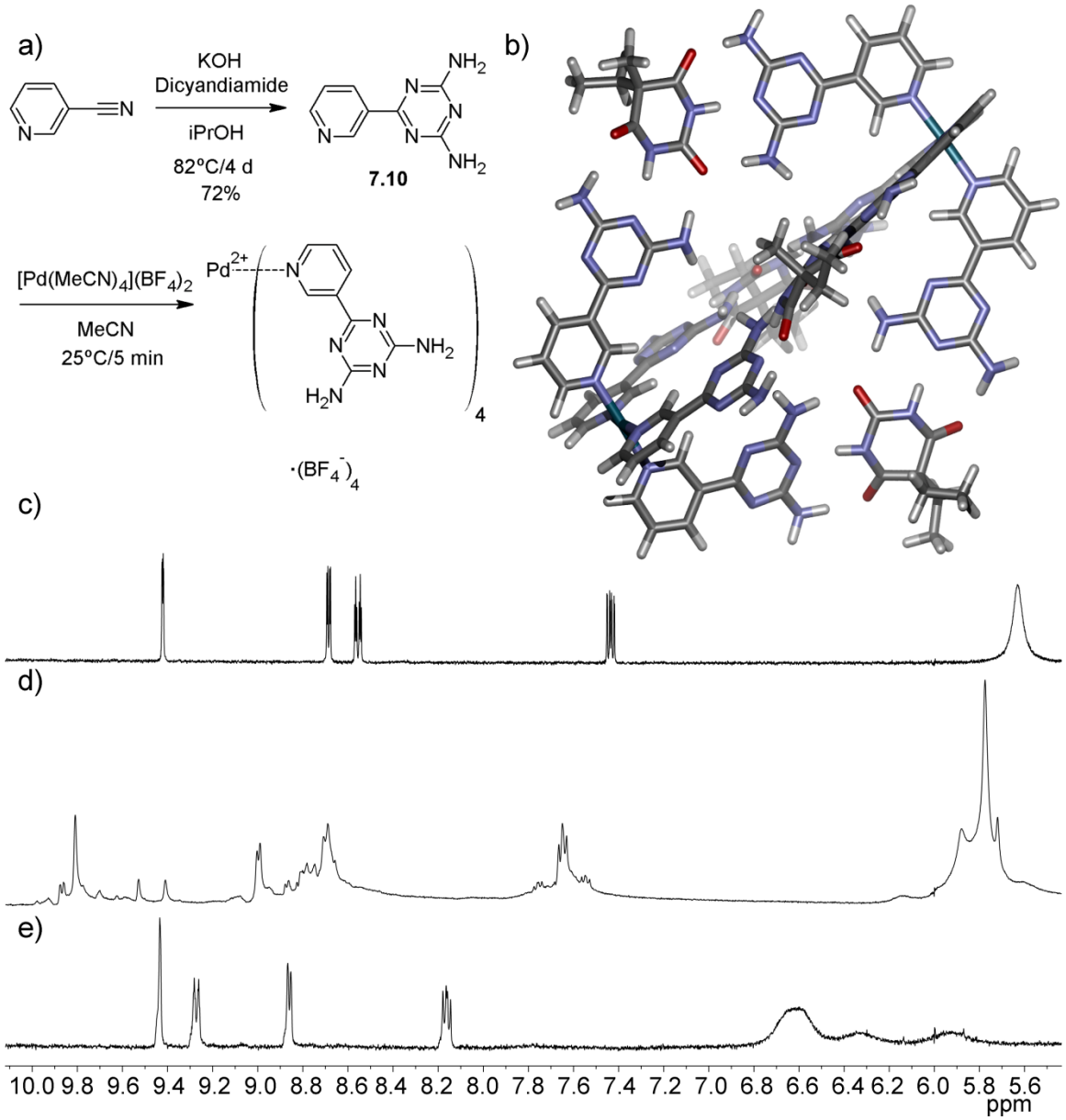

Figure 7.6: Synthesis of **7.10** and self-assembly with $[Pd(MeCN)_4](BF_4)_2$: a) Synthesis of ligand **7.10**; b) SPARTAN model of **{[7.10$_4$•Pd]$_2^{4+}$•7.9a$_4$}** (AM1 forcefield); c) ^{1}H NMR spectrum of **7.10**; d) ^{1}H NMR spectrum of **[7.10$_4$•Pd](BF$_4$)$_2$**; e) ^{1}H NMR spectrum of **{[7.10$_4$•Pd]$_2^{4+}$•7.9a$_4$}** (CD_3CN, 400 MHz, 298 K).

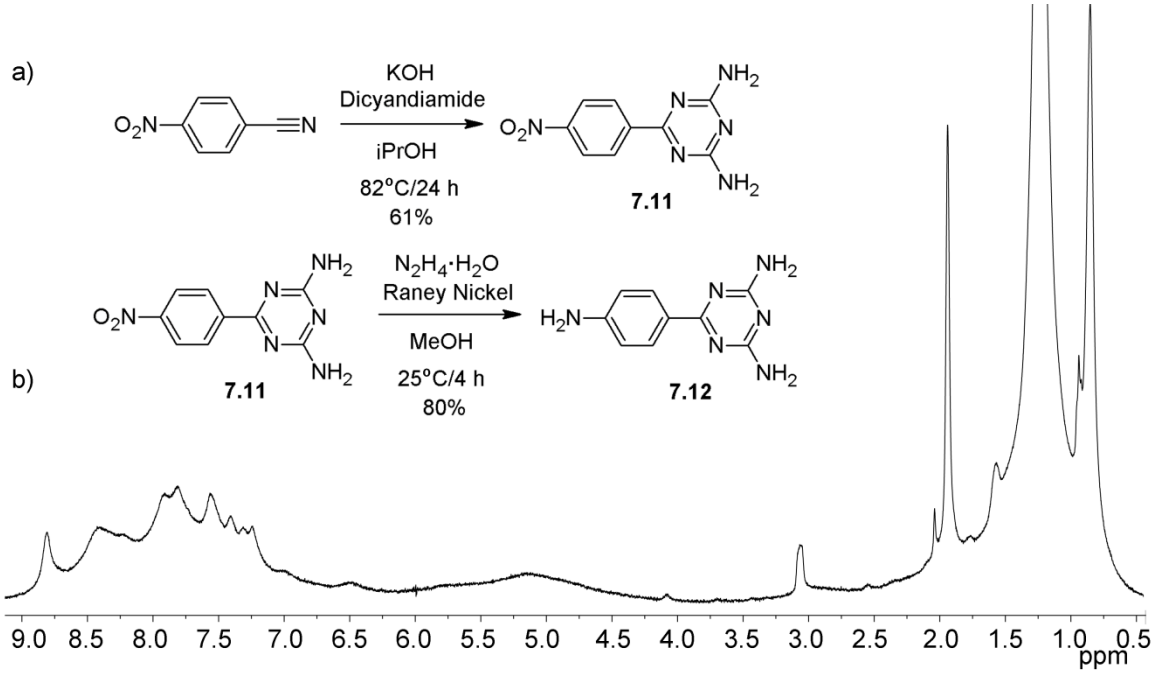

Figure 7.7: Multicomponent self-assembly of **7.12**: a) Synthesis of **7.12**; b) Multi-component self-assembly of **7.12** with 2-formyl pyridine, iron(II) perchlorate, and **7.9a** (CD_3CN, 400 MHz, 298 K).

It was also possible to prepare an iron(II)-iminopyridine precursor with the 3,5-diaminotriazine group by performing a dicyandiamide cyclization with *p*-nitrobenzaldehyde to give **7.11**, followed by reduction to the aniline **7.12** (Figure 7.7a). Although multi-component self-assembly using iron perchlorate, 2-formylpyridine and **7.9a** gave purple complexes, no discrete assembly was detected. The reversibility of the hydrogen bonds led to undefined oligomers in solution (Figure 7.7b).

7.4 Hybrid Self-Assemblies Displaying Spin Crossover Behavior

The monotriazine analogue of **7.5**, **7.13**, was expected to be more soluble than the bistriazine species. Ligand **7.13** can be prepared beginning with the synthesis of mono-

N-oxide **7.14** (Figure 7.8). This can be synthesized in excellent yield by combining an excess of hydrogen peroxide with 2,2'-bipyridine in trifluoroacetic acid.[9] The N-oxide can then be converted into mononitrile **7.15** by benzoyl chloride activation and subsequent attack by trimethylsilylcyanide.[10] Cyclization of **7.15** with dicyandiamide also proceeds in very good yield to give monotriazine **7.13**.[11]

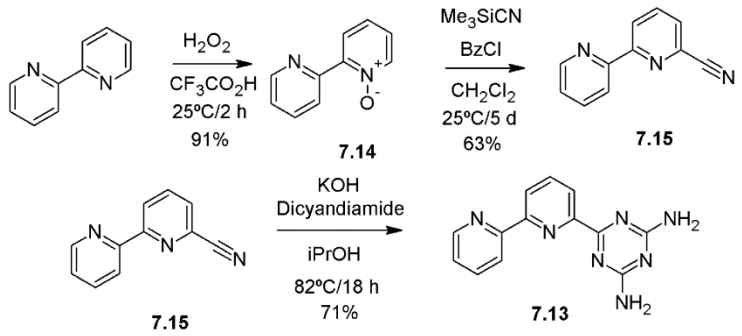

Figure 7.8: Synthesis of **7.13** from 2,2'-bipyridine *via* unsymmetrical N-oxide **7.14**.

Initial screens showed no complexation between **7.13** and either $Bi(OTf)_3$ or $Sm(OTf)_3$. The reason for this is not clear, as terpyridine complexes of both are known.[12] Addition of iron(II) perchlorate to **7.13** in DMSO, however, led to the immediate formation of a purple complex.[13] A titration experiment followed by ^1H in DMSO showed that this complex formed in a 2:1 ligand to metal ratio, consistent with the ligand acting as a tridentate chelator. All of the proton resonances for **$[7.13_2 \bullet Fe](ClO_4)_2$** were broad and spread out over a range of 20 ppm in the ^1H NMR spectrum (Figure 7.9). This suggests a paramagnetic complex, although the purple color is consistent with it being diamagnetic.[14] The complex could be made by combining the insoluble ligand **7.13** in solvents such as water, acetone, ethanol, or acetonitrile in the presence of iron(II) perchlorate. All of these displayed a purple color and similar NMR spectra.

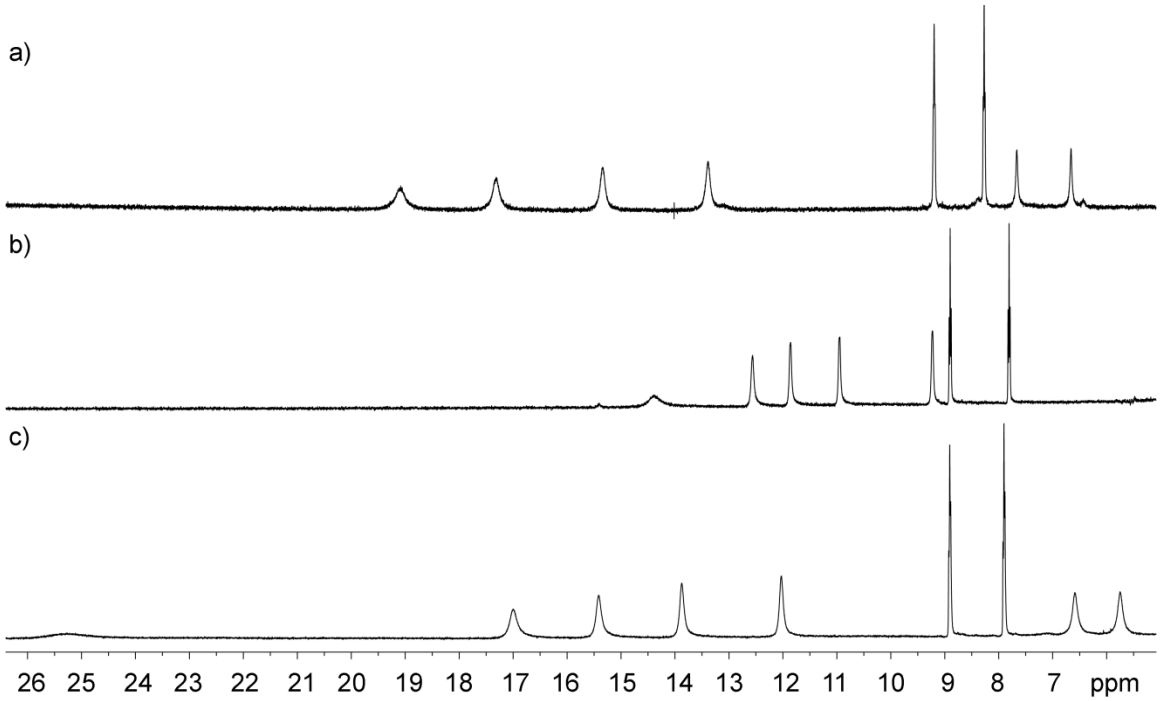

Figure 7.9: Representative ^{1}H NMR spectra of **[7.13$_2$•Fe](ClO$_4$)$_2$** in different solvents: a) Me_2CO-d_6; b) D_2O; c) CD_3CN (400 MHz, 298 K).

X-ray quality crystals of **[7.13$_2$•Fe](ClO$_4$)$_2$** were obtained by diffusion of benzene into an acetonitrile solution of the complex. In the crystal structure (Figure 7.10), the iron complex existed as a distorted octahedron, with an overall 161° angle between the outside chelating nitrogens, almost 20° away from the expected angles for an octahedral complex. The bond distances between the various Fe-N connections ranged from 1.89 Å to 2.05 Å. These distances were consistent with a low spin, diamagnetic octahedral Fe(II) complex.[15] Although there was evidence of hydrogen bonding between triazine protons and perchlorate anions in the crystal structure, **[7.13$_2$•Fe](BF$_4$)$_2$** and **[7.13$_2$•Fe](BPh$_4$)$_2$** were both prepared and show similar paramagnetic spectra.

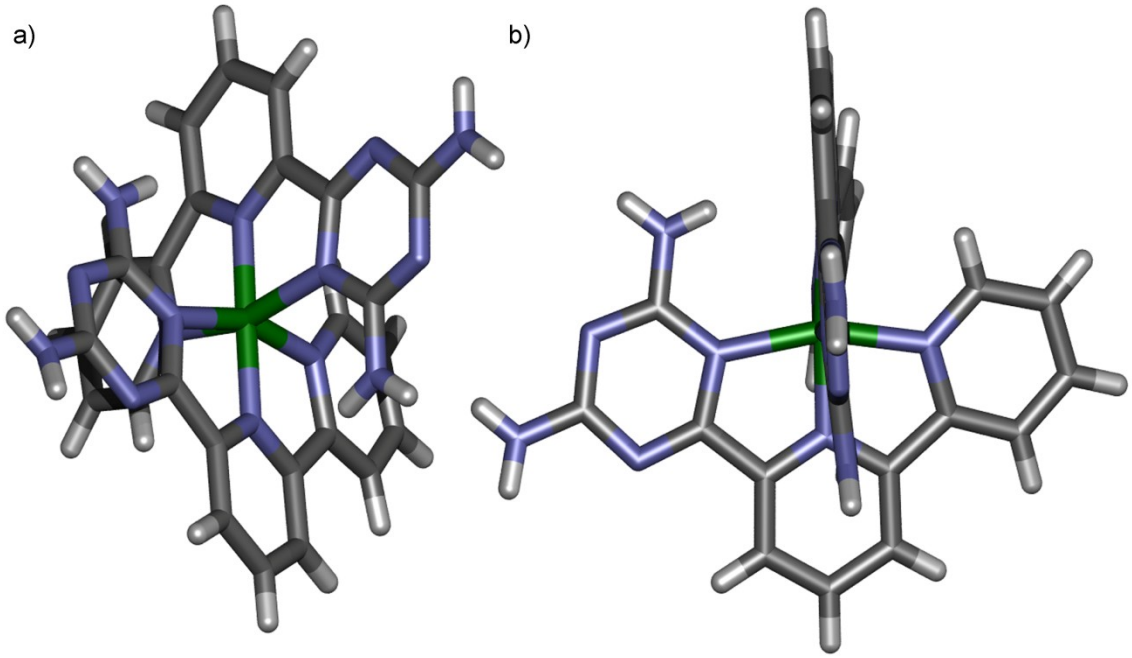

Figure 7.10: Crystal structure of **[7.13$_2$•Fe](ClO$_4$)$_2$**: a) Perspective showing octahedral Fe(II) center; b) Side perspective showing ligand twisting.

UV/Vis spectroscopy was employed to further characterize **[7.13$_2$•Fe](ClO$_4$)$_2$** (Figure 7.11). As expected, there was a peak at 557 nm, which corresponds to the metal-to-ligand charge transfer band expected for low spin Fe(II)-terpyidine complexes. When these spectra were taken at lower temperatures, however, the concentration of this peak increased. Increasing the temperature caused a decrease in the MLCT band at 557 nm.

The presence of both diamagnetic and paramagnetic iron pointed towards a spin transition on the iron. Iron(II) spin crossover (SCO) complexes are one of the most commonly studied for SCO behavior, owing to the change from S = 0 (fully diamagnetic) complexes to S = 2 (highly paramagnetic).[16] The complex **[7.13$_2$•Fe](ClO$_4$)$_2$** displayed SCO behavior because of similarity between the d-orbital splitting and spin pairing energy. Once these terms become the same, the two spin states become degenerate.

SCO behavior can be controlled thermally, as well as by photoexcitation and varying the pressure.[17]

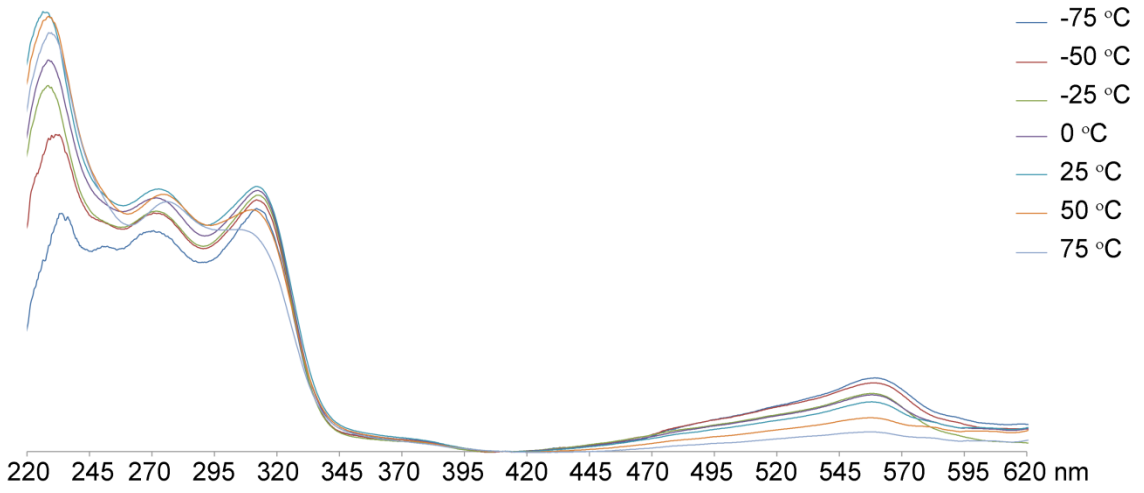

Figure 7.11: Variable temperature UV/Vis spectra of **[7.13$_2$•Fe](ClO$_4$)$_2$** (EtOH, 2.87 x 10^{-4} M).

The magnetic susceptibility of **[7.13$_2$•Fe](ClO$_4$)$_2$** was determined by the Evans NMR method (Equation 7.1).[18] In DMSO the measurement was relatively straightforward, and analysis provided a μ_{eff} at room temperature of 4.4. This is consistent with an approximately 3:1 mixture of high spin (S = 2) to low spin (S = 2) iron(II) under these conditions. Measuring this value in acetonitrile required a significant correction for the solvent density to give similar results.

Equation 7.1: Formula used to calculate magnetic susceptibility *via* the Evans NMR method where χ_g = magnetic susceptibility (cm^3/g), f = spectrometer frequency, m = mass, and χ_o = magnetic susceptibility of solvent (cm^3/g), d_o = initial density of solvent (g/cm^3), and d_s = density of solution (g/cm^3).

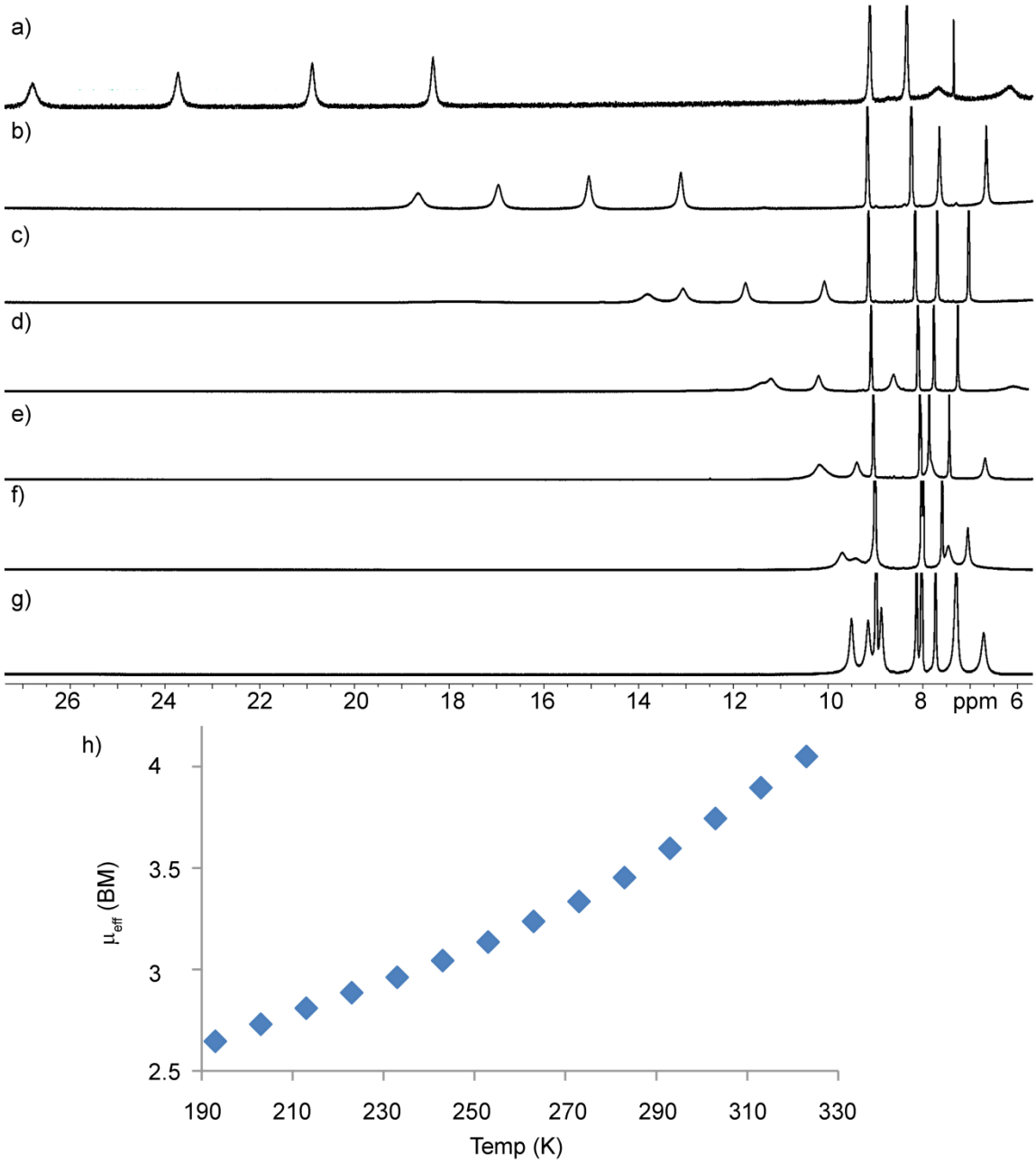

Figure 7.12: Variable temperature ^{1}H NMR spectra detailing magnetic behavior of **[7.13$_2$•Fe](ClO$_4$)$_2$**: a) 50 °C; b) 25 °C; c) 0 °C; d) -20 °C; e) -40 °C; f) -60 °C; g) -80 °C (Me_2CO-d_6, 500 MHz); h) Variable temperature magnetic data determined using the Evan's method (Me_2CO-d_6, 500 MHz, 8.2 x 10^{-3} M).

The spin transition of **[7.13$_2$•Fe](ClO$_4$)$_2$** should also be observable by VT NMR.[19] At higher temperatures there would be more paramagnetic character, and at lower temperatures the sample would appear more diamagnetic. VT NMR analysis shows a small spectral range at low temperatures, while the peaks shift greatly downfield as the temperature is increased (Figure 7.12), consistent with a spin transition as the temperature is increased. Applying the Evans method across this temperature range shows that the magnetic susceptibility increases as a function of temperature (Figure 7.12h). This is further evidence that **[7.13$_2$•Fe](ClO$_4$)$_2$** exists as a mixture of high and low spin Fe(II) in solution.

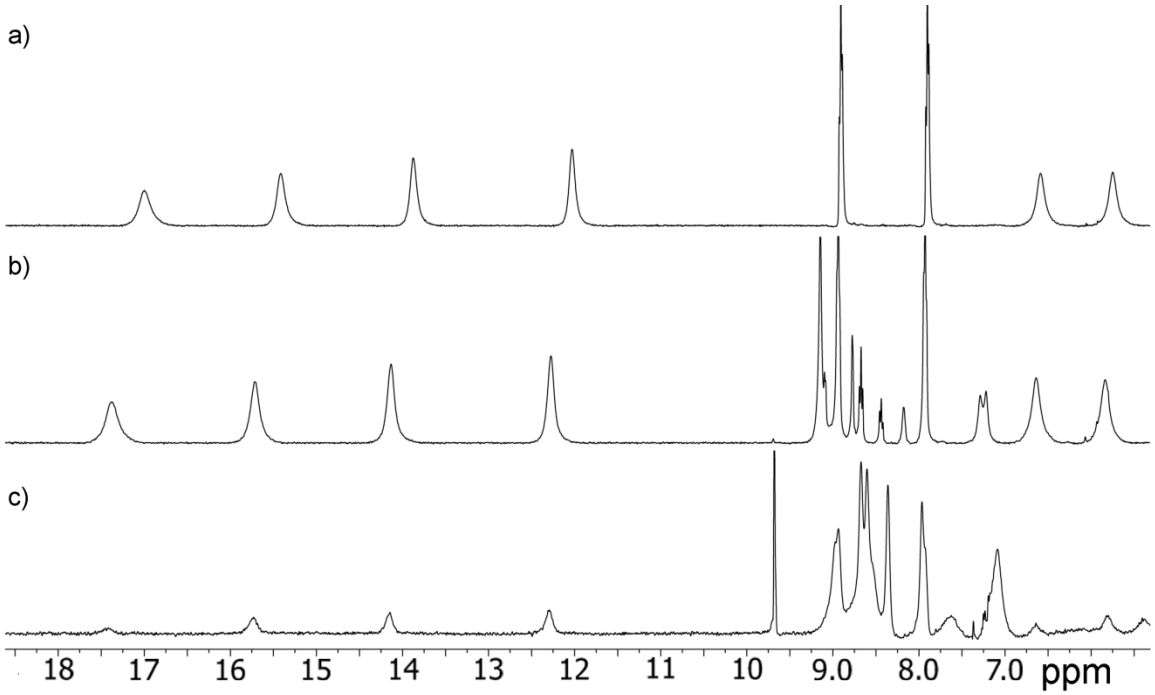

Figure 7.13: Titration of **7.9a** into **[7.13$_2$•Fe](ClO$_4$)$_2$**: a) ^{1}H-NMR spectrum of **[7.13$_2$•Fe](ClO$_4$)$_2$**; b) the mixture of species observed upon addition of **7.9a** to **[7.13$_2$•Fe](ClO$_4$)$_2$**; c) addition of excess **7.9a** to **[7.13$_2$•Fe](ClO$_4$)$_2$** (CD_3CN, 400 MHz, 1.4 x 10^{-2} M, 298 K).

The self-assembly of **[7.13$_2$•Fe](ClO$_4$)$_2$** was studied in CD_3CN by treatment with increasing amounts of the dioctyl barbituric acid **7.9a** (Figure 7.13). Many of the peaks shifted downfield. These shifts indicate an assembly process that occurs faster than the NMR timescale. In addition to the parent resonances of **[7.13$_2$•Fe](ClO$_4$)$_2$** shifting downfield, there was also evidence of new peaks in the upfield portion of the spectrum (Figure 7.13b). Further addition of **7.9a** (Figure 7.13c) caused these peaks to increase in intensity while the original, shifted peaks decreased.

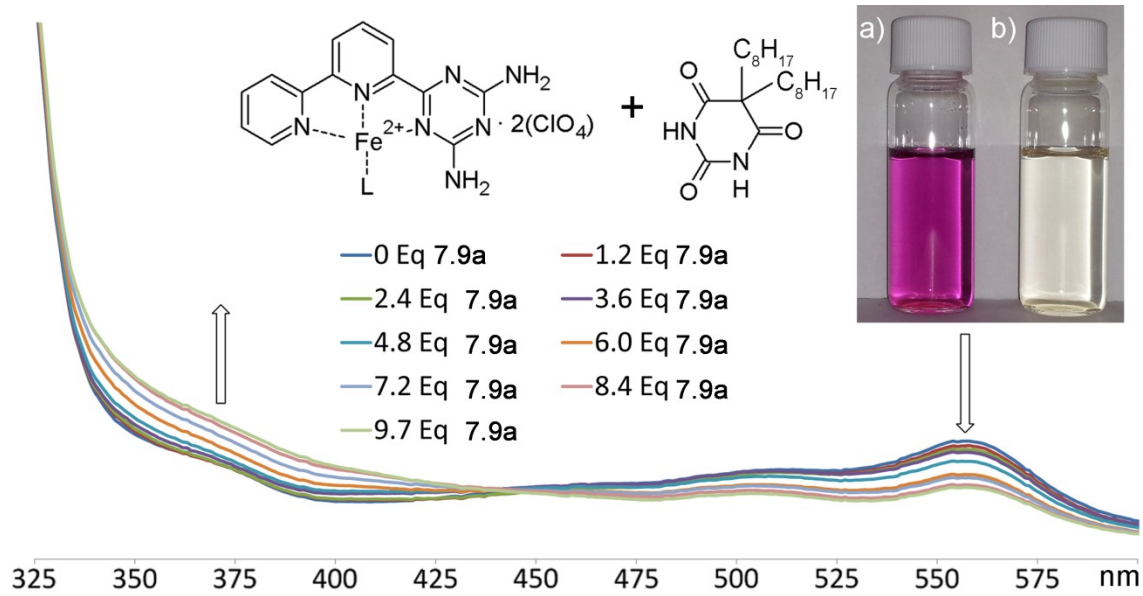

Figure 7.14: UV/Vis spectra showing decrease in the low spin MLCT band at 557 nm as **7.9a** is added to **[7.13$_2$•Fe](ClO$_4$)$_2$** (2.6 x 10^{-6} M, MeCN). Insert: a) **[7.13$_2$•Fe](ClO$_4$)$_2$**; b) + 20 eq. **7.9a**.

Similar results were obtained when **[7.13$_2$•Fe](ClO$_4$)$_2$** was added to a solution of **7.9a**, as well as when the titration was repeated with **[7.13$_2$•Fe](BF$_4$)$_2$**. Switching to the non-competitive solvent Me_2CO-d_6 also gave similar results. The titration of **7.9a** into **[7.13$_2$•Fe](ClO$_4$)$_2$** showed a *decrease* in the MLCT band at 557 nm with higher concentrations of **7.9a** by UV/Vis spectroscopy (Figure 7.14). In addition to this

decrease, however, there was also an *increase* in a band at 370 nm. As **7.9a** is added, the low spin population of **[7.13$_2$•Fe](ClO$_4$)$_2$** (represented by the band at 557 nm) decreases, while the high spin population (represented by the band at 370 nm) increases. Spin crossover by supramolecular assembly has only been seen before in iron-based metal-organic frameworks where SCO is modulated by guest uptake.[20]

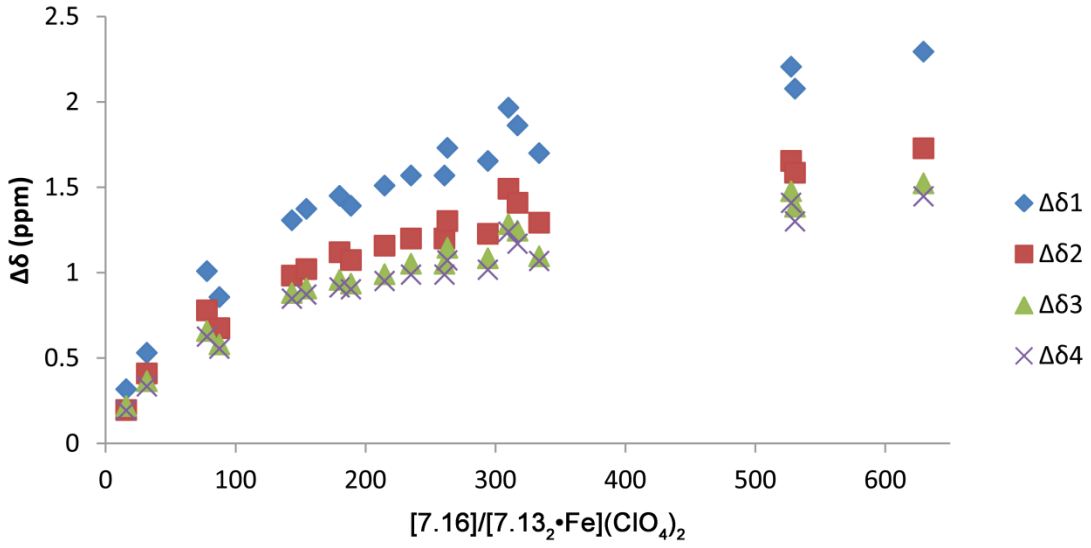

Figure 7.15: Changes in chemical shift of selected proton resonances (19.21, 17.42, 15.40, and 13.46 ppm in the initial spectrum) of **[7.13$_2$•Fe](ClO$_4$)$_2$** as a function of the concentration of **7.9a** (Me_2CO-d_6, 500 MHz, 3.71 x 10^{-3} M).

The hydrogen bond-driven self-assembly may be the cause of the SCO event. This was tested by adding a complementary hydrogen bonder which can only form one base pair with **[7.13$_2$•Fe](ClO$_4$)$_2$**, limiting it to the assembly of an HG_2 structure rather than any larger aggregates. The complementary hydrogen bonder 3,3-dimethylglutarimide (**7.16**) was prepared in excellent yield by reacting molten ammonium acetate and 3,3-dimethylglutaric anhydride. Titration of **7.16** into **[7.13$_2$•Fe](ClO$_4$)$_2$** showed a downfield shift of resonances in the ^{1}H NMR spectrum of the iron complex (Figure 7.15), but

nearing saturation of the guest there was no sign of a second species. Likewise, addition of **7.16** to a solution of **[7.13$_2$•Fe](ClO$_4$)$_2$** showed no decrease in the MLCT band at 557 nm.

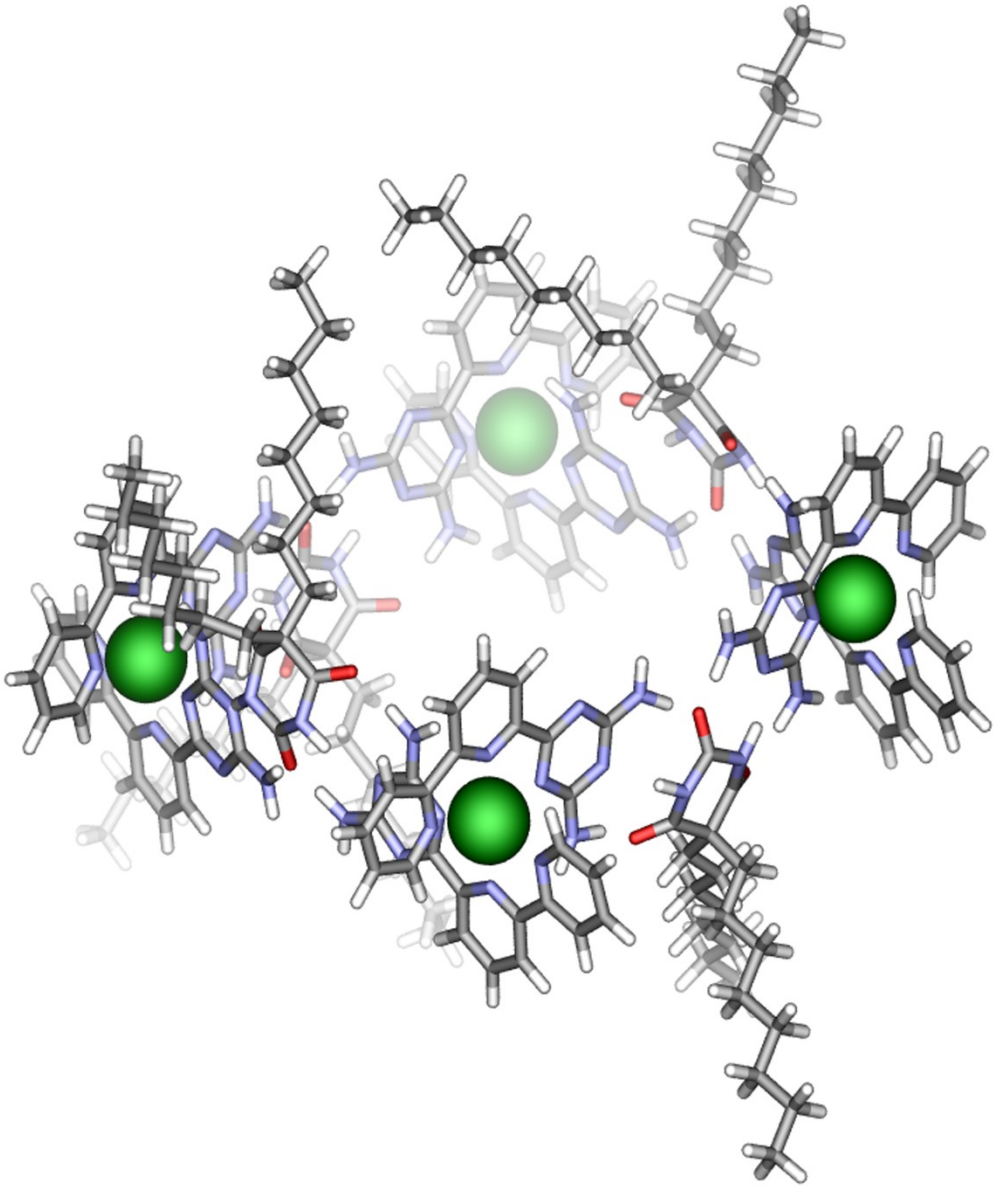

Figure 7.16: SPARTAN model of a proposed **{[7.13$_2$•Fe]$_4^{8+}$•7.9a$_4$}** square (AM1 forcefield).

Evidence supported that SCO for the **{[7.13$_2$•Fe]$_x^{2x+}$•7.9a$_y$}** assembly was an effect of supramolecular aggregation, but it was unclear the exact nature of the assembly. Previous work on melamine-barbiturate systems showed hydrogen bonded assemblies would form small, closed structures, but over time would equilibrate to become larger species that eventually precipitated out of solution.[7] Molecular modeling suggested the smallest closed structure possible was **{[7.13$_2$•Fe]$_4^{8+}$•7.9a$_4$}** (Figure 7.16). This square-shaped structure would have an inversion plane with alternating orientation of the alkyl chains of **7.9a**.

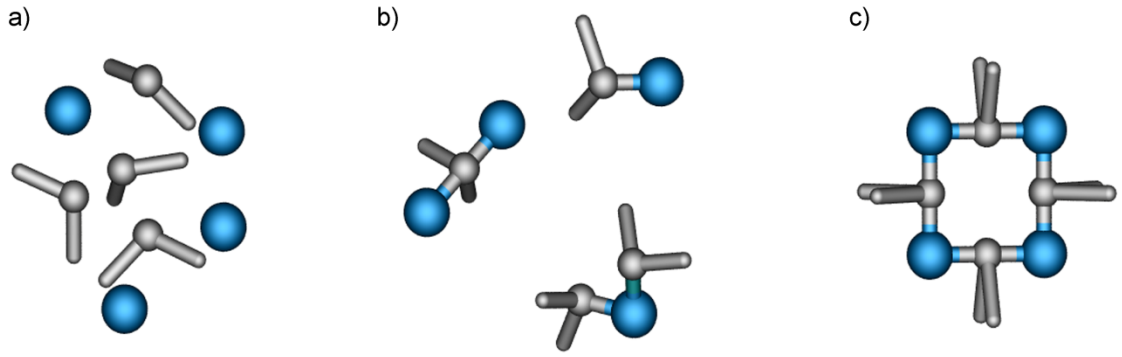

Figure 7.17: Cartoon representation of the self-assembly of **{[7.13$_2$•Fe]$_4^{8+}$•7.9a$_4$}**: a) Free **[7.13$_2$•Fe]$^{2+}$** and **7.9a**; b) Partially assembled **{[7.13$_2$•Fe]$_x^{2x+}$•7.9a$_y$}**; c) Closed **{[7.13$_2$•Fe]$_4^{8+}$•7.9a$_4$}**.

The presence of two different sets of **[7.13$_2$•Fe](ClO$_4$)$_2$** resonances in the ^{1}H NMR spectrum upon addition of **7.9a** suggests the assembly process looks like the cartoon in Figure 7.17. Free **[7.13$_2$•Fe](ClO$_4$)$_2$** equilibrates between various, “open” aggregates in solution. This process is fast on the NMR timescale, leading the proton resonances to shift downfield as a weighted average of all the possible assemblies. These aggregates can eventually become large enough to form “closed” structures, which give rise to the

change in spin state. The closed structure is in slow exchange with the "open" aggregates and can therefore be distinguished from them by ^{1}H NMR.

There is also a kinetic component to the formation of these complexes.[21] The decrease in the MLCT band at 557 nm was not only concentration dependent, but also time dependent. The initial rate of change in the MLCT band at 557 nm was dependent on the ratio of **7.9a** to **[7.13$_2$•Fe](ClO$_4$)$_2$** (Figure 7.18). Regardless of the initial rate, however, the change in absorbance becomes negligible after approximately five hours.

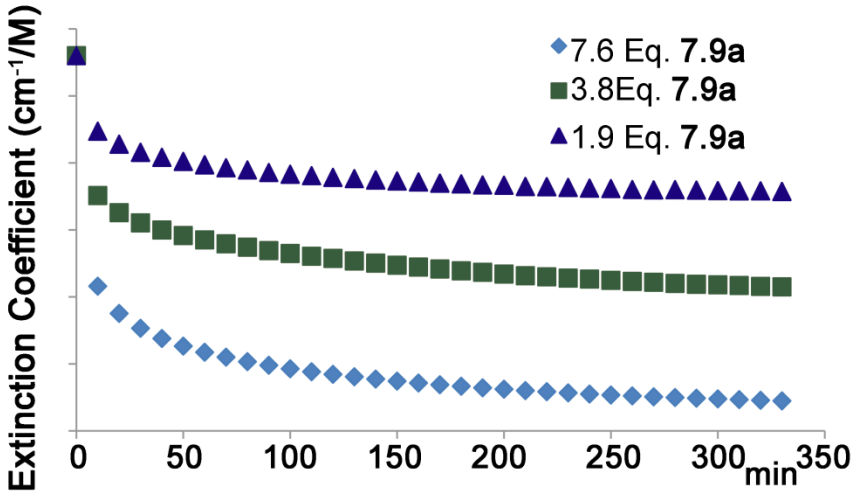

Figure 7.18: Kinetic formation of **{[7.13$_2$•Fe]$_4^{8+}$•7.9a$_4$** assembly determined by UV/Vis spectroscopy (MeCN, 5.0 x 10^{-5} M).

Addition of **[7.13$_2$•Fe](ClO$_4$)$_2$** and **7.9a** to solutions of acetonitrile containing different quantities of ethanol showed different rates of MLCT loss (Figure 7.19a). Increasing concentrations of the competitive hydrogen bonder ethanol led to a decrease in the self-assembled species, and the MLCT band for low spin iron in **[7.13$_2$•Fe](ClO$_4$)$_2$** is retained. If a solution that has undergone complete spin transition is left sitting long enough, it can

absorb water and re-equilibrate back to the free iron complex, complete with recovery of the MLCT band at 557 nm (Figure 7.19b).

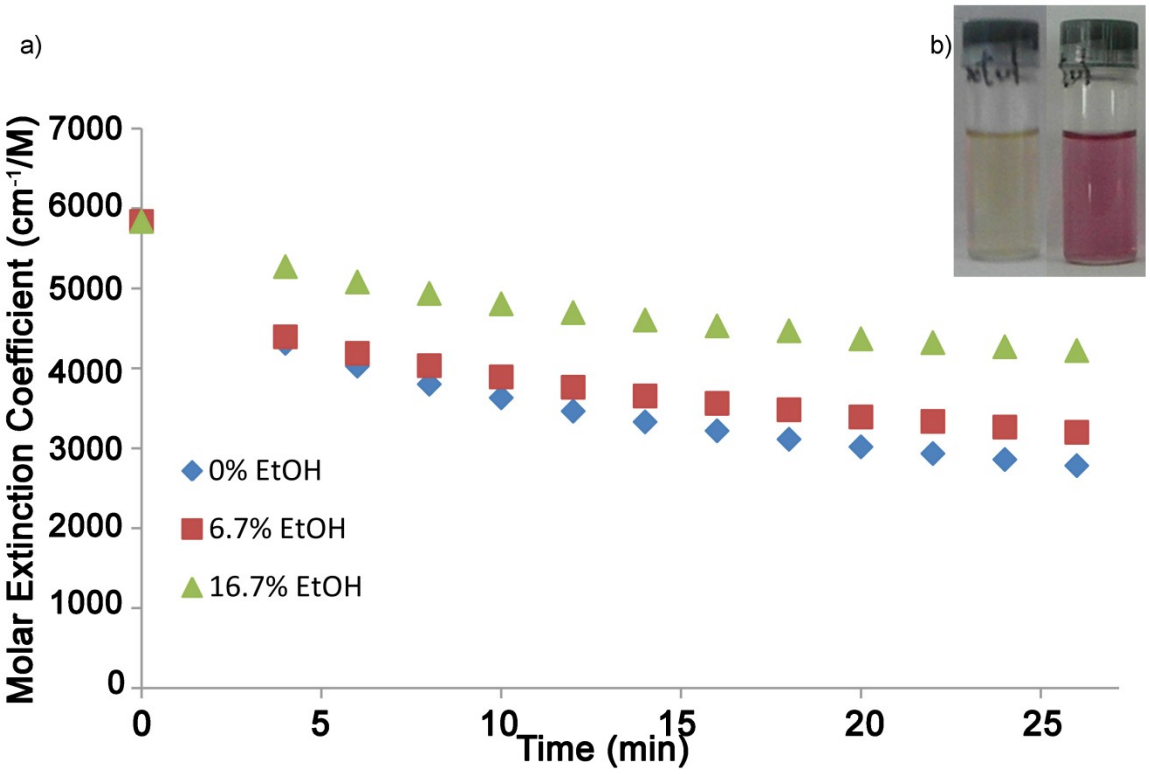

Figure 7.19: Effect of competitive hydrogen bonding on the formation of **{[7.13$_2$•Fe]$_4^{8+}$•7.9a$_4$}**: a) Competition studied by UV/Vis in increasing amounts of ethanol (MeCN, 2.25 x 10^{-5} M); b) A sample at t = 4d (left) and t = 10 d (right).

Attempts to characterize the self-assembly in the solid state were unsuccessful. Growing co-crystals by slow evaporation, vapor diffusion, and biphasic mixing all failed. Attempts to grow co-crystals of **7.9a** with **[7.13$_2$•Fe](BPh$_4$)$_2$** were also unsuccessful, as were attempts at using the less flexible pyromellitic diimide in place of **7.9a**. The assembly of **[7.13$_2$•Fe](ClO$_4$)$_2$** and **7.9a** was not amenable to analysis by MALDI-MS or ESI-MS, and even DOSY NMR was ineffective, as the relaxation rate was too quick to allow for the necessary diffusion time.

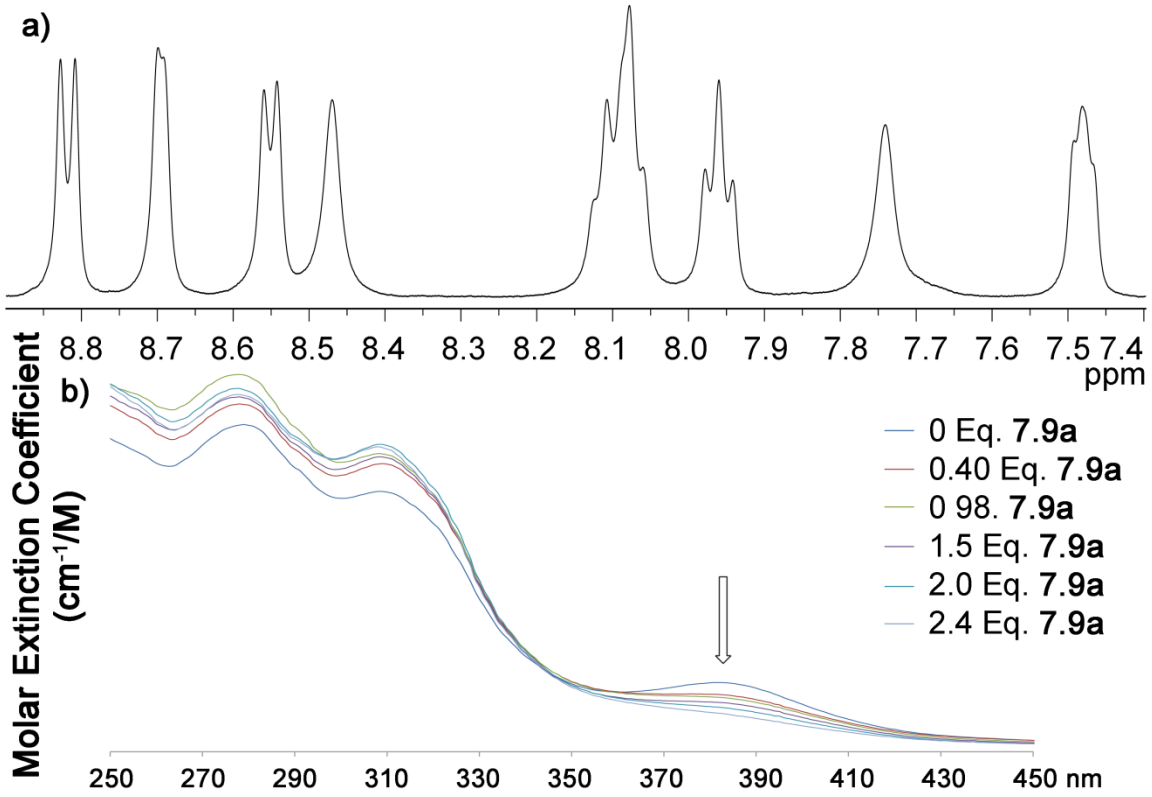

Figure 7.20: Characterization of **[7.13$_2$•Fe^{III}](ClO$_4$)$_3$**: a) ^{1}H NMR spectrum of **[7.13$_2$•Fe^{III}](ClO$_4$)$_3$** (DMSO-d_6, 400 MHz, 298 K); b) UV/Vis titration of **7.9a** into a solution of **[7.13$_2$•Fe^{III}](ClO$_4$)$_3$** (CH_3CN, 2.4 x 10^{-5} M).

The iron(III) analogue could also be prepared by treating **7.13** with iron(III) perchlorate in acetonitrile to give an orange complex. This complex was less paramagnetic than the iron(II) species with μ_{eff} = 3.5. The ^{1}H NMR spectrum of **[7.13$_2$•Fe^{III}](ClO$_4$)$_3$** was captured in a standard window (Figure 7.20a). The ^{1}H resonances shifted when **[7.13$_2$•Fe^{III}](ClO$_4$)$_3$** was treated with **7.9a**, however, no new peaks were observed in the ^{1}H NMR spectrum. Analysis by UV/Vis shows that the MLCT band for this complex, which is at 380 nm, readily decreases upon addition of **7.9a** (Figure 7.20b).

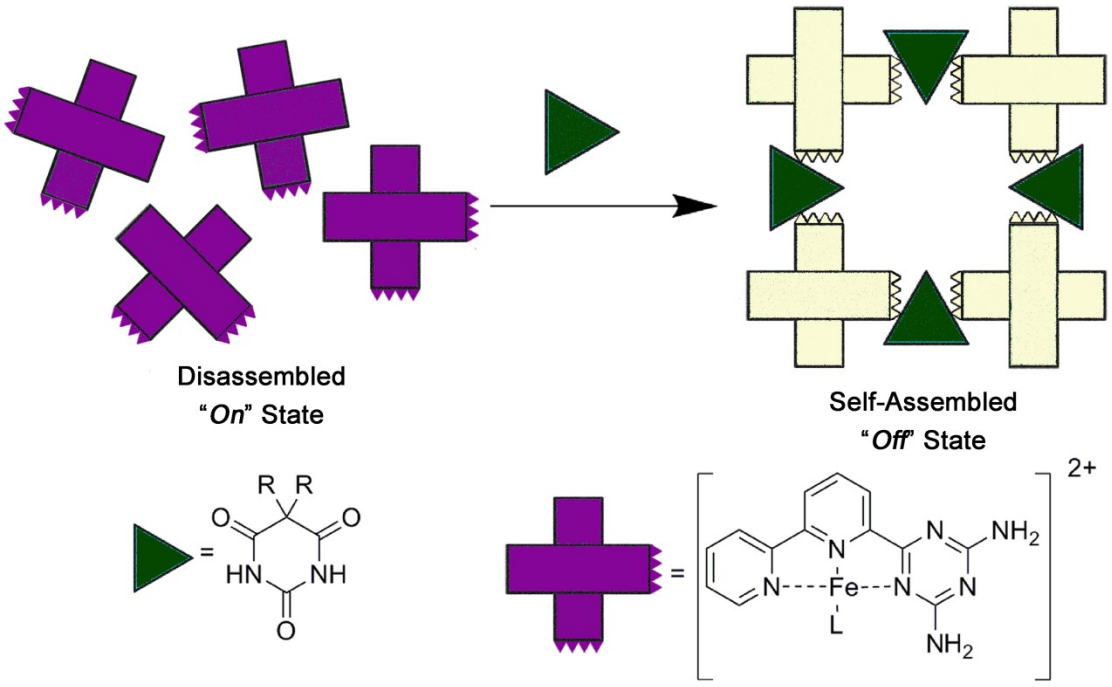

Figure 7.21: Use of **[7.13$_2$•Fe](ClO$_4$)$_2$** as a colorimetric sensor for barbituric acids.

The noticeable change in color of both **[7.13$_2$•Fe](ClO$_4$)$_2$** and **[7.13$_2$•Fe^{III}](ClO$_4$)$_3$** upon hydrogen bonding self-assembly with **7.9a** suggested they might serve as colorimetric sensors for neutral barbituric acids. Although there are chemical sensors known for barbituric acids, most notably the Hamilton-type receptors,[22] detection requires observing the change in fluorescence emission or by sensing barbiturates with chromophores attached.[23] These complexes could fill the need for a broad colorimetric sensor for barbiturates which doesn't suffer from challenges with selectivity.[24] Diethyl barbiturate (**7.9b**) and dibutyl barbiturate (**7.9c**) were synthesized for this study. Both caused a similar color change from "on" to "off" when combined with **[7.13$_2$•Fe](ClO$_4$)$_2$** (Figure 7.21). The differences in the side chains of **7.9a**-**c** suggested **[7.13$_2$•Fe](ClO$_4$)$_2$** should be able to detect a wide range of barbiturates.

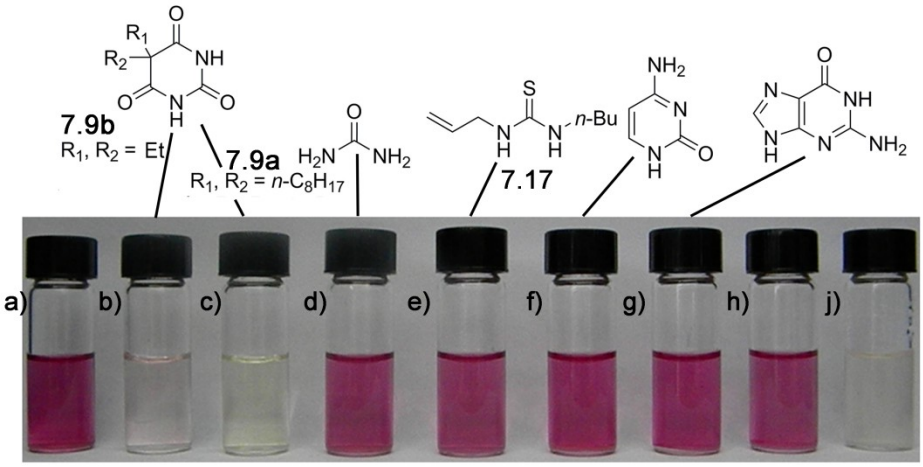

Figure 7.22: Colorimetric detection of different hydrogen bonders (1 x 10^{-2} M, 87 eq. ea.) using **[7.13$_2$•Fe](ClO$_4$)$_2$** (CH_3CN, 1.15 x 10^{-4} M): a) **[7.13$_2$•Fe](ClO$_4$)$_2$** only; b) **7.9b**; c) **7.9a**; d) urea; e) thiourea **7.17**; f) Saturated cytosine; g) Saturated guanine; h) Mixture of urea, **7.17**, and cytosine; j) Mixture of **7.9a,** urea, **7.17**, and cytosine.

Significant quantities of competitive hydrogen bonders (ethanol or water) could deactivate the sensing ability of **[7.13$_2$•Fe](ClO$_4$)$_2$**, but it was not clear whether or not complementary hydrogen bonders could lead to false positives. To test the sensitivity, the complex **[7.13$_2$•Fe](ClO$_4$)$_2$** was added to acetonitrile as a control for the "on" state (Figure 7.22a). It was also mixed with **7.9b** and **7.9a** (Figure 7.22b and c respectively) as a control for the "off" state. When the complex was mixed with a significant excess of urea (Figure 7.22d), thiourea **7.17** (Figure 7.22e), cytosine (Figure 7.22f) or guanine (Figure 7.22g), there was no sign of a color change. If these four hydrogen bonders were combined together (Figure 7.22h), there was still no sign of a color change. In the presence of these competitive hydrogen bonders, **[7.13$_2$•Fe](ClO$_4$)$_2$** was still able to sense **7.9a** (Figure 7.22j).

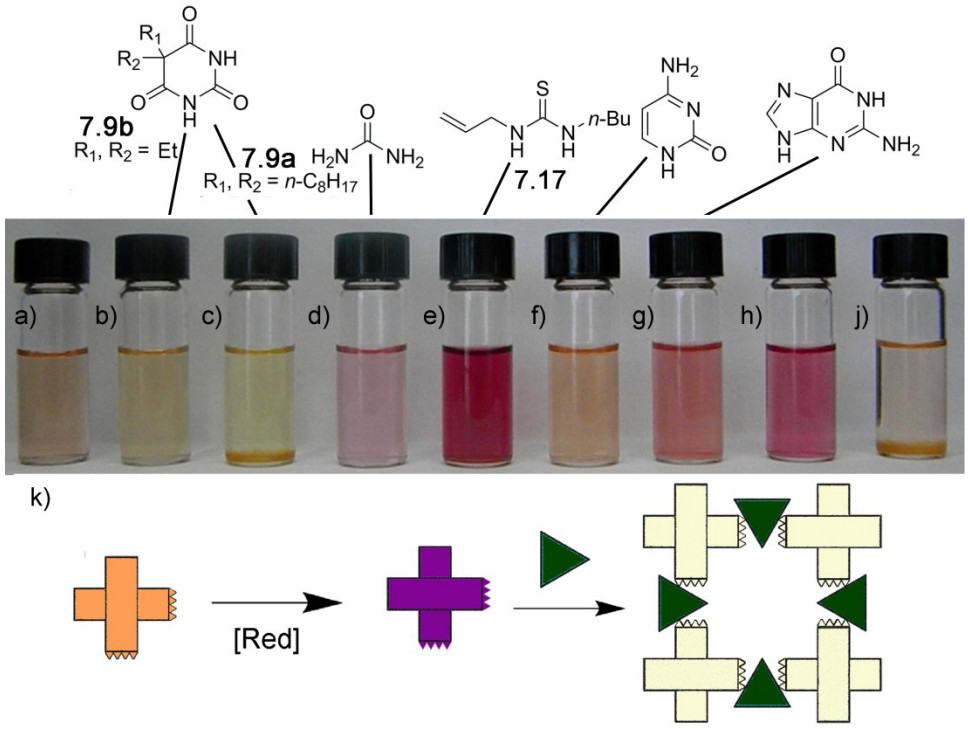

Figure 7.23: Colorimetric detection of different hydrogen bonders (1 x 10^{-2} M, ~22 eq. ea.) using **[7.13$_2$•Fe^{III}](ClO$_4$)$_3$** (CH_3CN, 4.6 x 10^{-4} M): a) **[7.13$_2$•Fe^{III}](ClO$_4$)$_3$** only; b) **7.9b**; c) **7.9a**; d) urea; e) thiourea **7.17**; f) Saturated cytosine; g) Saturated guanine; h) Mixture of urea, **7.17**, and cytosine; j) Mixture of **7.9a,** urea, **7.17**, and cytosine.

Tests with the iron(III) analogue gave a more sensitive response when followed by UV/Vis. The loss of the MLCT band at 380 nm, however, resulted in a less obvious difference between the “on” control (Figure 7.23a) and the “off” controls (Figure 7.23b and c). Addition of the hydrogen bonders individually (Figure 7.23d-g) resulted in a slight to dramatic change in color back towards the purple of the **[7.13$_2$•Fe](ClO$_4$)$_2$** complex. The process took longer for cytosine and guanine (Figure 7.23f and g respectively), and the presence of other species retarded the process when all four were mixed together (Figure 7.23h). Analysis by UV/Vis confirmed the iron in these samples had returned to the +2 oxidation state, complete with the expected MLCT band at 557 nm. Analysis of

the complexes by cyclic voltammetry (Figure 7.24) suggests a large difference between charge states.

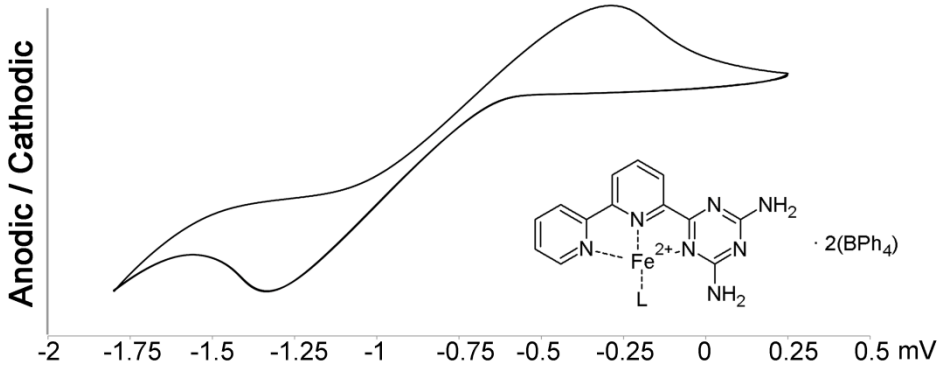

Figure 7.24: Cyclic voltammogram of **[7.13$_2$•Fe](ClO$_4$)$_2$** (MeCN, 5.0 x 10^{-4} M Bu_4NBF_4 buffer, 4.8 x 10^{-5} M, Scan Rate = 0.05 V/s).

7.5 Hybrid Self-Assemblies Based on Ureidopyrimidinones

One limitation of the diaminotriazine motif for hydrogen bonding is the low binding association between complementary pairs. To make robust assembled cages using this strategy, a stronger hydrogen bonding motif was required. Ureidopyrimidinones offer increased strength.[25] The addition of an extra contact adds approximately 2 kcal mol^{-1} to the overall stability of the association. There are also more favorable "secondary" interactions when matched groups are adjacent (such as two donor pairs together) and can add stabilization on the order of 0.8 kcal mol^{-1} due to positive interactions across a diagonal association.

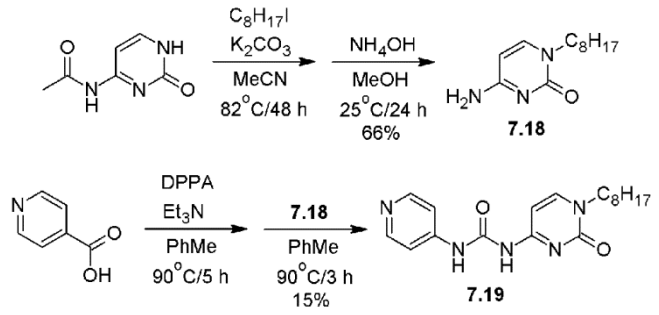

Figure 7.25: Synthesis of 4-pyridyl UPy **7.19** from N^4-acetylcytosine and isonicotinic acid.

Commercially available N^4-acetylcytosine was alkylated by heating with 1-iodooctane and potassium carbonate in acetonitrile (Figure 7.25). The crude amide was then deprotected withammonium hydroxide in methanol at room temperature to give the desired product **7.18** in great yield after recrystallization from EtOH. In a second step, isonicotinic acid was treated in anhydrous toluene with diphenylphosphorylazide and triethylamine to afford the Curtius rearrangement product *in situ*, followed by addition of **7.18**. This led to the desired 4-pyridyl UPy **7.19**. Unfortunately, this was unable to form a single discrete self-assembly when complexed with Pd(II), Mn(I), or Re(I).

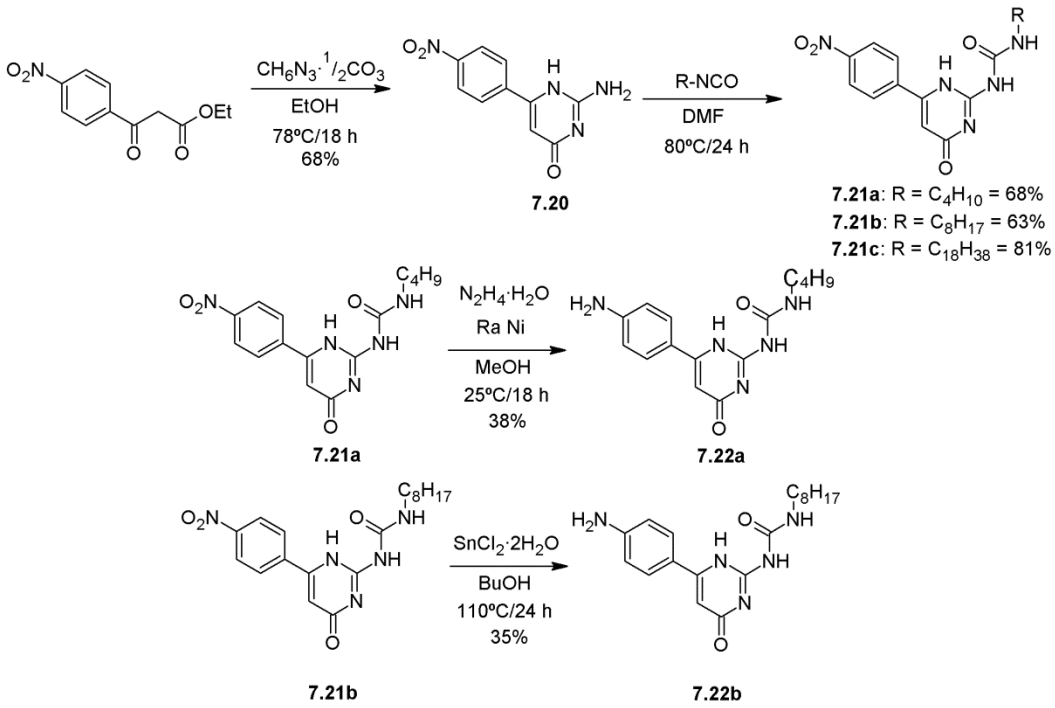

Figure 7.26: Synthesis of isocytosine **7.20** and UPy derivatives **7.21a**-**c**.

Condensation of ethyl 4-nitrophenylacetoacetate with guanidine carbonate gave isocytosine **7.20** in good yield (Figure 7.26). Treatment of **7.20** with different alkyl isocyanates led to formation of nitro-ureidopyrimidinones **7.21a**-**c**. These could be reduced either using Raney nickel (in the case of **7.21a**) or with tin dichloride (**7.21b**) to afford the necessary anilines **7.22a** and **7.22b** for multi-component self-assembly. Reduction of **7.21c** was unsuccessful under a variety of conditions due to its insolubility.

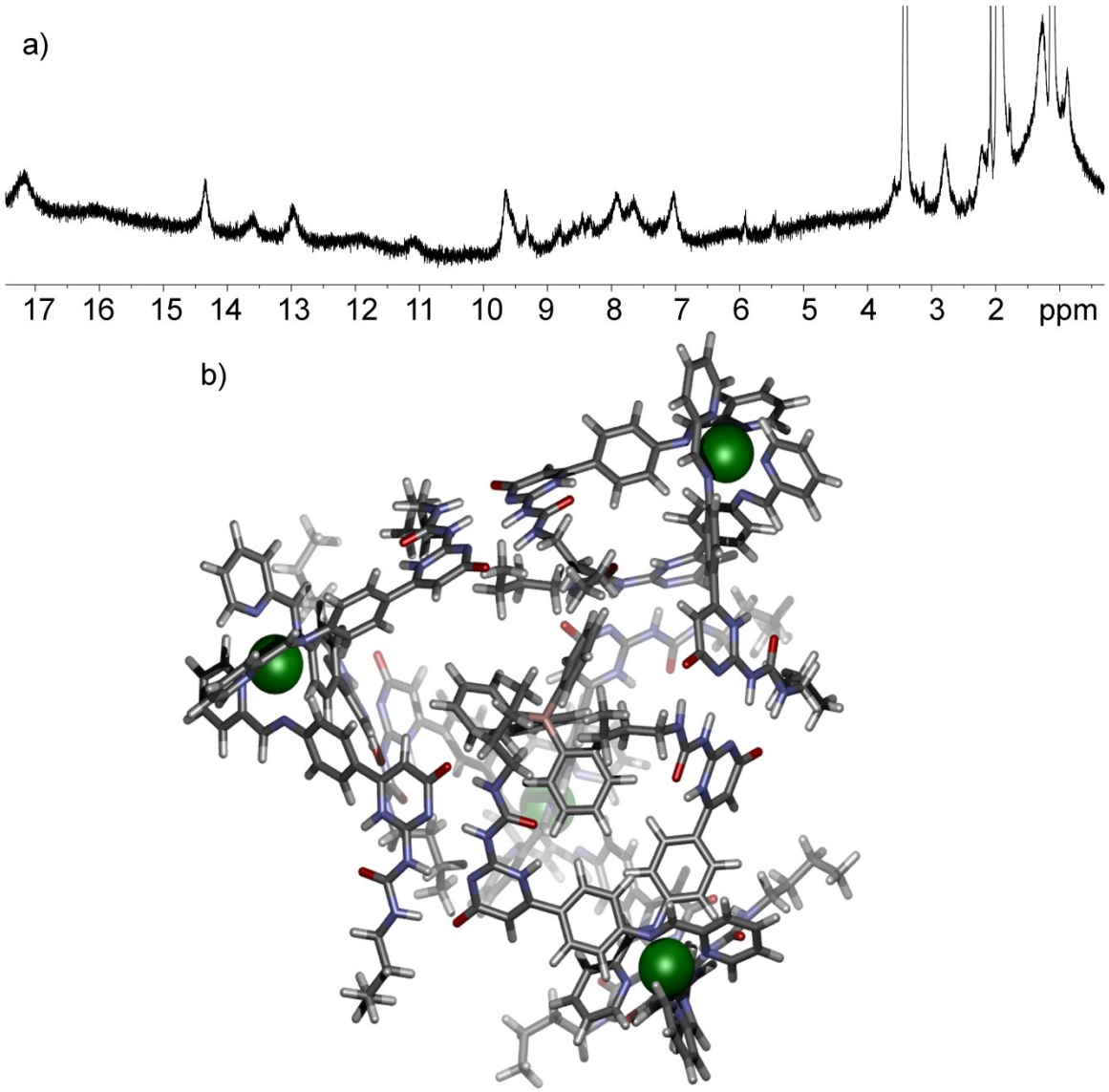

Figure 7.27: Hybrid tetrahedron: a) ^{1}H NMR spectra of **[7.23b$_x$•Fe$_y$]$^{2y+}$** (Me_2CO-d_6, 400 MHz, 298K); b) SPARTAN model of **[(BPh$_4$)⊂[7.23b$_{12}$•Fe$_4$]$^{7+}$** (AM1 forcefield).

Multi-component self-assembly of **7.22a** with 2-formylpyridine and $Fe(ClO_4)_2$•xH_2O followed by precipitation with diethyl ether gave **[7.23a$_x$•Fe$_y$]$^{2y+}$** as a purple complexes, but this was not very soluble. Attempts to redissolve samples required treatment in a sonicator bath with heating, giving rise to broad ^{1}H NMR spectra consistent with the

formation of mostly undefined aggregates. Addition of methanol broke apart the aggregate and led to better dissolution, although it failed to give a ^{1}H NMR spectrum that could be attributed to a single product.

The low solubility of the **[7.23a$_x$•Fe$_y$]$^{2y+}$** species necessitated study of aniline **7.22b**. Multi-component self-assembly using **7.22b**, 2-formylpyridine, and $Fe(ClO_4)_2$•xH_2O gave conversion to the product **[7.23b$_x$•Fe$_y$]$^{2y+}$**. As seen from the ^{1}H NMR spectrum (Figure 7.27a), this species exhibits many broad peaks, but this is likely a consequence of paramagnetism, not poor association. Molecular modeling suggests an M_4L_{12} is being formed (Figure 7.27b). Further characterization is currently underway to establish the identity of this assembly.

7.6 Conclusions

Preparation of hybrid metal-organic self-assemblies that utilize both dative and hydrogen bonding to self-assemble presents numerous challenges. They require careful choice of metal coordination motif to have the necessary solubility in solvents that are amenable to hydrogen bonding. They also provide some benefits, such as the preparation larger cages (such as **[7.23b$_{12}$•Fe$_4$]$^{8+}$**), without the need to construct exceptionally long ligands. Continued work in this area will have to address the subtle differences between strength of hydrogen bonding interactions with viable metal chelation strategies.

7.7 References

1) Pichlmaier, M.; Winter, R. F.; Zabel, M.; Záliš, S. “Electron Transfer Across Multiple Hydrogen Bonds: The Case of Ureapyrimidinedione-Substituted Vinyl Ruthenium and Osmium Complexes.” *J. Am. Chem. Soc.*, **2009**, *131*, 4892-4903.

2) a) Jang, J.-J.; Li, L.; Yang, T.; Kuang, D.-B.; Wang, W.; Su, C.-Y. “Self-Assembly of 2D Borromean Networks Through Hydrogen-Bonding Recognition.” *Chem. Commun*., **2009**, 2387-2389; b) Chen, C.-L.; Beatty, A. M. “Guest Inclusion and Structural Dynamics in 2-D Hydrogen-Bonded Metal-Organic Frameworks.” *J. Am. Chem. Soc.*, **2008**, *130*, 17222-17223.

3) Ilmain, F.; Tanaka, T.; Kokufuta, E. “Volume Transition in a Gel Driven by Hydrogen Bonding.” *Nature*, **1991**, *349*, 400-401.

4) Miyoshi, D.; Karimata, H.; Wang, Z.-M.; Koumoto, K.; Sugimoto, N. “Artificial G-Wire Switch with 2,2’-Bipyridine Units Responsive to Divalent Metal Ions.” *J. Am. Chem. Soc.*, **2007**, *129*, 5919-5925.

5) Ihara, T.; Shirasaka, Y.; Sato, Y.; Kitamura, Y.; Okada, K.; Tazaki, M.; Jyo, A. “Synthesis of the Amidite Reagent to Build Bipyridine Units into DNA Backbone.” *Heterocycles*, **2005**, *65*, 293-301.

6) Janeba, Z.; Balzarini, J.; Andrei, G.; Snoeck, R.; De Clercq, E.; Robins, M. J. “Synthesis and Biological Evaluation of 5-(Alkynyl)-1-(p-toluenesulfonyl)uracil Derivatives” *Can. J. Chem.*, **2006**, *84*, 580-586.

7) Mathias, J. P.; Simanek, E. E.; Zerkowski, J. A.; Seto, C. T.; Whitesides, G. M. “Structural Preferences of Hydrogen-Bonded Networks in Organic Solution – the Cyclic $CA_3 \bullet M_3$ “Rosette”” *J. Am. Chem. Soc.*, **1994**, *116*, 4316-4325.

8) Chauhan, S. M. S.; Giri, N. G. “Rosette Formation by Hydrogen Bonding of 5,5-Dialkylbarbituric Acids with 2-Amino-4,6-bis[5-(4’-aminophenyl)porphyrinatozinc]-1,3,5-triazines in Solution.” *Supramol. Chem.*, **2008**, *20*, 743-752.

9) Demnitz, F. W. J.; D’heni, M. B. “A High Yielding Preparation of 2,2’-Bipyridine-1-Oxide.” *Org. Prep. Proced. Int.*, **1998**, *30*, 467-469.

10) Van der Vlugt, J. I.; Demeshko, S.; Dechert, S.; Meyer, F. “Tetranuclear Co^{II}, Mn^{II}, and Cu^{II} Complexes of a Novel Binucleating Pyrazolate Ligand Preorganized for the Self-Assembly of Compact [2 x 2]-Grid Structures.” *Inorg. Chem.*, **2008**, *47*, 1576-1585.

11) a) Case, F. H. “The Preperation of Triazines Related to 6-Cyano-2,2’-bipyridine.” *J. Org. Chem.*, **1966**, *31*, 2398-2400; b) Duong, A.; Maris, T.; Lebel, O.; Wuest, J. D. “Synthesis and Structures of Isomeric Diaminotriazinyl-Substituted 2,2’-Bipyridines and 1,10-Phenanthrolines.” *J. Org. Chem.*, **2011**, *76*, 1333-1341.

12) a) Lewis, K. M.; Kelley, J.; Peterson, L. Jr.; Smith, M. D.; Severance, R. C.; Vaughn, S. A.; zur Loye, H.-C. “Synthesis and Crystal Structure of an Iodobismuthate Incoporporating Both a Cationic and Anionic Bi(III) Complex Ion.” *J. Chem. Cryst.*, **2010**, *40*, 867-871; b) Semenova, L. I.; Sobolev, A. N.; Skelton, B. W.; White, A. H. “Structure Systematics of Rare Earth Complexes. XV. Tris(2,2’:6’,2-terpyridine)lanthanoid(III) Tris(perchlorate) Complexes.” *Aus. J. Chem.*, **1999**, *52*, 519-529.

13) Young, M. C.; Liew, E.; Ashby, J.; McCoy, K. E.; Hooley, R. J. “Spin State Modulation of Iron Spin Crossover Complexes *via* Hydrogen-Bonding Self-Assembly.” *Chem. Commun.*, **2013**, *49*, 6331-6333.

14) Constable, E. C.; Baum, G.; Bill, E.; Dyson, R.; van Eldik, R.; Fenske, D.; Kaderli, S.; Morris, D.; Neubrand, A.; Neuburger, M.; Smith, D. R.; Wieghardt, K.; Zehnder, M.; Zuberbühler, “Control of Iron(II) Spin States in 2,2’:6’,2”-Terpyridine Complexes Through Ligand Substitution.” *Chem.-Eur. J.*, **1999**, *5*, 498-508.

15) Medlycott, E. A.; Hanan, G. S.; Abedin T. S. M.; Thompson, L. K. “The Effect of Steric Hindrance on the Fe(II) Complexes of Triazine-Containing Ligands.” *Polyhedron*, 2008, **27**, 493-501.

16) a) Bousseksou, A.; Molnár, G.; Salmon, L.; Nicolazzi, W. “Molecular Spin Crossover Phenomenon: Recent Achievements and Prospects.” *Chem. Soc. Rev.*, **2011**, *40*, 3313-3335; b) Machan, C. W.; Adelhardt, M.; Sarjeant, A. A.; Stern, C. L.; Sutter, J.; Meyer, K.; Mirkin, C. A. “One-Pot Synthesis of an Fe(II) Bis-Terpyridine Complex with Allosterically Regulated Electronic Properties.” *J. Am. Chem. Soc.*, **2012**, *134*, 16921-16924; c) Olguín, J.; Brooker, S. “Spin Crossover Active Iron(II) Complexes of Selected Pyrazole-Pyridine/Pyrazine Ligands.” *Coord. Chem. Rev.*, **2011**, *255*, 203-240.

17) a) Scepaniak, J. J.; Harris, T. D.; Vogel, C. S.; Sutter, J.; Meyer, K.; Smith, J. M. “Spin Crossover in a Four-Coordinate Iron(II) Complex.” *J. Am. Chem. Soc.*, **2011**, *133*, 3824-3827; b) Gütlich, P.; Ksenofontov, V.; Gaspar, A. B. “Pressure Effect Studies on Spin Crossover Systems.” *Coord Chem. Rev.*, **2005**, *249*, 1811-1829.

18) a) Schuber, E. M. “Utilizing the Evans Method with a Superconducting NMR Spectrometer in the Undergraduate Laboratory.” *J. Chem. Educ.*, **1992**, *69*, 62; b) Loliger, J.; Scheffold, R. “Paramagnetic Moment Measurements by NMR. A Micro Technique.” *J. Chem. Educ.*, **1972**, *49*, 646-647.

19) King, E. R.; Sazama, G. T.; Betley, T. A. “Co(III) Imidos Exhibiting Spin Crossover and C-H Bond Activation.” *J. Am. Chem. Soc.*, **2012**, *134*, 17858-17861.

20) a) Southon, P. D.; Liu, L.; Fellows, E. A.; Price, D. J.; Halder, G. J.; Chapman, K. W.; Moubaraki, B.; Murray, K. S.; Létard, J.-F.; Kepert, C. J. “Dynamic Interplay Between Spin-Crossover and Host-Guest Function in a Nanoporous Metal-Organic Framework Material.” *J. Am. Chem. Soc.*, **2009**, *131*, 10998-11009; b) Halder, G. J.;

Kepert, C. J.; Moubaraki, B.; Murray, K. S.; Cashion, J. D. “Guest-Dependent Spin Crossover in a Nanoporous Molecular Framework Material.” *Science*, **2002**, *298*, 1762-1765.

21) Young, M. C.; Liew, E.; Hooley, R. J. “Colorimetric Barbiturate Sensing with Hybrid Spin Crossover Assemblies.” *Chem. Commun.*, **2014**, *50*, 5043-5045.

22) a) McGrath, J. M.; Pluth, M. D. “Understanding the Effects of Preorganization, Rigidity, and Steric Interactions in Synthetic Barbiturate Receptors.” *J. Org. Chem.*, **2014**, *79*, 711-719; b) Chang, S.-K.; Hamilton, A. D. “Molecular Recognition of Biologically Interesting Substrates: Synthesis of an Artificial Receptor for Barbiturates Employing Six Hydrogen Bonds.” *J. Am. Chem. Soc.*, **1988**, *110*, 1318-1319.

23) Tecilla, P.; Dixon, R. P.; Slobodkin, G.; Alavi, D. S.; Waldeck, D. H.; Hamilton, A. D. “Hydrogen-Bonding Self-Assembly of Multichromophore Structures.” *J. Am. Chem. Soc.*, **1990**, *112*, 9408-9410.

24) Westwood, J.; Coles, S. J.; Collinson, S. R.; Gasser, G.; Green, S. J.; Hursthouse, M. B.; Light, M. E.; Tucker, J. H. R. “Binding and Electrochemical Recognition of Barbiturate and Urea Derivatives by a Regioisomeric Series of Hydrogen-Bonding Ferrocene Receptors.” *Organometallics*, **2004**, *23*, 946-951.

25) Rieth, S.; Baddeley, C.; Badjic, J. D. “Prospects in Controlling Morphology, Dynamics, and Responsiveness of Supramolecular Polymers.” *Soft Matter*, **2007**, *3*, 137-154.

Chapter 8 – Experimental

8.1 General Information

^{1}H, gCOSY and ^{13}C spectra were recorded on either a Varian Inova 400 MHz or 500 MHz NMR spectrometer, or a Bruker 600 MHz spectrometer and processed using MestReNova by Mestrelab Research S.L. NOESY, ROESY, TOCSY, and DOSY NMR were recorded on a Bruker 600 MHz spectrometer equipped with TopSpin. Proton (^{1}H) chemical shifts are reported in parts per million (δ) with respect to tetramethylsilane (TMS, δ=0), and referenced internally with respect to the protio solvent impurity. Deuterated NMR solvents were obtained from Cambridge Isotope Laboratories, Inc., Andover, MA, and used without further purification. Mass spectra were recorded on an Agilent 6210 LC TOF mass spectrometer using electrospray ionization with fragmentation voltage set at 115 V and processed with an Agilent MassHunter Operating System. X-ray diffraction data were collected at 100(2) K on a Bruker APEX2 platform-CCD X-ray diffractometer system. Room temperature UV/Vis spectroscopy was performed on a Cary 50 Photospectrometer using the Varian Scans program to collect data. Variable temperature UV/Vis spectra were obtained by suspending a cuvette in a dewar filled with an acetone/dry ice bath for low temperatures and a heated beaker of water for warmer temperatures, with spectra collected using a home-built Ocean Optics system. Cyclic voltammetry was performed using a CH Instruments Electrochemical Analyzer with a glassy carbon working electrode, a Pt wire auxiliary, and Ag/AgCl for the reference electrode. Magnetic susceptibility measurements were performed according to the Evans method, with the deuterated solvent used as the reference, and the chemical shift difference between the reference and solution used to determine the paramagnetic

contribution of the solute. All other materials were obtained from Aldrich Chemical Company, St. Louis, MO and were used as received. Solvents were dried through a commercial solvent purification system (Pure Process Technologies, Inc.). Molecular modeling (semi-empirical calculations) was performed using the AM1 force field using SPARTAN.[1]

8.2 Chapter 2 Experimental

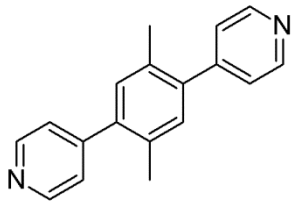

2.1a

2,5-bis(4-pyridyl)-*p*-xylene (2.1a):

The reagent 2,5-dibromo-*p*-xylene (250 mg, 0.95 mmol), 4-pyridine boronic acid (291 mg, 2.4 mmol), [1,1′-Bis(diphenylphosphino)ferrocene]dichloropalladium(II), complex with dichloromethane (77 mg, 110 μmol) and cesium carbonate (926 mg, 2.8 mmol) were combined in a 50 mL round bottomed flask with stir bar and attached reflux condenser. The system was placed under N_2 using a Schlenk line, followed by addition of anhydrous PhMe (10 mL) and EtOH (10 mL). The reaction was subjected to three more purge cycles, followed by heating to reflux. The reaction was cooled after 72 h, followed by diluting with Et_2O (200 mL). This was filtered through celite to remove palladium black and other salts, followed by removing the organic solvent *in vacuo*. The resulting solid was recrystallized from absolute EtOH to give product as a tan product (209 mg, 84%). ^{1}H NMR (400 MHz; $CDCl_3$) δ 8.67 (dd, *J* = 4.4, 1.6 Hz, 4H), 7.30 (dd, *J* =

4.4, 1.6 Hz, 4H), 7.15 (s, 2H), 2.29 (s, 6H); ^{13}C NMR (100 MHz; $CDCl_3$) δ 149.8, 149.4, 139.3, 132.9, 131.7, 124.3, 19.8.

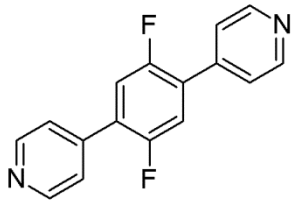

2.1b

2,5-bis(4-pyridyl)-*p*-difluorobenzene (2.1b):

The reagent 2,5-dibromo-*p*-difluorobenzene (250 mg, 0.92 mmol), 4-pyridine boronic acid (283 mg, 2.3 mmol), [1,1′-Bis(diphenylphosphino)ferrocene]dichloropalladium(II), complex with dichloromethane (77 mg, 110 μmol) and cesium carbonate (1498 mg, 3.07 mmol) were combined in a 50 mL round bottomed flask with stir bar and attached reflux condenser. The system was placed under N_2 using a Schlenk line, followed by addition of anhydrous PhMe (10 mL) and EtOH (10 mL). The reaction was subjected to three more purge cycles, followed by heating to reflux. The reaction was cooled after 72 h, followed by diluting with Et_2O (480 mL). This was filtered through celite, and the celite was then rinsed with DCM (75 mL). This organic layer was washed with deionized H_2O (3 x 100 mL), dried over $MgSO_4$, then evaporated *in vacuo* to give product as a tan solid (27 mg, 11%). ^{1}H NMR (400 MHz; $CDCl_3$) δ 8.74 (d, *J* = 4.1 Hz, 4H); 7.51 (d, *J* = 3.8 Hz, 4H); 7.35 (t, *J* = 8.4 Hz, 2H).

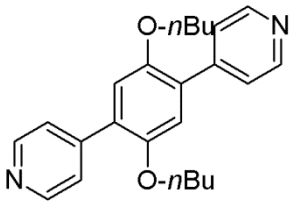

2.1c

2,5-bis(4-pyridyl)-*p*-dibutyloxybenzene (2.1c):

The reactant 2,5-diiodo-*p*-dibutyloxybenzene (240 mg, 0.52 mmol), 4-pyridine boronic acid (160 mg, 1.3 mmol), [1,1′-Bis(diphenylphosphino)ferrocene]dichloropalladium(II), complex with dichloromethane (54 mg, 77 μmol) and cesium carbonate (500 mg, 1.5 mmol) were combined in a 50 mL round bottomed flask with stir bar and attached reflux condenser. The system was placed under N_2 using a Schlenk line, followed by addition of DMF (5 mL). The reaction was subjected to three more purge cycles, followed by heating to 110°C. The reaction was cooled after 20 h, followed by diluting with EtOAc (500 mL). This was filtered through celite, followed by evaporating *in vacuo*. The residue of this was recrystallized from EtOH to give a tan solid (18 mg, 9%). ^{1}H NMR (400 MHz; $CDCl_3$) δ 7.72 (m, 4H), 7.50 (m, 2H), 7.44 (m, 4H), 3.92 (t, *J* = 6.4 Hz, 4H), 1.77 (quin, *J* = 8.1 Hz, 4H), 1.53 (sex, *J* = 7.5 Hz, 4H), 0.99 (t, *J* = 7.4 Hz, 6H); ^{13}C NMR (100 MHz; $CDCl_3$) δ 152.9, 133.4, 132.6, 132.4, 132.3, 131.6, 128.7, 128.5, 122.8, 86.4, 70.1, 31.3, 19.4, 13.9.

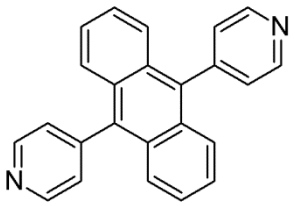

2.1d

9,10-bis(4-pyridyl)-anthracene (2.1d):

The reagent 9,10-dibromoanthracene (300 mg, 0.89 mmol), 4-pyridine boronic acid (283 mg, 2.23 mmol), [1,1′-Bis(diphenylphosphino)ferrocene]dichloropalladium(II), complex with dichloromethane (62 mg, 88 μmol) and cesium carbonate (872 mg, 2.68 mmol) were combined in a 50 mL round bottomed flask with stir bar and attached reflux condenser. The system was placed under N_2 using a Schlenk line, followed by addition of DMF (25 mL). The reaction was subjected to three more purge cycles, followed by heating to reflux. The reaction was cooled after 34 h, followed by diluting with deionized H_2O (100 mL). This was filtered through celite, and the celite was then rinsed with CH_2Cl_2 (75 mL). This organic layer was washed with deionized H_2O (3 x 100 mL), dried over $MgSO_4$, then evaporated *in vacuo* to give product as a tan solid (291 mg, 98%). ^{1}H NMR (400 MHz; $CDCl_3$) δ 8.88 (d, *J* = 5.5 Hz, 4H), 7.61 (dd, *J* = 6.8, 3.3 Hz, 4H), 7.44 (d, *J* = 5.5 Hz, 4H), 7.40 (dd, *J* = 6.8, 3.2 Hz, 4H); ^{13}C NMR (100 MHz; $CDCl_3$) δ 150.2, 147.5, 134.8, 129.1, 126.6, 126.4, 126.1.

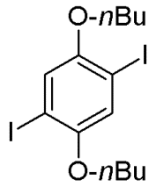

2.2

2,5-diiodo-*p*-dibutyloxybenzene (2.2):

Hydroquinone (1.34 g, 12.1 mmol) and potassium hydroxide (2.9 g, 51.7 mmol) were combined in a 50 mL round bottomed flask with stir bar and attached reflux condenser. The system was placed under N_2 using a Schlenk line, followed by addition of DMF (10 mL). The mixture was heated to 60°C for 1 h, followed by addition of 1-iodobutane (4.8

mL, 42.3 mmol). After 15 h the reaction was cooled, diluted with deionized H_2O, and filtered to give a light brown glassy solid. A portion of the resulting solid (350 mg 1.6 mmol) was then added to a mixture of iodine monochloride (1.85 g, 11.4 mmol) in MeOH (3 mL), followed by heating under reflux. After 8 h the reaction was cooled, followed by evaporation of the solvent *in vacuo*. The resulting oil was treated with saturated $Na_2SO_{3(aq)}$ followed by extraction with CH_2Cl_2. The organic layer was dried over $MgSO_4$ and evaporated *in vacuo* to give product as a green solid (666 mg, 89%). ^{1}H NMR (400 MHz; $CDCl_3$) δ 7.17 (s, 2H), 3.94 (t, *J* = 6.4 Hz, 4H), 1.79 (quin, *J* = 6.9 Hz, 4H), 1.53 (sex, *J* = 4.6 Hz, 4H), 0.98 (t, *J* = 7.4 Hz, 6H).

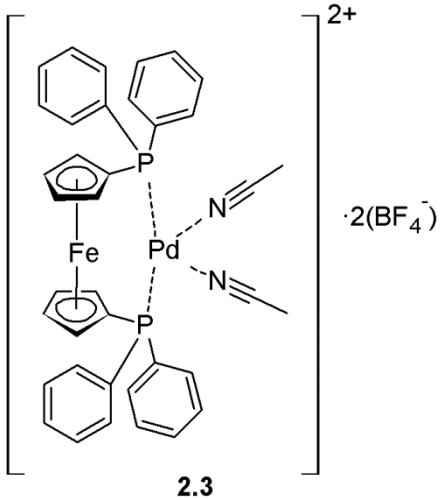

2.3

[1,1′-bis(diphenylphosphino)ferrocene]bis-acetonitrilepalladium(II) tetrafluoroborate (2.3):

[1,1′-Bis(diphenylphosphino)ferrocene]dichloropalladium(II) complex with dichloromethane (100 mg, 0.12 mmol) were combined in MeCN (8 mL) and CH_2Cl_2 (5 mL) in a 25 mL round bottom flask. To this was added silver tetrafluoroborate (47.7 mg, 0.25 mmol) in MeCN (2 mL). The solution was submerged in an ultrasonification bath for

5 min, followed by centrifugation of the resulting white precipitate. The organic layer was then evaporated *in vacuo* to give product as a purple solid (99 mg, 90%). ^{1}H NMR (400 MHz; CD_3CN) δ 7.81 (br s, 8H), 7.72 (t, *J* = 7.3 Hz, 4H), 7.57 (t, *J* = 7.3 Hz, 8H), 4.72 (br s, 8H), 1.96 (s, 6H).

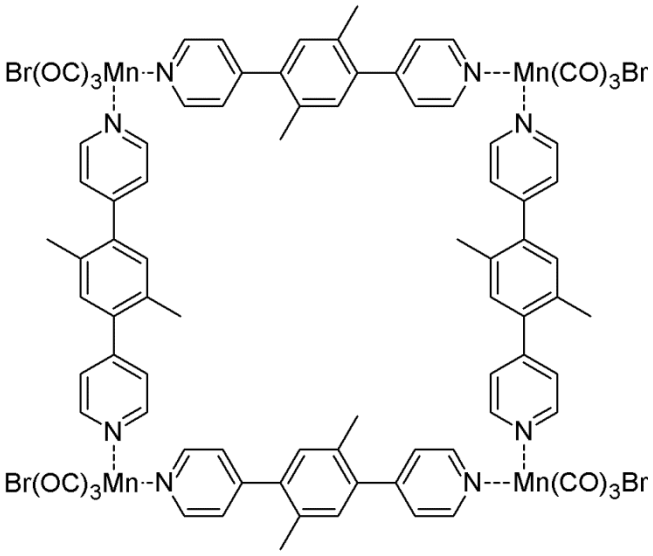

[2.1a$_4$·Mn$_4$](CO)$_{12}$Br$_4$

[2.1a$_4$•Mn$_4$](CO)$_{12}$Br$_4$:

Ligand **2.1a** (68.0 mg, 0.26 mmol) was combined with $Mn(CO)_5Br$ in a 25 mL round bottom flask, followed by addition of Me_2CO (10 mL). The mixture was stirred in the dark for 9 h, followed by filtration of the desired complex as a yellow solid (75.0 mg, 53%). ^{1}H NMR (400 MHz; Me_2CO-d_6) δ 8.94 (br s, 16H), 7.60 (br s, 16H), 7.34 (br s, 8H), 2.36 (s, 24H); HRMS (ESI) m/z calcd for $C_{86}H_{69}Br_3Mn_4N_9O_{12}$ ([M-Br+MeCN]+) 1876.0132, found 1875.9850.

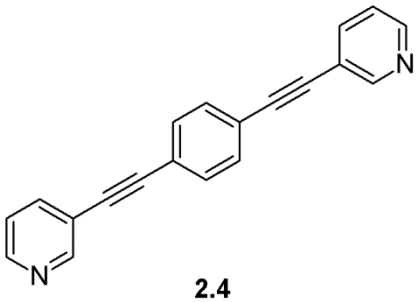

2.4

1,4-bis[(3-pyridyl)ethynyl]benzene (2.4):

The reagent p-diidodobenzene (150 mg, 0.45 mmol), 3-ethynylpyridine (100 mg, 0.97 mmol), [1,1′-Bis(diphenylphosphino)ferrocene]dichloropalladium(II), complex with dichloromethane (37 mg, 0.045 mmol) and copper(I) iodide (7 mg, 0.04 mmol) were combined in a 50 mL round bottomed flask with stir bar and attached reflux condenser. The system was placed under N_2 using a Schlenk line, followed by addition of anhydrous THF (10 mL) and diisopropylamine (3 mL). The reaction was subjected to three more purge cycles, followed by heating under reflux. The reaction was cooled after 36 h, followed by evaporating *in vacuo*. The residue was dissolved in CH_2Cl_2, followed by washing with $KOH_{(aq)}$ (3 M, 3 x 50 mL). The organic layer was then dried over $MgSO_4$ and evaporated *in vacuo* to give the desired product as a brown solid (52 mg, 41%). ^{1}H NMR (400 MHz; $CDCl_3$) δ 8.59 (s, 2H), 8.40 (d, *J* = 4.4 Hz, 2H), 7.68 (dt, *J* = 7.9, 1.6 Hz, 2H), 7.40 (s, 4H), 7.18 (dd, *J* = 7.8, 7.4 Hz, 2H).

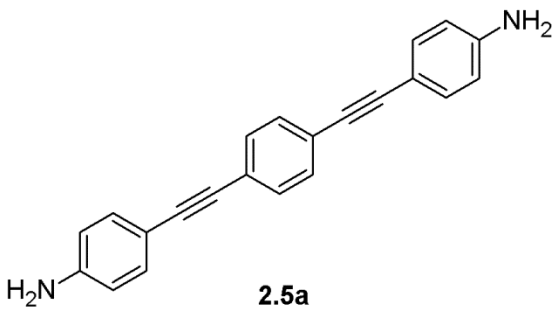

2.5a

1,4-bis[(4-aminophenyl)ethynyl]benzene (2.5a):

The reagent p-Diiodobenzene (500 mg, 1.5 mmol), 4-ethynylaniline (379 mg, 3.2 mmol), [1,1′-Bis(diphenylphosphino)ferrocene]dichloropalladium(II) complex with dichloromethane (62 mg, 0.076 mmol), and copper(I) iodide (14 mg, 0.074 mmol) were combined in a 25 mL round bottom flask with stir bar and attached reflux condenser. The system was placed under N_2 using a Schlenk line, followed by addition of anhydrous THF (10 mL) and diisopropylamine (3 mL), followed by heating the reaction mixture at 70°C. After 24 h the reaction was cooled, and some precipitate was filtered. The filtrate was evaporated *in vacuo*, and the crude product was triturated in Et_2O and filtered to give product as a tan solid (560 mg, 79%). ^{1}H NMR (400 MHz; $CDCl_3$) δ 7.44 (s. 4H), 7.33 (d, *J* = 8.4 Hz, 4H), 6.63 (d, *J* = 8.5 Hz, 4H), 3.84 (br s, 4H).

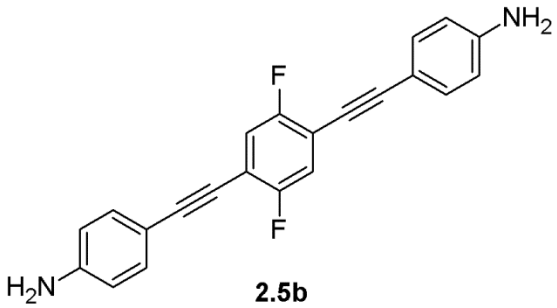

2.5b

1,4-bis[(4-aminophenyl)ethynyl]2,5-difluorobenzene (2.5b):

The reagent 2,5-Dibromo-p-Difluorobenzene (300 mg, 1.1 mmol), 4-ethynylaniline (294 mg, 2.5 mmol), [1,1′-Bis(diphenylphosphino)ferrocene]dichloropalladium(II) complex with dichloromethane (70 mg, 0.086 mmol), and copper(I) iodide (11 mg, 0.06 mmol) were combined in a 50 mL round bottom flask with stir bar and attached reflux condenser. The system was placed under N_2 using a Schlenk line, followed by addition of anhydrous THF (15 mL) and diisopropylamine (5 mL), followed by heating the reaction mixture at

80°C. After 40 h the reaction was cooled, followed by filtering through celite. The filtrate was evaporated *in vacuo*, and the crude product was purified by column chromatography over silica using 1:2 EtOAc/hexanes to give the product as a tan solid (121 mg, 32%). ^{1}H NMR (400 MHz; $CDCl_3$) δ 7.35 (d, *J* = 8.3 Hz, 4H), 7.16 (t, *J* = 7.5 Hz, 2H), 6.64 (d, *J* = 8.3 Hz, 4H), 3.88 (br s, 4H).

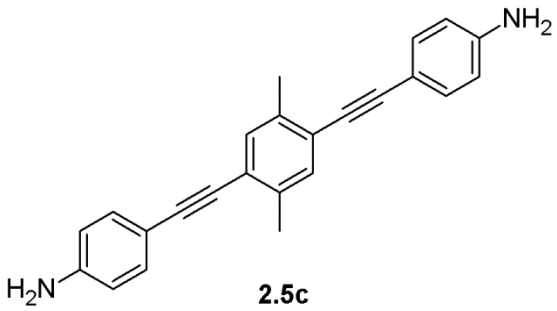

2.5c

2,5-bis[(4-aminophenyl)ethynyl]p-xylene (2.5c):

2,5-Dibromo-p-xylene (500 mg, 1.9 mmol), 4-ethynylaniline (379 mg, 3.9 mmol), [1,1′-Bis(diphenylphosphino)ferrocene]dichloropalladium(II) complex with dichloromethane (77 mg, 0.094 mmol), and copper(I) iodide (23 mg, 0.12 mmol) were combined in a 25 mL round bottom flask with stir bar and attached reflux condenser. The system was placed under N_2 using a Schlenk line, followed by addition of anhydrous THF (10 mL) and diisopropylamine (1 mL), followed by heating the reaction mixture at 70°C. After 40 h the reaction was cooled, diluted with EtOAc (100 mL), then filtered through celite and evaporated *in vacuo*. Recrystallization of this residue from MeOH gave product as a brown solid (357 mg, 56%). ^{1}H NMR (400 MHz; $CDCl_3$) δ 7.35 (s, 2H), 7.32 (d, *J* = 5.3 Hz, 4 H), 6.64 (d, *J* = 8.3 Hz, 4H), 3.82 (br s, 4H), 2.43 (s, 6H).

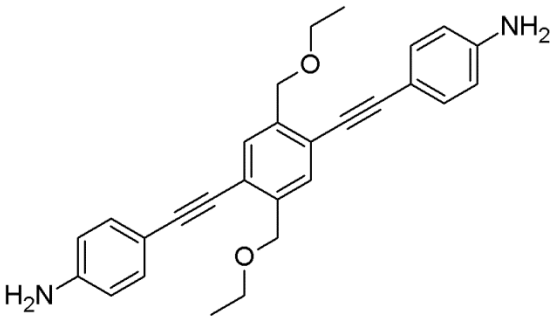

2.5d

1,4-bis[(4-aminophenyl)ethynyl]2,5-bis(ethoxyethyl)benzene (2.5d):

The intermediate **2.6b** (232 mg, 0.66 mmol), 4-ethynylaniline (170 mg, 1.45 mmol), [1,1′-Bis(diphenylphosphino)ferrocene]dichloropalladium(II) complex with dichloromethane (27 mg, 0.033 mmol), and copper(I) iodide (6 mg, 0.03 mmol) were combined in a 25 mL round bottom flask with stir bar and attached reflux condenser. The system was placed under N_2 using a Schlenk line, followed by addition of anhydrous THF (10 mL) and diisopropylamine (1 mL), followed by heating the reaction mixture at 80°C. After 40 h the reaction was cooled, diluted with Et_2O (100 mL), followed by filtration through celite. The filtrate was evaporated *in vacuo*, and the crude product was recrystallized from 95% EtOH to give product as a tan solid (126 mg, 45%). ^{1}H NMR (400 MHz; $CDCl_3$) δ 7.59 (s, 2H), 7.33 (d, *J* = 8.3 Hz, 4H), 6.65 (d, *J* = 8.4 Hz, 4H), 4.71 (s, 4H), 3.87 (br s, 4H), 3.63 (q, *J* = 7.0 Hz, 4H), 1.29 (t, *J* = 7.0 Hz, 6H).

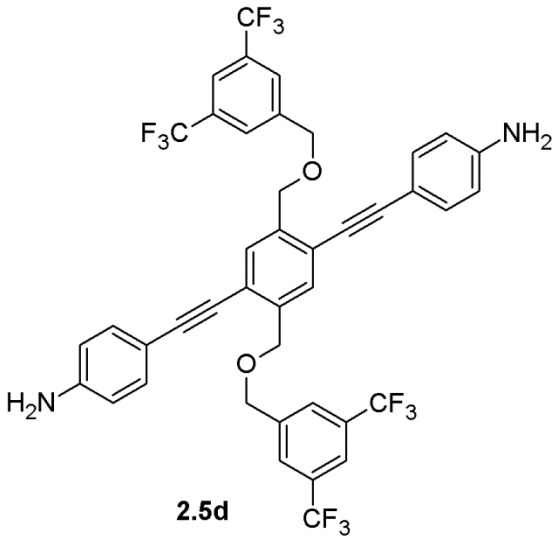

2.5d

1,4-bis[(4-aminophenyl)ethynyl]2,5-bis[(3,5-bis-trifluoromethylphenylmethoxy)methyl]benzene (2.5d):

The intermediate **2.6c** (471 mg, 0.63 mmol), 4-ethynylaniline (170 mg, 1.45 mmol), [1,1′-Bis(diphenylphosphino)ferrocene]dichloropalladium(II) complex with dichloromethane (26 mg, 0.032 mmol), and copper(I) iodide (7 mg, 0.04 mmol) were combined in a 30 mL sealed tube. The flask was filled with anhydrous THF (20 mL) and diisopropylamine (1 mL), followed by purging with N_2 and then heating the reaction mixture at 80°C. After 42 h the reaction was cooled, and filtered through celite. The filtrate was diluted with deionized H_2O (100 mL), followed by extraction with CH_2Cl_2 (3 x 125 mL). The combined organic layers were dried over $MgSO_4$, followed by evaporating *in vacuo*. The residue was recrystallized from 95% EtOH to give product as a brown solid (148 mg, 29 %). ^{1}H NMR (400 MHz; $CDCl_3$) δ 7.85 (s, 4H), 7.78 (s, 2H), 7.62 (s, 2H), 7.26 (d, *J* = 8.3 Hz, 4H), 6.63 (d, *J* = 8.3 Hz, 4H), 4.85 (s, 4H), 4.73 (s, 4H), 3.86 (br s, 4H).

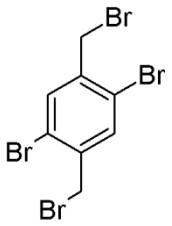

2.6a

2,5-Dibromo-α,α'-dibromo-p-xylene (2.6a):

The reagents 2,5-dibromo-p-xylene (2.03 g, 7.69 mmol), N-bromosuccinimide (3.00 g, 16.9 mmol), and 2,2′-azobis(2-methylpropionitrile) were combined in benzene (50 mL) in a 100 mL round bottom flask with attached reflux condenser and stir bar, followed by heating under reflux. After 24 h the reaction was cooled and the solvent evaporated *in vacuo*. The resulting solid was recrystallized from absolute EtOH to give the desired product as a white solid (1.69 g, 52%). ^{1}H NMR (400 MHz; $CDCl_3$) δ 7.66 (s, 2H), 4.51 (s, 4H).

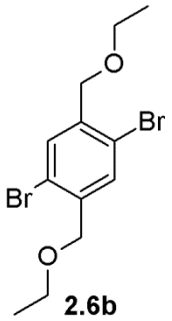

2.6b

1,4-dibromo-2,5-bis(ethoxymethyl)benzene (2.6b):

Intermediate **2.6a** (500 mg, 1.19 mmol) was added to absolute EtOH (3 mL) in a 25 mL round bottom flask with stir bar and attached reflux condenser, followed by 21 weight % NaOEt in EtOH (5 mL). The reaction was heated to 70°C. After 3 h the reaction was cooled, and the solvent evaporated *in vacuo*. The residue was treated with CH_2Cl_2 (250

mL) followed by washing with H_2O. The organic layer was then dried over $MgSO_4$ and evaporated *in vacuo* to give the product as a faint orange product which retained its color after washing with cyclohexane (404 mg, 97%). ^{1}H NMR (400 MHz; $CDCl_3$) δ 7.63 (s, 2H), 4.49 (s, 4H), 3.61 (q, *J* = 7.0 Hz, 4H), 1.28 (t, *J* = 7.0 Hz, 6H); ^{13}C NMR (100 MHz; $CDCl_3$) δ 138.7, 132.2, 121.2, 71.2, 66.6, 15.3.

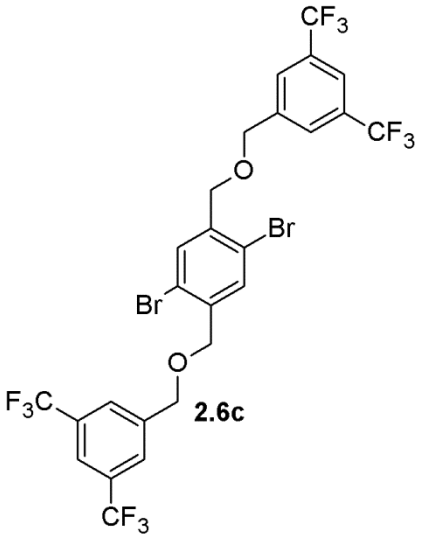

2.6c

1,4-dibromo-2,5-bis(ethoxymethyl)benzene (2.6b):

3,5-Bis(trifluoromethyl)benzyl alcohol (683 mg, 2.80 mmol) was added to anhydrous THF (30 mL) in a 50 mL round bottom flask with stir bar and attached reflux condenser. System was purged with N_2, followed by addition of 60 weight % sodium hydride in mineral oil (130 mg, 3.25 mmol). After stirring for 30 min intermediate **2.6a** (590 mg, 1.40 mmol) was added and the reaction was heated to 66°C. After 24 h the reaction was cooled, followed by diluting with deionized H_2O. The resulting precipitate was filtered and dried to give the desired product as a light yellow solid (935 mg, 89%). ^{1}H NMR (400 MHz; $CDCl_3$) δ 7.84 (s, 4H), 7.83 (s, 2H), 7.68 (s, 2H), 4.74 (s, 4H), 4.65 (s, 4H).

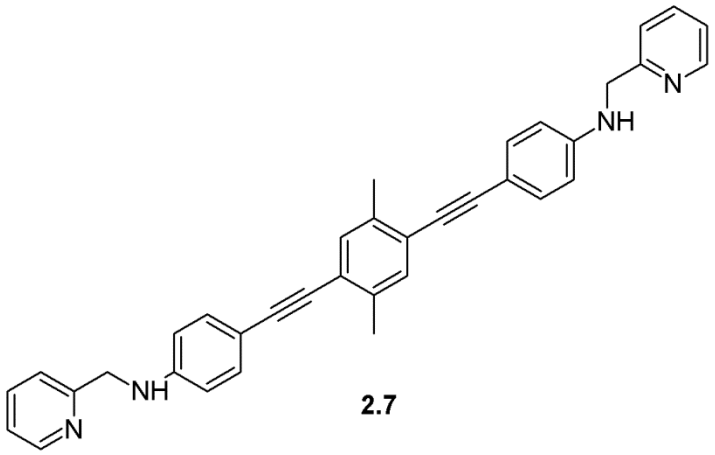

2.7

2,5-bis{[N-(2-pyridylmethyl)aminophenyl]ethynyl}-p-xylene (2.7a):

Dianiline **2.5c** (267 mg, 0.79 mmol) was combined with 2-formylpyridine (151 µL, 1.58 mmol) in a 30 mL sealed tube with a stir bar. Absolute ethanol (18 mL) and anhydrous CH_2Cl_2 (2 mL) were added, followed by heating the reaction at 60°C for 2 h. After cooling, $NaBH_4$ (120 mg, 3.2 mmol) was added and the reaction was stirred at RT for an additional 6 h. The solvent was evaporated *in vacuo*, and the residue was triturated in deionized H_2O (20 mL), followed by filtration and drying to give the product as a dark yellow solid (380 mg, 92%).^{1}H NMR (400 MHz; $CDCl_3$) δ 8.60 (d, *J* = 4.9 Hz, 2H), 7.67 (td, *J* = 7.7, 1.8 Hz, 2H), 7.36 (d, *J* = 8.7 Hz, 4H), 7.32 (d, *J* = 7.9 Hz, 2H), 7.30 (s, 2H), 7.21 (dd, *J* = 7.1, 5.3 Hz, 2H), 4.49 (s, 4H), 2.42 (s, 6H); ^{13}C NMR (100 MHz; DMSO-d_6) δ 157.8, 149.3, 147.9, 137.0, 136.9, 133.0, 132.3, 123.1, 122.4, 121.8, 112.9, 112.0, 95.5, 86.6, 48.9, 20.2.

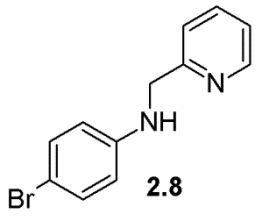

2.8

4-bromo-*N*-(pyridine-2-ylmethyl)aniline (2.8):

The reagents p-bromoaniline (9.07 g, 52.7 mmol) and 2-formylpyridine (5.00 mL, 52.3 mmol) were combined in a 250 round bottom flask with stir bar followed by addition of absolute EtOH (100 mL). The reaction was stirred at RT for 4 h before addition of $NaBH_4$ (4.00 g, 106 mmol). After an additional 10 h stirring at RT the reaction was diluted with deionized water, and a precipitate filtered. After washing with additional deionized water and drying, the crude product was recrystallized from 95% EtOH to give the desired product as a tan solid (5.04 g, 36.6%). ^{1}H NMR (400 MHz; DMSO-d_6) δ 8.52 (d, J = 4.3 Hz, 1H), 7.73 (t, J = 7.5 Hz, 1H), 7.32 (d, J = 7.8 Hz, 1H), 7.24 (m, 1H), 7.17 (d, J = 8.3 Hz, 2H), 6.57 (t, J = 6.0 Hz, 1H), 6.53 (d, J = 8.4 Hz, 2H), 4.33 (d, J = 6.0 Hz, 2H).

$[2.7_4 \bullet Cr_4](NO_3)_{12}$:

Ligand **2.7** was added to an NMR tube followed by DMSO-d_6. $Cr(NO_3)_3 \bullet 9H_2O$ (1.0 eq.) was added, followed by shaking the tube for 10 s, resulting in complexation. ^{1}H NMR (400 MHz, DMSO-d_6) δ 8.69 (d, J = 4.6 Hz, 8H). 8.16 (t, J = 7.4 Hz, 8H), 7.64 (t, J = 8.4 Hz, 8H), 7.31 (s, 8H), 7.27 (d, J = 8.0 Hz, 16H), 6.63 (d, J = 7.6 Hz, 16H), 4.57 (s, 16H), 2.35 (s, 24H).

8.3 Chapter 3 Experimental

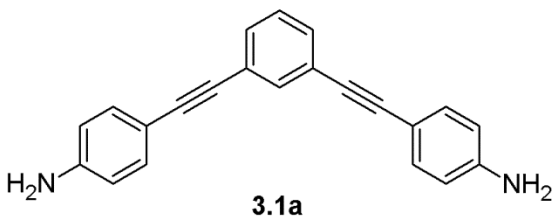

3.1a

1,3-Bis[(4-aminophenyl)ethynyl]benzene (3.1a):

m-Diiodobenzene (500 mg, 1.52 mmol) was combined with 4-ethynylaniline (443 mg, 3.78 mmol), [1,1′-Bis-(diphenylphosphino)ferrocene] dichloropalladium(II) complexed with CH_2Cl_2 (62 mg, 76 µmol), and copper iodide (14 mg, 74 µmol) in a 25 mL round-bottomed flask with attached reflux condenser. The system was purged using a Schlenk line. Anhydrous iPr_2NH (2 mL) and anhydrous PhMe (8 mL) were added, followed by three additional purge cycles. The reaction was then heated to 100°C for 48 h. After cooling, the reaction was diluted with Et_2O (250 mL) and filtered through celite. The solvent was then evaporated *in vacuo*. The residue from this was purified by column chromatography (SiO_2; hexanes/ethyl acetate 3:1 + 1% Et_3N to hexanes/ethyl acetate 1:1 + 1% Et_3N). Collection of fractions and evaporation of solvent *in vacuo* gave product as a dull yellow solid (132 mg, 28%). ^1H NMR (400 MHz; $CDCl_3$) δ 7.63 (s, 1H), 7.39 (dd, *J* = 7.5, 1.1 Hz, 2H), 7.33 (d, *J* = 8.6 Hz, 4H), 7.28 (d, *J* = 7.5 Hz, 1H), 6.64 (d, *J* = 8.6 Hz, 4H), 3.82 (br, 4H). ^{13}C NMR (100 MHz; $CDCl_3$) δ 146.9, 134.2, 133.2, 130.6, 128.4, 124.3, 114.9, 90.7, 86.9. HRMS (ESI) m/z calcd for $C_{22}H_{16}N_2$ ($[M+H]^+$) 309.1386, found 309.1389.

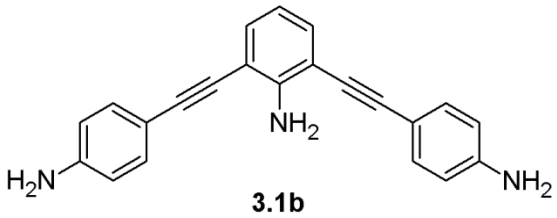

3.1b

2,6-Bis[(4-aminophenyl)ethynyl)]aniline (3.1b):

2,6-Dibromoaniline (380 mg, 1.51 mmol), 4-ethynylaniline (443 mg, 3.78 mmol), [1,1'-bis(diphenylphosphino)ferrocene]dichloropalladium(II), complex with dichloromethane (62 mg, 76 µmol), and copper iodide (14 mg, 74 µmol) were combined in a 25 mL round-

bottomed flask with attached reflux condenser. The system was purged using a Schlenk line. Anhydrous iPr_2NH (2 mL) and anhydrous PhMe (8 mL) were added, followed by three additional purge cycles. The reaction was then heated to 100°C for 48 h. After cooling, the reaction was diluted with Et_2O (250 mL) and filtered through celite. The solvent was then evaporated *in vacuo*. The residue from this was purified by column chromatography (SiO_2; hexanes/ethyl acetate 3:1 + 1% Et_3N to hexanes/ethyl acetate 1:1 + 1% Et_3N). Collection of fractions and evaporation of solvent *in vacuo* gave product as an orange solid (102 mg, 21%). ^1H NMR (400 MHz; $CDCl_3$) δ 7.33 (d, *J* = 8.4 Hz, 4H), 7.28 (d, *J* = 7.5 Hz, 2H), 6.65 (t, *J* = 7.5 Hz, 1H), 6.64 (d, *J* = 8.4 Hz, 4H), , 4.86 (br, 2H), 3.83 (br, 4H). ^{13}C NMR (100 MHz; $CDCl_3$) δ 148.7, 146.8, 133.0, 131.8, 117.3, 114.9, 112.7, 108.2, 95.7, 83.5. HRMS (ESI) m/z calcd for $C_{22}H_{17}N_3$ ($[M^{\bullet}]^+$) 323.1417, found 323.1427.

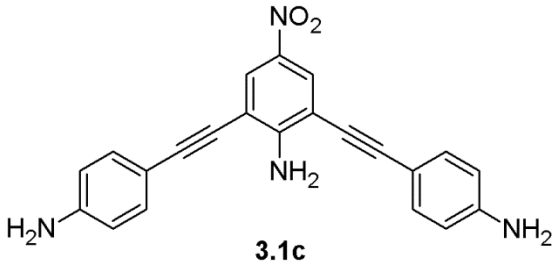

3.1c

2,6-Bis[(4-aminophenyl)ethynyl]4-nitroaniline (3.1c):

To a 2-neck 25 mL round-bottom flask equipped with a stir bar and reflux condenser was added 2,6-diiodo-4-nitroaniline (100 mg, 25 mmol), 4-ethynylaniline (58 mg, 50 mmol), bis(triphenylphosphino)dichloropalladium(II) (17.5 mg 2.5 mmol) and copper iodide (2.5 mg 1.3 mmol). The mixture was placed under nitrogen and anhydrous iPr_2NH (5 mL) was added. The reaction was stirred at room temperature for 40 h. The solvent was removed by rotary evaporation and the remaining solid was dissolved in a mixture of

methylene chloride and methanol. The mixture was then filtered through celite and the solvent from the filtrate was removed by rotary evaporation. The product was recrystallized from methylene chloride twice to give an orange powder (32 mg, 33% yield). ^{1}H NMR (400 MHz; $CDCl_3$) δ 8.19 (s, 2H), 7.34 (d, *J* = 8.6 Hz, 4H), 6.66 (d, *J* = 8.6 Hz, 4H), 5.53 (br, 2H), 3.91 (br, 4H); ^{1}H NMR (400 MHz; DMSO-d_6) δ= 8.00 (s, 2H), 7.34 (d, *J* = 8.6 Hz, 4H), 6.68 (br, 2H), 6.57 (d, *J* = 8.6 Hz, 4H), 5.64 (br, 4H). ^{13}C NMR (100 MHz; DMSO-d_6) δ 153.4, 149.8, 136.1, 133.0, 126.5, 113.4, 107.5, 107.0, 98.0, 81.1. HRMS (ESI) m/z calcd for $C_{22}H_{16}N_4O_2$ ($[M+H]^+$) 369.1346, found 369.1382.

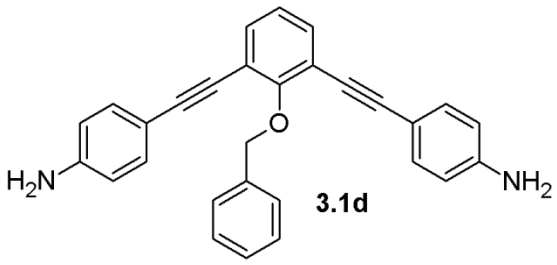

3.1d

O-Benzyl 2,6-bis[(4-aminophenyl)ethynyl]phenol (3.1d):

3.2a (250 mg, 0.73 mmol), 4-ethynylaniline (214 mg, 1.83 mmol), bis(triphenylphosphino)dichloropalladium(II) (60 mg, 0.09 mmol), and copper iodide (14 mg, 0.07 mmol) were combined in a 25 mL round-bottomed flask with attached reflux condenser. The system was purged using a Schlenk line. Anhydrous iPr_2NH (8 mL) and anhydrous THF (8 mL) were added, followed by three additional purge cycles. The reaction was then heated under reflux for 72 h. After cooling, the reaction was diluted with Et_2O (400 mL) and filtered through celite. The solvent was then evaporated *in vacuo*. The residue from this was triturated in 3 M aqueous KOH (20 mL) in an ultrasonication bath, followed by filtration and drying. The solid was purified by column

chromatography (SiO_2; hexanes/ethyl acetate 3:1 + 1% Et_3N to hexanes/ethyl acetate 1:1 + 1% Et_3N). Collection of fractions and evaporation of solvent *in vacuo* gave product as a light orange solid (32 mg, 10%). ^1H NMR (400 MHz; $CDCl_3$) δ 7.62 (d, *J* = 7.2 Hz, 2H), 7.42 (d, *J* = 7.7 Hz, 2H), 7.32 (m, 3H), 7.28 (d, *J* = 8.0 Hz, 4H), 7.04 (t, *J* = 7.7 Hz, 1H), 6.63 (d, *J* = 8.0 Hz, 4H), 5.34 (s, 2H), 3.83 (br, 4H). ^{13}C NMR (100 MHz; $CDCl_3$) δ 160.1, 146.9, 137.7, 133.1, 132.7, 128.6, 128.5, 128.0, 123.8, 118.7, 114.9, 112.7, 94.9, 83.7, 75.6. HRMS (ESI) m/z calcd for $C_{29}H_{22}N_2O$ ($[M+Na]^+$) 437.1624, found 437.1646.

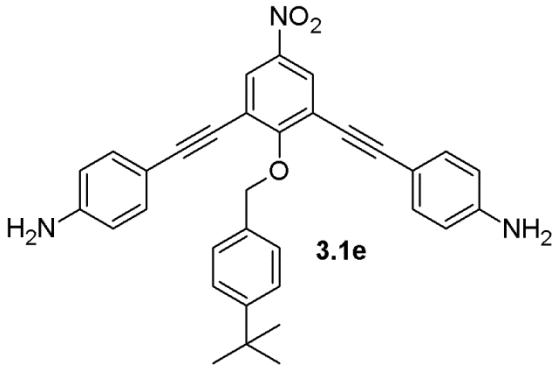

3.1e

O-4-(t-Butyl)benzyl 2,6-bis[(4-aminophenyl)ethynyl]4-nitrophenol (3.1e):

3.2b (638 mg, 1.19 mmol), 4-ethynylaniline (348 mg, 2.97 mmol), bis(triphenylphosphino)dichloropalladium(II) (42 mg, 0.06 μmol), and copper iodide (12 mg, 0.06 μmol) were combined in a 50 mL round-bottomed flask with attached reflux condenser. The system was purged using a Schlenk line. Anhydrous iPr_2NH (10 mL) and anhydrous PhMe (10 mL) were added, followed by three additional purge cycles. The reaction was then heated under reflux for 68 h. After cooling, the solvent was diluted with Et_2O (200 mL), followed by filtering through celite. The solvent was then removed *in vacuo*. The residue was dissolved in EtOAc (10 mL), followed by addition of hexanes (90 mL) to give a precipitate. The mixture was filtered through celite and rinsed with

additional hexanes (100 mL), causing new precipitate to form. The fine solid was filtered through celite, rinsed with hexanes (50 mL), then washed off of the celite with EtOAc (50 mL). Solvent was removed *in vacuo* to give product as an orange solid (264 mg, 41%). ^{1}H NMR (400 MHz; $CDCl_3$) δ 8.23 (s, 2H), 7.52 (d, *J* = 8.2 Hz, 2H), 7.39 (d, *J* = 8.2 Hz, 2H), 7.29 (d, *J* = 8.4 Hz, 4H), 6.63 (d, *J* = 8.4 Hz, 4H), 5.48 (s, 2H), 3.71 (br, 2H), 1.33 (s, 9H). ^{13}C NMR (100 MHz; $CDCl_3$) δ 164.5, 151.4, 147.5, 143.1, 133.8, 133.3, 128.3, 127.3, 125.5, 119.3, 114.8, 111.6, 97.3, 82.3, 75.7, 34.7, 31.5. HRMS (ESI) m/z calcd for $C_{33}H_{29}N_3O_3$ ($[M+H]^+$) 516.2281, found 516.2354.

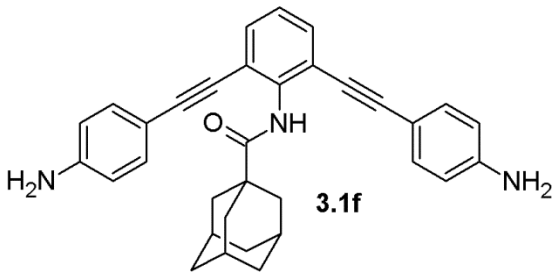

3.1f

N-(2,6-bis[(4-aminophenyl)ethynyl]phenyl)adamantanecarboxamide (3.1f):

3.2d (103 mg, 0.25 mmol), 4-ethynylaniline (73 mg, 0.62 mmol), bis(triphenylphosphino)dichloropalladium(II) (18 mg, 0.03 μmols), and copper iodide (5 mg, 0.03 μmols) were combined in a 25 mL round-bottomed flask with attached reflux condenser. The system was purged using a Schlenk line. Anhydrous iPr_2NH (5 mL) and anhydrous PhMe (10 mL) were added, followed by three additional purge cycles. The reaction was then heated under reflux for 72 h. After cooling, the reaction was filtered through celite, followed by removal of solvent *in vacuo*. The residue was then purified by column chromatography (SiO_2; hexanes/ethyl acetate 2:1 + 1% Et_3N to hexanes/ethyl acetate 1:1 + 1% Et_3N) to give the product as a light orange solid (17 mg, 14%). ^{1}H NMR

(400 MHz; $CDCl_3$) δ 7.56 (br, 1H), 7.45 (d, *J* = Hz, 2H), 7.30 (d, *J* = Hz, 4H), 7.15 (t, *J* = Hz, 1H), 6.62 (d, *J* = Hz, 4H), 3.87 (br, 4H), 2.07 (s, 9H), 1.75 (s, 6 H). ^{13}C NMR (100 MHz; $CDCl_3$) δ 175.5, 146.9, 138.8, 133.1, 131.8, 125.9, 121.5, 114.9, 112.6, 95.5, 84.3, 41.6, 39.7, 36.7, 28.4. HRMS (ESI) m/z calcd for $C_{33}H_{31}N_3O$ ($[M+H]^+$) 486.2539, found 486.2609.

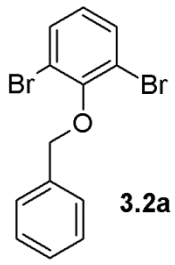

3.2a

Benzyl 2,6-Dibromophenyl Ether (3.2a):

2,6-Dibromophenol (580 mg, 2.3 mmol), benzyl bromide (274 µL, 2.3 mmol), potassium carbonate (479 mg, 3.47 mmol), and sodium iodide (33 mg, 0.22 mmol) were combined in a 25 mL round-bottomed flask with attached reflux condenser. MeCN (7 mL) was added, and reaction was heated under reflux for 16 h. After cooling, water was added, followed by extraction with Et_2O. The combined organic fractions were washed with brine, dried over $MgSO_4$, followed by evaporation of solvent *in vacuo*. The crude product was then filtered through a silica plug with hexanes to yield a white solid (645 mg, 82%). ^1H NMR (400 MHz; $CDCl_3$) δ 7.61 (d, *J* = 7.2 Hz, 2H), 7.54 (d, *J* = 8.0 Hz, 2H), 7.44-7.35 (m, 3H), 6.90 (t, *J* = 8.0 Hz, 1H), 5.04 (s, 2H) . ^{13}C NMR (100 MHz; $CDCl_3$) δ 153.0, 136.4, 132.9, 128.6, 128.5, 126.6, 118.9, 74.7 (two resonances are overlapping). HRMS (ESI) m/z calcd for $C_{13}H_{14}Br_2NO$ ($[M+NH_4]^+$) 359.9417, found 359.9432.

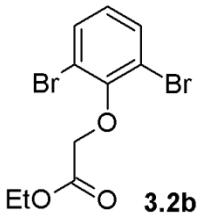

3.2b

Ethyl (2,6-dibromophenoxy)acetate (3.2b):

2,6-Dibromophenol (200 mg, 0.79 mmol), ethyl bromoacetate (88 µL, 0.80 mmol), and potassium carbonate (150 mg, 1.09 mmol) were combined in a 25 mL round-bottomed flask with attached reflux condenser and stir bar. MeCN (10 mL) was added, and reaction was heated under reflux for 24 h. After cooling, water was added, followed by extraction with CH_2Cl_2 (3 x 50 mL). The combined organic fractions were dried over $MgSO_4$, followed by evaporation of solvent *in vacuo*. The product was isolated as a clear oil (173 mg, 65%). ^{1}H NMR (400 MHz; $CDCl_3$) δ 7.34 (d, *J* = 8.0 Hz, 2H), 6.77 (t, *J* = 8.0 Hz, 1H), 4.45 (s, 2H), 4.15 (q, *J* = 7.1 Hz, 2H), 1.18 (t, *J* = 7.1 Hz, 3H). ^{13}C NMR (100 MHz; $CDCl_3$) δ 167.2, 151.7, 132.5, 126.8, 117.6, 68.6, 60.9, 13.9.

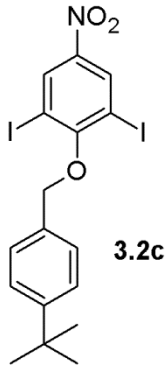

3.2c

4-(t-Butyl)benzyl 2,6-Diiodo-4-nitrophenyl Ether (3.2c):

2,6-Diiodo-4-nitrophenol (640 mg, 1.64 mmol), 4-(t-butyl) benzyl bromide (300 µL, 1.64 mmol), and potassium carbonate (283 mg, 2.05 mmol) were combined in a 25 mL round-

bottomed flask with attached reflux condenser. MeCN (10 mL) was added, and reaction was heated under refluxed for 24 h. After cooling, water (100 mL) was added, followed by extraction with CH_2Cl_2 (3 x 50 mL). The combined organic fractions were dried over $MgSO_4$, followed by evaporation of solvent *in vacuo* to give a faint yellow solid (708 mg, 80%). ^{1}H NMR (400 MHz; $CDCl_3$) δ 8.69 (s, 2H), 7.60 (d, *J* = 8.3 Hz, 2H), 7.48 (d, *J* = 8.3 Hz, 2H), 5.06 (s, 2H), 1.37 (s, 9H). ^{13}C NMR (100 MHz; $CDCl_3$) δ 162.9, 152.1, 144.8, 135.2, 132.2, 128.6, 125.7, 90.6, 75.0, 34.8, 31.5. HRMS (ESI) m/z calcd for $C_{17}H_{17}I_2NO_3$ ($[M]^{\bullet+}$) 536.9292, found 536.9290.

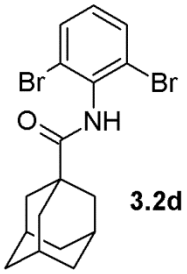

3.2d

1-(N-(2,6-Dibromophenyl))Adamantane Carboxamide (3.2d):

2,6-Dibromoanline (250 mg, 1.0 mmol) and 1-adamantanecarboxylic acid chloride (160 mg, 0.81 mmol) were combined in a 10 mL round-bottomed flask with attached reflux condenser. System was purged using a Schlenk line, followed by addition of anhydrous PhMe (5 mL). Reaction was heated under reflux for 28 h, followed by cooling and then evaporating the solvent *in vacuo*. The residue was then recrystallized from 95% EtOH to give the product as a white powder (103 mg, 31%). ^{1}H NMR (400 MHz; $CDCl_3$) δ 7.55 (d, *J* = 8.1 Hz, 2H), 7.21 (br, 1H), 6.99 (t, *J* = 8.1 Hz, 1H), 2.10 (s, 3H), 2.05 (s, 6H), 1.77 (s, 6H). ^{13}C NMR (100 MHz; $CDCl_3$) δ 175.6, 135.1, 132.3, 129.3, 124.0, 41.6, 39.3, 36.6, 28.3. HRMS (ESI) m/z calcd for $C_{17}H_{19}Br_2NO$ ($[M+H]^+$) 411.9906, found 411.9913.

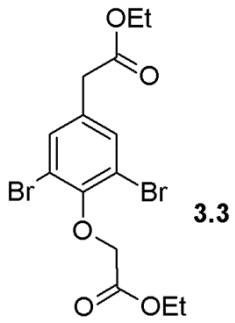

3.3

Ethyl [3,5-dibromo-4-(2-ethoxy-2-oxoethoxy)phenyl]acetate (3.3):

2,6-Dibromophenol (500 mg, 1.98 mmol), ethyl bromoacetate (220 µL, 1.99 mmol), and potassium carbonate (550 mg, 3.98 mmol) were combined in a 50 mL round-bottomed flask with attached reflux condenser and stir bar. MeCN (25 mL) was added, and reaction was heated under reflux for 24 h. After cooling, water was added, followed by extraction with CH_2Cl_2 (3 x 50 mL). The combined organic fractions were dried over $MgSO_4$, followed by evaporation of solvent *in vacuo*. The product was isolated as a clear oil (459 mg, 54%). ^{1}H NMR (400 MHz; $CDCl_3$) δ 7.61 (s, 2H), 4.54 (s, 2H), 4.27 (q, *J* = 7.2 Hz, 2H), 4.19 (s, 2H), 4.18 (q, *J* = 7.1 Hz, 2H), 1.29 (t, *J* = 7.1 Hz, 3H). 1.24 (t, *J* = 7.2 Hz, 3H). ^{13}C NMR (100 MHz; $CDCl_3$) δ 169.7, 167.4, 151.7, 135.1, 118.7, 118.3, 61.5, 61.0, 14.2.

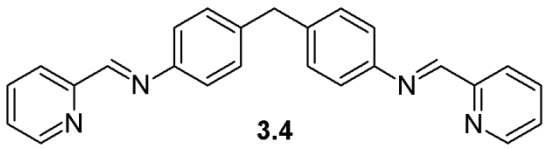

3.4

4,4'-Methylene-bis[N-(2-pyridinylmethylene)benzenamine (3.4):

4,4'-diaminodiphenylmethane (512 mg, 2.58 mmol) and 2-pyridinecarboxaldehyde (500 µL, 5.27 mmol) were combined in a 50 mL Erlenmeyer flask with stir bar. MeOH (25 mL) was added, followed by stirring for 24 h, after which point a precipitate was filtered. The crude product was rinsed with hexanes (25 mL) and dried to give a cream solid (712 mg, 73%). ^{1}H NMR (400 MHz; $CDCl_3$) δ 8.73 (dq, *J* = 4.8, 0.8 Hz, 2H), 8.65 (s, 2H), 8.22 (d, *J* = 7.8 Hz, 2H), 7.82 (td, *J* = 7.8, 1.1 Hz, 2H), 7.38 (ddd, *J* = 7.8, 4.8, 1.1 Hz, 2H), 7.29 (s, 8H), 4.07 (s, 2H). ^{13}C NMR (100 MHz; $CDCl_3$) δ 160.1, 154.8, 149.8, 149.1, 139.9, 136.8, 129.9, 125.1, 122.0, 121.5, 41.2. HRMS (ESI) m/z calcd for $C_{25}H_{20}N_4$ ($[M+H]^+$) 377.1760, found 377.1719.

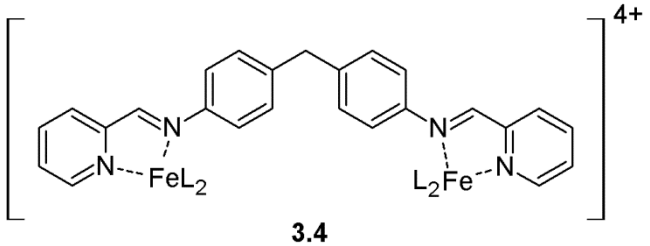

3.4

[3.4$_3$•Fe$_2$](ClO$_4$)$_2$ (Method A):

3.4 (25.0 mg, 66.0 µmol) and $Fe(ClO_4)_2$•xH_2O (17.2 mg) were combined in anhydrous MeCN (10 mL) in a 25 mL round-bottomed flask under a blanket of N_2, followed by submerging in an ultrasonication bath for two minutes. The solution was then diluted with Et_2O (200 mL), followed by filtration of the resulting precipitate. After drying, product was isolated as a purple solid (35.5 mg, 98%).

[3.4$_3$•Fe$_2$](ClO$_4$)$_4$ (Method B):

4,4'-Diaminodiphenylmethane (66 mg, 330 µmol) and 2-pyridinecarboxaldehyde (59 µL, 670 µmol) were combined in anhydrous MeCN (2 mL) in a 10 mL round-bottomed flask

under a blanket of N_2. To this solution was added $Fe(ClO_4)_2 \bullet xH_2O$ (122 mg). The mixture was then submerged in an ultrasonication bath for two minutes. The solution was then diluted with Et_2O (14 mL), and cooled to -25°C. This gave a fine precipitate which was collected by centrifugation to give a purple solid (183 mg, 82%). ^1H NMR (400 MHz; CD_3CN) δ 8.93 (s, 2H), 8.56 (d, *J* = 7.7 Hz, 2H), 8.37 (t, *J* = 7.7 Hz, 2H), 7.75 (t, *J* = 6.7 Hz, 2H), 7.35 (d, *J* = 5.2 Hz, 2H), 6.94 (br s, 4H), 5.52 (br s, 4H), 4.01 (s, 2H).

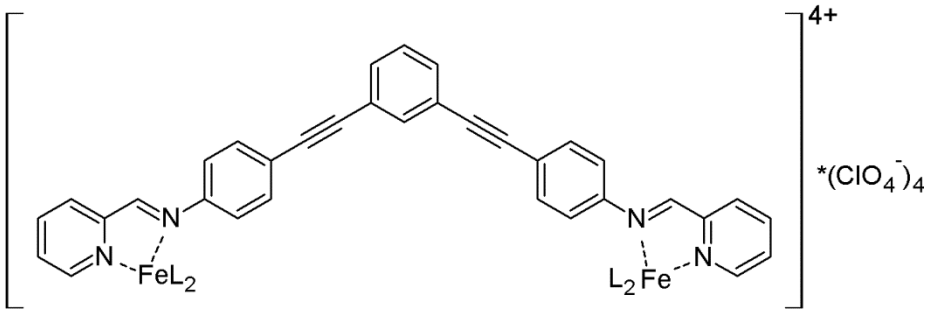

$[3.5a_3Fe_2](ClO_4)_4$

$[3.5a_3 \bullet Fe_2](ClO_4)_4$:

Compound **3.1a** (3.9 mg, 13 μmol) and 2-pyridinecarboxaldehyde (2.5 μL, 26 μmol) were combined in anhydrous MeCN (1 mL) in a 10 mL round-bottomed flask under a blanket of N_2. To this solution was added $Fe(ClO_4)_2 \bullet xH_2O$ (3.0 mg). The mixture was then submerged in an ultrasonication bath for two minutes. The solution was then diluted with Et_2O (14 mL), and cooled to -25°C. This gave a fine precipitate which was collected by centrifugation to give a purple solid (7.5 mg, 90%). ^1H NMR (500 MHz; CD_3CN) δ 8.93 (s, 2H), 8.54 (d, *J* = 7.5 Hz, 2H), 8.39 (t, *J* = 7.72 Hz, 2H), 7.85 (s, 1H), 7.79 (t, *J* = 6.0

Hz, 2H), 7.58 (d, *J* = 7.2 Hz, 2H), 7.45 (m, 7H), 5.33 (d, *J* = 8.2 Hz, 4H). HRMS (ESI) m/z calcd for $C_{102}H_{66}Cl_4Fe_2N_{12}O_{16}$ ($[M+2H]^{2+}$) 984.1159, found 984.1167.

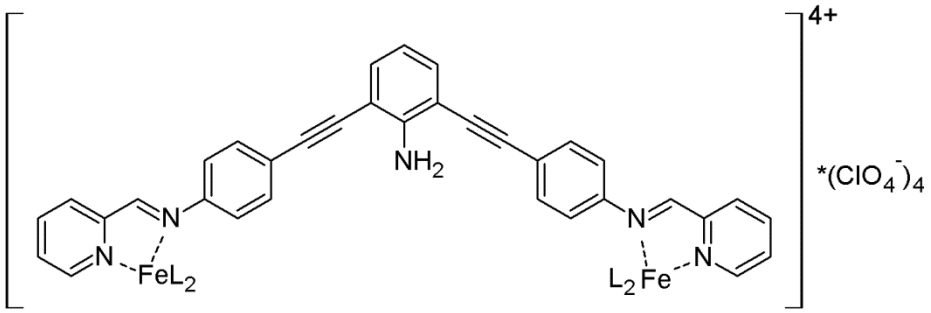

$[3.5b_3Fe_2](ClO_4)_4$

$[3.5b_3{\bullet}Fe_2](ClO_4)_4$:

Compound **3.1b** (8.5 mg, 26 μmol) and 2-pyridinecarboxaldehyde (5.5 μL, 58 μmol) were combined in anhydrous MeCN (1 mL) in a 10 mL round-bottomed flask under a blanket of N_2. To this solution was added $Fe(ClO_4)_2{\bullet}xH_2O$ (7.1 mg). The mixture was then submerged in an ultrasonication bath for two minutes. The solution was then diluted with Et_2O (14 mL), and cooled to -25°C. This gave a fine precipitate which was collected by centrifugation to give a purple solid (49.2 mg, 94%). ^1H NMR (400 MHz; CD_3CN) δ 8.89 (s, 2H), 8.52 (d, *J* = 7.6 Hz, 2H), 8.39 (t, *J* = 7.6 Hz, 2H), 7.77 (t, *J* = 6.1 Hz, 2H), 7.47 (d, *J* = 8.4 Hz, 4H), 7.38 (m, 4H), 6.71 (t, *J* = 7.6 Hz, 1H), 5.47 (br, 2H), 5.31 (d, *J* = 8.4 Hz, 4H). HRMS (ESI) m/z calcd for $C_{102}H_{69}Cl_4Fe_2N_{15}O_{16}$ ($[M-3(ClO_4)]^{3+}$) 571.4676, found 571.4686.

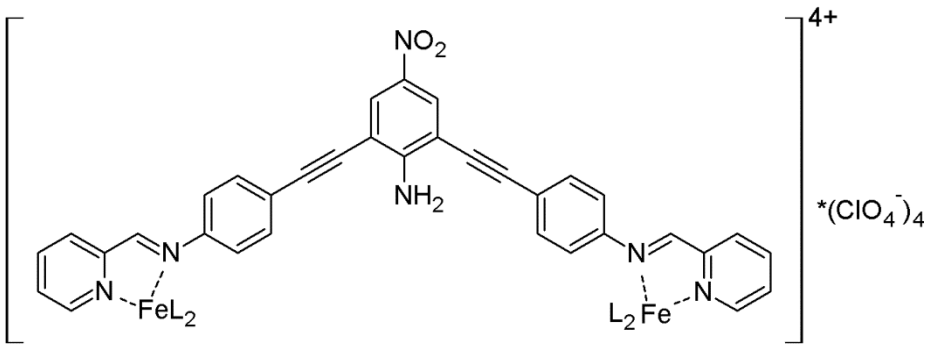

[3.5c$_3$Fe$_2$](ClO$_4$)$_4$

[3.5c$_3$•Fe$_2$](ClO$_4$)$_4$:

Compound **3.1c** (10.6 mg, 29 μmol) and 2-pyridinecarboxaldehyde (6.0 μL, 63 μmol) were combined in anhydrous MeCN (1 mL) in a 10 mL round-bottomed flask under a blanket of N_2. To this solution was added $Fe(ClO_4)_2$•xH_2O (7.0 mg). The mixture was then submerged in an ultrasonication bath for two minutes. The solution was then diluted with Et_2O (14 mL), and cooled to -25°C. This gave a fine precipitate which was collected by centrifugation to give a purple solid (15.6 mg, 76 %). ^{1}H NMR (500 MHz; CD_3CN) δ 8.87 (s, 2H), 8.53 (t, *J* = 8.2 Hz, 2H), 8.39 (t, *J* = 7.5 Hz, 2H), 8.24 (s, 2H), 7.77 (m, 2H), 7.57 (m, 4H), 7.39 (d, *J* = 8.1 Hz, 2H), 6.57 (br, 2H), 5.32 (d, *J* = 8.1 Hz, 4H). HRMS (ESI) m/z calcd for $C_{102}H_{66}Cl_4Fe_2N_{18}O_{22}$ ($[M-3(ClO_4)]^{3+}$) 616.4526, found 616.4522.

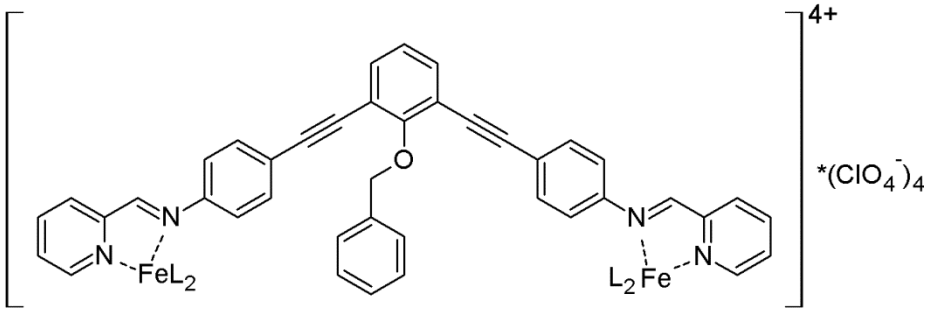

[3.5d$_3$Fe$_2$](ClO$_4$)$_4$

[3.5d$_3$•Fe$_2$](ClO$_4$)$_4$:

Compound **3.1d** (23.8 mg, 57 μmol) and 2-pyridinecarboxaldehyde (11.0 μL, 116 μmol) were combined in anhydrous MeCN (1 mL) in a 10 mL round-bottomed flask under a blanket of N_2. To this solution was added $Fe(ClO_4)_2$•xH_2O (13.9 mg). The mixture was then submerged in an ultrasonication bath for two minutes. The solution was then diluted with Et_2O (14 mL), and cooled to -25°C. This gave a fine precipitate which was collected by centrifugation to give a purple solid (35.8 mg, 82%). ^{1}H NMR (400 MHz; CD_3CN) δ 8.91 (s, 2H), 8.54 (d, *J* = 7.6 Hz, 2H), 8.39 (t, *J* = 8.0 Hz, 2H), 7.79 (t, *J* = 5.8 Hz, 2H), 7.59 (d, *J* = 7.6 Hz, 2H), 7.43 (m, 4H), 7.28 (d, *J* = 7.7 Hz, 4H), 7.22 (t, *J* = 7.7 Hz, 1H), 7.09 (t, *J* = 8.0 Hz, 2H), 6.83 (t, *J* = 7.7 Hz, 1H), 5.36 (d, *J* = 7.7 Hz, 4H), 5.19 (s, 2H). HRMS (ESI) m/z calcd for $C_{123}H_{84}Cl_4Fe_2N_{12}O_{19}$ ($[M-2(ClO_4)]^{2+}$) 1043.2223, found 1043.2203.

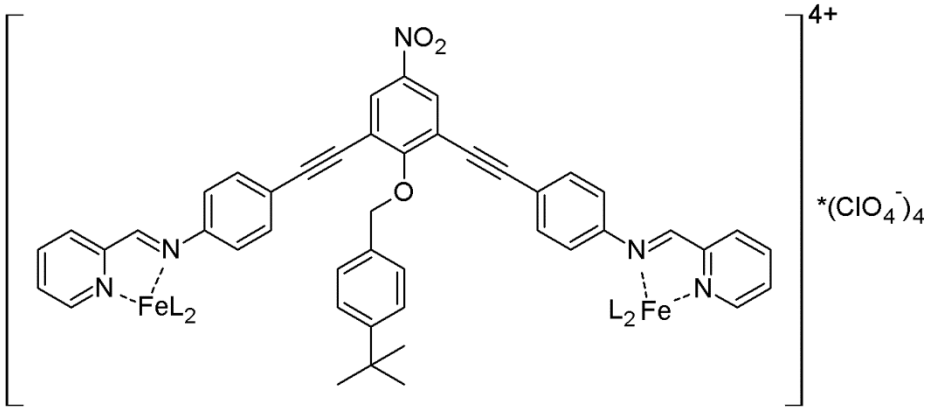

[3.5c$_3$Fe$_2$](ClO$_4$)$_4$

[3.5e$_3$•Fe$_2$](ClO$_4$)$_4$:

Compound **3.1e** (54.6 mg, 0.11 mmols) and 2-pyridinecarboxaldehyde (21 μL, 0.22 mmols) were combined in anhydrous MeCN (5 mL) in a 10 mL round-bottomed flask

under a blanket of N_2. To this solution was added $Fe(ClO_4)_2 \cdot xH_2O$ (26 mg). The mixture was then submerged in an ultrasonication bath for five minutes. The solution was then diluted with Et_2O (10 mL), and cooled to -25°C. This gave a fine precipitate which was collected by centrifugation to give a purple solid (41.4 mg, 45%). ^1H NMR (500 MHz; CD_3CN) δ 8.81 (s, 2H), 8.58 (d, *J* = 7.3 Hz, 2H), 8.42 (s, 2H), 8.40 (m, 2H), 7.77 (dd, *J* = 9.8 Hz, 3.7 Hz, 2H), 7.34 (d, *J* = 5.4 Hz, 2H), 7.29 (d, *J* = 8.2 Hz, 2H), 7.19 (d, *J* = 8.0 Hz, 4H), 7.13 (d, *J* = 8.2 Hz, 2H), 5.7 (s, 2H), 5.17 (d, *J* = 8.0 Hz, 4H), 1.09 (s, 9H). HRMS (ESI) m/z calcd for $C_{135}H_{105}Cl_4Fe_2N_{15}O_{25}$ ($[M-4(ClO_4)]^{4+}$) 547.9224, found 547.9227.

8.4 Chapter 4 Experimental

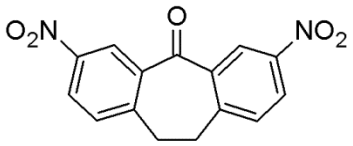

4.1a

3,7-Dinitrodibenzosuberone (4.1a):

Dibenzosuberone (10.4 g, 49.9 mmol) was added to a 100 mL round bottom flask with stir bar, followed by attaching a drop-addition funnel and placing the system under N_2, followed by placing the flask into an ice bath. Fuming nitric acid (90%, 25 mL) cooled to 0°C was added to the drop-addition funnel, followed by slowly adding this to the dibenzosuberone over 10 min. The flask was then placed into an oil bath and heated to 100°C while stirring. After 2 h the reaction was allowed to cool, followed by pouring into vigorously stirred ice water (1 L). The resulting precipitate was filtered, followed by rinsing with additional deionized water (1 L). After drying, the crude product was

recrystallized from $MeNO_2$ to give product as a light yellow solid (5.86 g, 39%). ^{1}H NMR (400 MHz; DMSO-d_6) δ 8.69 (d, J = 2.5 Hz, 2H), 8.39 (dd, J = 8.4, 2.6 Hz, 2H), 7.72 (d, J = 8.4 Hz, 2H), 3.37 (s, 4H). ^{13}C NMR (100 MHz; DMSO-d_6) δ 190.3, 149.5, 146.4, 137.7, 131.9, 127.0, 125.3, 33.3. HRMS (ESI) m/z calcd for $C_{15}H_{11}N_2O_5$ ($[M+H]^+$) 299.0662, found 299.30677.

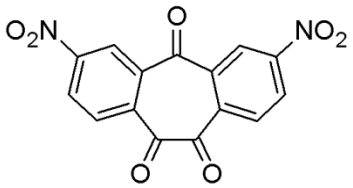

4.1b

3,7-Diamino-5*H*-dibenzo[*a*,*d*][7]annulene-5,10,11-trione (4.1b):

Dibenzosuberone (10.4 g, 49.9 mmol) was added to a 100 mL round bottom flask with stir bar, followed by attaching a drop-addition funnel and placing the system under N_2, followed by placing the flask into an ice bath. Fuming nitric acid (90%, 25 mL) cooled to 0°C was added to the drop-addition funnel, followed by slowly adding this to the dibenzosuberone over 10 min. The flask was then placed into an oil bath and heated to 100°C while stirring. After 12 h the reaction was allowed to cool, followed by pouring into vigorously stirred ice water (1 L). The resulting precipitate was filtered, followed by rinsing with additional deionized water (1 L). After drying, the crude product was hot filtered from $MeNO_2$ to give product as a white solid (488 mg, 3%). ^{1}H NMR (400 MHz; DMSO-d_6) δ 8.90 (d, J = 1.9 Hz, 2H), 8.60 (dd, J = 8.5, 2.0 Hz, 2H), 8.32 (d, J = 8.3 Hz, 2H).

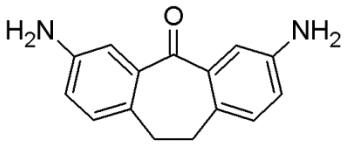

4.2a

3,7-Diaminodibenzosuberone (4.2a):

Compound **4.2a** (400 mg, 1.34 mmol) was added to a 50 mL round bottom flask with stir bar, followed by addition of Raney© 2800 Ni suspension in water (1.0 mL) and MeOH (25 mL). The flask was purged with nitrogen gas using a Schlenk line. Hydrazine monohydrate (2.0 mL, 41.2 mmol) was slowly added. After the addition was complete, the reaction was stirred at room temperature. After 24 h the reaction mixture was diluted with acetone (100 mL) followed by filtering through celite. After evaporating the solvent *in vacuo*, the residue was triturated in deionized water (200 mL) before being filtered using celite. The filter was rinsed clean using MeOH (150 mL) before evaporating the solvent *in vacuo* to give an orange-yellow solid. This was recrystallized from EtOH to give product as a yellow solid (162 mg, 50 %). ^{1}H NMR (400 MHz; DMSO-d_6) δ 7.30 (d, J = 2.6 Hz, 2H), 7.00 (d, J = 8.0 Hz, 2H), 6.76 (dd, J = 8.0, 2.6 Hz, 2H), 3.68 (br s, 4H), 3.05 (s, 4H). ^{1}H NMR (400 MHz; DMSO-d_6) δ 7.05 (d, J = 2.3 Hz, 2H), 6.94 (d, J = 8.1 Hz, 2H), 6.69 (dd, J = 8.1, 2.3 Hz, 2H), 5.11 (br s, 4H), 2.89 (s, 4H). ^{13}C NMR (100 MHz; DMSO-d_6) δ 195.7, 146.9, 138.7, 130.1, 129.3, 118.2, 114.3, 33.9. HRMS (ESI) m/z calcd for $C_{15}H_{15}N_2O$ ($[M+H]^+$) 239.1178, found 239.1248.

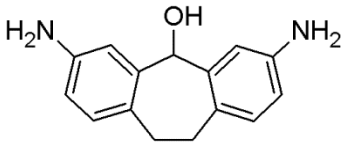

4.2b

3,7-Diaminodibenzosuberol (4.2b):

Compound **4.2a** (503 mg, 2.1 mmol) was added to a 25 mL round bottom flask with stir bar, followed by partially dissolving in absolute EtOH (20 mL). $NaBH_4$ (3.00 g, 79.3 mmol) was added slowly, followed by allowing the reaction to stir overnight at room temperature. After 12 h had elapsed, the reaction mixture was slowly diluted with water (280 mL). After being allowed to sit, a precipitate slowly settled to the bottom, which was filtered and dried to give product as a light-orange solid (416 mg, 81%). ^{1}H NMR (400 MHz; DMSO-d_6) δ 6.73 (d, J = 2.4 Hz, 2H), 6.69 (d, J = 8.0 Hz, 2H), 6.30 (dd, J = 8.0 Hz, 2.4 Hz, 2H), 5.76 (d, 4.5 Hz, 1H), 5.54 (d, J = 4.0 Hz, 1H), 4.74 (bs, 4H), 2.98 (m, 2H), 2.83 (m, 2H). ^{13}C NMR (100 MHz; DMSO-d_6) δ 146.1, 143.7, 129.7, 124.1, 112.0, 110.7, 70.6, 31.1. HRMS (ESI) m/z calcd for $C_{15}H_{16}N_2O$ ($[M\cdot]^+$) 240.1257, found 240.1267.

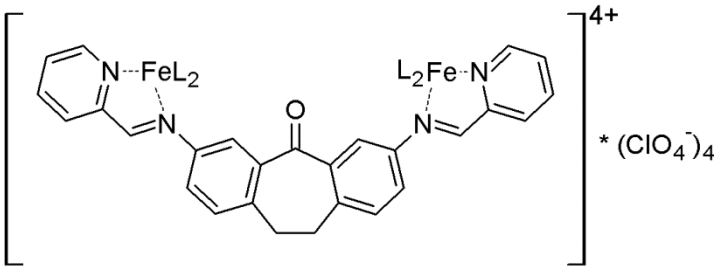

[4.3a$_3$·Fe$_2$](ClO$_4$)$_4$

[4.3a$_3$•Fe$_2$](ClO$_4$)$_4$:

Dianiline **4.2a** (28.5 mg, 120 μmol), 2-formylpyridine (24.0 μL, 253 μmol) and $Fe(ClO_4)_2$•xH_2O (30.2 mg) were combined in anhydrous MeCN (2 mL) in a 25 mL round-bottomed flask under a blanket of N_2, followed by submerging in an ultrasonication bath for two minutes. The solution was then diluted with Et_2O (15 mL), cooled to -25°C followed by filtration of the resulting precipitate. After drying, product was isolated as a

purple solid (65.0 mg, 92%). ^{1}H NMR (400 MHz; CD_3CN) δ 8.71 (s, 6H), 8.46 (d, *J* = 7.4 Hz, 6H), 8.39 (t, *J* = 7.6 Hz, 6 H), 7.75 (t, *J* = 6.1 Hz, 6H), 7.38 (d, *J* = 5.3 Hz, 6 H), 7.17 (d, *J* = 8.1 Hz, 6H), 6.28 (br s, 6H), 5.52 (d, *J* = 7.1 Hz, 6H), 3.30 (d, *J* = 9.5 Hz, 6H), 3.17 (dd, *J* = 15.0, 9.9 Hz, 6H). ^{13}C NMR (100 MHz; CD_3CN) δ 190.1, 176.2, 159.3, 156.8, 149.3, 145.4, 140.7, 139.3, 132.0, 131.8, 130.7, 125.8, 124.2, 35.6. HRMS (ESI) m/z calcd for $C_{81}H_{60}Fe_2N_{12}O_3$ ($[M-4ClO_4]^{4+}$) 340.0897, found 340.0898.

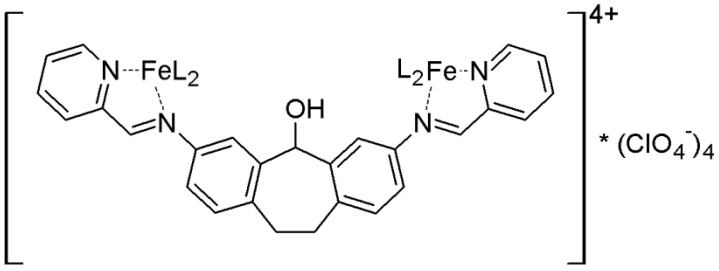

$[4.3b_3 \cdot Fe_2](ClO_4)_4$

$[4.3b_3 \bullet Fe_2](ClO_4)_4$:

Dianiline **4.2b** (150 mg, 0.62 mmol), 2-formylpyridine (120 µL, 1.25 mmol) and $Fe(ClO_4)_2 \bullet xH_2O$ (150 mg) were combined in anhydrous MeCN (20 mL) in a 50 mL round-bottomed flask under a blanket of N_2, followed by heating to 60°C for 24 h. The solution was then cooled to room temperature, diluted with Et_2O (300 mL), and cooled to -25°C followed by filtration of the resulting precipitate. Drying product *in vacuo* gave product as a purple solid (362 mg, 98%). ^{1}H NMR (400 MHz; CD_3CN) δ 8.73 (s, 6H), 8.02 (m, 12H), 7.93 (dd, *J* = 15.7, 7.6 Hz, 6H), 7.52 (m, 12H), 6.81 (d, *J* = 8.0 Hz, 6H), 6.07 (d, *J* = 5.5 Hz, 9H), 3.32 (dd, *J* = 16.3, 7.7 Hz, 6H), 2.83 (m, 6H), 2.54 (d, *J* = 5.2 Hz, 3H). ^{13}C NMR (100 MHz; CD_3CN) δ 171.1, 160.1, 156.1, 146.3, 144.5, 139.4, 138.6, 131.2, 130.2, 129.5, 121.8, 120.8, 67.9, 31.4. HRMS (ESI) m/z calcd for $C_{81}H_{66}Cl_2Fe_2N_{12}O_{11}$ ($[M-2ClO_4]^{2+}$) 782.1519, found 782.1547.

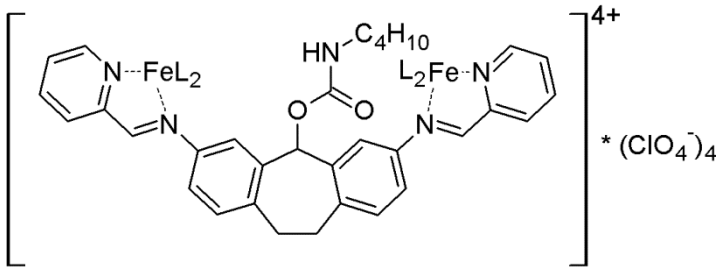

[4.3c$_3$·Fe$_2$](ClO$_4$)$_4$

[4.3c$_3$•Fe$_2$](ClO$_4$)$_4$:

Complex **[4.3b$_3$•Fe$_2$](ClO$_4$)$_4$** (25.9 mg, 15 μmol) and butyl isocyanate (30.0 μL, 266 μmol) were combined in anhydrous MeCN (5 mL) in a 25 mL round-bottomed flask under a blanket of N_2, followed by heating under reflux for 24 h. The solution was then cooled to room temperature and diluted with Et_2O (250 mL), then cooled to -25°C followed by filtration of the resulting precipitate through celite. The filter was rinsed with additional Et_2O (50 mL), followed by rinsing the product off of the filter using acetone (75 mL). After evaporating the solvent *in vacuo* product was obtained as a purple solid (24.3 mg, 80 %). ^{1}H NMR (400 MHz; CD_3CN) δ 9.10 (s, 1H), 9.03 (s, 1H), 8.96 (s, 1H), 8.90 (s, 1H), 8.29-7.93 (m, 10H), 7.60-7.37 (m, 4H), 7.15 (d, *J* = 5.5 Hz, 1H), 6.99 (d, *J* = 5.3 Hz), 3.76-3.45 (m, 2H), 3.30 (ttd, *J* = 18.7, 9.7, 5.0 Hz, 4H), 3.11-2.81 (m, 4H), 1.64-1.00 (m, 12H), 0.97-0.87 (m, 2H), 0.78 (dd, *J* = 7.7, 7.0 Hz, 3H), 0.70 (td, 7.4, 3.0 Hz, 3H). ^{13}C NMR (125 MHz; CD_3CN) δ 172.1, 172.3, 172.1, 171.9, 160.0, 159.5, 159.4, 159.1, 156.4, 156.0, 155.6, 139.6, 139.5, 139.3, 130.1, 129.9, 129.8, 129.5, 129.0, 128.8, 128.5, 60.1, 59.9, 59.5, 32.0, 31.9, 29.6, 20.5, 20.4, 20.3, 13.8, 13.6. HRMS (ESI) m/z calcd for $C_{98}H_{96}Cl_3Fe_2N_{16}NaO_{18}$ ([M-ClO_4+Na+CH_3CN]$^+$) 1012.2369, found 1012.3002.

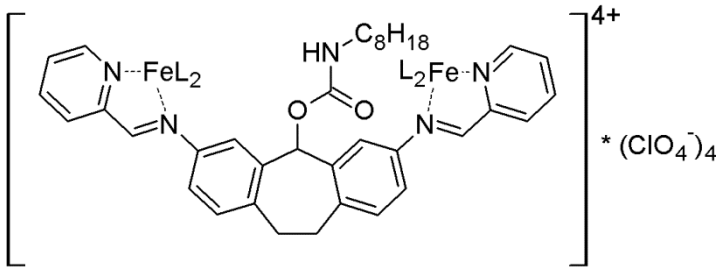

[4.3d$_3$·Fe$_2$](ClO$_4$)$_4$

[4.3d$_3$•Fe$_2$](ClO$_4$)$_4$:

Complex **[4.3b$_3$•Fe$_2$](ClO$_4$)$_4$** (30.3 mg, 17 μmol) and octyl isocyanate (50.0 μL, 283 μmol) were combined in anhydrous MeCN (5 mL) in a 25 mL round-bottomed flask under a blanket of N_2, followed by heating under reflux for 14 h. The solution was then cooled to room temperature and diluted with Et_2O (300 mL), cooled to -25°C followed by filtration of the resulting precipitate. After drying the product was recovered as a purple solid (26.0 mg, 67 %). For NMRs see pages *S*-23 through *S*-24. ESI-MS led to decomposition in which no parent ion or fragments reminiscent of self-assembly were observed.

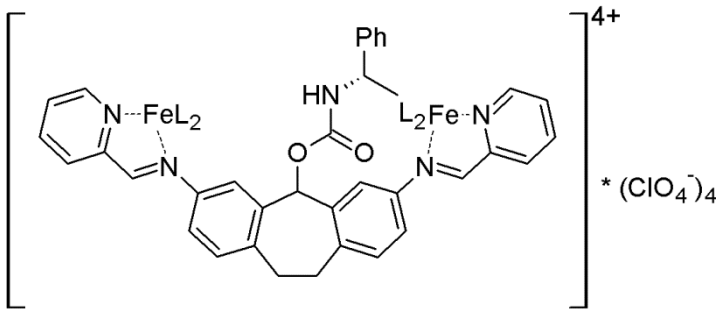

[(*S*)-4.3e$_3$·Fe$_2$](ClO$_4$)$_4$

[(*S*)-4.3e$_3$•Fe$_2$](ClO$_4$)$_4$:

Complex **[4.3b$_3$•Fe$_2$](ClO$_4$)$_4$** (27.4 mg, 16 μmol) and (S)-(−)-α-methylbenzyl isocyanate (50.0 μL, 355 μmol) were combined in anhydrous MeCN (5 mL) in a 25 mL round-bottomed flask under a blanket of N_2, followed by heating under reflux for 14 h. The solution was then cooled to room temperature and diluted with Et_2O (300 mL), cooled to -25°C followed by filtration of the resulting precipitate. After drying the product was recovered as a purple solid (28.7 mg, 83 %). ^{1}H NMR (400 MHz; CD_3CN) δ 8.71 (s, 2H), 7.80 (td, *J* = 7.7, 1.3 Hz, 2H), 7.49-7.19 (m, 14H), 7.08-7.04 (m, 1H), 6.99-6.90 (m, 4H), 6.55 (d, *J* = 7.2 Hz, 2H), 5.35 (br s, 1H), 5.3 (m, 1H), 1.33 (d, *J* = 7.0 Hz, 3H). For NMRs see pages *S*-25 through *S*-26. ESI-MS led to decomposition in which no parent ion or fragments reminiscent of self-assembly were observed.

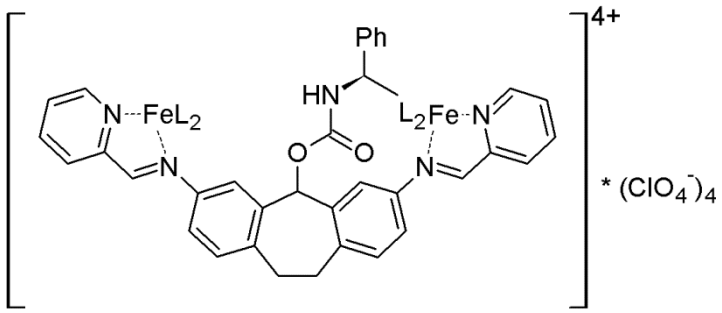

[(*R*)-4.3e$_3$·Fe$_2$](ClO$_4$)$_4$

[(*R*)-4.3e$_3$•Fe$_2$](ClO$_4$)$_4$:

Complex **[4.3b$_3$•Fe$_2$](ClO$_4$)$_4$** (6.6 mg, 3.7 μmol) and (R)-(−)-α-methylbenzyl isocyanate (50.0 μL, 355 μmol) were combined in anhydrous MeCN (5 mL) in a 25 mL round-bottomed flask under a blanket of N_2, followed by heating under reflux for 24 h. The solution was then cooled to room temperature and diluted with anhydrous Et_2O (45 mL), cooled to -25°C followed by filtration of the resulting precipitate. After drying the product was rinsed with EtOAc (50 mL), then filtered and dried to give a purple solid (6.1 mg, 74

%). ^{1}H NMR (400 MHz; CD_3CN) δ 8.71 (s, 2H), 7.80 (td, *J* = 7.7, 1.3 Hz, 2H), 7.49-7.19 (m, 14H), 7.08-7.04 (m, 1H), 6.99-6.90 (m, 4H), 6.55 (d, *J* = 7.2 Hz, 2H), 5.35 (br s, 1H), 5.3 (m, 1H), 1.33 (d, *J* = 7.0 Hz, 3H). For ^{1}H NMR see page *S*-27. ESI-MS led to decomposition in which no parent ion or fragments reminiscent of self-assembly were observed.

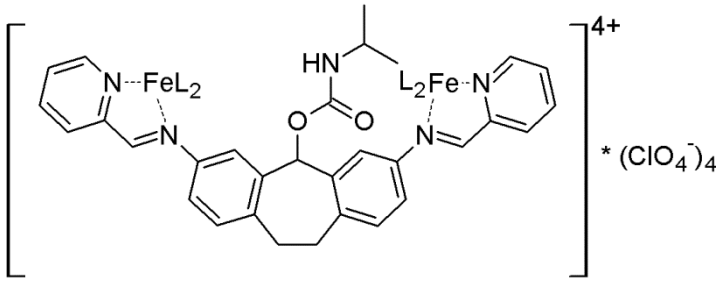

[4.3f$_3$·Fe$_2$](ClO$_4$)$_4$

[4.3f$_3$•Fe$_2$](ClO$_4$)$_4$:

Complex **[4.3b$_3$•Fe$_2$](ClO$_4$)$_4$** (20 mg, 11 μmol) and isopropyl isocyanate (100.0 μL, 102 μmol) were combined in anhydrous MeCN (10 mL) in a 50 mL round-bottomed flask under a blanket of N_2, followed by heating under reflux for 15 h. Excess isocynate was required to achieve reaction completion. The solution was then cooled to room temperature and diluted with Et_2O (300 mL), cooled to -25°C followed by filtration of the resulting precipitate. After drying the product was recovered as a purple solid mixed with N,N'-diisopropyl urea which could not be removed without destroying the self-assembly. For ^{1}H NMR see page *S*-27. ESI-MS led to decomposition in which no parent ion or fragments reminiscent of self-assembly were observed.

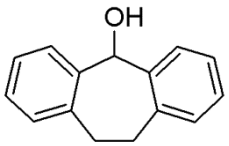

4.4

Dibenzosuberol (4.4):

Dibenzosuberone (916 mg, 4.40 mmol) and $NaBH_4$ (333 mg, 8.80 mmol) were combined in a 50 mL round bottom flask with stir bar. MeOH (20 mL) was added, and the reaction was stirred at room temperature. After 24 h the reaction was diluted with deionized H_2O (300 mL) to give a precipitate. This was filtered, and rinsed with additional deionized H_2O (300 mL) and dried to give product as a white solid (691 mg, 74%). ^{1}H NMR (400 MHz; $CDCl_3$) δ 7.46 (dd, *J* = 6.3, 2.0 Hz, 2H), 7.19 (m, 6H), 5.96 (d, *J* = 1.7 Hz, 1H), 3.43 (m, 2H), 3.12 (m, 2H), 2.29 (d, *J* = 2.5 Hz, 1H). ^{13}C NMR (100 MHz; $CDCl_3$) δ 140.6, 139.0, 130.3, 128.1, 127.2, 126.3, 76.6, 32.5. HRMS (ESI) m/z calcd for $C_{15}H_{14}O$ ($[M\cdot]^+$) 210.1039, found 210.1033.

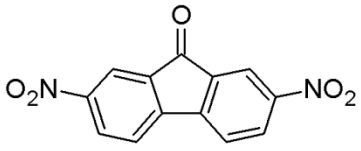

4.5a

2,7-Dinitrofluorenone (4.5a):

Fluorenone (5.00 g, 27.7 mmol) was placed under N_2. An attached drop-addition funnel was then charged with a solution of 1:1 conc. H_2SO_4/conc. HNO_3 (30 mL). This mixture was slowly added over 20 minutes, followed by slowly bringing the system to 100 °C. After 2 h the drop-addition funnel was again charged with a solution of 1:1 conc. H_2SO_4/conc. HNO_3 (15 mL), followed by slow addition over 20 minutes. Following

heating for an additional 3 h, the reaction mixture was allowed to cool. The reaction mixture was then poured into a rapidly stirred ice-water (600 mL) bath, followed by filtration. After washing with additional deionized water (1 L) followed by subsequent air-drying, the resulting solid was recrystallized from nitromethane to give a yellow solid (3.10 g, 41 %). ^{1}H NMR (400 MHz; DMSO-d_6) δ 8.61 (dd, J = 8.2, 2.2 Hz, 2H), 8.36 (d, J = 1.8 Hz, 2H), 8.34 (d, J = 8.2 Hz, 2H).

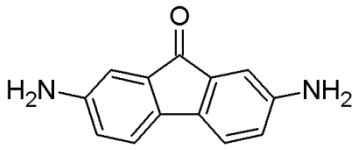

4.6a

2,7-Diaminofluorenone (4.6a):

Ketone **4.5a** (500 mg, 1.85 mmol) $NaBH_4$ (1.17 g, 30.9 mmol), and 10% Pd on carbon (100 mg, 0.08 mmol) were combined in a 50 mL round bottom flask with stir bar. This was sealed with a septum, and N_2 was used to purge the system. A balloon with attached syringe was affixed to the septum, followed by addition of anhydrous THF (5 mL). The reaction mixture was stirred at RT, followed by slow addition of MeOH (4 mL) over 1 h, causing the balloon to inflate. After 12 h the reaction was filtered through celite, followed by rinsing the celite with Me_2CO. The organic phase was evaporated *in vacuo*, followed by treating the residue with deionized water (1 L). The resulting precipitate was filtered and dried to give product as an orange solid (179 mg, 46%). ^{1}H NMR (400 MHz; DMSO-d_6) δ 7.13 (d, J = 8.0 Hz, 2H), 6.73 (d, J =1.8 Hz, 2H), 6.46 (dd, J = 8.0, 2.1 Hz, 2H), 4.93 (s, 4H).

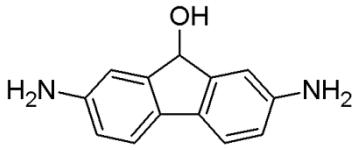

4.6b

2,7-Diaminofluorenol (4.6b):

4.5a (550 mg, 2.04 mmol) was suspended in MeOH (75 mL), followed by placing the flask under a blanket of N_2. To this was added Raney© 2800 Ni suspension in water (500 µL), followed by hydrazine monohydrate (500 µL, 10.3 mmol). The flask was stirred at room temperature for 8 h before being filtered through a pad of celite. After removal of the solvent *in vacuo* the product was recovered as a brown solid (263 mg, 61 %). ^{1}H NMR (400 MHz; DMSO-d_6) δ 7.13 (d, J = 7.9 Hz, 2H), 6.73 (s, 2H), 6.46 (d, J = 7.6 Hz, 2H), 5.44 (d, J = 7.8 Hz, 1H), 5.15 (d, J = 7.7 Hz, 1H), 4.96 (br s, 4H). ^{13}C NMR (125 MHz; DMSO-d_6) δ 147.2, 146.7, 129.1, 118.9, 117.7, 114.0, 112.8, 111.8, 110.6, 74.1, 73.0. HRMS (ESI) m/z calcd for $C_{13}H_{12}N_2O$ ($[(M)]^{\bullet+}$) 212.0944, found 212.0948.

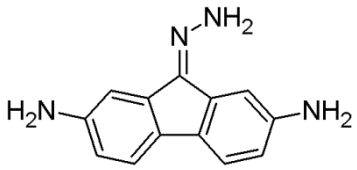

4.6c

9-Hydrazinylidene-9*H*-fluorene-2,7-diamine (4.6c):

4.5a (550 mg, 2.04 mmol) was suspended in MeOH (75 mL), followed by placing the flask under a blanket of N_2. To this was added 10% Pd on carbon (100 mg, 0.08 mmol), followed by hydrazine monohydrate (500 µL, 10.3 mmol). The flask was stirred at room temperature for 12 h before being filtered through a pad of celite. After removal of the

solvent *in vacuo* the product was recovered as an orange solid (421 mg, 91%). ^{1}H NMR (400 MHz; DMSO-d_6) δ 7.29 (d, *J* = 2.1 Hz, 1H), 7.15 (t, *J* = 7.9 Hz, 2H), 6.93 (d, *J* = 2.0 Hz, 1H), 6.53 (dd, *J* = 1.9, 1.0 Hz, 1H), 6.51 (dd, *J* = 1.9, 1.0 Hz, 1H), 5.12 (br s, 4H),

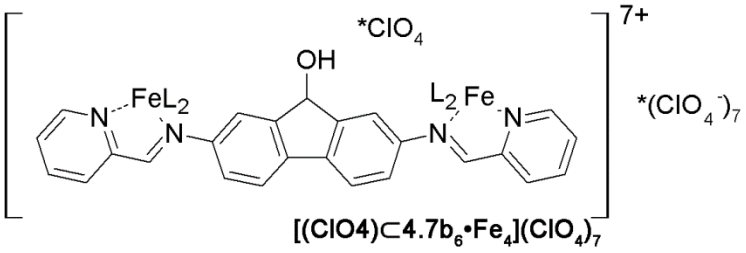

[(ClO$_4$)⊂4.7b$_6$•Fe$_4$](ClO$_4$)$_7$:

Dianiline **4.6b** (170 mg, 0.80 mmol) was combined in MeCN (10 mL) with 2-formylpyridine (160 µL, 1.67 mml), followed by purging with N_2. $Fe(ClO_4)_2$*xH_2O (200 mg) was then added, and the mixture was then heated at 82 °C for 3 h. Upon cooling, this was diluted with Et_2O (240 mL) and cooled to -25°C. The precipitate was then filtered and rinsed with additional Et_2O (50 mL) to give product as a dark purple solid (294 mg, 65%). See pages *S-6* through *S-10* for relevant NMR spectra. HRMS (ESI) m/z calcd for $C_{150}H_{108}Cl_4Fe_4N_{24}O_{22}$ ([(M-4ClO$_4$)]$^{4+}$) 740.8556, found 740.8462.

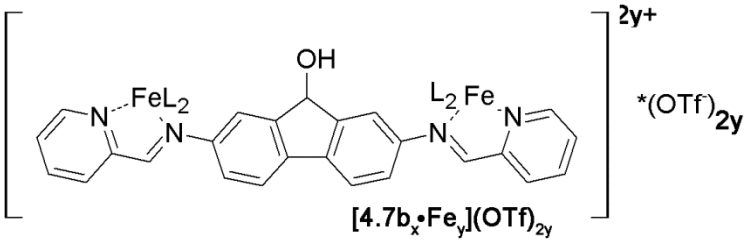

[4.7b$_x$•Fe$_y$](OTf)$_{2y}$:

Dianiline **4.6b** (190 mg, 0.90 mmol) was combined in MeCN (10 mL) with 2-formylpyridine (180 µL, 1.88 mml), followed by purging with N_2. Meanwhile, $FeCl_2$ (79 mg, 0.62 mmol) and AgOTf (325 mg, 1.26 mmol) were combined in MeCN (20 mL). This was suspended in an ultrasonification bath for 1 h, before AgCl was filtered off and the iron(II) triflate solution thus obtained was added to the solution of ligand. The mixture was then heated at 82 °C for 3 h. Upon cooling, this was diluted with Et_2O (470 mL) and cooled to -25°C. The precipitate was then filtered and rinsed with additional Et_2O (100 mL) to give product as a dark purple solid (498 mg, 88%).

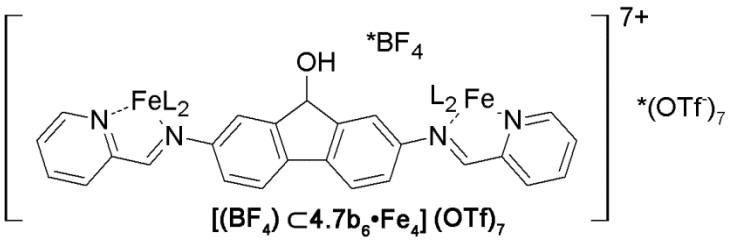

[(BF$_4$)⊂4.7b$_6$•Fe$_4$](OTf)$_7$:

The oligomer **[4.7b$_x$•Fe$_y$](OTf)$_{2y}$** (2.0 mg, 5.3 µmol) was added to CD_3CN (400 µL) in an NMR tube. To this was added excess $NaBF_4$ (this could also be achieved by adding 1 eq of $Bu_4N(BF_4)$). The solution was then placed in a sonicator bath at 60°C for 3 h to give the desired compound in solution.

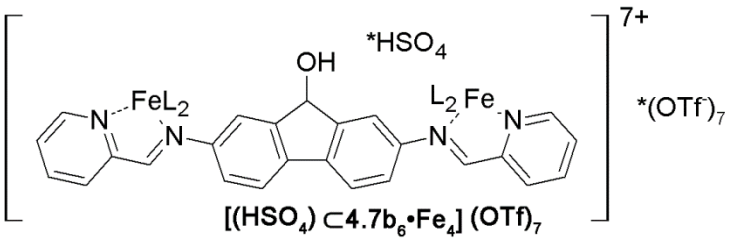

[(HSO$_4$)⊂4.7b$_6$•Fe$_4$](OTf)$_7$:

The oligomer **[4.7b$_x$•Fe$_y$](OTf)$_{2y}$** (2.0 mg, 5.3 μmol) was added to CD_3CN (400 μL) in an NMR tube. To this was added 1 eq of $Bu_4N(HSO_4)$. The solution was then placed in a sonicator bath at 60°C for 3 h to give the desired compound in solution.

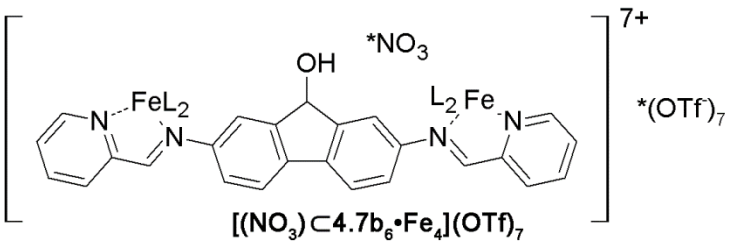

[(NO$_3$)⊂4.7b$_6$•Fe$_4$](OTf)$_7$

[(NO$_3$)⊂4.7b$_6$•Fe$_4$](OTf)$_7$:

The oligomer **[4.7b$_x$•Fe$_y$](OTf)$_{2y}$** (2.0 mg, 5.3 μmol) was added to CD_3CN (400 μL) in an NMR tube. To this was added 1 eq of $Bu_4N(NO_3)$. The solution was then placed in a sonicator bath at 60°C for 3 h to give the desired compound in solution.

8.5 Chapter 5 Experimental

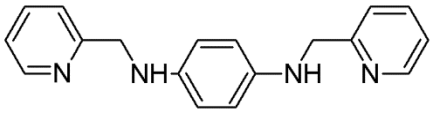

5.1

***N*,*N*'-bis(pyridin-2-ylmethyl)benzene-1,4-diamine (5.1)**:

p-Phenylene diamine (1.00 g, 9.25 mmol) and 2-pyridinecarboxaldehyde (1.75 mL, 18.3 mmol) were combined in a 50 mL Erlenmeyer flask with stir bar. MeOH (25 mL) was added, followed by stirring for 7 h, after which point sodium borohydride (1.40 g, 37.0 mmol) was added slowly. The reaction was then stirred at room temperature for 12 h. The reaction mixture was evaporated *in vacuo* to give a residue which was then triturated in dichloromethane. Evaporation of the organic phase *in vacuo* gave the desired product as a tan solid (1.12 g, 42%). ^{1}H NMR (400 MHz; $CDCl_3$) δ 8.56 (d, *J*=4.8 Hz, 2H), 7.61 (td, *J* =7.7, 1.8 Hz, 2H), 7.32 (d, *J* = 7.8 Hz, 2H), 7.14 (dd, *J* = 7.0, 5.2 Hz, 2H), 6.59 (s, 4H), 4.38 (s, 4H); ^{13}C NMR (100 MHz; $CDCl_3$) δ 159.3, 149.3, 149.2, 140.6, 136.6, 122.0, 121.8, 114.9, 50.7.

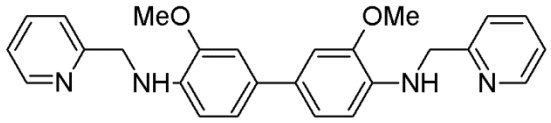

5.2a

***N,N*'-bis(pyridin-2-ylmethyl)-*o*-anisidine (5.2a)**:

o-Dianisidine (1.00 g, 4.09 mmol) and 2-pyridinecarboxaldehyde (780 µL, 8.16 mmol) were combined in a 50 mL Erlenmeyer flask with stir bar. EtOH (25 mL) was added, followed by stirring for 12 h, after which point sodium borohydride (619 mg, 16.4 mmol) was added slowly. The reaction was then stirred at room temperature for 24 h. The reaction mixture was evaporated *in vacuo* to give a residue which was then triturated in water, and the product filtered as a tan solid (1.48 g, 85%). ^{1}H NMR (400 MHz; $CDCl_3$) δ 8.60 (d, *J* = 4.8 Hz, 2H), 7.64 (t, *J* = 7.6 Hz, 2H), 7.38 (d, *J* = 7.9 Hz, 2H), 7.19 (t, *J* = 6.1 Hz, 2H), 6.99 (d, *J* = 7.8 Hz, 2H), 6.98 (s, 2H), 6.56 (d, *J* =7.8 Hz, 4.54 (s, 4H), 3.94 (s, 6H).

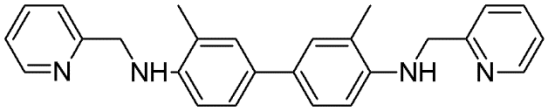

5.2b

***N,N'*-bis(pyridin-2-ylmethyl)-*o*-tolidine (5.2b)**:

o-Tolidine (1.50 g, 7.07 mmol) and 2-pyridinecarboxaldehyde (1.34 mL, 14.0 mmol) were combined in a 125 mL Erlenmeyer flask with stir bar. EtOH (100 mL) was added, followed by stirring for 6 h, after which point sodium borohydride (1.80 g, 47.6 mmol) was added slowly. The reaction was then stirred at room temperature for 12 h. The reaction mixture was then diluted with water (400 mL) and the resulting precipitate was filtered and dried. Recrystallization from 95% ethanol gave product as a yellow solid (2.26 g, 81%). ^{1}H NMR (400 MHz; $CDCl_3$) δ 8.62 (d, *J* = 3.6 Hz, 2H), 7.64 (t, *J* = 7.3 Hz, 2H), 7.33 (d, *J* = 7.7 Hz, 2H), 7.31 (s, 2H), 7.29 (t, *J* = 11.0 Hz, 2H), 7.19 (t, *J* = Hz, 2H), 6.62 (d, *J*= 8.0 Hz, 2H), 4.71 (br s, 2H), 4.54 (s, 4H), 2.32 (s, 6H). ^{13}C NMR (100 MHz; $CDCl_3$) δ 158.7, 149.3, 144.5, 136.7, 130.8, 128.5, 125.0, 122.7, 122.1, 121.7, 110.6, 49.5, 17.9.

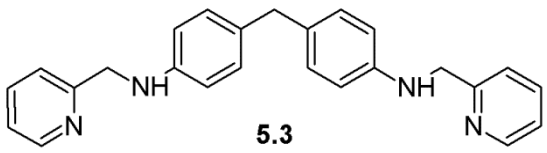

5.3

***N,N'*-bis(pyridin-2-ylmethyl)-4,4'-diaminodiphenylmethane (5.3)**:

4,4'-diaminodiphenylmethane (1.04 g, mmol) and 2-pyridinecarboxaldehyde (1.0 mL, mmol) were combined in a 125 mL Erlenmeyer flask with stir bar. EtOH (100 mL) was added, followed by stirring for 2 h, after which point sodium borohydride (800 mg, mmol)

was added slowly. The reaction was then stirred at room temperature for 24 h. The reaction mixture was then diluted with water (400 mL) and the solution was evaporated *in vacuo* to a volume of 425 mL. The resulting precipitate was filtered, washed with deionized water (200 mL) and dried to give product as a light yellow solid (1.33 g, 66%). ^{1}H NMR (400 MHz; $CDCl_3$) δ 8.57 (d, *J* = 4.5 Hz, 2H), 7.62 (td, *J* = 7.2, 5.0 Hz, 2H), 7.33 (d, *J*= 7.8 Hz, 2H), 7.17 (dd, *J* = 7.2, 5.0 Hz, 2H), 6.98 (d, *J* = 8.2 Hz, 4H), 6.59 (d, *J* = 8.1 Hz, 4H), 4.60 (br s, 2H), 4.43 (s, 4 H), 3.76 (s, 2H); ^{13}C NMR (100 MHz; $CDCl_3$) δ 158.9, 149.2, 146.1, 136.7, 131.2, 129.7, 122.1, 121.7, 113.3, 49.7, 40.2.

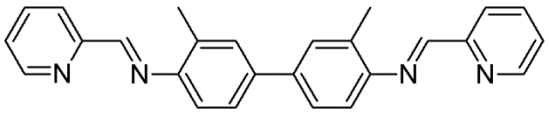

5.4

***N*,*N*'-bis(pyridin-2-ylmethylene)-*o*-tolidine (5.4):**

o-Tolidine (560 mg, 2.64 mmol) and 2-formylpyridine (500 µL, 5.28 mmol) were combined in a 125 mL Erlenmeyer flask with stir bar. MeOH (50 mL) was added, followed by stirring for 24 h at RT. The reaction mixture was then filtered and dried to give product as a yellow solid (609 mg, 59%). ^{1}H NMR (400 MHz; $CDCl_3$) δ 8.71 (d, *J* = 3.4 Hz, 2H), 8.59 (s, 2H), 8.27 (d, *J* = 7.7 Hz, 2H), 7.81 (t, *J* = 7.3 Hz, 2H), 7.52 (s, 2H), 7.49 (d, *J* = 8.6 Hz, 2H), 7.36 (t, *J* = 5.5 Hz, 2H), 7.11 (d, *J* = 7.9 Hz, 2H), 2.48 (s, 6H); ^{13}C NMR (100 MHz; $CDCl_3$) δ 159.7, 159.6, 155.0, 149.7, 149.1, 139.0, 136.7, 133.1, 129.0, 125.4, 125.1, 121.8, 118.0, 18.2.

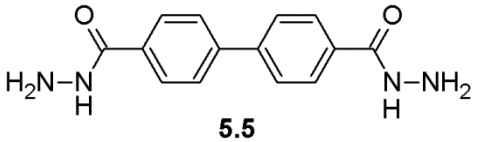

5.5

1,1'-Biphenyl-4,4'-dicarbohydrazide (5.5) (Method A):

To a round bottom flask equipped with stir bar was added 4,4'-biphenyl dicarboxylic acid (1.00 g, 4.13 mmol), 2-(6-Chloro-1H-benzotriazole-1-yl)-1,1,3,3-tetramethylaminium hexafluoro-phosphate [HCTU] (3.44 g, 8.32 mmol), acetonitrile (40 mL), and triethylamine (2.5 mL, 17.8 mmol). The reaction was stirred at room temperature for 5 h, followed by addition of triethylamine (2.5 mL, 17.8 mmol) and anhydrous hydrazine (300 µL, 9.60 mmol). The reaction was stirred at room temperature for an additional 16 h, followed by filtering a white precipitate, which was then rinsed with deionized water (200 mL), triturated in dichloromethane (50 mL), and refiltered to give an off-white solid (848 mg, 76%). ^{1}H NMR (400 MHz, DMSO-d_6) δ 9.91 (br, 2H); 7.94 (d, J=8.4 Hz, 4H); 7.84 (d, J=8.4 Hz, 4H); 4.83 (br, 4H); ^{13}C NMR (100 MHz, DMSO-d_6) δ 165.4; 141.6; 132.5; 127.7; 126.7; HRMS (ESI) m/z calcd for $C_{14}H_{14}N_4O_2$ $(M+H)^+$ 271.1189; found 271.1204.

1,1'-Biphenyl-4,4'-dicarbohydrazide (5.5) (Method B):

To a round bottom flask equipped with stir bar was added diethyl 4,4'-biphenyl dicarboxylate (1.00 g, 3.70 mmol) and hydrazine monohydrate (2.0 mL, 41.1 mmol). This was heated at 70 °C for 24 h, followed by cooling. The mixture was diluted with deionized water (250 mL), followed by filtering the resulting precipitate and drying to give product as a white solid (936 mg, 94%).

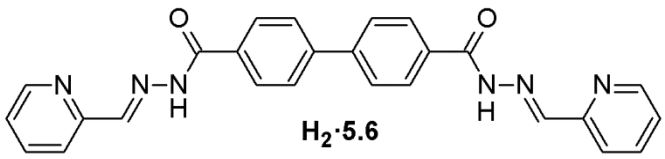

H_2·5.6

1,1'-Biphenyl-4,4'-dicarboxylic acid, bis-(2-pyridinylmethylidene)hydrazone (H_2•5.6):

To a round bottom flask equipped with stir bar and reflux condenser was added hydrazide **4** (500 mg, 5.27 mmol), 2-pyridinecarboxaldehyde (500 µL, 5.27 mmol), absolute ethanol (15 mL), and acetic acid (2 drops). The reaction was refluxed 24 h under N_2. After cooling to room temperature, a white precipitate was filtered and washed with 95 % ethanol (100 mL) to give product as a white solid (857 mg, 91%). ^{1}H NMR (400 MHz, DMSO-d_6) δ 12.15 (s, 2H); 8.62 (d, J=4.3 Hz, 2H); 8.54 (s, 2H); 8.08 (d, J=8.1 Hz, 4H); 8.00 (d, J=7.6 Hz, 2H); 7.94 (d, J=8.1 Hz, 4H); 7.88 (t, J=7.4 Hz, 2H); 7.42 (t, J=5.4 Hz, 2H); ^{13}C NMR (100 MHz, DMSO-d_6) δ 162.9; 153.3; 149.5; 148.2; 142.3; 136.9; 132.6; 128.5; 127.0; 124.4; 119.9; HRMS (ESI) m/z calcd for $C_{26}H_{20}N_6O_2$ $(M+H)^+$ 449.1721; found 449.1708.

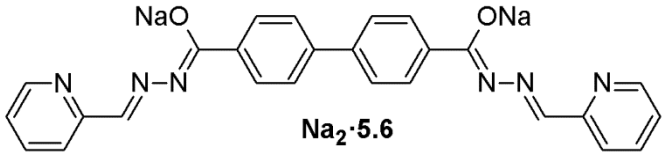

Na_2·5.6

1,1'-Biphenyl-4,4'-dicarboxylic acid, bis-(2-pyridinylmethylidene)hydrazone, disodium salt (Na_2•5.6):

To a round bottom flask equipped with stir bar and reflux condenser was added **4** (848 mg, 1.85 mmol), 2-pyridinecarboxaldehyde (600 µL, 6.33 mmol), absolute ethanol (35 mL), and acetic acid (2 drops). The reaction was refluxed 24 h under N_2. After cooling to room temperature, a white precipitate was filtered and washed with 6M NaOH (50 mL) and deionized water (100 mL) to give product as a light yellow solid (1.52 g, 98%). ^{1}H NMR (400 MHz, DMSO-d_6) δ 8.58 (d, J=4.8 Hz, 2H); 8.45 (s, 2H); 8.11 (d, J=7.9 Hz, 2H); 7.94 (d, J=7.8 Hz, 2H); 7.82 (m, 3H); 7.34 (dd, J=6.2, 4.8 Hz, 2H); ^{13}C NMR (100

MHz, DMSO-d_6) δ 165.7; 154.7; 149.5; 146.7; 141.3; 136.5; 128.6; 126.3; 123.3; 120.2; HRMS (ESI) m/z calcd for $C_{26}H_{18}Na_2N_6O_2$ $(M\text{-}Na+2H)^+$ 471.1539; found 471.1526.

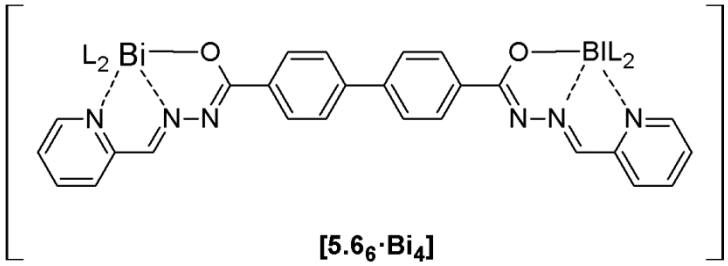

[5.6$_6$·Bi$_4$]

[5.6$_6$•Bi$_4$]:

Ligand **Na$_2$•5.6** was added to an NMR tube followed by DMSO-d_6. $Bi(OTf)_3$ (0.66 eq.) was added, followed by shaking the tube for 10 s, resulting in complexation. ^{1}H NMR (400 MHz, DMSO-d_6) δ 8.62 (d, J=4.6 Hz, 2H); 8.49 (s, 2H); 8.09 (d, J=8.1 Hz, 4H); 8.00 (d, J=7.6 Hz, 2H); 7.93 (d, J=8.1 Hz, 4H); 7.89 (t, J=7.8 Hz, 2H); 7.41 (t, J=5.8 Hz, 2H); ^{13}C NMR (100 MHz, DMSO-d_6) δ 172.4, 154.1, 149.8, 149.4, 142.0, 140.2, 133.4, 129.0, 127.1, 124.3, 120.7 (q, J=322.2 Hz).

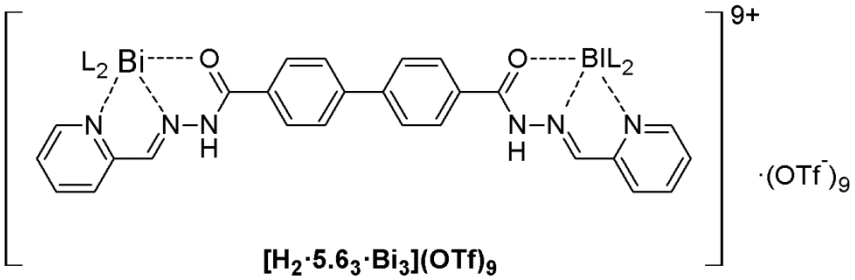

[H$_2$·5.6$_3$·Bi$_3$](OTf)$_9$

[(H$_2$•5.6)$_3$•Bi$_3$](OTf)$_9$:

Ligand **H$_2$•5.6** was added to an NMR tube followed by CD_3CN. $Bi(OTf)_3$ (2.1 eq.) was added, followed by shaking the tube for 10 s, resulting in complexation. ^{1}H NMR (400 MHz, CD_3CN) δ 9.79 (s, 2H), 9.37 (d, J=5.1 Hz, 2H); 8.51 (t, J=7.7 Hz, 2H); 8.38 (d,

J=7.6 Hz, 2H); 8.31 (d, J=8.4 Hz, 4H); 8.11 (partially overlapped t, J=6.6 Hz, 2H); 8.08 (d, J=8.4 Hz, 4H); 5.58 (br, 2H); (100 MHz, CD_3CN) δ 168.9; 154.4; 153.0; 148.4; 146.7; 144.2; 131.1; 129.6; 127.9; 125.9; 121.1 (q, J=318.6 Hz); HRMS (ESI) m/z calcd for $C_{78}H_{54}Bi_3N_{18}O_6$ (M-6(HOTf)-3(OTF))$^{3+}$ 655.1289; found 655.1290.

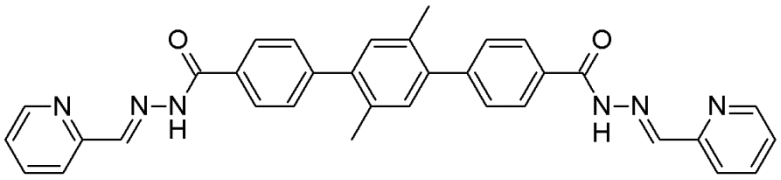

H_2·5.7

2',5'-Dimethyl-1,1':4',1''-terphenyl-4,4''-dicarboxylic acid, bis-(2-pyridylmethylidene)hydrazone (H_2•5.7):

Bis-hydrazide **5.11** (267 mg, 0.71 mmol) was combined in a 50 mL round bottom flask with stir bar and attached reflux condenser with 2-formyl pyridine (140 µL, 1.48 mmol), acetic acid (2 drops), and absolute ethanol (10 mL). The reaction mixture was heated under reflux for 12 h and then cooled, followed by filtration of the resulting precipitate. This was washed with absolute EtOH (25 mL) followed by drying to give product as a tan solid (298 mg, 76%). ^{1}H NMR (400 MHz, DMSO-d_6) δ 12.13 (s, 2H), 8.63 (d, *J* = 4.7 Hz, 2H), 8.51 (s, 2H), 8.02 (m, 6H), 7.92 (d, *J* = 7.6 Hz, 2H), 7.59 (d, *J* = 7.9 Hz, 4H), 7.44 (t, *J* = 6.1 Hz, 2H), 7.24 (s, 2H), 2.29 (s, 6H).

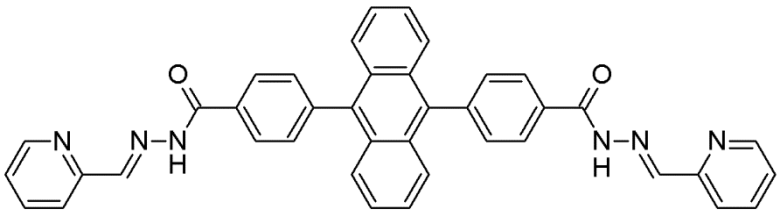

H_2·5.8

4,4'-(Anthracen-9,10-diyl)bis-N-(pyridine-2-ylmethylidene)benzohydrazone (H_2•5.8):

Bis-hydrazide **5.12** (100 mg, 0.22 mmol) was combined in a 50 mL round bottom flask with stir bar and attached reflux condenser with 2-formyl pyridine (42 µL, 0.44 mmol), acetic acid (2 drops), and absolute ethanol (10 mL). The reaction mixture was heated under reflux for 12 h and then cooled, followed by filtration of the resulting precipitate. This was washed with absolute EtOH (25 mL) followed by drying to give product as a tan solid (121 mg, 86%). ^{1}H NMR (400 MHz, DMSO-d_6) δ 12.28 (s, 2H), 8.66 (d, *J* = 4.6 Hz, 2H), 8.56 (s, 2H), 8.23 (d, *J* = 7.9 Hz, 4H), 8.06 (d, *J* = 7.7 Hz, 2H), 7.95 (t, *J* = Hz, 2H), 7.68 (d, *J* = 7.8 Hz, 4H), 7.61 (dd, *J* = 6.4, 3.4 Hz, 4H), 7.48 (m, 6H). ^{13}C NMR (100 MHz, DMSO-d_6) δ 163.3, 153.1, 149.4, 147.9, 141.9, 137.2, 136.0, 132.8, 131.1, 129.0, 128.2, 126.3, 125.9, 124.6, 120.1.

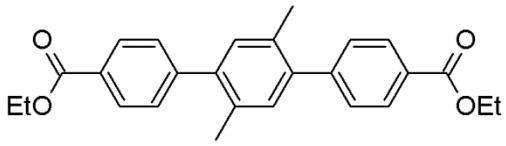

5.9

Diethyl-2',5'-dimethyl-1,1':4',1''-terphenyl-4,4''-dicarboxylate (5.9):

The reagent 2,5-dibromo-*p*-xylene (500 mg, 1.89 mmol), 4-ethoxycarbonylphenyl boronic acid (930 mg, 4.80 mmol), cesium carbonate (4.96 g, 15.2 mmol), and palladium(bis-triphenylphosphine)dichloride (133 mg, 0.19 mmol) were combined in a 50 mL round bottom flask with attached reflux condenser and stir bar. After purging the system using a Schlenk line and filling with dry N_2, absolute ethanol (10 mL) and anhydrous toluene (10 mL) were added, followed by three additional purge cycles. The reaction was then brought to 80 °C. After 48 h the reaction was cooled. The resulting

solution was diluted with diethyl ether (250 mL), followed by filtering through celite. The organic solvents were evaporated *in vacuo*, and the resulting residue was recrystallized from absolute ethanol to give the product as a beige solid (382 mg, 50%). ^{1}H NMR (400 MHz, $CDCl_3$) δ 8.12 (d, *J* = 8.1 Hz, 4), 7.44 (d, *J* = 8.1 Hz, 4H), 7.16 (s, 2H), 4.42 (q, *J* = 7.1 Hz, 4H), 2.27 (s, 6H), 1.42 (t, *J* = 7.1 Hz, 6H).

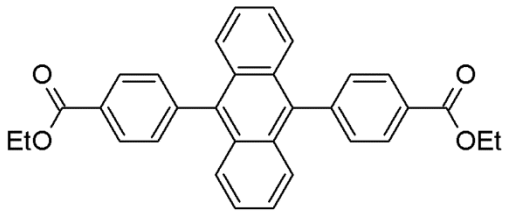

5.10

Diethyl-4,4'-(anthracen-9,10-diyl)dibenzoate (5.10):

The reagent 9,10-dibromoanthracene (300 mg, 0.89 mmol), 4-ethoxycarbonylphenyl boronic acid (693 mg, 3.6 mmol), cesium carbonate (1.16 g, 3.56 mmol), and palladium(bis-triphenylphosphine)dichloride (63 mg, 0.09 mmol) were combined in a 50 mL round bottom flask with attached reflux condenser and stir bar. After purging the system using a Schlenk line and filling with dry N_2, dimethylformamide (15 mL) was added, followed by three additional purge cycles. The reaction was then brought to 80 °C. After 96 h the reaction was cooled. The resulting solution was diluted with deionized water (250 mL), followed by filtering through celite. The filter cake was washed with ethyl acetate (100 mL), followed by washing with dichloromethane until the washing were no longer fluorescent. Removal of solvent *in vacuo* gave product as a beige solid (162 mg, 45%). ^{1}H NMR (400 MHz, $CDCl_3$) δ 8.30 (d, *J* = Hz, 4H), 7.63 (dd, *J* = 6.8, 3.3 Hz, 4H), 7.58 (d, *J* = Hz, 4H), 7.35 (dd, *J* = 6.9, 3.2 Hz, 4H), 4.49 (q, *J* = 7.1 Hz, 4H), 1.48 (t, *J* =

7.1 Hz, 6H). ^{13}C NMR (100 MHz, $CDCl_3$) δ 166.7, 144.1, 136.5, 131.6, 130.0, 129.9, 129.6, 126.8, 125.6, 61.3, 14.6;

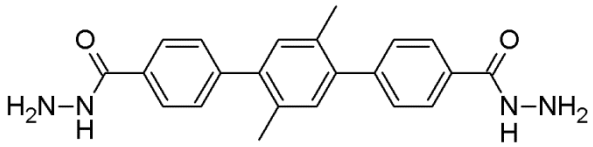

5.11

2',5'-Dimethyl-1,1':4',1''-terphenyl-4,4''-dicarbohydrazide (5.11):

Diester **5.9** (877 mg, 2.18 mmol) was added to hydrazine monohydrate (4.5 mL), followed by heating the mixture at 80 °C. After 12 h the reaction mixture was diluted with deionized water (200 mL), followed by filtration of the resulting precipitate. Drying gave the desired product as a tan solid (538 mg, 65%). ^{1}H NMR (400 MHz, DMSO-d_6) δ 10.09 (br s, 2H), 8.16 (d, *J* = 8.3 Hz, 4H), 7.73 (d, *J*= 8.3 Hz, 4H), 7.44 (s, 2H), 4.62 (br s, 4H), 2.75 (s, 6H).

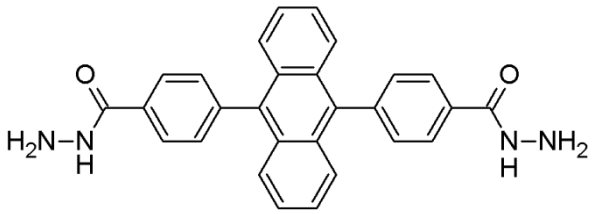

5.12

4,4'-(Anthracen-9,10-diyl)dibenzohydrazide (5.12):

Diester **5.10** (312 mg, 0.66 mmol) was added to hydrazine monohydrate (4.0 mL) and anhydrous toluene (4 mL) and absolute ethanol (4 mL), followed by heating the mixture at 80 °C. After 12 h the reaction was cooled and the resulting precipitate was filtered and

dried to give the desired product as a tan solid (274 mg, 93%). ^{1}H NMR (400 MHz, DMSO-d_6) δ 9.99 (s, 2H), 8.10 (d, *J* = 7.3 Hz, 4H), 7.55 (m, 8H), 7.45 (dd, *J* = 6.6, 3.2 Hz, 4H), 4.47 (br s, 4H).

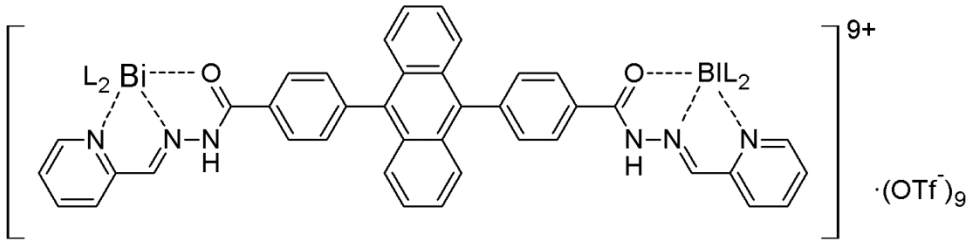

$[H_2 \cdot 5.8_3 \cdot Bi_3](OTf)_9$

$[(H_2 \bullet 5.8)_3 \bullet Bi_3](OTf)_9$:

Ligand **H_2•5.8** was added to an NMR tube followed by CD_3CN. $Bi(OTf)_3$ (2.1 eq.) was added, followed by shaking the tube for 10 s, resulting in complexation. ^{1}H NMR (400 MHz, CD_3CN) δ 9.80 (s, 2H), 9.36 (s, 2H), 8.52 (t, *J* = 7.7 Hz, 2H), 8.47 (d, *J* = 7.4 Hz, 4H), 8.39 (d, *J* = 7.4 Hz, 2H), 8.11 (t, *J* = 6.0 Hz, 2H), 7.83 (d, *J* = 7.3 Hz, 4H), 7.61 (d, *J* = 6.6 Hz, 4H), 7.47 (d, *J* = 6.6 Hz, 4H), 5.69 (br s, 2H). HRMS (ESI) m/z calcd for $C_{78}H_{54}Bi_3N_{18}O_6$ (M-6(HOTf)-3(OTF))$^{3+}$ 655.1289; found 655.1290.

8.6 Chapter 6 Experimental

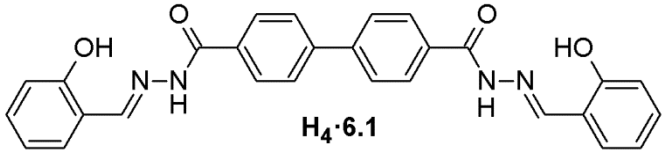

$H_4 \cdot 6.1$

1,1'-Biphenyl-4,4'-dicarboxylic acid, bis-((2-hydroxyphenyl)methylidene)hydrazone (H_4•6.1):

Bis-hydrazide **5.5** (900 mg, 3.33 mmol) was combined in a 50 mL round bottom flask with stir bar and attached reflux condenser with salicylaldehyde (750 µL, 7.06 mmol), acetic acid (2 drops), and absolute ethanol (20 mL). The reaction mixture was heated under reflux for 20 h and then cooled, followed by filtration of the resulting precipitate. This was washed with iPrOH (100 mL) followed by drying to give product as an off-white solid (1.47 g, 92%). ^{1}H NMR (400 MHz, DMSO-d_6) δ; 12.21 (s, 2H), 11.31 (s, 2H), 8.69 (s, 2H), 8.10 (d, J = 8.3 Hz, 4H), 7.96 (d, J = 8.3, 4H), 7.57 (d, J = 6.6 Hz, 2H), 7.32 (t, J = 7.1 Hz, 2H), 6.94 (m, 4H) ^{13}C NMR (100 MHz, DMSO-d_6) δ 162.3, 157.5, 148.3, 142.2, 132.2, 131.4, 129.5, 128.4, 127.1, 119.3, 118.7, 116.4.

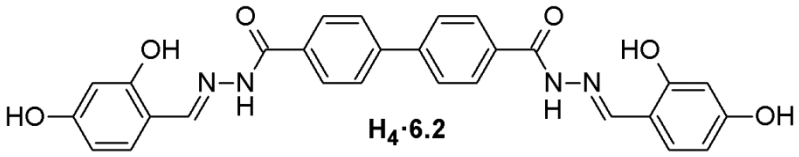

H_4·6.2

1,1'-Biphenyl-4,4'-dicarboxylic acid, bis-((2,4-dihydroxyphenyl)methylidene)hydrazone (H_4•6.2):

Bis-hydrazide **5.5** (138 mg, 0.51 mmol) was combined in a 50 mL round bottom flask with stir bar and attached reflux condenser with 2,4-dihydroxybenzaldehyde (148 mg, 1.07 mmol), acetic acid (1 drop), and absolute ethanol (5 mL). The reaction mixture was heated under reflux for 24 h and then cooled, followed by filtration of the resulting precipitate. This was washed with iPrOH (10 mL) followed by drying to give product as a tan solid (217 mg, 83%). ^{1}H NMR (400 MHz, DMSO-d_6) δ 12.01 (s, 2H), 11.48 (s, 2H), 9.97 (s, 2H), 8.54 (s, 2H), 8.06 (d, J = 8.3 Hz, 4H), 7.95 (d, J = 4H), 7.33 (d, J = 8.4 Hz, 2H), 6.37 (dd, J = 8.4, 2.0 Hz, 2H), 6.33 (d, J = 2.0 Hz, 2H).

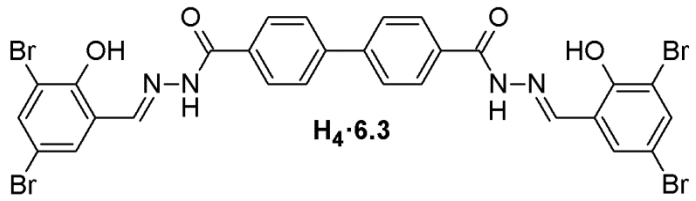

H_4·6.3

1,1'-Biphenyl-4,4'-dicarboxylic acid, bis-((3,5-dibromo-2-hydroxyphenyl)methylidene)hydrazone (H_4•6.3):

Bis-hydrazide **5.5** (100 mg, 0.37 mmol) was combined in a 50 mL round bottom flask with stir bar and attached reflux condenser with 3,5-dibromosalicylaldehyde (213 mg, 0.76 mmol), acetic acid (2 drops), and absolute ethanol (10 mL). The reaction mixture was heated under reflux for 24 h and then cooled, followed by filtration of the resulting precipitate. This was washed with iPrOH (10 mL) followed by drying to give product as an off-white solid (272 mg, 92%). ^{1}H NMR (400 MHz, DMSO-d_6) δ 12.76 (s, 2H), 12.64 (s, 2H), 8.58 (s, 2H), 8.11 (d, J = 8.4 Hz, 4H), 7.99 (d, J = 8.4 Hz, 4H), 7.85 (s, 4H).

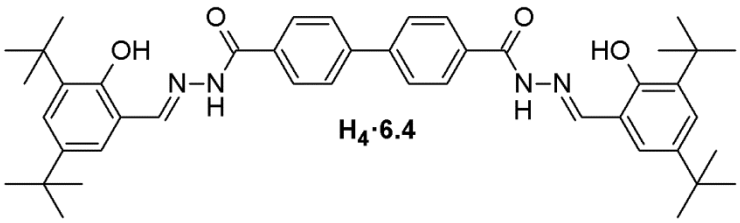

H_4·6.4

1,1'-Biphenyl-4,4'-dicarboxylic acid, bis-((3,5-*tert*-butyl-2-hydroxyphenyl)methylidene)hydrazone (H_4•6.4):

Bis-hydrazide **5.5** (75 mg, 0.28 mmol) was combined in a 50 mL round bottom flask with stir bar and attached reflux condenser with 3,5-di-*tert*-butylsalicylaldehyde (130 mg, 0.55 mmol), acetic acid (1 drop), and absolute ethanol (5 mL). The reaction mixture was heated under reflux for 24 h and then cooled, followed by filtration of the resulting

precipitate. This was washed with iPrOH (10 mL) followed by drying to give product as an off-white solid (113 mg, 58%). ^{1}H NMR (400 MHz, DMSO-d_6) δ 12.31 (s, 2H), 8.62 (s, 2H), 8.10 (d, J = 8.3 Hz, 4H), 7.99 (d, J = 8.4 Hz, 4H), 7.33 (s, 2H), 7.24 (s, 2H), 1.43 (s, 18H), 1.30 (s, 18H).

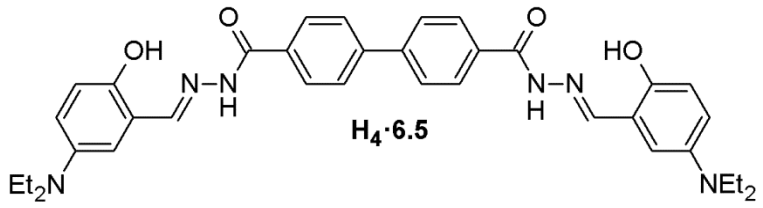

H_4·6.5

1,1'-Biphenyl-4,4'-dicarboxylic acid, bis-((4-(diethylamino)-2-hydroxyphenyl)methylidene)hydrazone (H_4•6.5):

Bis-hydrazide **5.5** (200 mg, 0.74 mmol) was combined in a 50 mL round bottom flask with stir bar and attached reflux condenser with 4-(diethylamino)salicylaldehyde (286 mg, 1.48 mmol), acetic acid (1 drop), and absolute ethanol (10 mL). The reaction mixture was heated under reflux for 16 h and then cooled, followed by filtration of the resulting precipitate. This was washed with MeOH (50 mL) followed by drying to give product as an off-white solid (442 mg, 96%). ^{1}H NMR (400 MHz, DMSO-d_6) δ 11.89 (s, 2H), 11.48 (s, 2H), 8.46 (s, 2H), 8.05 (d, J = 8.4 Hz, 4H), 7.94 (d, J = 8.3 Hz, 4H), 7.21 (d, J = 8.8 Hz, 2H), 6.28 (d, J = 7.3 Hz, 2H), 6.14 (s, 2H), 3.38 (q, J = 6.9 Hz, 4H), 1.11 (t, J = 6.9 Hz, 6H).

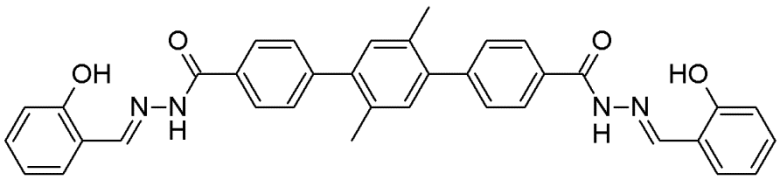

H_4·6.6

2',5'-Dimethyl-1,1':4',1''-terphenyl-4,4''-dicarboxylic acid, bis-(2-pyridylmethylidene)hydrazone (H_2•5.6):

Bis-hydrazide **5.11** (118 mg, 0.32 mmol) was combined in a 50 mL round bottom flask with stir bar and attached reflux condenser with salicylaldehyde (68 µL, 0.64 mmol), acetic acid (2 drops), and absolute ethanol (10 mL). The reaction mixture was heated under reflux for 24 h and then cooled, followed by filtration of the resulting precipitate. This was washed with absolute EtOH (25 mL) followed by drying to give product as a white solid (164 mg, 89%). ^{1}H NMR (400 MHz, DMSO-d_6) δ 12.19 (s, 2H), 11.31 (s, 2H), 8.67 (s, 2H), 8.04 (d, *J* = 8.2 Hz, 4H), 7.59 (m, 6H), 7.32 (t, *J* = 7.6 Hz, 2H), 7.24 (s, 2H), 6.96 (m, 4H), 2.29 (s, 2H).

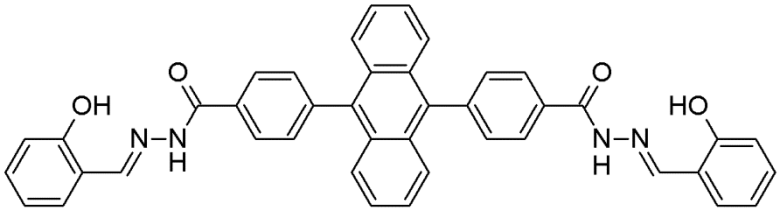

H_4·6.7

4,4'-(Anthracen-9,10-diyl)bis-N-((2-hydroxyphenyl)methylidene)benzohydrazone (H_4•6.7):

Bis-hydrazide **5.12** (43 mg, 96 µmol) was combined in a 50 mL round bottom flask with stir bar and attached reflux condenser with salicylaldehyde (22 µL, 210 µmol), acetic acid (2 drops), and absolute ethanol (10 mL). The reaction mixture was heated under reflux for 30 h and then cooled, followed by addition of CH_2Cl_2 (50 mL), followed by filtration of the resulting precipitate. This was dried to give product as a tan solid (50 mg,

79%). ^{1}H NMR (400 MHz, DMSO-d_6) δ 12.32 (br s, 2H), 11.33 (s, 2H), 8.72 (s, 2H), 8.24 (d, *J*= 8.1 Hz, 4H), 7.69 (d, *J*= 8.1 Hz, 4H), 7.60 (m, 6H), 7.49 (dd, *J* = 6.9, 3.2 Hz, 4H), 7.33 (dd, *J* = 12.0, 4.9 Hz, 2H), 6.97 (m, 4H).

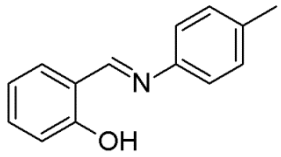

6.8

2-{(*E*)-[(4-Methylphenyl)imino]methyl}phenol (6.8):

p-Toluidine (2.02 g, 18.9 mmol) was combined in a 50 mL round bottom flask with stir bar with salicylaldehyde (2.0 mL, 18.8 mmol), and methanol (50 mL). The reaction mixture was stirred for 12 h, followed by filtration of the resulting precipitate. This was washed with hexanes (25 mL) and dried to give product as a yellow solid (3.12 g, 78%). ^{1}H NMR (400 MHz, $CDCl_3$) δ 13.39 (br s, 1H), 8.63 (s 1H), 7.38 (d, *J* = 8.1 Hz, 2H), 7.37 (td, *J* = 7.4, 1.7 Hz, 1H), 7.23 (m, 1H), 7.22 (d, *J* = 8.1 Hz, 2H), 6.94 (td, *J* = 7.5, 0.9 Hz, 1H), 2.39 (s, 3H); ^{13}C NMR (100 MHz, DMSO-d_6) δ 161.8, 161.2, 146.0, 137.0, 133.0, 132.2, 130.1, 121.1, 119.4, 119.1, 117.3, 21.2.

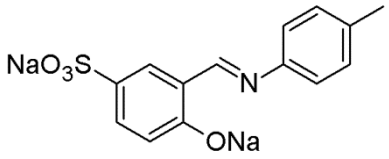

Na_2·6.9

Disodium 3-{(*E*)-[(4-methylphenyl)imino]methyl}-4-oxidobenzenesulfonate (Na_2•6.9):

The imine **6.8** (3.12 g, 14.8 mmol) was combined in a 50 mL round bottom flask with stir bar and reflux condenser with concentrated sulfuric acid (10 mL). The reaction mixture was stirred at 110 °C for 3 h, followed by pouring into ice-water (88 mL). The resulting suspension was heating to reflux, followed by hot filtration of the precipitate. This was then treated with saturated sodium bicarbonate (200 mL), followed by evaporation of the solvent by passing air over the mixture while heat was applied (50 °C). The resulting solid was washed with CH_2Cl_2, followed by triturating in MeOH (3 x 200 mL). The solvent was evaporated *in vacuo* to give product as a yellow solid (1.84 g, 37%). ^{1}H NMR (400 MHz, DMSO-d_6) δ 9.00 (s, 1H), 7.93 (d, *J* = 2.1 Hz, 1H), 7.60 (dd, *J* = 8.5, 2.2 Hz, 1H), 7.35 (d, *J* = 8.3 Hz, 2H), 7.26 (d, *J* = 8.0 Hz, 2H), 6.88 (d, *J* = 8.5 Hz, 1H), 2.34 (s, 3H); ^{13}C NMR (100 MHz, DMSO-d_6) δ 162.3, 160.4, 145.3, 139.7, 136.5, 130.5, 129.9, 129.6, 121.3, 118.0, 115.7, 20.6.

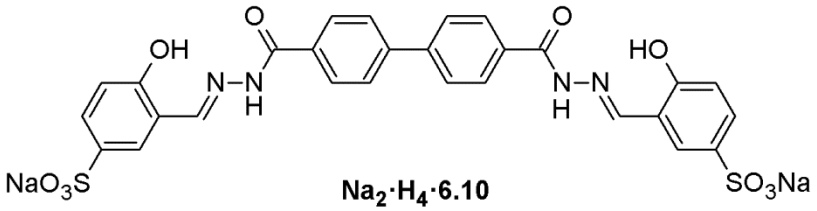

Na_2·H_4·6.10

1,1'-Biphenyl-4,4'-dicarboxylic acid, bis-((5-(sodiumsulfonyl)-2-hydroxyphenyl)methylidene)hydrazone (H_4•Na_2•6.10):

Bis-hydrazide **5.5** (67 mg, 0.25 mmol) was combined in a 50 mL round bottom flask with stir bar and attached reflux condenser with **Na_2•6.9** (100 mg, 0.30 mmol), acetic acid (100 µL), and absolute ethanol (10 mL). The reaction mixture was heated under reflux for 24 h and then cooled, followed by addition of Et_2O (10 mL) and filtration of the subsequent precipitate. Drying gave product as a light green solid (139 mg, 68%). ^{1}H

NMR (400 MHz, DMSO-d_6) δ 12.21 (s, 2H), 11.38 (s, 2H), 8.68 (br s, 2H), 8.10 (d, *J* = 8.4 Hz, 4H), 7.97 (d, *J* = 8.4 Hz, 4H), 7.52 (dd, *J* = 8.5, 2.1 Hz, 2H), 6.88 (d, *J* = 8.5 Hz, 2H).

8.7 Chapter 7 Experimental

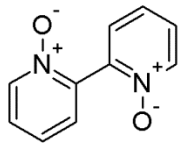

7.3

2,2'-Bipyridine-N,N'-dioxide (7.3):

The reagent 2,2'-bipyridine (1.54 g, 9.86 mmol) was dissolved in AcOH (10 mL) in a 50 mL round bottom flask with attached reflux condensor and stir bar, followed by heating to 75°C. Hydrogen peroxide (30 %, 10 mL) was then added slowly, and heating was continued. After 4.5 h the solvent was partially evaporated *in vacuo* to approximately 7 mL, followed by addition of acetone (1 L) and cooling to -25°C to give product as an off-white precipitate after collection by filtration. (1.56 g, 84%). ^{1}H NMR (400 MHz; D_2O) δ 8.49 (m, 2H), 7.86 (m, 2H), 7.78 (dd, *J* = 3.6, 1.8 Hz, 2H), 7.76 (dd, *J* = 4.5, 1.9 Hz, 2H).

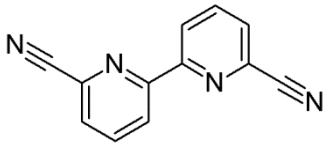

7.4

6,6'-Dicyano-2,2'-Bipyridine (7.4):

The intermediate **7.3** (1.88 g, 10 mmol) was combined with trimethylsilylcyanade (6.0 mL, 48 mmol) and benzoyl chloride (2.5 mL, 22 mmol) in a 100 mL round bottom flask with stir bar containing anhydrous dichloromethane (40 mL). After 5 d of stirring at room temperature the solvent was evaporated *in vacuo* to give a solid. This was triturated in $NaOH_{(aq)}$ followed by H_2O then filitered and dried to give product as a white solid. (1.58 g, 76%). ^{1}H NMR (400 MHz; $CDCl_3$) δ 8.72 (d, *J* = 8.1 Hz, 2H), 8.02 (t, *J* = 8.1 Hz, 2), 7.78 (d, *J* = 7.6 Hz, 2H).

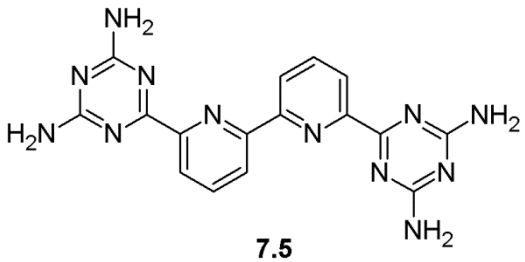

7.5

6,6'-Bis(3,5-diamino-2,4,6-triazinyl)2,2'-bipyridine (7.5):

The dinitrile **7.4** (100 mg, 0.48 mmol) was combined with dicyandiamide (86 mg, 1.0 mmol) and KOH (30 mg, 0.53 mmol) in a 50 mL round bottom flask with attached reflux condensor and stir bar. To this was added isopropanol (20 mL), followed by heating to reflux. After 24 h the reaction was cooled to room temperature and a precipitate was filtered, washed with deionized H_2O, then dried to give give product as a tan solid (123 mg, 68%). ^{1}H NMR (400 MHz; $CDCl_3$) δ 8.54 (d, *J* = 7.8 Hz, 2H), 8.24 (d, *J* = 7.7 Hz, 2H), 8.11 (t, *J* = 7.8 Hz, 2H), 6.96 (br s, 4H), 6.86 (br s, 4H).

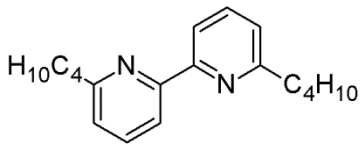

7.6

6,6'-Dibutyl-2,2'-bipyridine (7.6):

2,2'-Bipyridine (0.800 g, 5.1 mmol) was added to anhydrous diethyl ether (50 mL) in a 100 mL round bottom flask. This was purged with N_2, followed by cooling to -78 °C, followed by slow addition of 1.6 M n-BuLi in hexanes (11.2 mL, 28 mmol). After stirring for 2 h the reaction was warmed to room temperature, followed by stirring for an additional 6 h. The reaction was quenched with deionized H_2O, followed by extraction with dichloromethane (3 x 50 mL). The organic phase was dried over $MgSO_4$ followed by addition of MnO_2 (3.55 g, 40.8 mmol). This was stirred at room temperature for 24 h, followed by filtration through celite and evaporation of the solvent *in vacuo* to give product as a black oil (1.22 g, 89%). ^{1}H NMR (400 MHz; DMSO-d_6) δ 7.49 (d, *J* = 7.5 Hz, 2H), 7.42 (d, *J* = 7.4 Hz, 2H), 7.32 (t, *J* = 7.8 Hz, 2H), 2.78 (t, *J* = 7.8 Hz, 4H), 1.59 (quin, *J* = 7.4 Hz, 2H), 1.34 (sex, *J* = 7.3 Hz, 2H), 0.90 (t, *J* = 6.8 Hz, 6H).

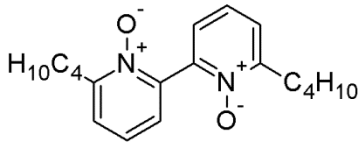

7.7

6,6'-Dibutyl-2,2'-bipyridine-N,N'-dioxide (7.7):

The oil **7.6** (1.22 g, 4.53 mmol) was added to AcOH (5 mL) and 30% H_2O_2 (40 mL), followed by heating to 75 °C for 8 h. The reaction was then treated with 6M $NaOH_{(aq)}$

(100 mL), followed by extraction with dichloromethane (3 x 100 mL). This was dried over $MgSO_4$, followed by evaporation *in vacuo* to give product as a clear oil (1.07 g, 79%). ^{1}H NMR (400 MHz; DMSO-d_6) δ 7.51 (d, *J* = 7.7 Hz, 2H), 7.45 (d, *J* = 7.9 Hz, 2H), 7.33 (t, *J* = 7.7 Hz, 2H), 2.79 (t, *J* = 8.4 Hz, 4H), 1.63 (quin, *J* = 5.8 Hz, 2H), 1.36 (sex, *J* = 7.3 Hz, 2H), 0.92 (t, *J* = 7.2 Hz, 6H).

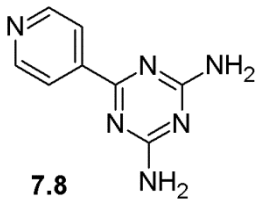

7.8

6-(Pyridin-4-yl)-1,3,5-triazine-2,4-diamine (7.8):

4-Cyanopyridine (2.03 g, 19.5 mmol), dicyandiamide (2.04 g, 24.3 mmol), and potassium hydroxide (194 mg, 3.5 mmol) were combined in a 50 mL round bottom flask with stir bar and attached reflux condenser. Isopropanol (20 mL) was added, followed by heating the reaction to 82 °C for 24 h. Afterwards the reaction was cooled, followed by filtration of the resulting precipitate. Washing with deionized water and drying gave product as a white solid (3.15 g, 86%). ^{1}H NMR (400 MHz; DMSO-d_6) δ 8.71 (d, *J* = 6.0 Hz, 2H), 8.06 (d, *J* = 6.0 Hz, 2H), 6.93 (br s, 4H). ^{13}C NMR (100 MHz; $CDCl_3$) δ 168.7, 167.5, 150.1, 144.5, 121.5.

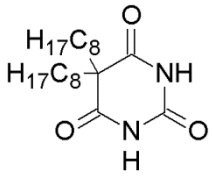

7.9a

5,5-Dioctylbarbituric Acid (7.9a):

Diethylmalonate (2.50 mL, 16.4 mmol) was slowly syringed into a 100 mL round-bottomed flask with stir bar containing anhydrous THF (50 mL), KI (260 mg, 1.57 mmol) and NaH suspended in mineral oil (1.36 g, 34.0 mmol). Once H_2 production ceased, 1-octylbromide (7.00 mL, 40.6 mmol) was added along with a reflux condensor, and reaction was purged using N_2, followed by heating under reflux. After 24 h, urea (990 mg, 16.5 mmol) was added, followed by addition of additional NaH suspended in mineral oil (1.34 g, 33.5 mmol). Reaction was then heated under reflux. After 24 h the reaction was cooled to room temperature, followed by addition of 10% aqueous HCl to lower the pH to approximately 1. The volume was reduced *in vacuo* until all of the THF had been removed, giving rise to a precipitate. This was filtered and dried. The precipitate was then triturated in hexanes (100 mL), filtered, and rinsed with additional hexanes (100 mL). After drying, product was recovered as a faint-beige solid (1.25 g, 21%). ^{1}H NMR (400 MHz; $CDCl_3$) δ 8.71 (s, 2H), 1.96 (m, 4H), 1.22 (m, 24H), 0.87 (t, *J* = 6.8 Hz, 6H). ^{13}C NMR (100 MHz; $CDCl_3$) δ 178.0, 175.4, 58.0, 34.5, 32.0, 29.8, 29.3, 27.4, 24.6, 22.8, 14.2. HRMS (ESI) m/z calcd for $C_{20}H_{36}N_2O_3$ ([M-H]$^+$) 352.2642, found 351.2563.

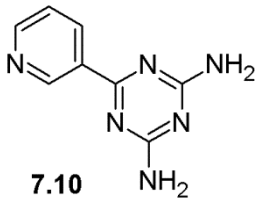

7.10

6-(Pyridin-3-yl)-1,3,5-triazine-2,4-diamine (7.10):

3-Cyanopyridine (1.00 g, 9.61 mmol), dicyandiamide (889 mg, 10.6 mmol), and KOH (250 mg, 4.46 mmol) were combined in a 100 mL round bottom flask with stir bar and attached reflux condenser. Isopropanol (50 mL) was added, and the reaction heated

under reflux. After 4 d the reaction was cooled and a precipitate was filtered. Washing with deionized water (100 mL) and drying gave product as a white solid (1.31 g, 72%). ^{1}H NMR (400 MHz; DMSO-d_6) δ 9.34 (d, J = 1.3 Hz, 1H), 8.68 (dd, J = 4.7, 1.5 Hz, 1H), 8.48 (dt, J = 8.0, 1.9 Hz, 1H), 7.50 (dd, J = 7.9, 4.8 Hz, 1H), 6.87 (br s, 8H). ^{13}C NMR (100 MHz; DMSO-d_6) δ 168.8, 167.3, 151.7, 149.0, 135.0, 132.5, 123.4.

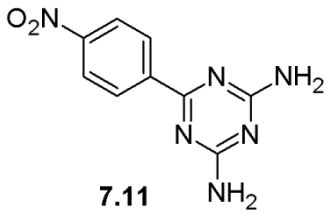

7.11

6-(4-Nitrophenyl)-1,3,5-triazine-2,4-diamine (7.11):

4-Nitrobenzonitrile (500 mg, 3.38 mmol), dicyandiamide (312 mg, 3.71 mmol), and KOH (102 mg, 1.82 mmol) were combined in a 50 mL round bottom flask with stir bar and attached reflux condenser. Isopropanol (20 mL) was added, and the reaction heated under reflux. After 18 h the reaction was cooled and a precipitate was filtered. Washing with deionized water (100 mL) and drying gave product as a tan solid (483 mg, 61%). ^{1}H NMR (400 MHz; DMSO-d_6) δ 8.45 (d, J = 8.9, 2H), 8.34 (d, J = 8.9 Hz, 2H), 6.95 (br s, 4H). ^{13}C NMR (100 MHz; $CDCl_3$) δ 168.4, 167.4, 149.0, 143.2, 128.8, 123.5.

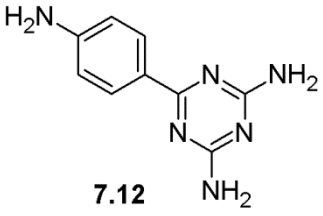

7.12

6-(4-Aminophenyl)-1,3,5-triazine-2,4-diamine (7.12):

Nitro compound **7.11** (470 mg, 2.02 mmol) was added to a 100 mL round bottom flask with stir bar, followed by addition of methanol (90 mL). Hydrazine monohydrate (2 mL, 41.2 mmol) and Raney© 2800 Ni suspension in water (1.0 mL), followed by stirring at room temperature for 4 h. The reaction mixture was then filtered through celite and solvent evaporated *in vacuo* to give product as a light yellow solid (328 mg, 80%). ^{13}C NMR (100 MHz; DMSO-d_6) δ 170.3, 167.2, 151.8, 129.3, 123.9, 112.7.

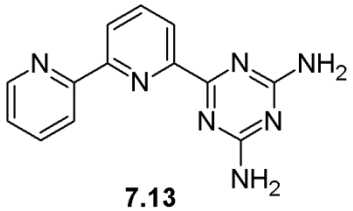

7.13

6-(3,5-Diamino-2,4,6-triazinyl)2,2'-bipyridine (7.13):

Nitrile **7.15** (248 mg, 1.37 mmol) was added to a 50 mL round-bottomed flask with stir bar, along with dicyandiamide (124 mg, 1.47 mmol) and KOH (34 mg, .61 mmol). A reflux condensor was attached, and iPrOH (20 mL) was added, followed by heating under reflux. After 18 h the reaction was cooled, and the precipitate was filtered. The filter cake was rinsed with iPrOH (120 mL) and deionized water (120 mL), then dried to give product as an off-white solid (259 mg, 71%). ^{1}H NMR (400 MHz; DMSO) δ 8.71(dd, *J* = 4.7, 0.7 Hz, 1H), 8.48 (d, *J* = 7.8 Hz, 2H), 8.20 (dd, *J* = 7.7, 0.9 Hz, 1H), 8.06 (td, *J* = 7.8 Hz, 1H), 7.98 (td, *J* = 7.7, 1.8 Hz, 1H), 7.48 (ddd, *J* = 7.4, 4.7, 1.0 Hz, 1H), 6.93 (br d, 4H). ^{13}C NMR (100 MHz; $CDCl_3$) δ 170.5, 167.6, 155.2, 155.0, 154.8, 149.3 (d, *J* = 6.4 Hz), 137.8, 137.2, 124.3, 123.6 (d, *J* = 6.5 Hz), 121.7 (d, *J* = 10.0Hz), 120.9 (d, *J* = 9.1 Hz). HRMS (ESI) m/z calcd for $C_{13}H_{11}N_7$ ($[M+H]^+$) 266.1148, found 266.1166.

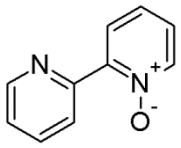

7.14

2,2'-Bipyridyl-N-Oxide (7.14):

2,2'-Bipyridine (1.248 g, 8.00 mmol) was added to a 50 mL round-bottomed flask with stir bar, followed by dissolution in trifluoroacetic acid (6.0 mL). This was cooled to room temperature, followed by slow addition of 30% H_2O_2 (1.2 mL, 12 mmol). Reaction was stirred at room temperature for 2 h, followed by addition of chloroform (25 mL). This was washed with 6M aqueous NaOH (3 x 10 mL), followed by back extraction of the combined aqueous phase with dichloromethane (4 x 20 mL). The combined organic phase was dried over $MgSO_4$, followed by evaporation *in vacuo* to give an oil. This was dried under vacuum overnight to give a beige solid (1.25 g, 91%). ^{1}H NMR (400 MHz; $CDCl_3$) δ 8.90 (d, *J* = 8.0 Hz, 1H), 8.74 (d, *J* = 4.2 Hz, 1H), 8.33 (d, *J* = 6.3 Hz, 1H), 8.20 (dd, *J* = 8.0, 2.0 Hz, 1H), 7.84 (td, *J* = 7.9, 1.8 Hz, 1H), 7.41-7.34 (m, 2H), 7.29 (m, 1H). HRMS (ESI) m/z calcd for $C_{10}H_8N_2O$ ($[M+H]^+$) 173.0709, found 173.0625.

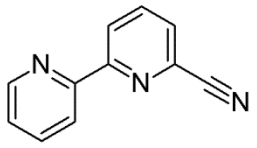

7.15

2,2'-Bipyridyl-6-Carbonitrile (7.15):

N-oxide **7.14** (3.635 g, 21.1 mmol) and trimethylsilylcyanide (6.60 mL, 52.6 mmol) were combined in a 50 mL round-bottomed flask with stir bar. Anhydrous CH_2Cl_2 (75 mL) was added to dissolve reagents, followed by placing the flask in an ice bath. Benzoyl chloride

(2.45 mL, 21.1 mmol) was added slowly to this, followed by stirring at room temperature under a blanket of nitrogen. After five days all volatiles were evaporated *in vacuo*. The resulting solid was triturated with 1M aqueous NaOH (200 mL) and collected by filtration. The filter cake was then washed with 1M aqueous NaOH (50 mL) and deionized water (250 mL). The obtained dried off-white solid was determined to be spectroscopically pure product (2.438 g, 63%). ^{1}H NMR (400 MHz; $CDCl_3$) δ 8.70-8.65 (m, 2H), 8.46 (d, *J* = 8.0 Hz, 1H), 7.95 (t, *J* = 7.9 Hz, 1H), 7.85 (td, *J* = 7.8, 1.8 Hz, 1H), 7.70 (dd, *J* = 7.6, .9 Hz, 1H), 7.37 (ddd, *J* = 7.5, 4.8, 1.1 Hz, 1H). HRMS (ESI) m/z calcd for $C_{11}H_7N_3$ ($[M+H]^+$) 182.0712, found 182.0736.

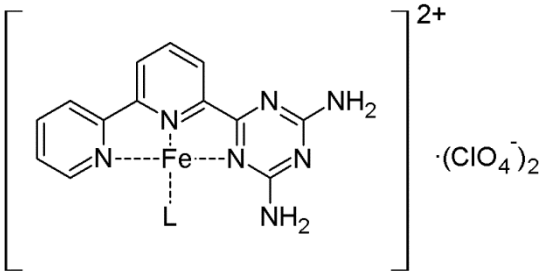

[7.13$_2$·Fe](ClO$_4$)$_2$

[7.13$_2$•Fe](ClO$_4$)$_2$:

Ligand **7.13** (35.0 mg, .132 mmol) was added to a 25 mL round-bottomed flask and suspended in MeCN (10 mL). This was followed by addition of $Fe(ClO_4)_2 \cdot xH_2O$ (24.0 mg). Upon stirring the triazine began to dissolve and the solution took a deep purple color. After 5 min all of the triazine was observed to have dissolved, and the reaction mixture was diluted with Et_2O (240 mL), causing a purple precipitate to form. This was collected by vacuum filtration and dried *in vacuo* to give product as a purple powder (49.2 mg, 95%). ^{1}H NMR (400 MHz; DMSO-d_6) δ 19.79 (br s, 1H), 17.97 (br s, 1H), 15.61 (br s, 1H), 13.87 (br s, 1H), 9.23 (br s, 1H), 8.66 (br s, 1H), 8.24 (br s, 1H), 7.20

(br s, 1H); (400 MHz; CD_3CN) δ 25.27 (br s, 1H), 17.00 (br s, 1H), 15.41 (br s, 1H), 13.87 (br s, 1H), 12.03 (br s, 1H), 8.91 (t, *J* = 7.2 Hz, 1H), 7.90 (t, *J* = 7.3 Hz, 1H), 6.59 (br s, 1H), 5.75 (br s, 1H), 0.05 (br s, 2H); (400 MHz; Acetone-d_6) δ 19.21 (br s, 1H), 17.42 (br s, 1H), 15.40 (br s, 1H), 13.46 (br s, 1H), 9.21 (t, *J* = 7.0 Hz, 1H), 8.28 (t, *J* = 7.0 Hz, 1H), 7.67 (br s, 1H), 6.66 (br s, 1H); (400 MHz; D_2O) δ 14.41 (br s, 1H), 12.56 (br s, 1H), 11.85 (br s, 1H), 10.95 (br s, 1H), 9.23 (br s, 1H), 8.90 (t, *J* = 7.9 Hz, 1H), 7.81 (t, *J* = 7.6 Hz, 1H). HRMS (ESI) m/z calcd for $C_{26}H_{22}ClFeN_{14}O_4$ ($[M\text{-}ClO_4]^+$) 685.0981, found 685.0996.

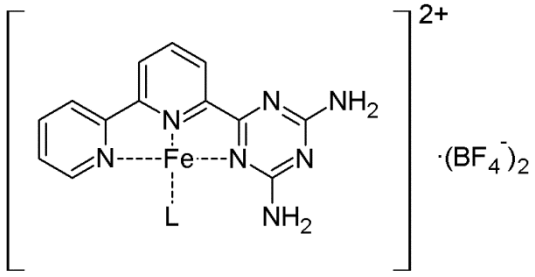

[7.13$_2$·Fe](BF$_4$)$_2$

[7.13$_2$•Fe](BF$_4$)$_2$:

Ligand **7.13** (2.0 mg, 7.5 μmol) was suspended in CD_3CN (500 μL) in an NMR tube. Meanwhile, $FeCl_2$ (11.5 mg, 91 μmol) and $AgBF_4$ (35.3 mg, 180 μmol) were combined in CD_3CN (1.0 mL), followed by vigorous shaking. After removal of AgCl by centrifugation, $Fe(BF_4)_2$ solution (42 μL, 3.8 μmol) was added to the tube, immediately causing the solution to turn purple. Sample was placed in an ultrasonification bath until no further residual solid was observed in the tube. ^{1}H NMR (400 MHz; CD_3CN) δ 25.76 (br s, 2H), 17.27 (br s, 1H), 15.61 (br s, 1H), 14.04 (br s, 1H), 12.19 (br s, 1H), 8.94 (br s, 1H), 7.93 (br s, 1H), 6.61 (br s, 1H), 5.77 (br s, 1H), 5.04 (br s, 2H).

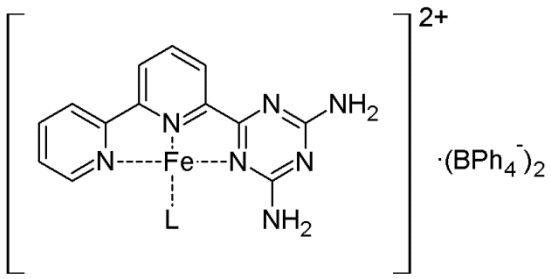

[7.13$_2$·Fe](BPh$_4$)$_2$

[7.13$_2$•Fe](BPh$_4$)$_2$:

Ligand **7.13** (166 mg, 630 μmol) was suspended in CH_3CN (25 mL) along with $Fe(ClO_4)_2 \cdot xH_2O$ (114 mg) and sodium tetraphenylborate (214 mg, 630 μmol) in a 100 mL round-bottomed flask with star bar. This was stirred for ten minutes until all solids had dissolved, followed by dilution with deionized water (150 mL). The resulting fine precipitate was filtered through celite, followed by rinsing with additional deionized water (100 mL). The filter was then rinsed with Me_2CO (400 mL) to dissolve the precipitate. Removal of the solvent *in vacuo* gave product as a fluffy purple solid (203 mg, 53%). ^{1}H NMR (400 MHz; DMSO) δ 17.52 (br s, 2H), 15.77 (br s, 2H), 14.18 (br s, 2H), 12.34 (br s, 2H), 8.91 (t, *J* = 7.5 Hz, 2H), 7.91 (t, *J* = 7.5 Hz, 2H), 7.27 (br s, 16H), 6.99 (t, *J* = 7.4 Hz, 16H), 6.83 (t, *J* = 7.1 Hz, 8H), 6.62 (br s, 2H), 5.75 (br s, 2H).

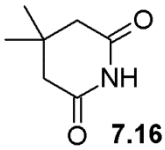

7.16

3,3-Dimethylglutarimide (7.16):

3,3-Dimethylglutaric anhydride (1.00 g, 7.03 mmol) and ammonium acetate (750 mg, 9.73 mmol) were combined in a 25 mL round-bottomed flask equipped with a reflux condenser. After purging with N_2 the mixture was heated to 155 °C. After 12 h the

reaction was cooled. The solidified mixture was dissolved in CH_2Cl_2 (20 mL), followed by washing with deionized water (2 x 20 mL). The organic layer was dried over anhydrous $MgSO_4$ then evaporated *in vacuo* to give product as an off-white solid (717 mg, 71%). ^{1}H NMR (400 MHz; $CDCl_3$) δ 8.15 (br s, 1H), δ=2.44 (s, 4H), δ=1.12 (s, 6H). ^{13}C-NMR (100 MHz; $CDCl_3$) δ 172.2, 45.6, 30.6, 28.0. HRMS (ESI) m/z calcd for $C_7H_{11}NO_2$ ($[M+H]^+$) 142.0863, found 142.0866.

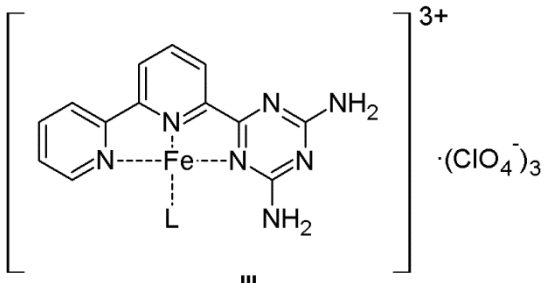

$[7.13_2 \cdot Fe^{III}](ClO_4)_3$

$[7.13_2 \bullet Fe^{III}](ClO_4)_3$:

Ligand **7.13** (25.0 mg, 94 μmol) was suspended in CH_3CN (10 mL) along with $Fe(ClO_4)_3 \cdot xH_2O$ (23.0 mg) in a 25 mL round-bottomed flask with star bar. This was stirred for ten minutes until all solids had dissolved, followed by dilution with Et_2O (50 mL). The mixture was cooled to -25 °C, and the resulting precipitate was filtered through celite, followed by rinsing with addition Et_2O (25 mL). The filter was then rinsed with Me_2CO (100 mL) and MeCN (100 mL) to dissolve the precipitate. Removal of the solvent *in vacuo* gave product as an orange solid (38.5 mg, 92%). ^{1}H NMR (400 MHz; DMSO) δ 8.82 (d, *J* = 7.7 Hz, 1H), 8.70 (d, 0.3 Hz, 1H), 8.55 (d, *J* = 6.8 Hz, 1H), 8.47 (br s, 1H), 8.09 (m, 2H), 7.96 (t, *J* = 7.2 Hz, 1H), 7.74 (t, *J* = 4.3 Hz, 1H); (400 MHz; CD_3CN) δ 8.82 (d, *J* = 4.9 Hz, 1H), 8.66 (d, *J* = 8.1 Hz, 1H), 8.48 (m, 1H), 8.29 (d, *J* = 7.4 Hz, 1H), 8.20 (t, *J* = 7.8 Hz, 1H), 8.13 (br s, 1H), 7.84 (m, 1H), 6.44 (br s, 1H); (400 MHz; Acetone-d_6)

δ 8.90 (d, *J* = 4.5 Hz, 1H), 8.85 (d, *J* = 8.0 Hz, 1H), 8.70 (d, *J* = 7.3 Hz, 1H), 8.48 (br s, 1H), 8.35 (t, *J* = 7.2 Hz, 1H), 8.26 (m, 2H), 7.82 (t, *J* = 5.6 Hz, 1H), 7.12 (br s, 1H).

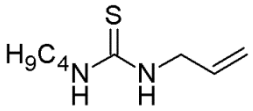

7.17

1-Allyl-3-butylthiourea (7.17):

Butylamine (1.05 mL, 10.6 mmol) was added to MeCN (10 mL), followed by addition of allyl isothiocyanate (1.00 mL, 10.2 mmol). This mixture was heat under reflux for 30 min, followed by cooling. The solvent and excess butylamine was evaporated *in vacuo* to give the desired product as a viscous yellow oil (1.45 g, 82%). ^{1}H NMR (400 MHz; $CDCl_3$) δ 6.64 (br s, 2H), 5.59 (ddd, *J* = 22.5, 10.5, 5.4 Hz, 1H), 4.94 (dt, *J* = 10.9 Hz, 5.4 Hz, 1H), 4.88 (dd, *J* = 10.2, 0.9 Hz, 1H), 3.85 (br s, 2H), 3.20 (br s, 2H), 1.29, (p, *J* = 7.3 Hz, 2H), 1.10 (sex, *J* = 7.4 Hz, 2H), 0.66 (t, *J* = 7.3 Hz, 3H). ^{13}C NMR (100 MHz; $CDCl_3$) δ 180.8, 133.1, 116.0, 46.1, 43.8, 30.5, 19.4, 13.1. HRMS (ESI) m/z calcd for $C_8H_{17}N_2S$ ($[M+H]^+$) 173.1106, found 173.1321.

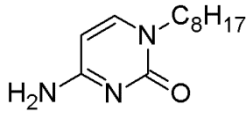

7.18

N^6-Octylcytosine (7.18):

N^4-Acetylcytosine (4.00 g, 26.1 mmol), 1-iodooctane (4.80 mL, 26.6 mmol), and potassium carbonate (7.30 g, 52.8 mmol) were combined in a 100 mL round bottom flask with stir bar and attached reflux condenser. Acetonitrile (50 mL) was added,

followed by heating the reaction to 82 °C for 48 h. After this the reaction was cooled, followed by evaporation of the solvent *in vacuo*. The residue from this was triturated in deionized water (100 mL), followed by filtration of the remaining solid. This was added to a 250 mL round bottom flask with stir bar, followed by methanol (75 mL) and ammonium hydroxide (75 mL). After stirring at room temperature for 24 h, a precipitate was filtered, rinsed with deionized water (200 mL), followed by drying. Recrystallization from absolute ethanol gave product as a beige solid (3.85 g, 66%). ^{1}H NMR (400 MHz; $CDCl_3$) δ 9.64 (br s, 2H), 7.56 (d, *J* = 7.2 Hz, 1H), 7.37 (d, *J* = 7.1 Hz, 1H), 3.86 (t, *J* = 7.3 Hz, 2H), 1.74 (quin, *J* = 5.6 Hz, 2H), 1.30 (m, 4H), 1.25 (m, 6H), 0.87 (t, *J* = 6.4 Hz, 3H)

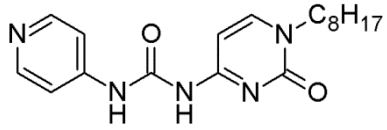

7.19

1-(1-Octyl-2-oxo-1,2-dihydropyrimidin-4-yl)-3-pyridin-4-ylurea (7.19):

Isonicotinic acid (500 mg, 4.06 mmol) was added to a 100 mL round bottom flask with stir bar and attached reflux condenser. After purging the system with N_2, anhydrous toluene (10 mL) was added. The reaction mixture was then treated with triethylamine (900 µL) and diphenylphoryl azide (900 µL, 4.19 mmol). The reaction was heated to 90 °C for 5 h, followed by addition of a suspension of **7.18** (900 mg, 4.03 mmol) in anhydrous toluene (50 mL). The reaction was heated at 90 °C for an additional 3 h before being allowed to cool. Solution was treated with 10% $NaOH_{(aq)}$ (50 mL), followed by evaporating the solvent *in vacuo*. The residue was triturated in methanol (20 mL), followed by hot filtering the precipitate to give product as a white solid (213 mg, 15%). ^{1}H NMR (400 MHz; $CDCl_3$) δ 11.63 (br s, 1H), 11.28 (br s, 1H), 8.46 (d, *J* = 5.1 Hz, 2H),

7.66 (d, *J* = 5.1 Hz, 2H), 7.60 (d, *J* = 7.2 Hz, 1H), 7.54 (d, *J* = 7.4, 1H), 3.91 (t, *J* = 7.2 Hz, 2H), 1.80 (quin, *J* = 6.4 Hz, 2H), 1.34 (m, 4H), 1.28 (m, 6H), 0.87 (t, *J* = 6.5 Hz, 3H); ^{13}C NMR (100 MHz; $CDCl_3$) δ 164.9, 157.5, 151.9, 150.5, 147.7, 146.6, 113.7, 98.0, 51.4, 31.9, 29.3, 29.1, 26.7, 22.7, 14.2.

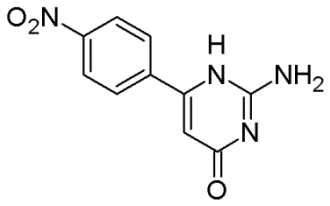

7.20

2-Amino-6-(4-nitrophenyl)pyrimidin-4(1*H*)-one (7.20):

p-Nitrobenzoylacetate (510 mg, 2.15 mmol) and guanidine carbonate (245 mg, 2.72 mmol) were combined in a 50 mL round bottom flask with stir bar and attached reflux condenser. To this was added absolute ethanol (20 mL), followed by purging with N_2. This was then heated to 78 °C for 18 h. Afterwards the reaction was cooled, followed by filtration followed by washing with water (100 mL) and acetone (50 mL). Drying gave product as a yellow solid (340 mg, 68%). ^{1}H NMR (400 MHz; DMSO-d_6) δ 10.99 (br s, 1H), 8.28 (d, *J* = 9.0 Hz, 2H), 8.20 (d, *J* = 9.0 Hz, 2H), 6.74 (br s, 2H), 6.28 (s, 1H).

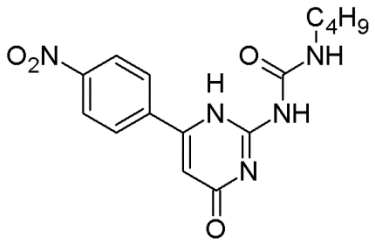

7.21a

1-Butyl-3-[6-(4-nitrophenyl)-4-oxo-1,4-dihydropyrimidin-2-yl]urea (7.21a):

Isocytosine **7.20** (228 mg, 0.98 mmol) was added to anhydrous DMF (3 mL) in a 10 mL round bottom flask with attached reflux condenser and stir bar, followed by purging with N_2. Butyl isocyanate (220 µL, 1.95 mmol) was added, and the reaction was heated to 80 °C for 24 h. The reaction was then cooled, diluted with Et_2O (25 mL), followed by filtering and drying to give product as a yellow solid (222 mg, 68%). ^{1}H NMR (400 MHz; DMSO-d_6) δ 11.95 (br s, 1H), 10.01 (br s, 1H), 8.32 (d, *J* = 8.9 Hz, 2H), 8.22 (d, *J* = 8.9 Hz, 2H), 7.15 (br s, 1H), 6.68 (s, 6.68), 3.17 (q, *J* = 6.1 Hz, 2H), 1.46 (quin, *J* = 7.0 Hz, 2H), 1.32 (sex, *J* = 7.7 Hz, 2H), 0.90 (t, *J* = 7.3 Hz, 3H).

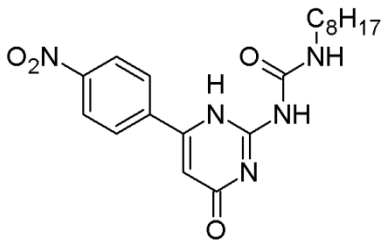

7.21b

1-Octyl-3-[6-(4-nitrophenyl)-4-oxo-1,4-dihydropyrimidin-2-yl]urea (7.21b):

Isocytosine **7.20** (325 mg, 1.40 mmol) was added to anhydrous DMF (3 mL) in a 10 mL round bottom flask with attached reflux condenser and stir bar, followed by purging with N_2. Octyl isocyanate (500 µL, 2.83 mmol) was added, and the reaction was heated to 80 °C for 24 h. The reaction was then cooled, diluted with Et_2O (25 mL), followed by filtering and drying. This was triturated in dichloromethane (25 mL), then filtered to give product as a yellow solid (342 mg, 63%). ^{1}H NMR (400 MHz; DMSO-d_6) δ 11.92 (br s, 1H), 9.99 (br s, 1H), 8.32 (d, *J* = 8.9 Hz, 2H), 8.22 (d, *J* = 8.9 Hz, 2H), 7.17 (br s, 1H), 6.67 (br s, 1H); 3.18 (q, *J* = 6.4 Hz, 2H), 1.46 (quin, *J* = 6.6 Hz, 2H), 1.27 (m, 4H), 1.24 (m, 6H), 0.85 (t, *J* = 6.7 Hz, 3H).

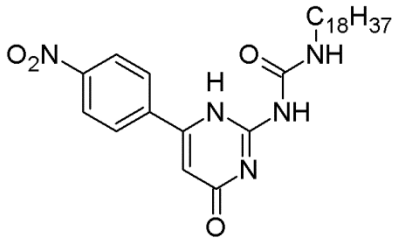

7.21c

1-Octadecyl-3-[6-(4-nitrophenyl)-4-oxo-1,4-dihydropyrimidin-2-yl]urea (7.21c):

Isocytosine **7.20** (213 mg, 0.92 mmol) was added to anhydrous DMF (3 mL) in a 10 mL round bottom flask with attached reflux condenser and stir bar, followed by purging with N_2. Octadecyl isocyanate (542 mg, 1.83 mmol) was added, and the reaction was heated to 80 °C for 24 h. The reaction was then cooled, diluted with dichloromethane (100 mL), followed by filtering and drying. This was triturated in dichloromethane (25 mL), then filtered to give product as a light yellow solid (264 mg, 54%). ^{1}H NMR (400 MHz; DMSO-d_6) δ 11.92 (br s, 1H), 9.99 (br s, 1H), 8.32 (d, J = 8.9 Hz, 2H), 8.22 (d, J = 8.9 Hz, 2H), 7.17 (br s, 1H), 6.67 (br s, 1H); 3.18 (q, J = 6.4 Hz, 2H), 1.46 (quin, J = 6.6 Hz, 2H), 1.27 (m, 4H), 1.24 (m, 6H), 0.85 (t, J = 6.7 Hz, 3H).

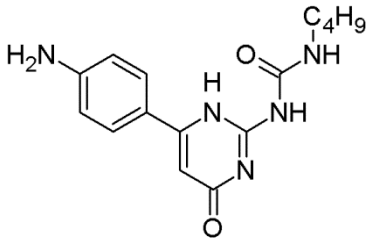

7.22a

1-Butyl-3-[6-(4-aminophenyl)-4-oxo-1,4-dihydropyrimidin-2-yl]urea (7.22a):

Nitro UPy **7.21a** (222 mg, 0.67 mmol) was added to MeOH (20 mL) with hydrazine monohydrate (2 mL, 41.2 mmol) and Raney© 2800 Ni suspension in water (1.0 mL) in a 100 mL round bottom flask with stir bar. This was stirred at room temperature for 2 h, followed by filtering through celite and evaporating *in vacuo* to give product as a tan solid (76 mg, 38%). ^{1}H NMR (400 MHz; DMSO-d_6) δ 11.47 (br s, 1H), 9.57 (br s, 1H), 7.67 (d, *J* = 8.4 Hz, 2H), 6.63 (d, *J* = 8.5 Hz, 2H), 6.24 (s, 1H), 3.18 (q, *J* = 6.2 Hz, 2H), 1.47 (quin, *J* = 7.1 Hz, 2H), 1.33 (sex, *J* = 7.4 Hz, 2H), 0.90 (t, *J* = 7.3 Hz, 3H).

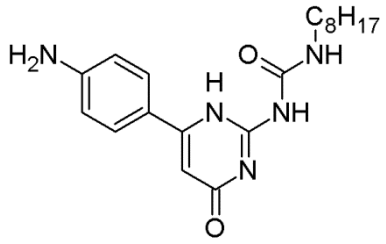

7.22b

1-Octyl-3-[6-(4-aminophenyl)-4-oxo-1,4-dihydropyrimidin-2-yl]urea (7.22b):

Nitro UPy **7.21b** (340 mg, 0.88 mmol) was added to BuOH (50 mL) with $SnCl_2$•$2H_2O$ in a 100 mL round bottom flask with stir bar. This was heated to 117 °C for 24 h. After cooling the reaction mixture was diluted with water, followed by filtering the precipitate and drying to give product as a light yellow solid (110 mg, 35%). ^{1}H NMR (400 MHz; DMSO-d_6) δ 11.38 (br s, 1H), 9.53 (br s, 1H), 7.63 (d, *J* = 8.4 Hz, 2H), 7.40 (br s, 1H), 6.55 (d, *J* = 8.5 Hz, 2H), 6.16 (s, 1H), 3.18 (q, *J* = 6.4 Hz, 2H), 1.46 (quin, *J* = 6.6 Hz, 2H), 1.27 (m, 4H), 1.24 (m, 6H), 0.85 (t, *J* = 6.7 Hz, 3H).

8.8 Selected NMR Spectra from Chapter 3

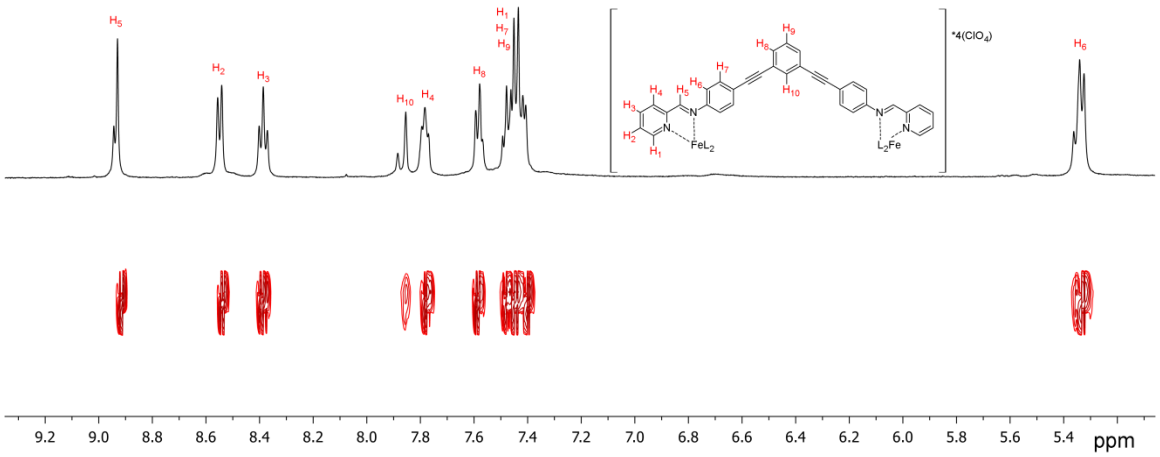

Figure 8.1: ^{1}H DOSY NMR spectrum of **[3.5a$_3$•Fe$_2$](ClO$_4$)$_4$** (CD_3CN, 600 MHz, 298 K, Δ = 17.0 ms, δ = 7000 μs, Diffusion Coefficient = 5.46x10^{-10} m^2/s vs. 3.85x10^{-9} m^2/s for the solvent).

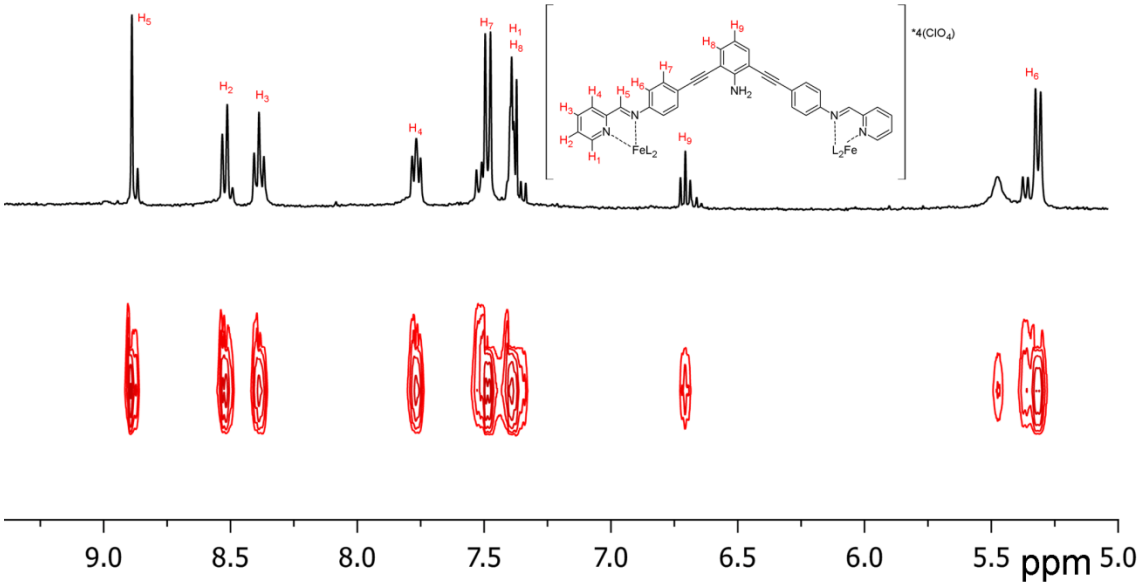

Figure 8.2: ^{1}H DOSY NMR spectrum of **[3.5b$_3$•Fe$_2$](ClO$_4$)$_4$** (CD_3CN, 600 MHz, 298 K, Δ = 17.0 ms, δ = 7000 μs, Diffusion Coefficient = 5.25x10^{-10} m^2/s vs. 3.47x10^{-9} m^2/s for the solvent).

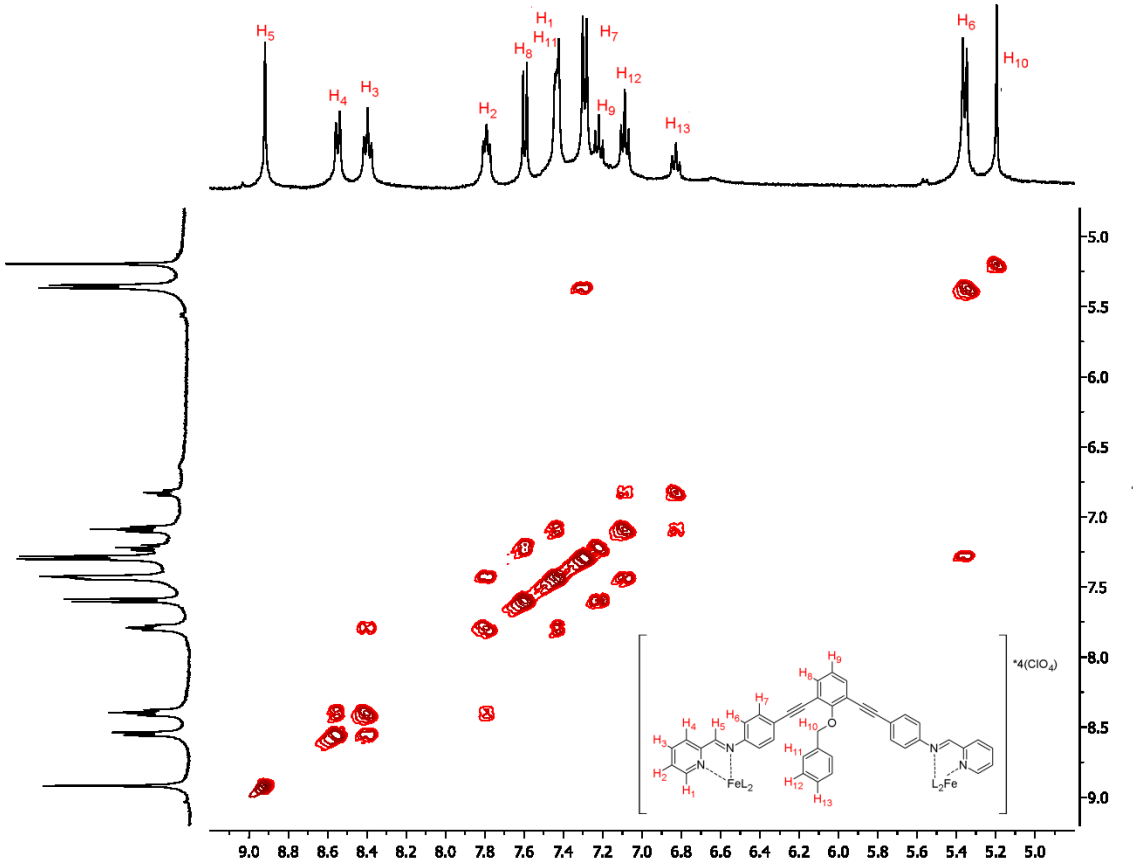

Figure 8.3: COSY spectrum of **[3.5d$_3$•Fe$_2$](ClO$_4$)$_4$** (CD_3CN, 500 MHz, 298 K).

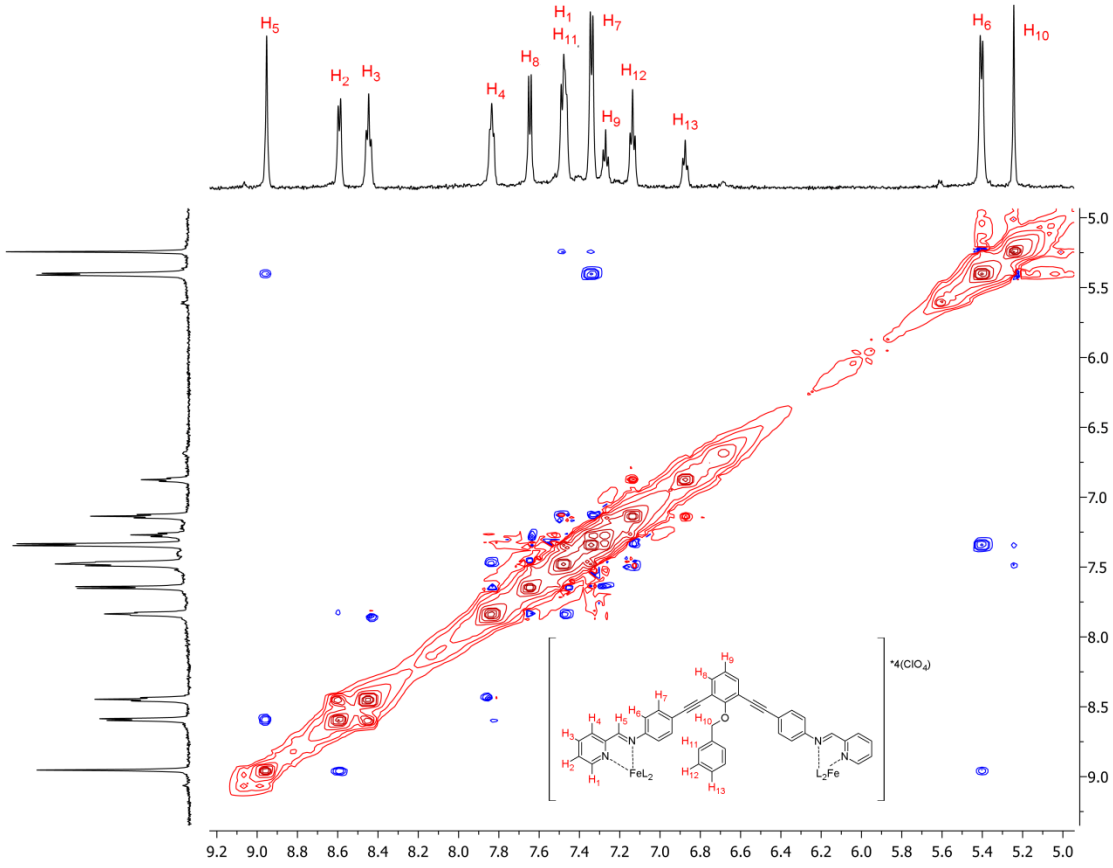

Figure 8.4: ROESY spectrum of **[3.5d$_3$•Fe$_2$](ClO$_4$)$_4$** (CD_3CN, 600 MHz, 298 K).

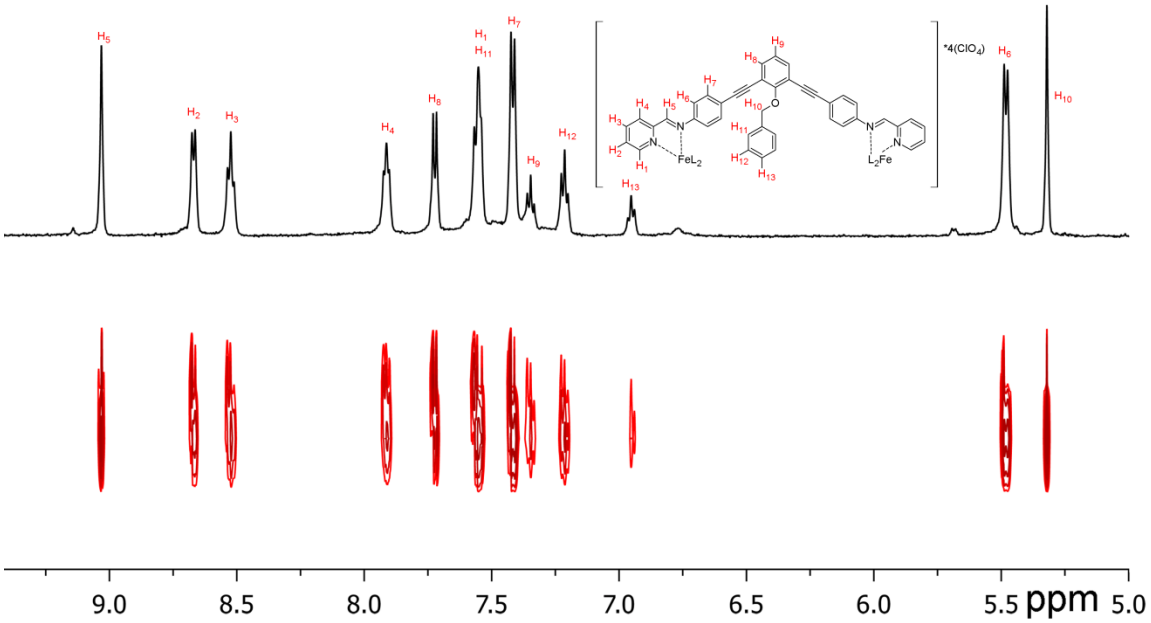

Figure 8.5: ^{1}H DOSY spectrum of **[3.5d$_3$•Fe$_2$](ClO$_4$)$_4$** (CD_3CN, 600 MHz, 298 K, Δ = 17.0 ms, δ = 7000 μs, Diffusion Coefficient = 5.51×10^{-10} m^2/s vs. 3.79×10^{-9} m^2/s for the solvent).

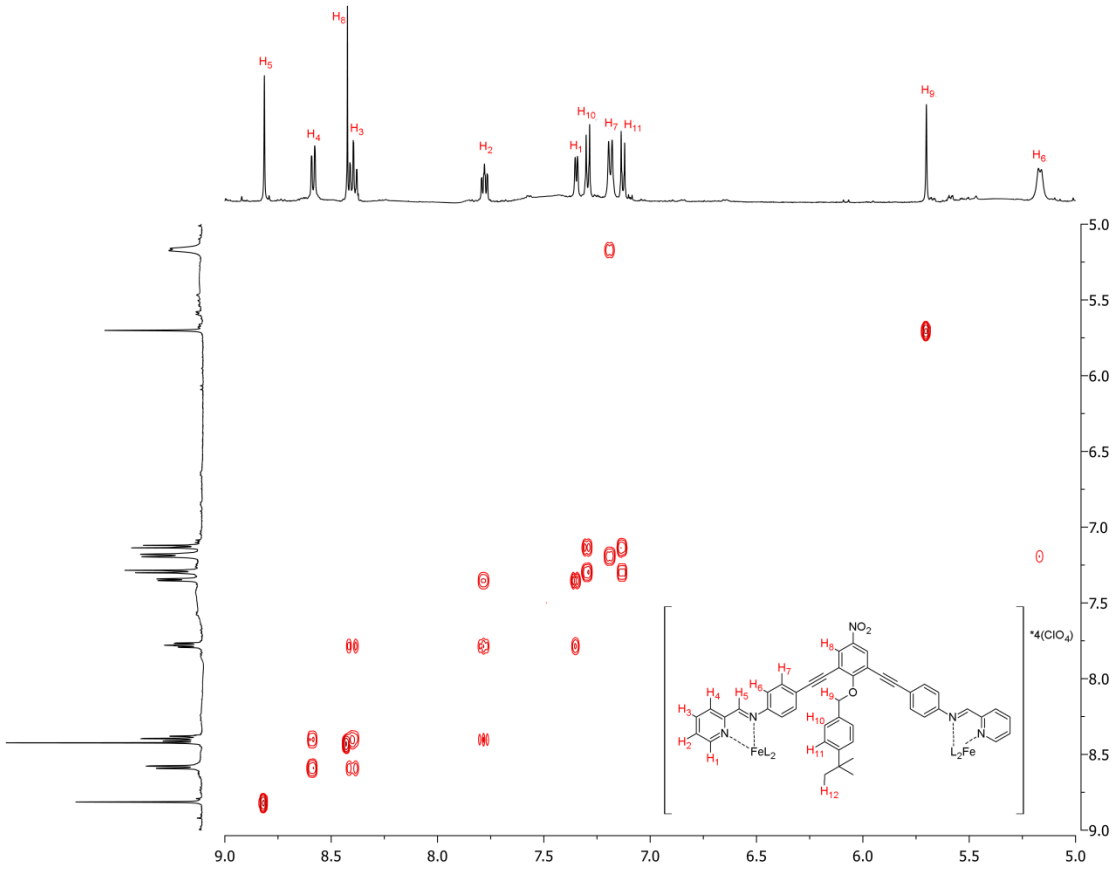

Figure 8.6: COSY spectrum of **[3.5e$_3$•Fe$_2$](ClO$_4$)$_4$** (CD_3CN, 500 MHz, 298 K).

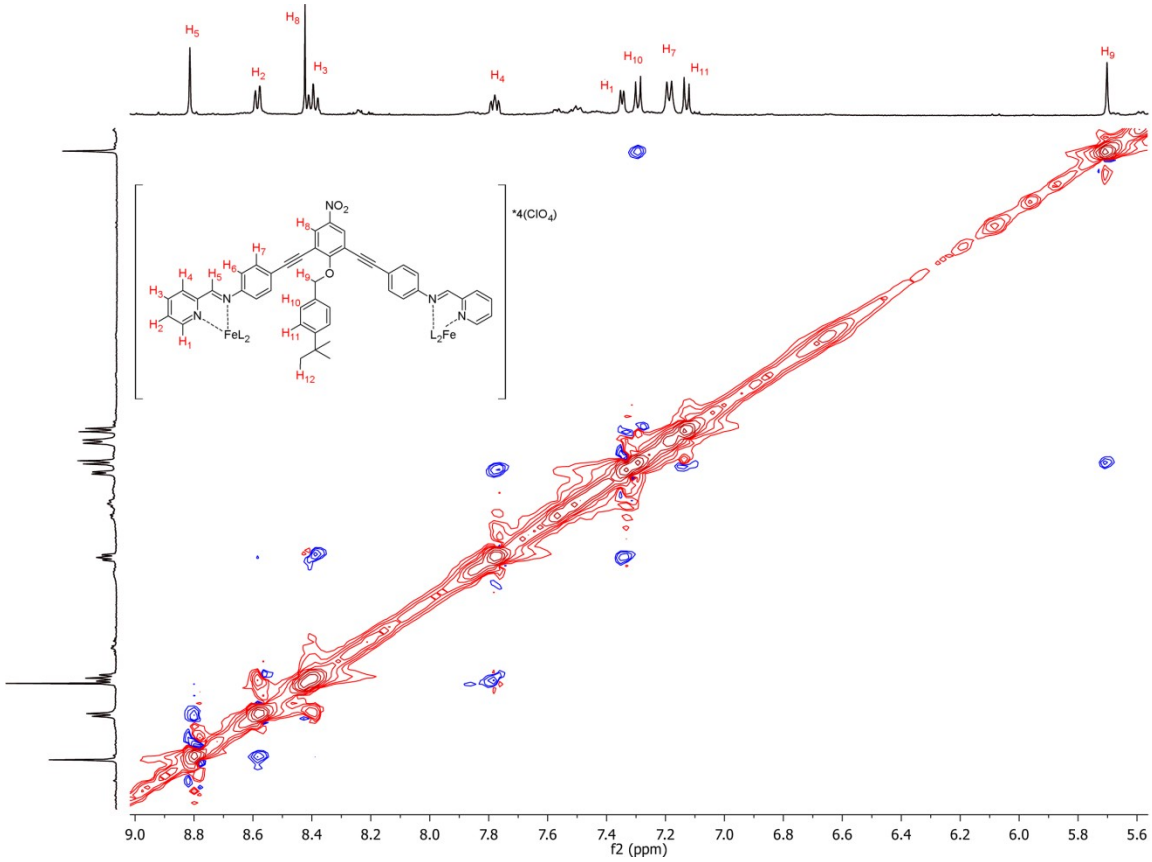

Figure 8.7: ROESY spectrum of **[3.5e$_3$•Fe$_2$](ClO$_4$)$_4$** (CD_3CN, 600 MHz, 298 K).

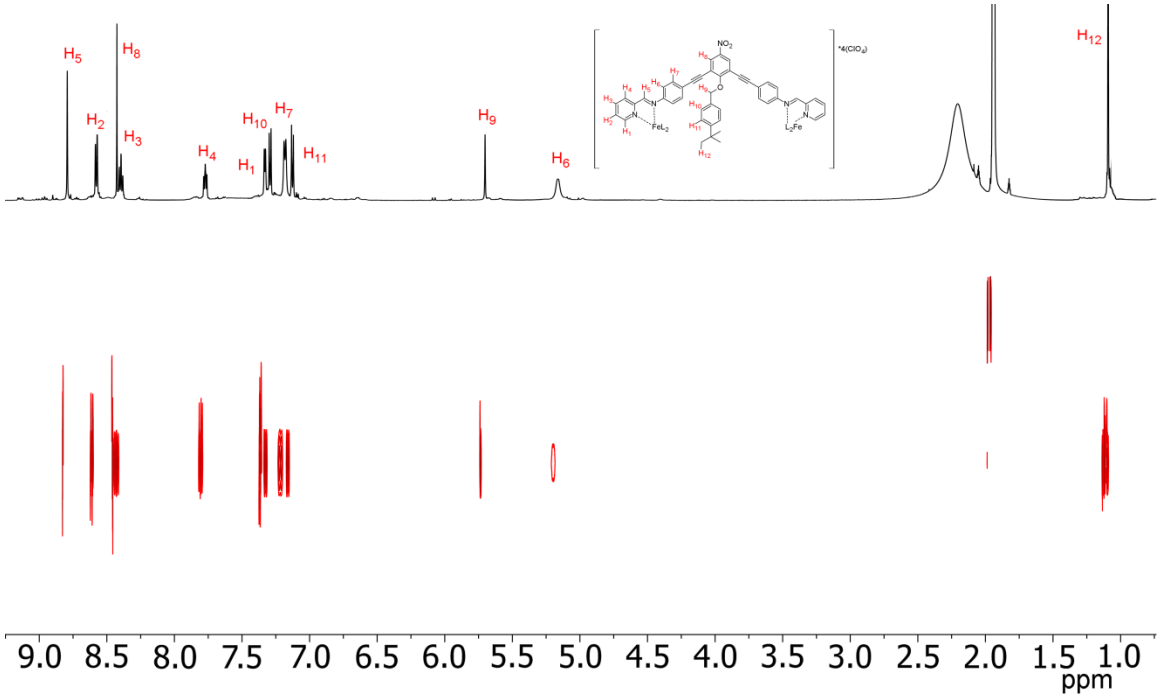

Figure 8.8: ^{1}H DOSY spectrum of **[3.5e$_3$•Fe$_2$](ClO$_4$)$_4$** (CD_3CN, 600 MHz, 298 K, Δ = 17.0 ms, δ = 7000 μs, Diffusion Coefficient = 4.20x10^{-10} m^2/s vs. 3.79x10^{-10} m^2/s for the solvent).

8.9 Selected NMR Spectra from Chapter 4

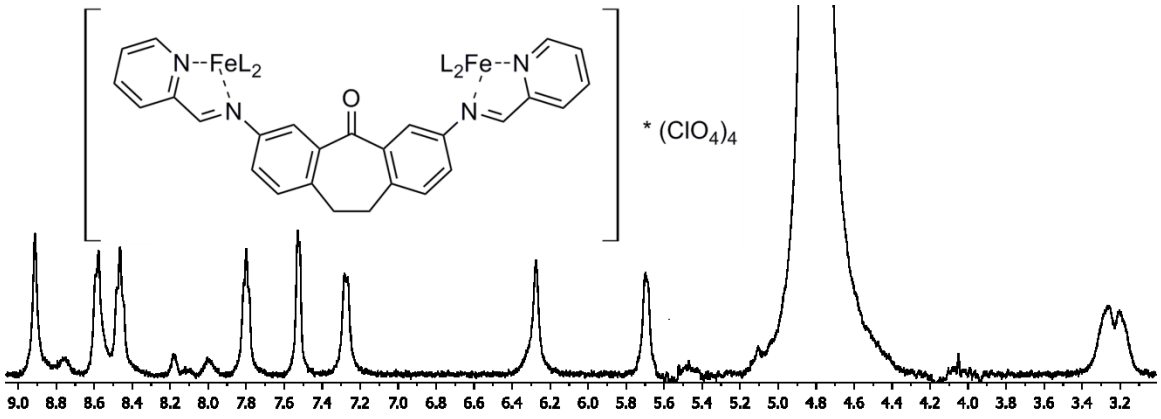

Figure 8.9: ^{1}H NMR spectrum of **[4.3a$_3$•Fe$_2$](ClO$_4$)$_4$** + 2 eq. LiCl (D_2O, 400 MHz, 298 K).

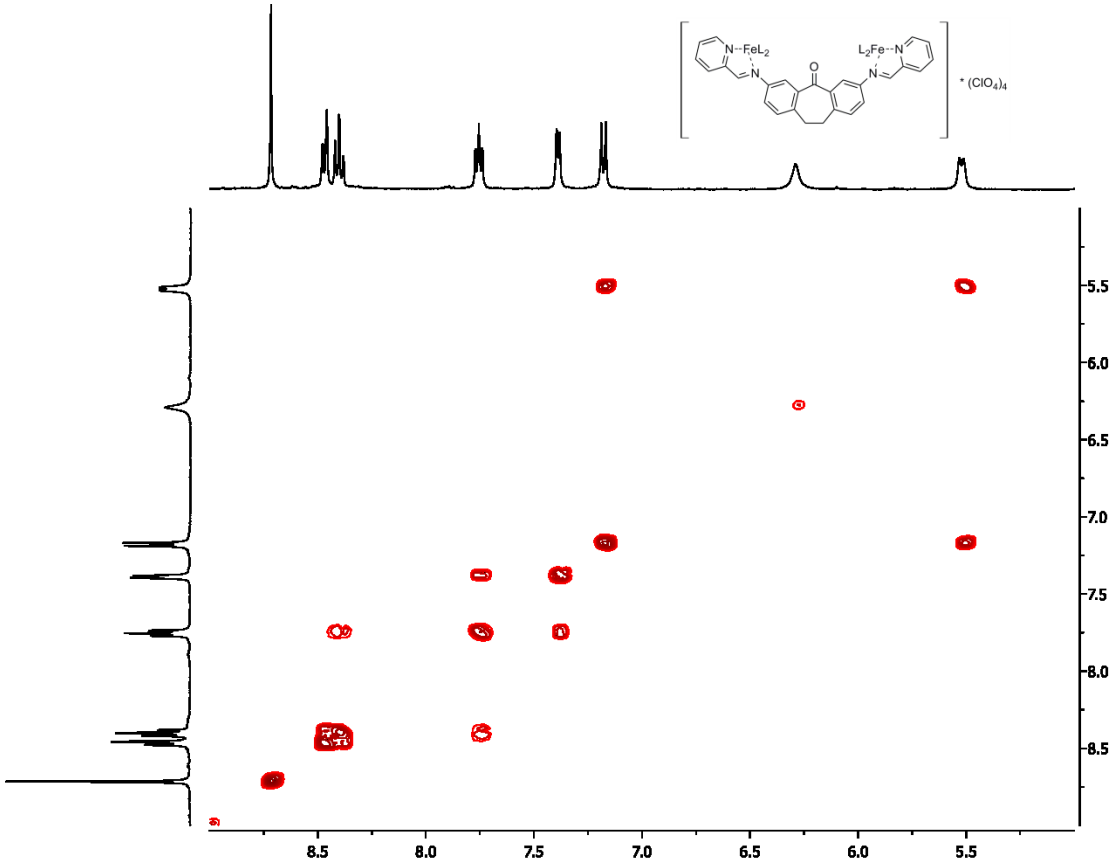

Figure 8.10: COSY spectrum of **[4.3a$_3$•Fe$_2$](ClO$_4$)$_4$** (CD_3CN, 600 MHz, 298 K).

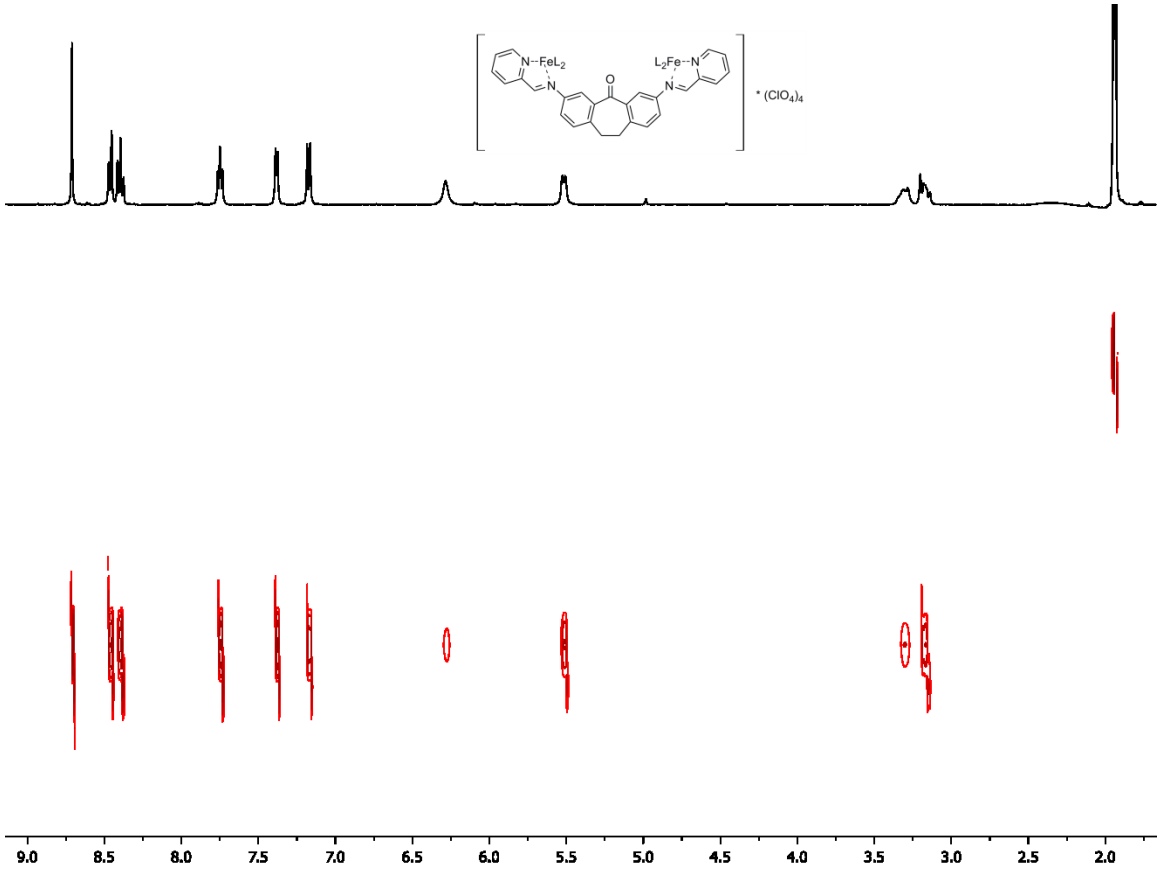

Figure 8.11: ^{1}H DOSY spectrum of **[4.3a$_3$•Fe$_2$](ClO$_4$)$_4$** (CD_3CN, 600 MHz, 298 K, Δ = 100 ms, δ = 2.6 μs, Diffusion Coefficient = 5.97 x 10^{-10} m^2/s vs. 3.95 x10^{-9} m^2/s for the solvent).

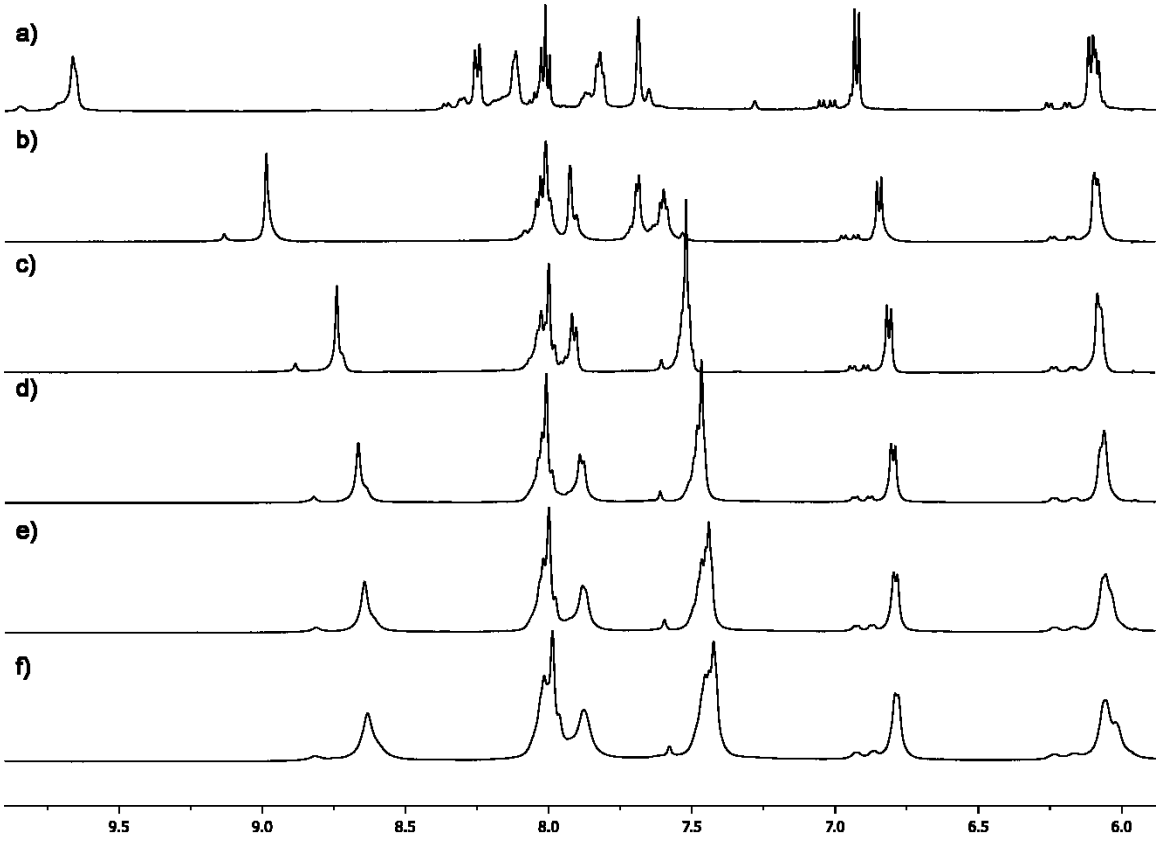

Figure 8.12: Variable temperature ^{1}H NMR spectra of **[4.3a$_3$•Fe$_2$](ClO$_4$)$_4$** (CD_3CN, 600 MHz): a) 75 °C; b) 50 °C; c) 25 °C; d) 0 °C; e) -20 °C; f) -40 °C.

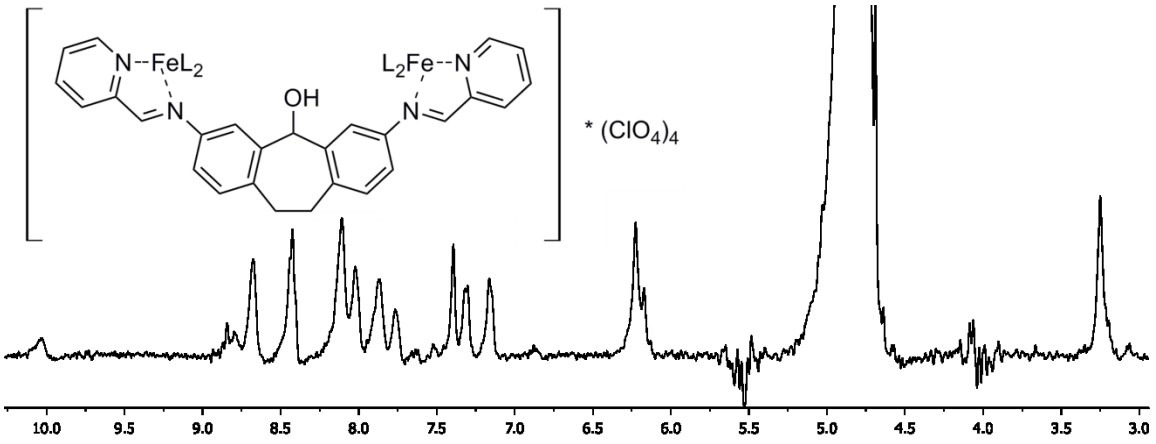

Figure 8.13: ^{1}H NMR spectrum of **[4.3b$_3$•Fe$_2$](ClO$_4$)$_4$** (D_2O, 400 MHz, 298 K).

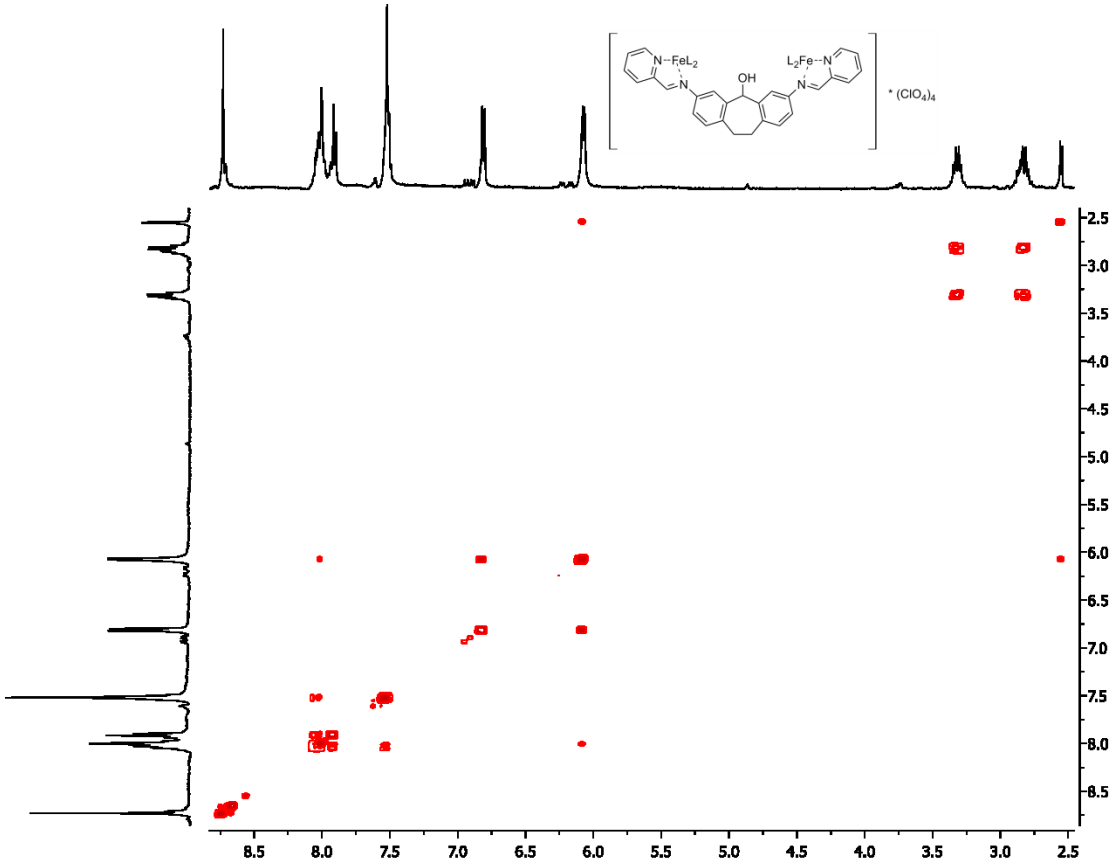

Figure 8.14: COSY spectrum of **[4.3b$_3$•Fe$_2$](ClO$_4$)$_4$** (CD_3CN, 600 MHz, 298 K).

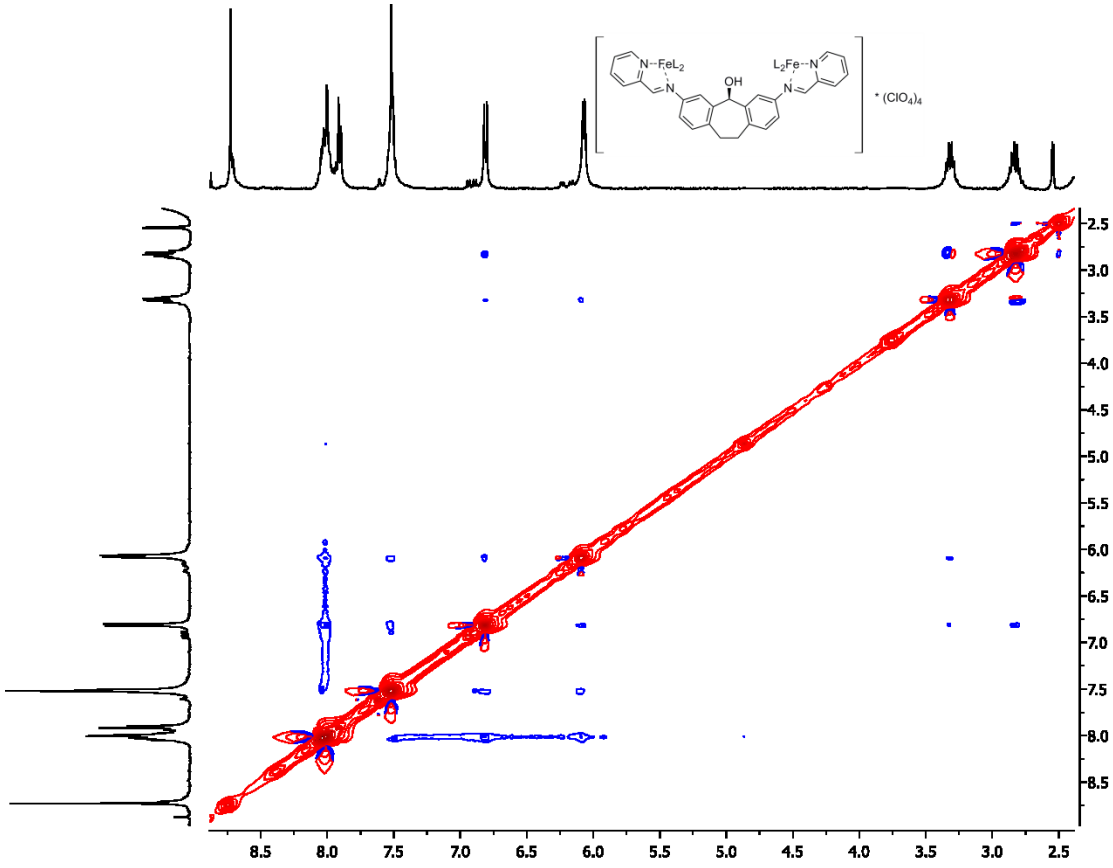

Figure 8.15: NOESY spectrum of **[4.3b$_3$•Fe$_2$](ClO$_4$)$_4$** (CD_3CN, 600 MHz, 298 K).

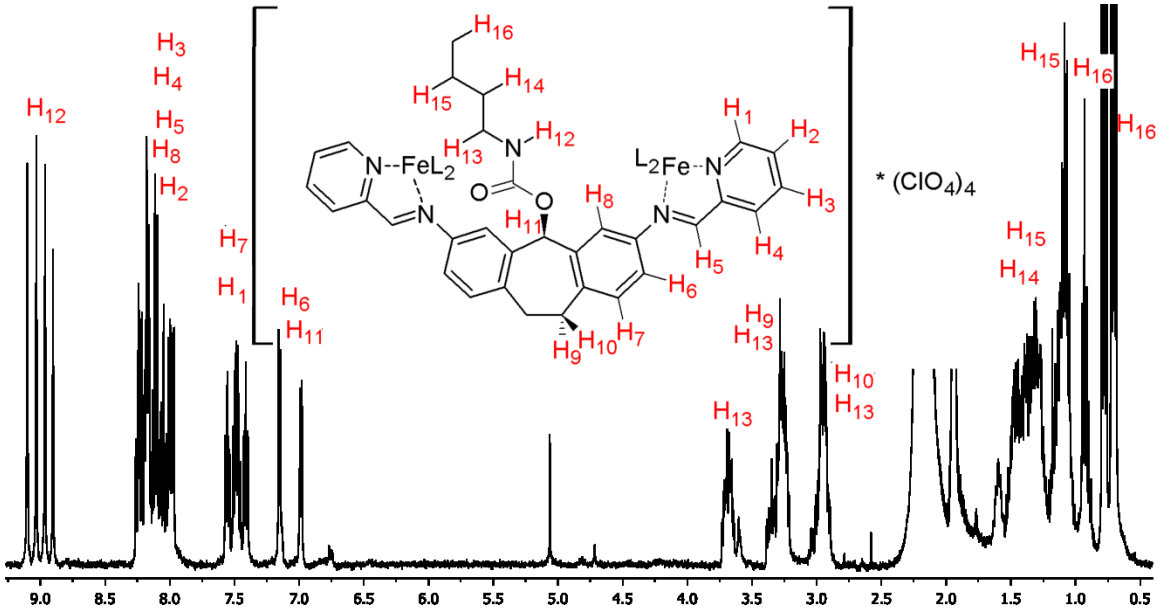

Figure 8.16: ^{1}H NMR spectrum of **[4.3c$_3$•Fe$_2$](ClO$_4$)$_4$** (CD_3CN, 400 MHz, 298 K).

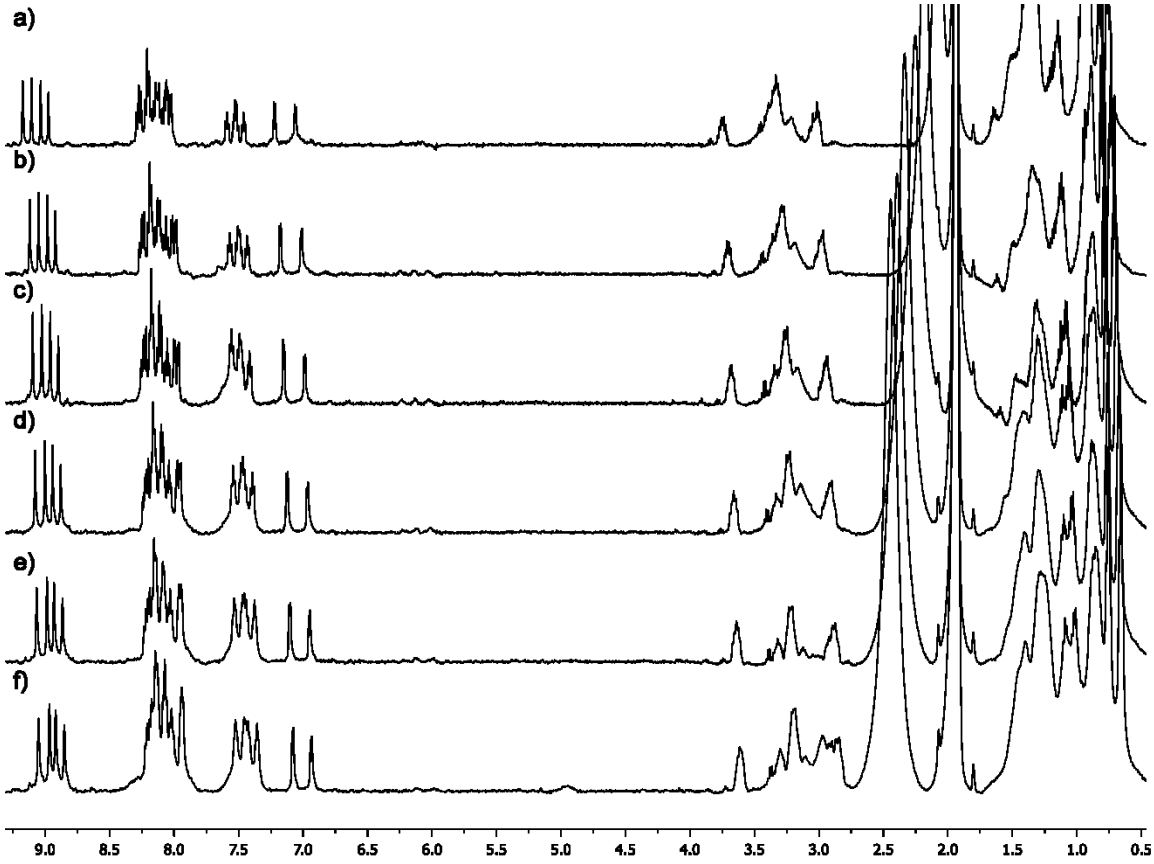

Figure 8.17: Variable temperature ^{1}H NMR spectra of **[4.3c$_3$•Fe$_2$](ClO$_4$)$_4$** (CD_3CN, 500 MHz): a) 75 °C; b) 50 °C; c) 25 °C; d) 0 °C; e) -20 °C; f) -40 °C.

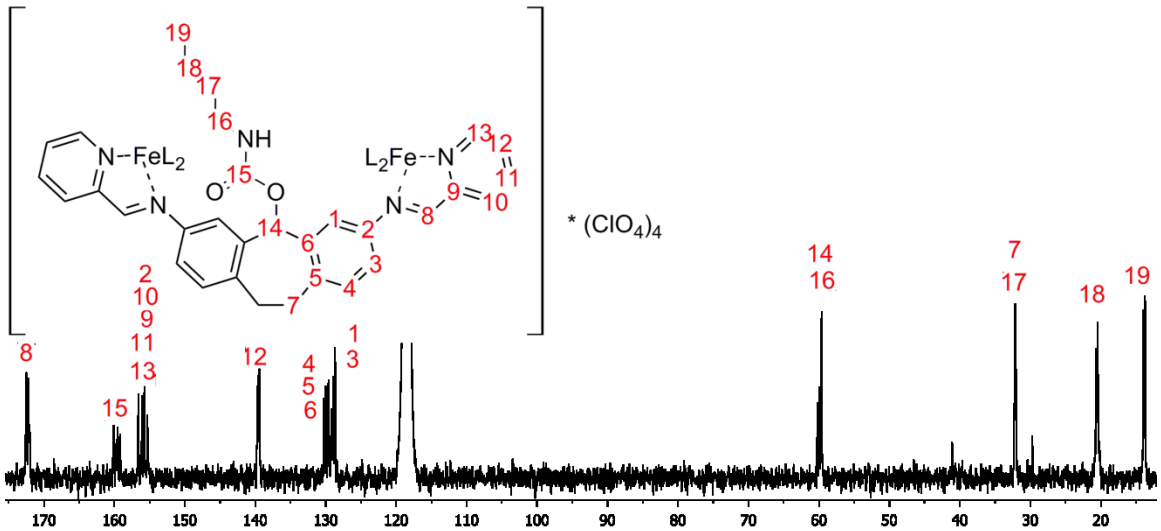

Figure 8.18: ^{13}C NMR spectrum of **[4.3c$_3$•Fe$_2$](ClO$_4$)$_4$** (CD_3CN, 125 MHz, 298 K).

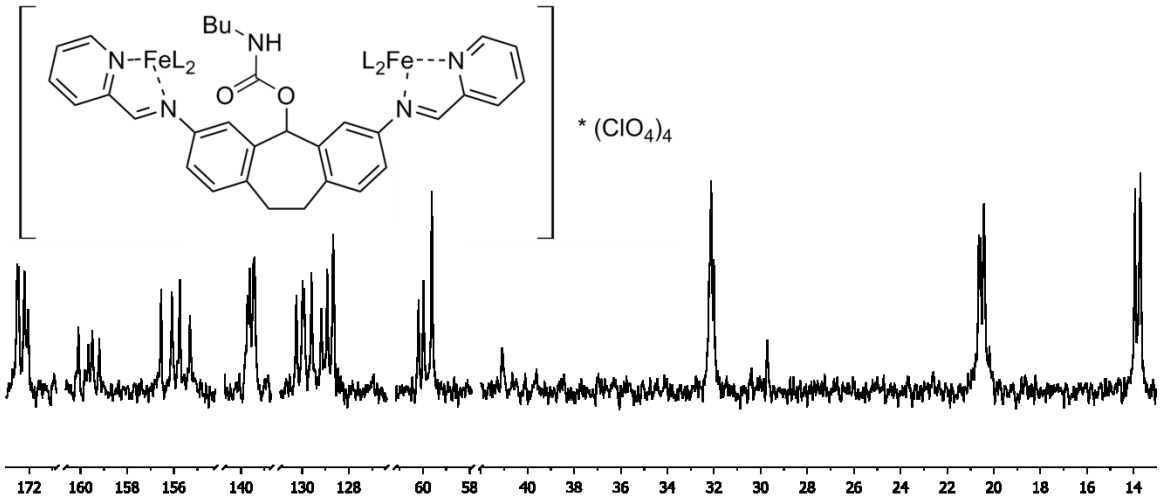

Figure 8.19: Close-up ^{13}C NMR spectrum of **[4.3c$_3$•Fe$_2$](ClO$_4$)$_4$** (CD_3CN, 125 MHz, 298 K).

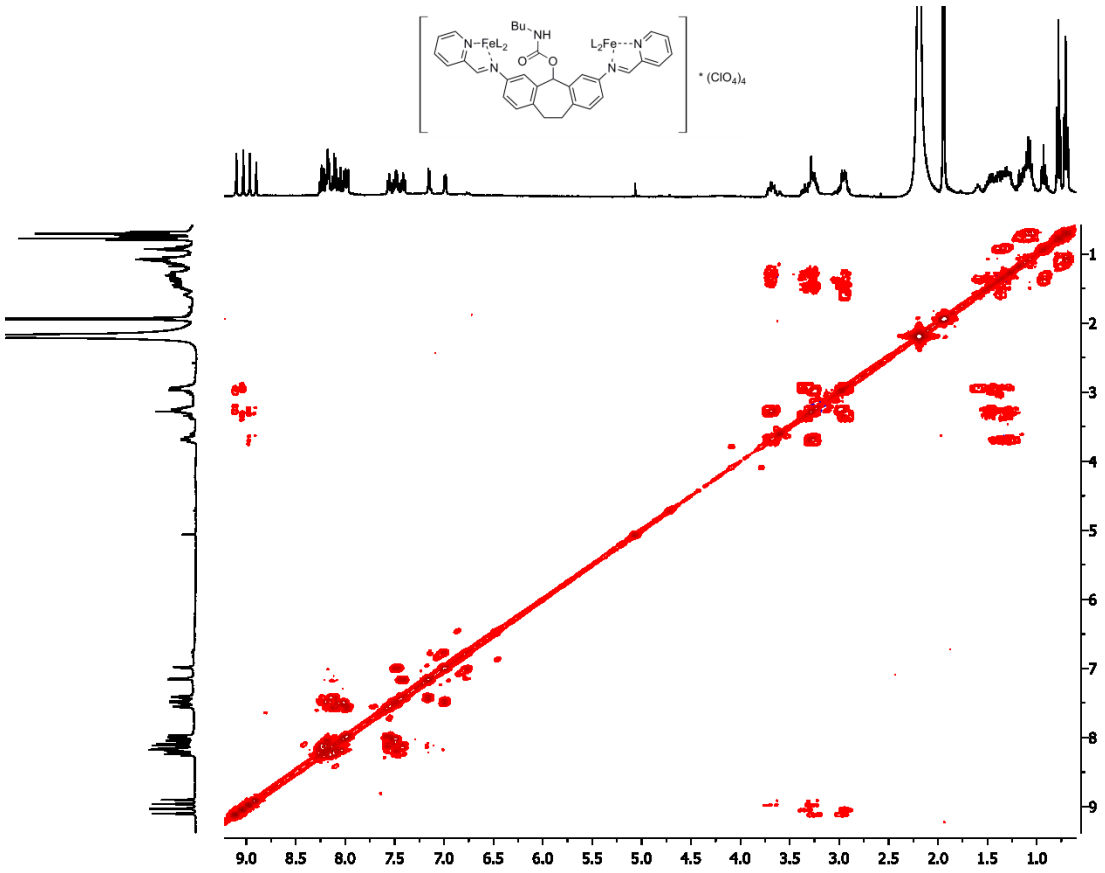

Figure 8.20: COSY spectrum of **[4.3c$_3$•Fe$_2$](ClO$_4$)$_4$** (CD_3CN, 600 MHz, 298 K).

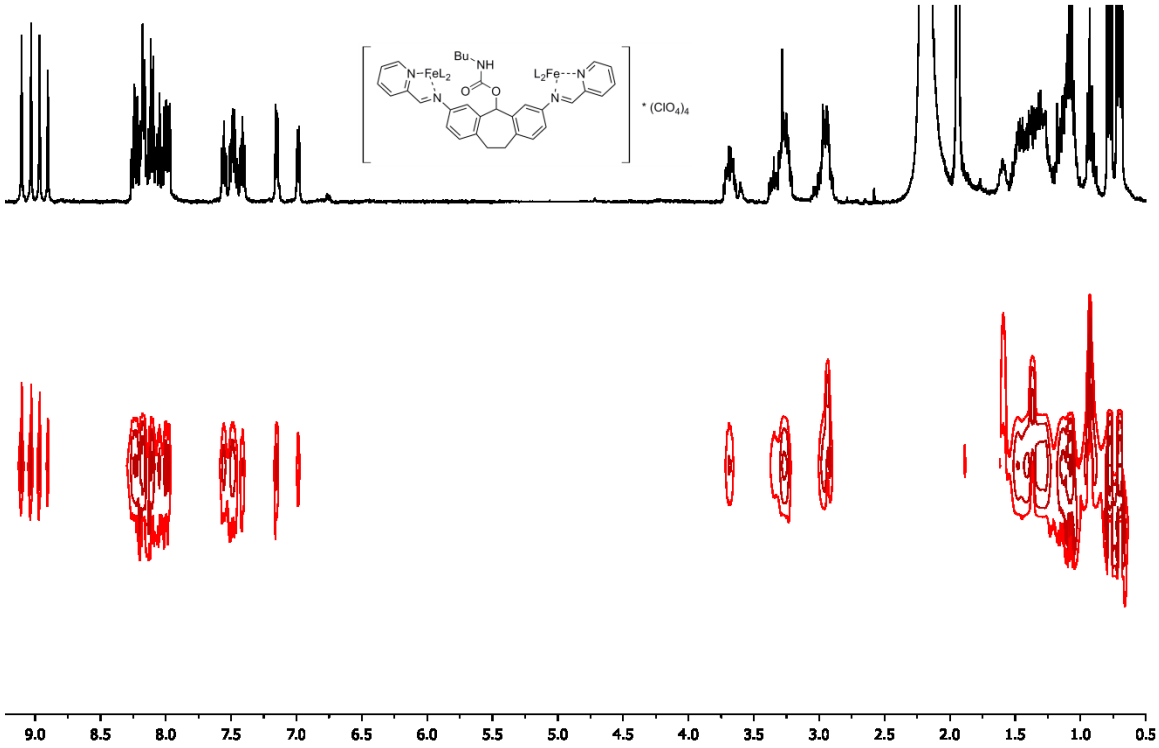

Figure 8.21: ^{1}H DOSY spectrum of **[4.3c$_3$•Fe$_2$](ClO$_4$)$_4$** (CD_3CN, 600 MHz, 298 K, Δ = 100 ms, δ = 2.6 μs, Diffusion Coefficient = 6.27 x 10^{-10} m^2/s vs. 3.95 x10^{-9} m^2/s for the solvent).

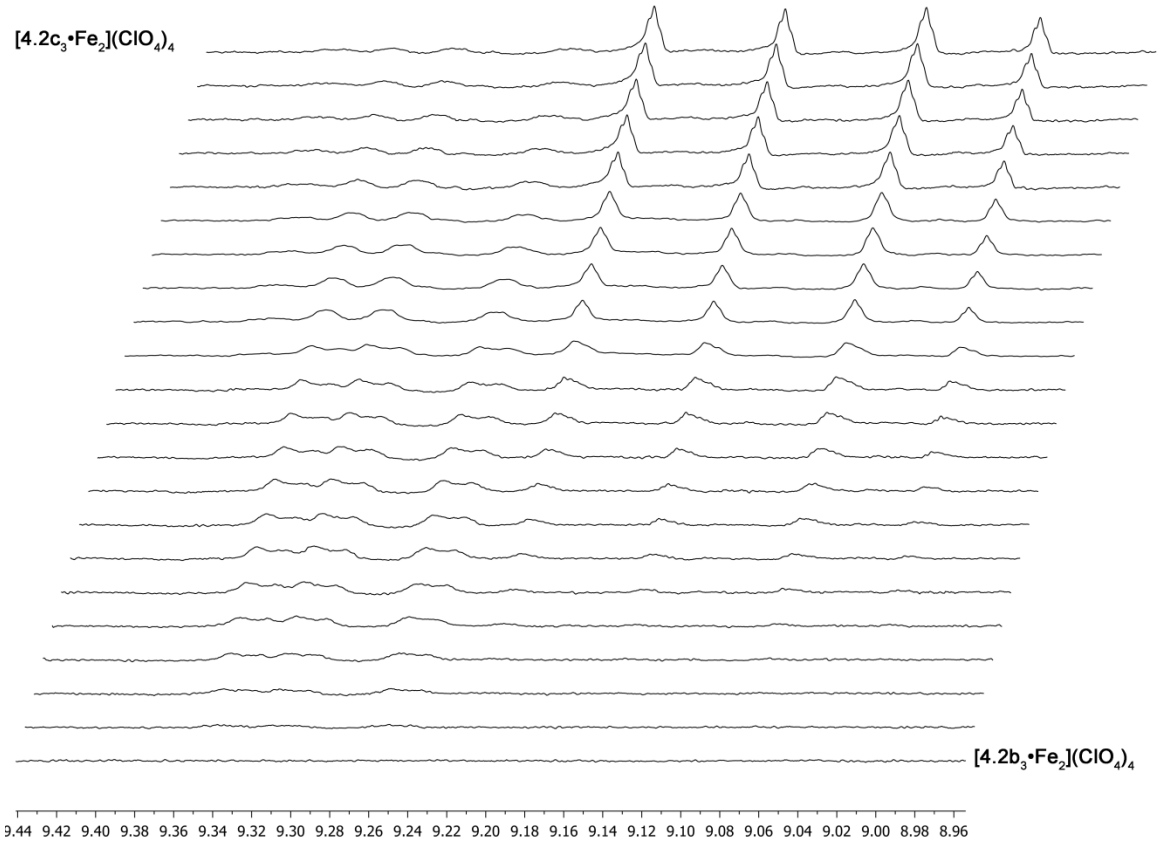

Figure 8.22: ^{1}H NMR spectra of the reaction of **[4.3b$_3$•Fe$_2$](ClO$_4$)$_4$** with butyl isocyanate to become **[4.3c$_3$•Fe$_2$](ClO$_4$)$_4$** in 15 minute intervals (0 – 6 h) (CD_3CN, 500 MHz, 253 K).

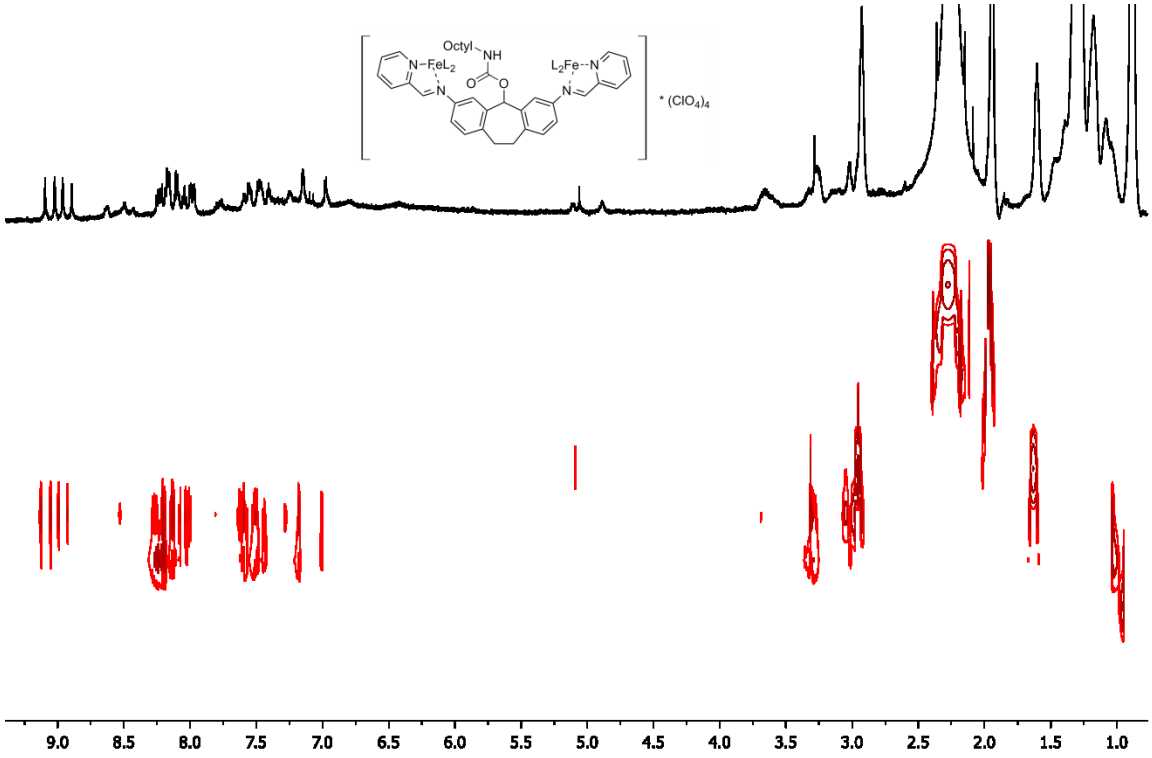

Figure 8.23: ^{1}H DOSY spectrum of **[4.3e$_3$•Fe$_2$](ClO$_4$)$_4$** (CD_3CN, 600 MHz, 298 K, Δ = 100 ms, δ = 2.6 μs, Diffusion Coefficient = 1.07 x10^{-9} m^2/s vs. 4.17 x10^{-9} m^2/s for the solvent).

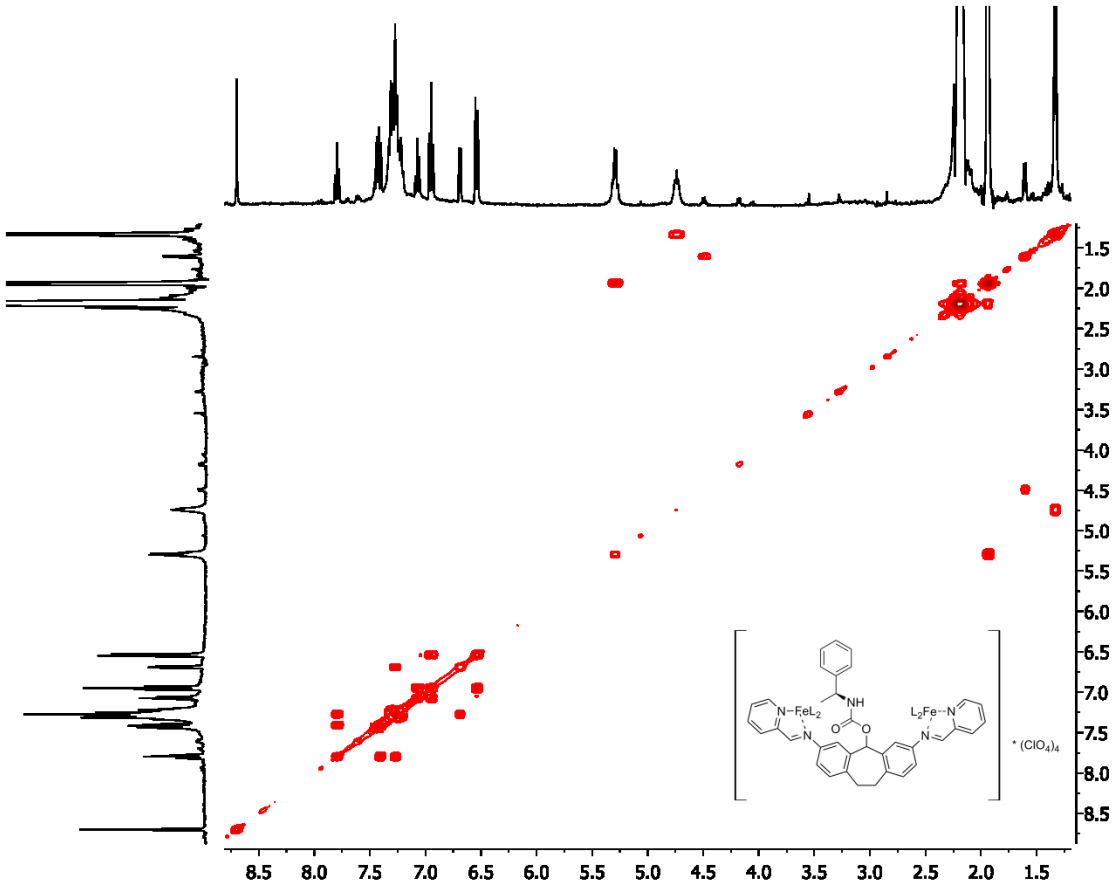

Figure 8.24: gCOSY spectrum of **[(*S*)-4.3f$_3$•Fe$_2$](ClO$_4$)$_4$** (CD_3CN, 600 MHz, 298 K).

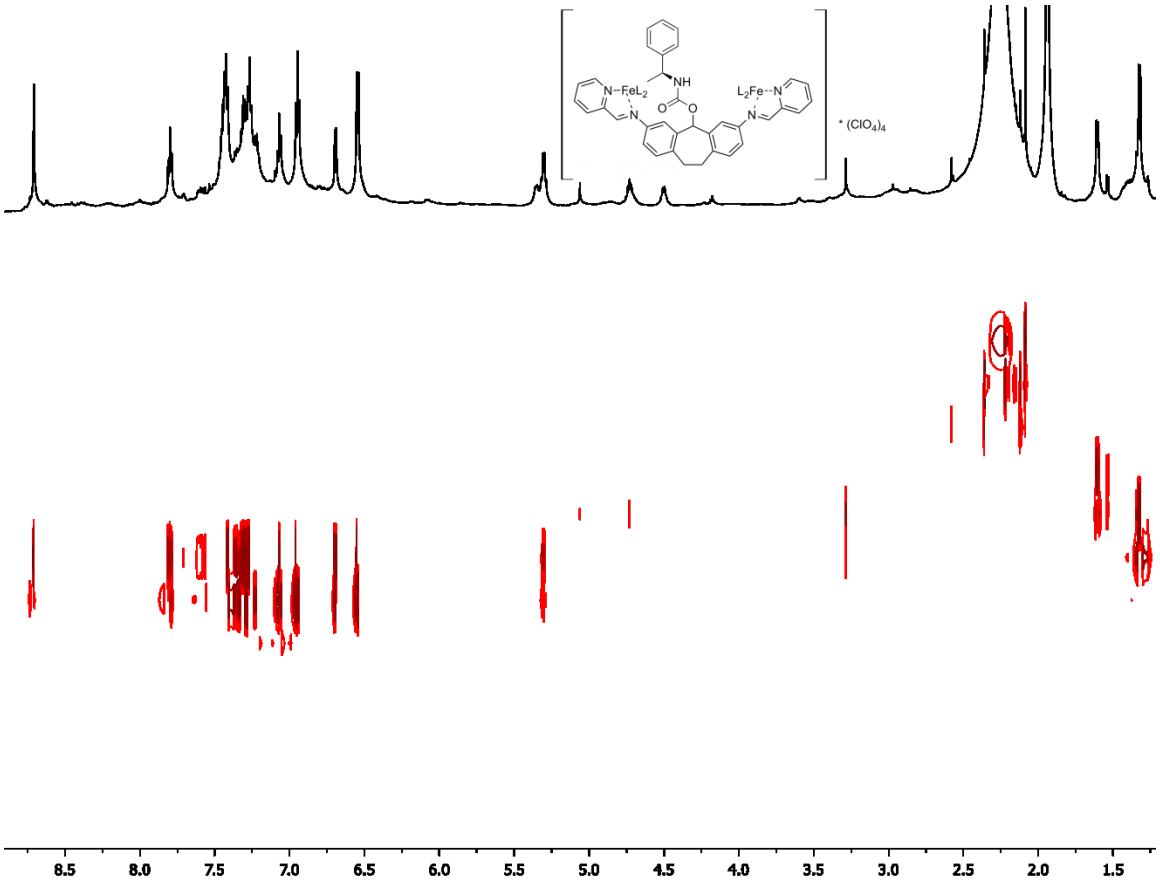

Figure 8.25: ^{1}H DOSY spectrum of **[(*S*)-4.3f$_3$•Fe$_2$](ClO$_4$)$_4$** (CD_3CN, 600 MHz, 298 K, Δ = 100 ms, δ = 2.6 μs, Diffusion Coefficient = 8.32 x10^{-10} m^2/s vs. 3.31 x10^{-9} m^2/s for the solvent).

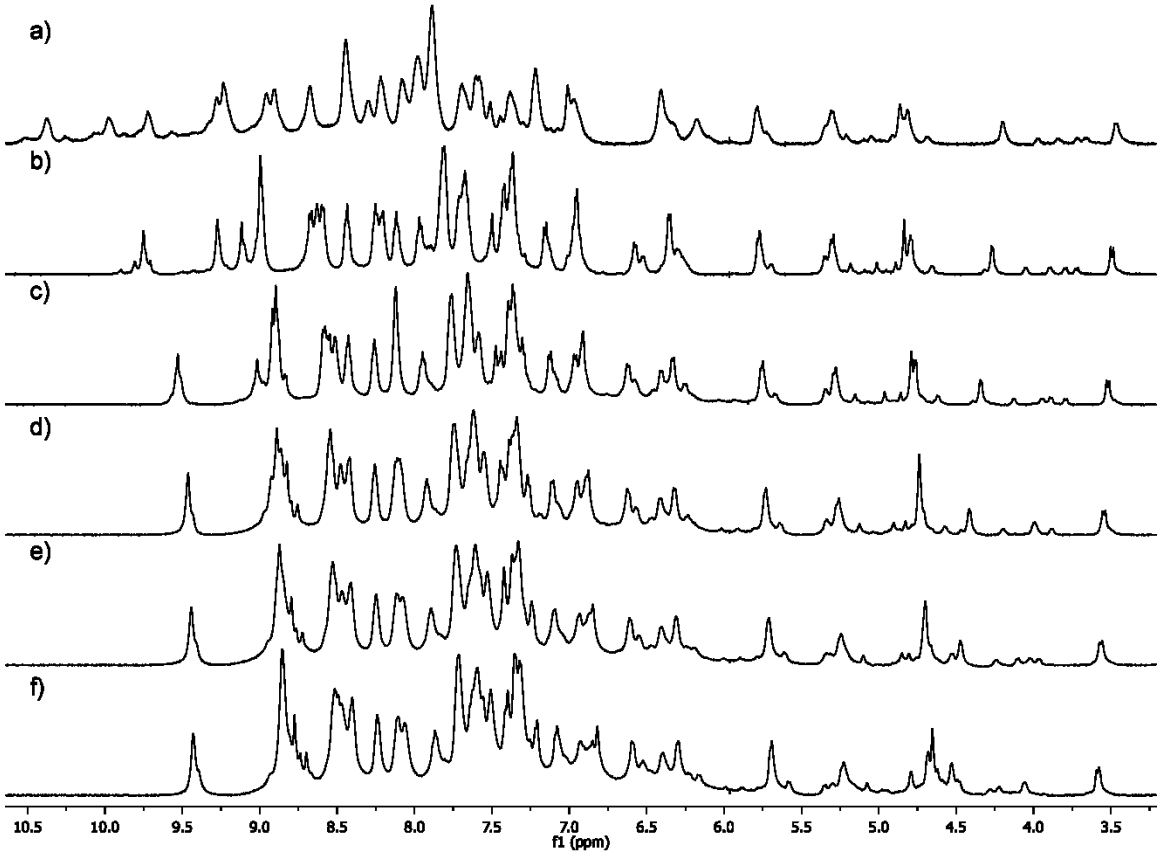

Figure 8.26: Variable temperature ^{1}H NMR spectra of **[4.7b$_6$•Fe$_4$](ClO$_4$)$_8$** (CD_3CN, 500 MHz): a) 75 °C; b) 50 °C; c) 25 °C; d) 0 °C; e) -20 °C; f) -40 °C.

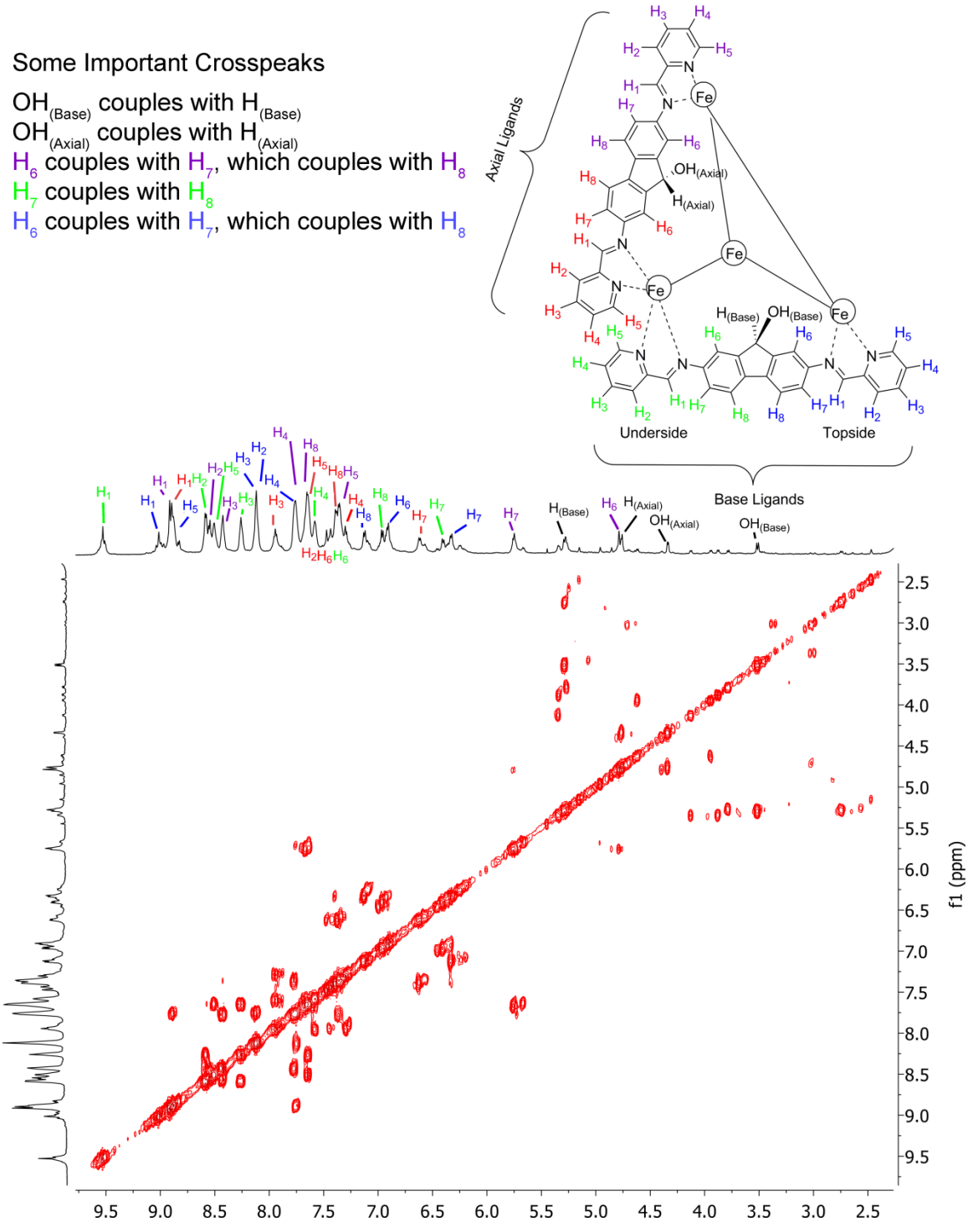

Figure 8.27: COSY spectrum of **[4.7b$_6$•Fe$_4$](ClO$_4$)$_8$** (CD_3CN, 600 MHz, 298 K).

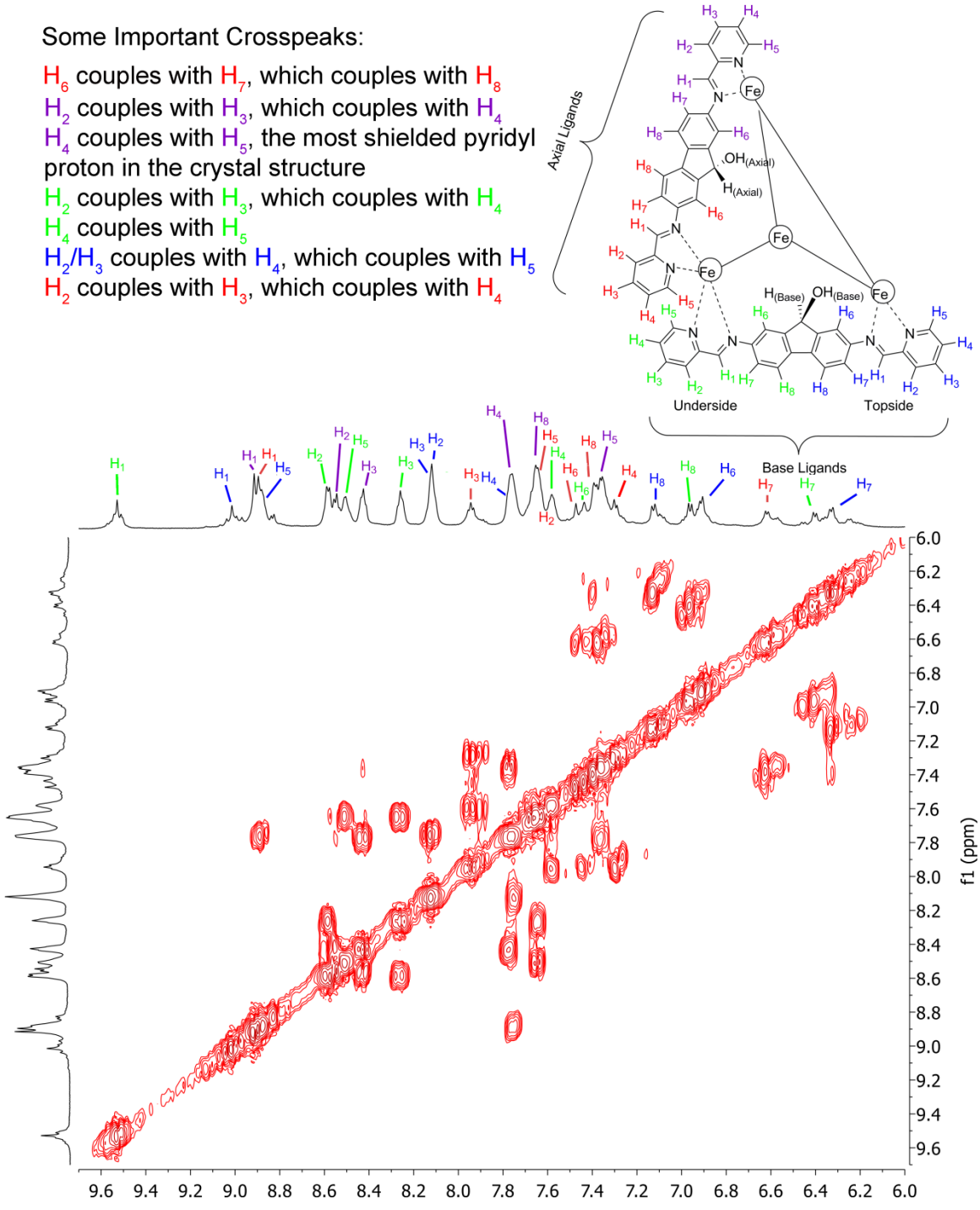

Figure 8.28: Close-up of downfield portion of COSY spectrum of **[4.7b$_6$•Fe$_4$](ClO$_4$)$_8$** (CD_3CN, 600 MHz, 298 K).

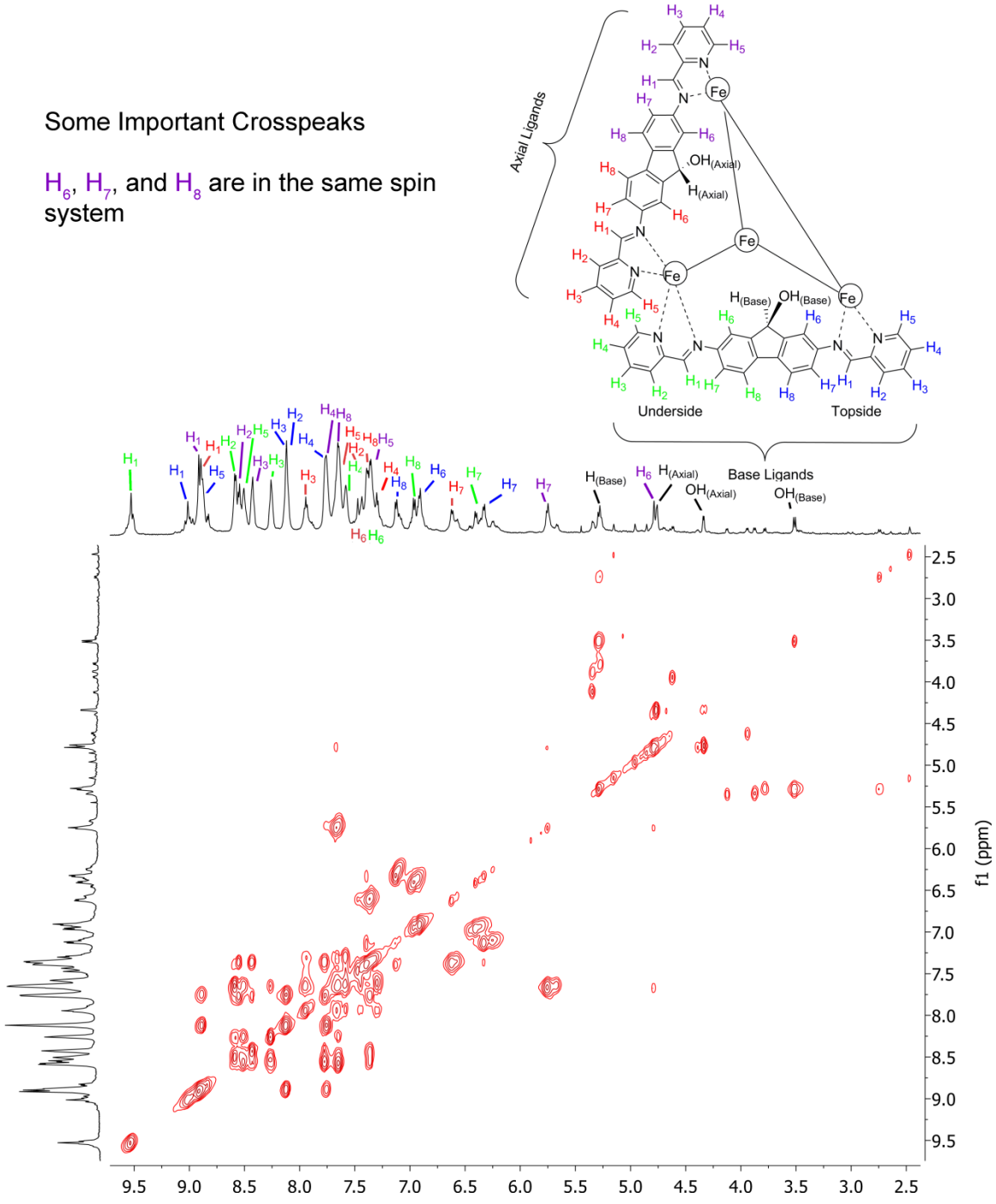

Figure 8.29: TOCSY spectrum of **[4.7b$_6$•Fe$_4$](ClO$_4$)$_8$** (CD_3CN, 600 MHz, 298 K).

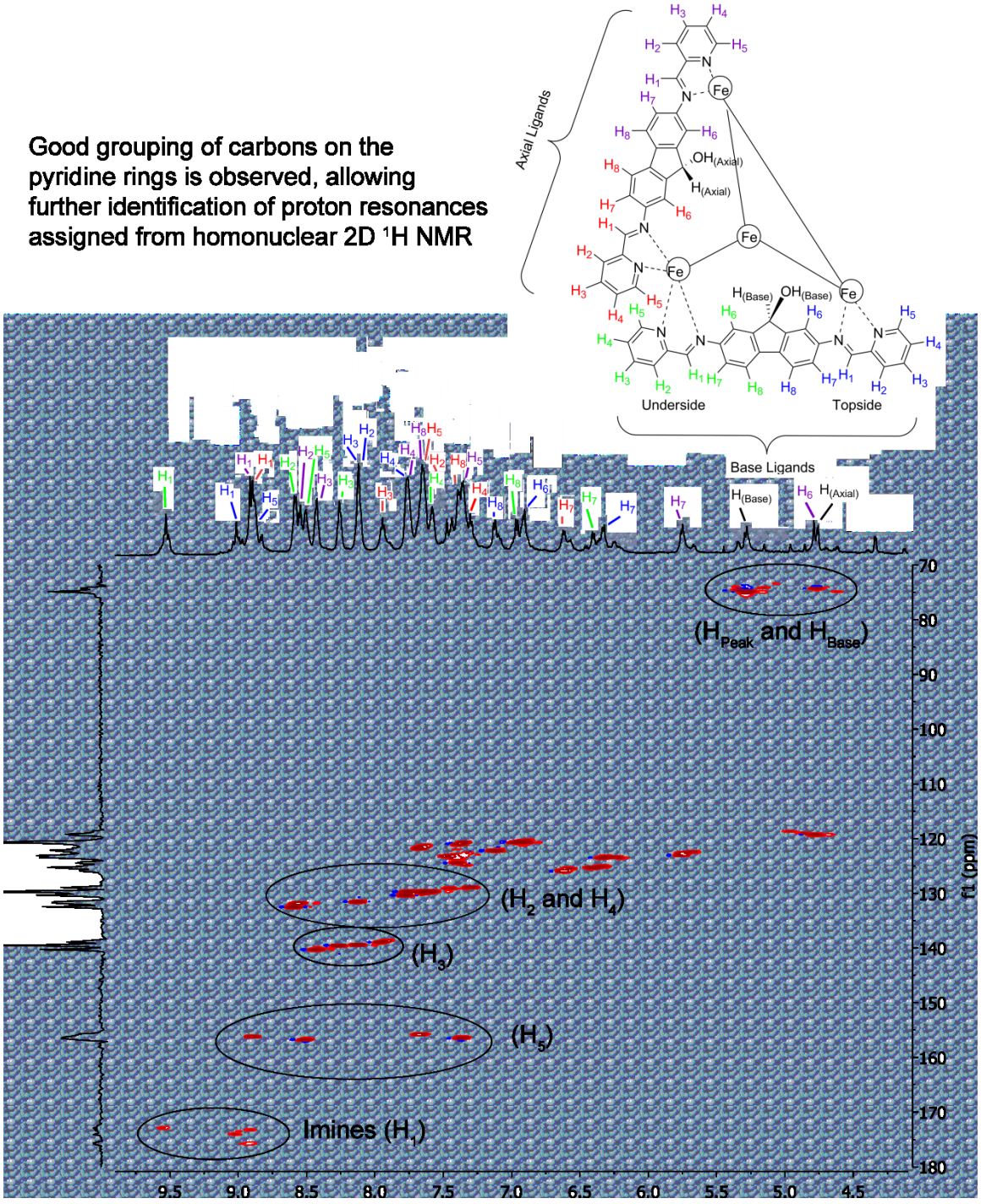

Figure 8.30: HSQC spectrum of **[4.7b$_6$•Fe$_4$](ClO$_4$)$_8$** (CD_3CN, 600 MHz, 298 K).

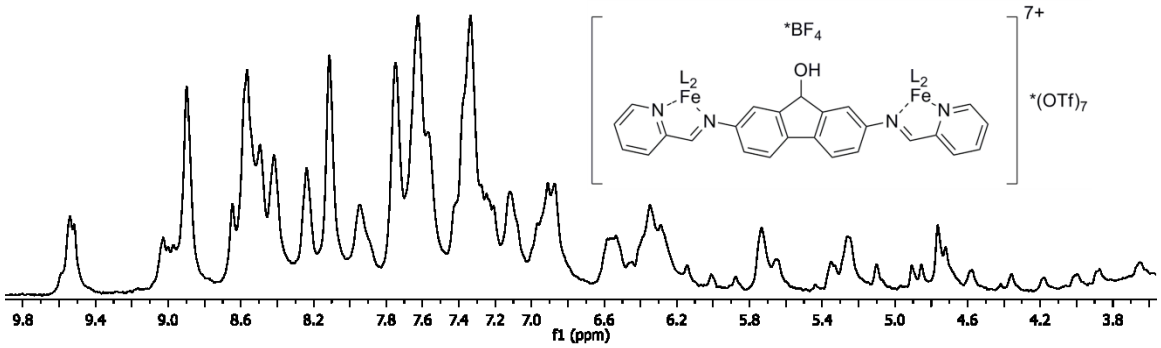

Figure 8.31: ^{1}H NMR spectrum of **[(BF_4)⊂4.7b_6•Fe_4]$(OTf)_7$** (CD_3CN, 400 MHz, 298 K).

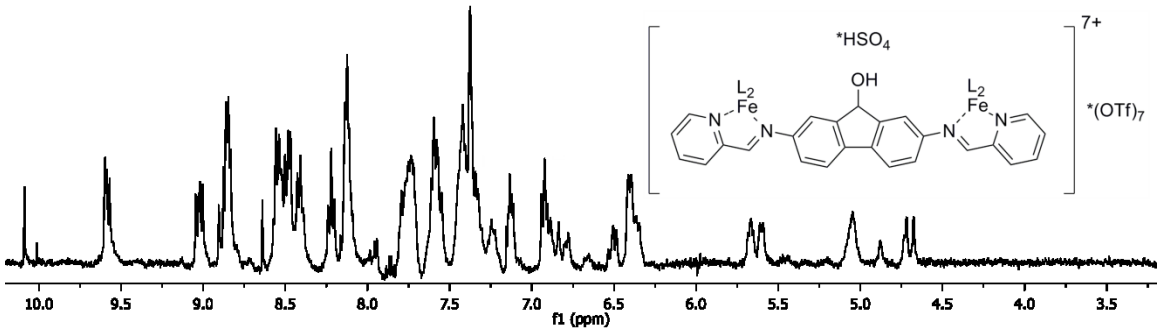

Figure 8.32: ^{1}H NMR spectrum of **[(HSO_4)⊂4.7b_6•Fe_4]$(OTf)_7$** (CD_3CN, 400 MHz, 298 K).

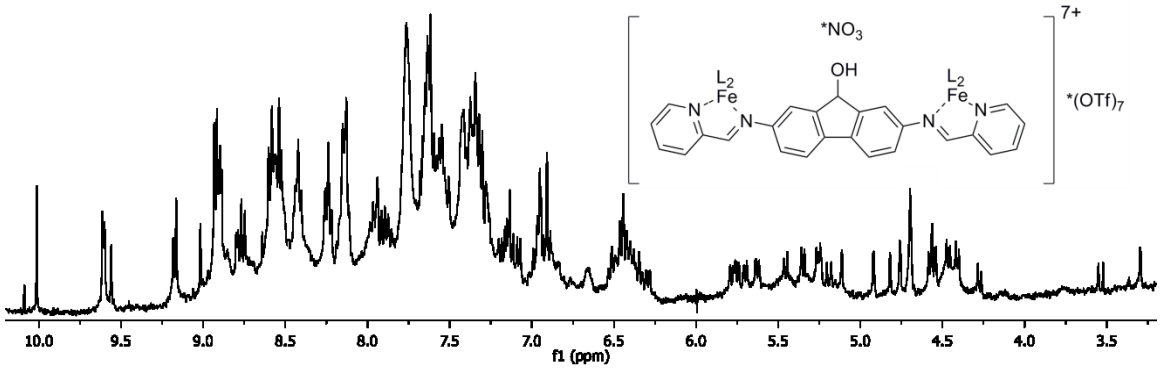

Figure 8.33: ^{1}H NMR spectrum of **[(NO_3)⊂4.7b_6•Fe_4]$(OTf)_7$** (CD_3CN, 400 MHz, 298 K).

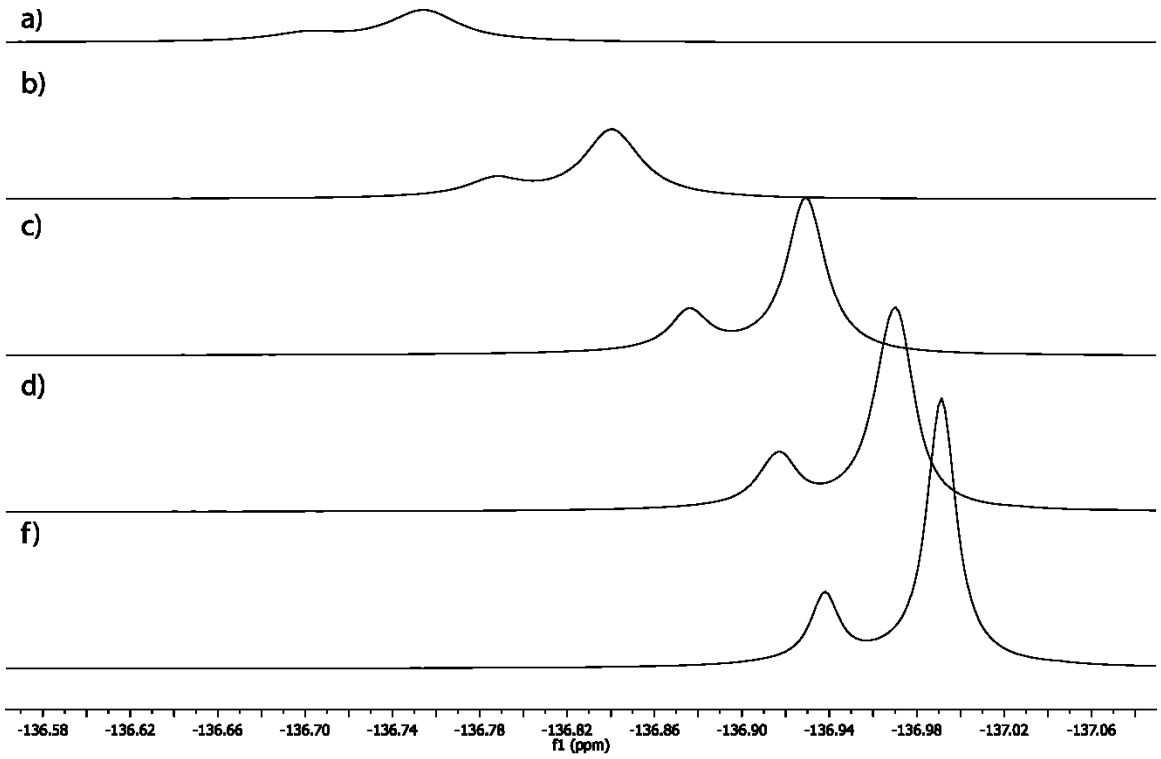

Figure 8.34: ^{1}H NMR spectra of Bu_4NBF_4 titrated into **[(BF$_4$)⊂4.7b$_6$•Fe$_4$](OTf)$_7$** (CD_3CN, 400 MHz, 298 K): a) 0 eq. Bu_4NBF_4; a) 4 eq. Bu_4NBF_4; a) 8 eq. Bu_4NBF_4; a) 16 eq. Bu_4NBF_4; a) 32 eq. Bu_4NBF_4.

8.10 Selected Mass Spectra

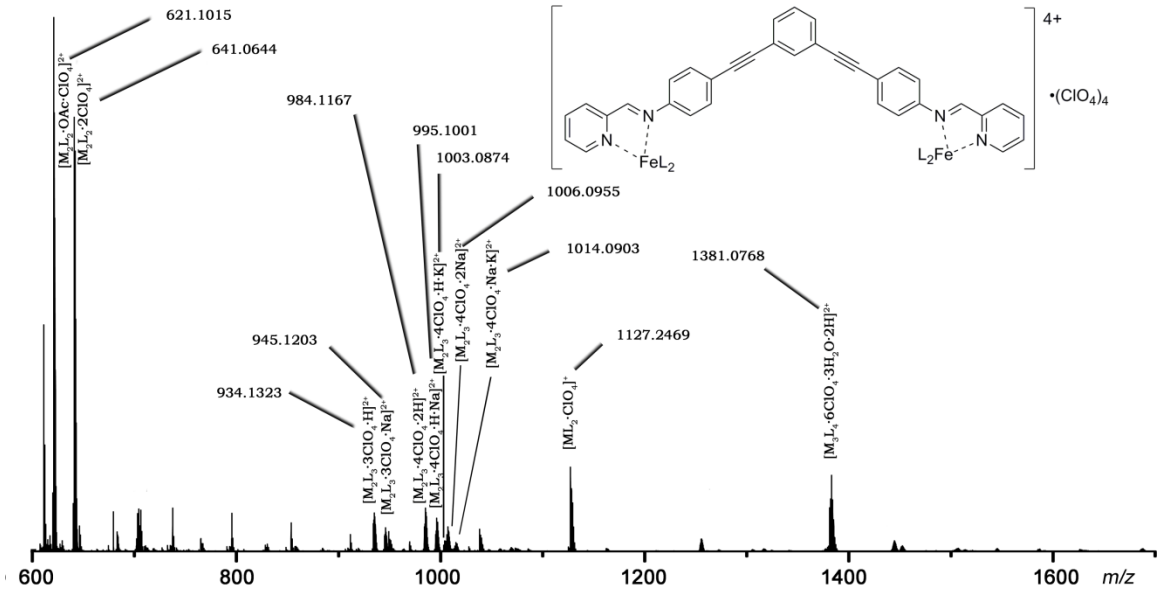

Figure 8.35: ESI-MS of **[3.5a$_3$•Fe$_2$](ClO$_4$)$_4$** (MeCN).

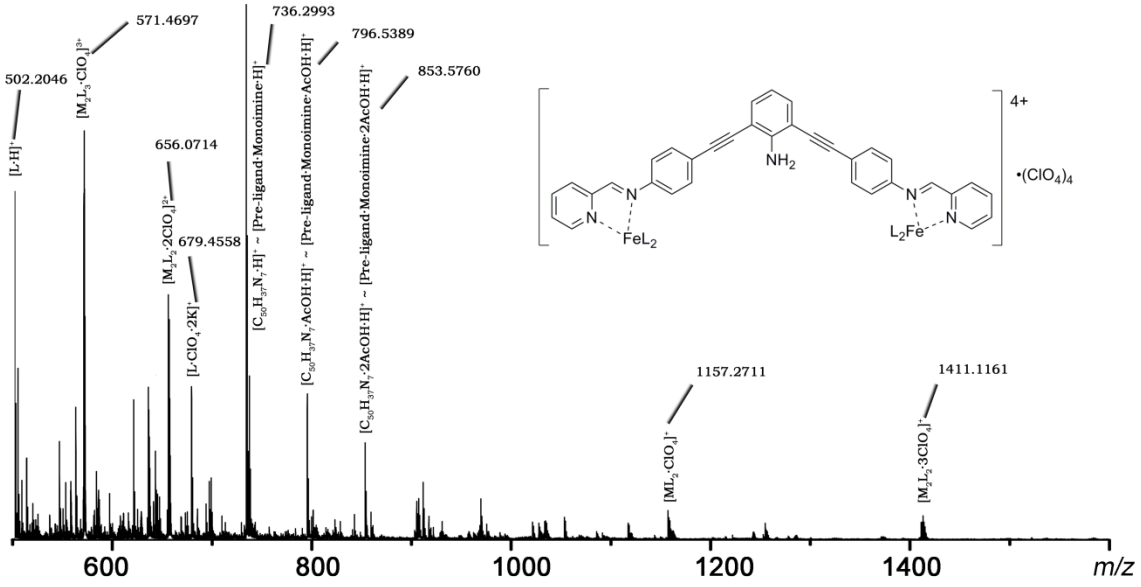

Figure 8.36: ESI-MS of **[3.5b$_3$•Fe$_2$](ClO$_4$)$_4$** (MeCN).

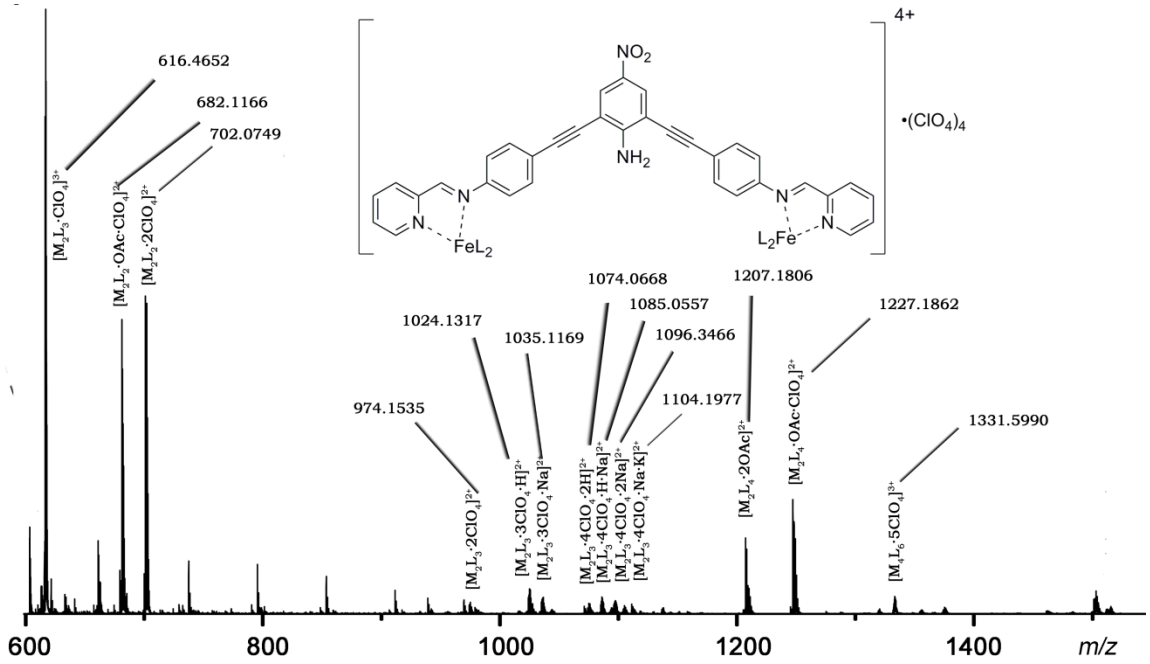

Figure 8.37: ESI-MS of **[3.5c$_3$•Fe$_2$](ClO$_4$)$_4$** (MeCN).

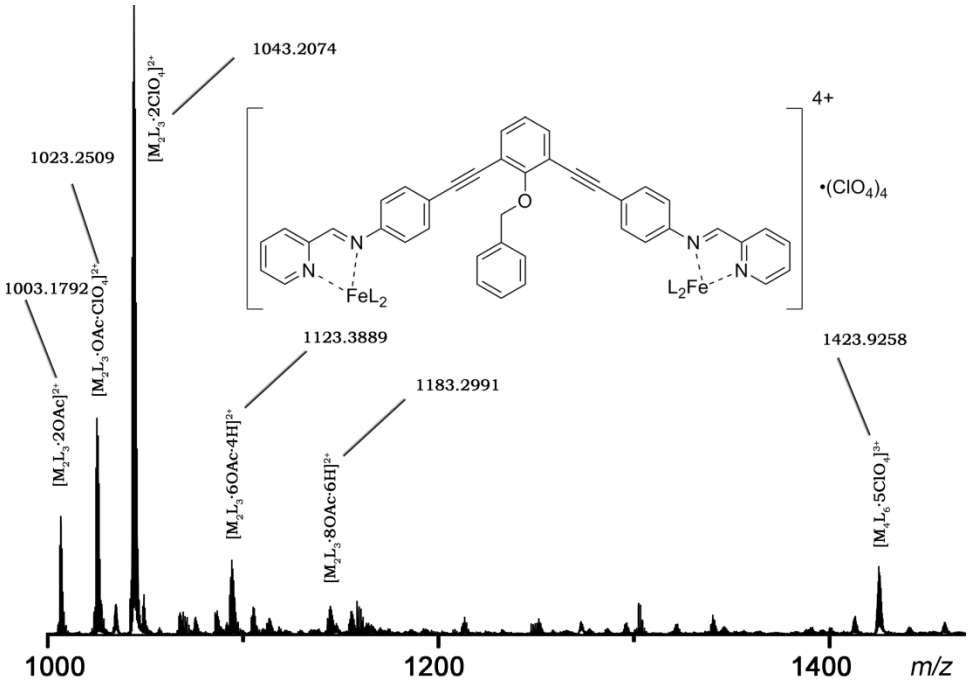

Figure 8.38: ESI-MS of **[3.5d$_3$•Fe$_2$](ClO$_4$)$_4$** (MeCN).

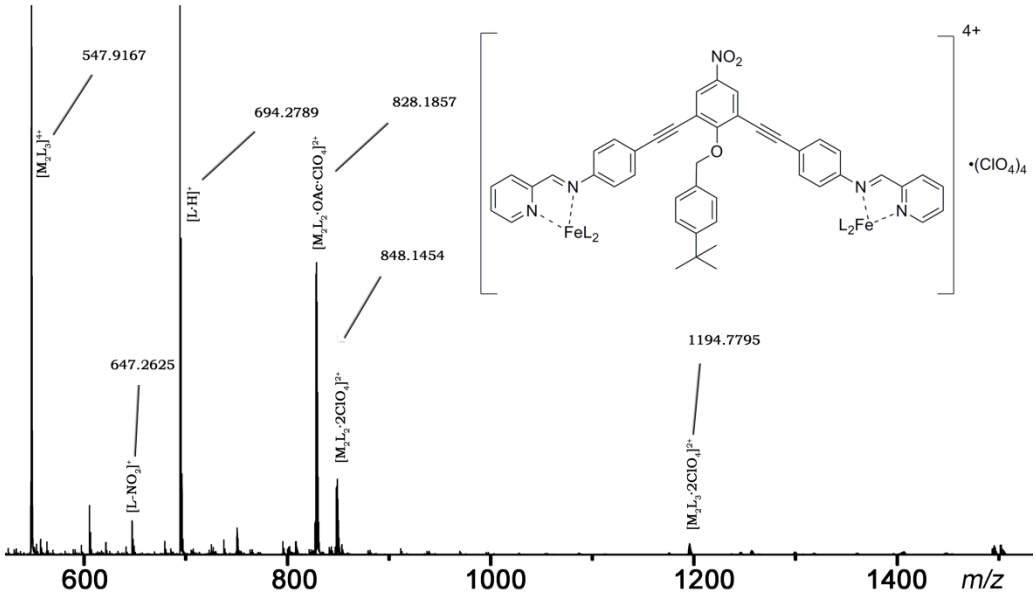

Figure 8.39: ESI-MS of **[3.5e$_3$•Fe$_2$](ClO$_4$)$_4$** (MeCN).

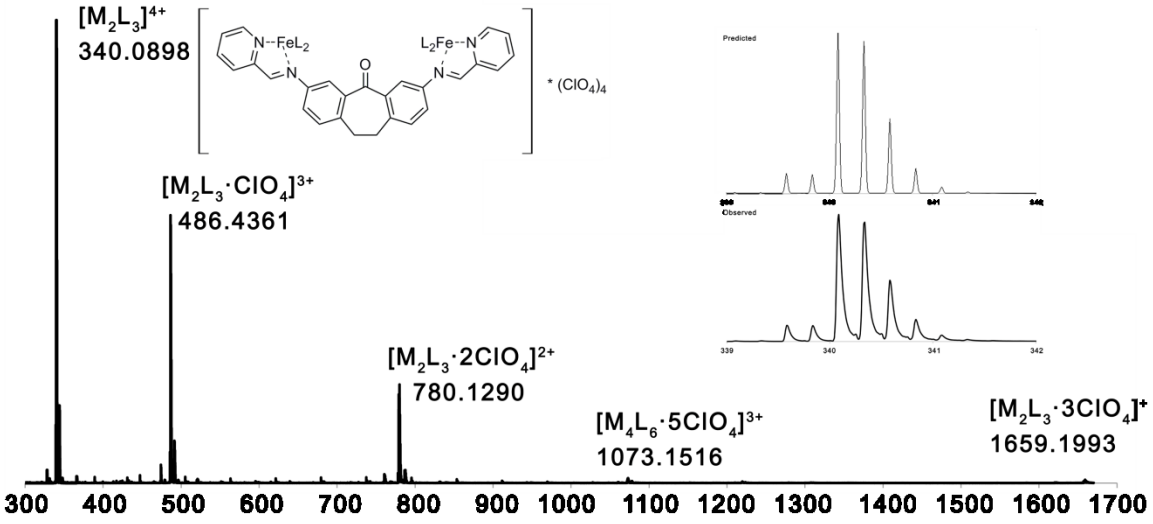

Figure 8.40: ESI-MS of **[4.2a$_3$•Fe$_2$](ClO$_4$)$_4$** (MeCN).

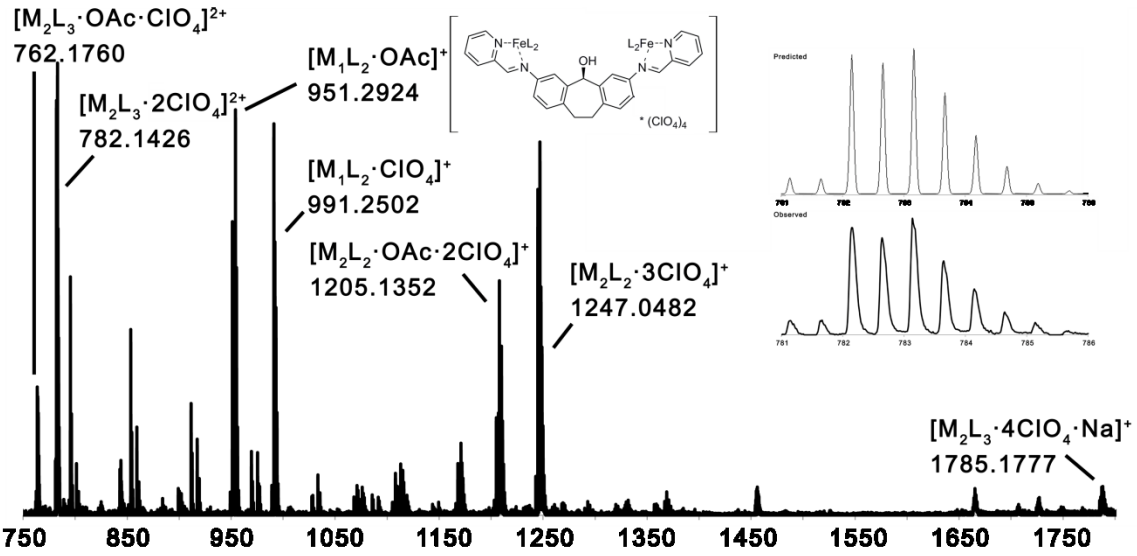

Figure 8.41: ESI-MS of **[4.2b$_3$•Fe$_2$](ClO$_4$)$_4$** (MeCN).

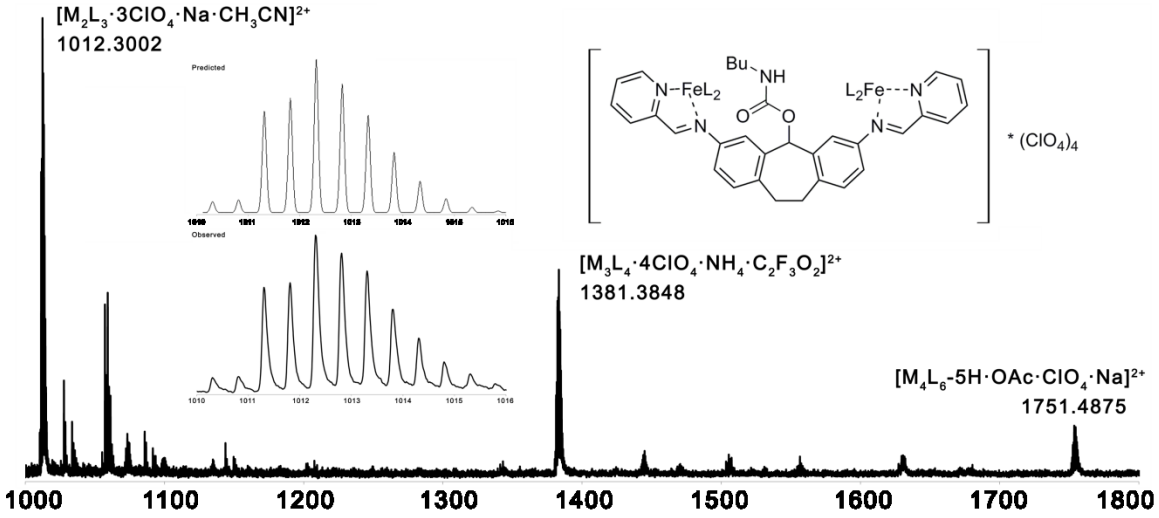

Figure 8.42: ESI-MS of **[4.2c$_3$•Fe$_2$](ClO$_4$)$_4$** (MeCN).

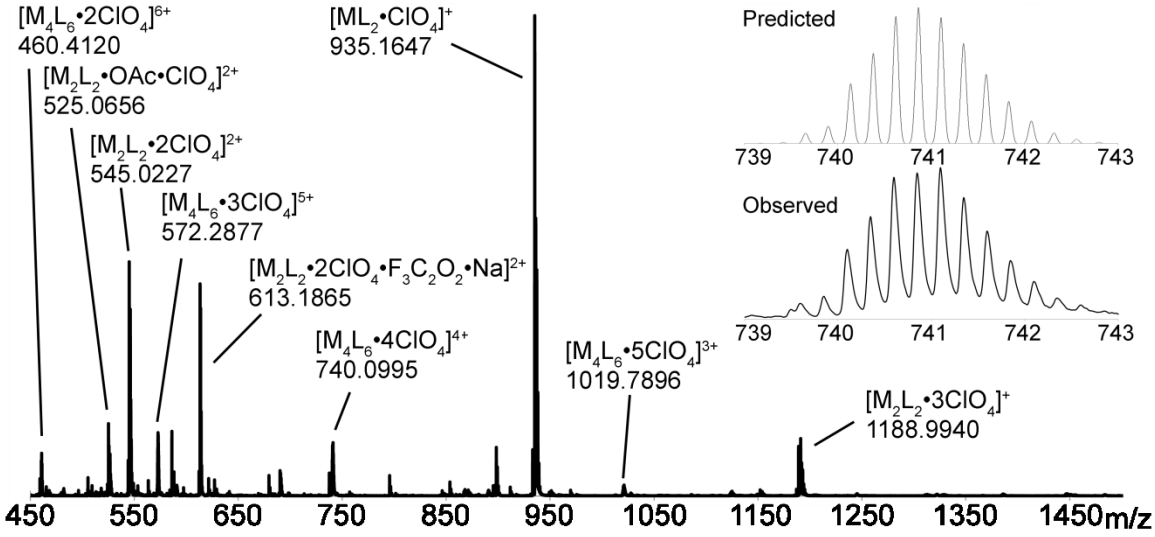

Figure 8.43: ESI-MS of **[4.7b$_6$•Fe$_4$](ClO$_4$)$_8$** (MeCN).

8.11 Selected Optical Spectra

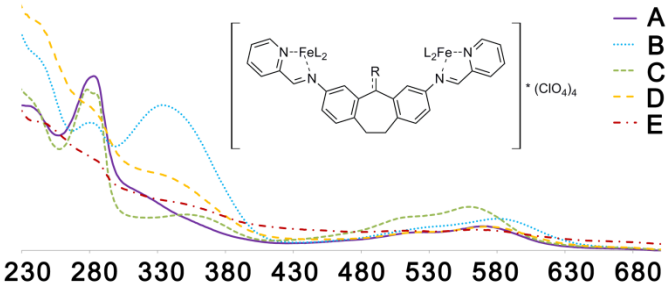

Figure 8.44: UV spectra of **[4.3(a-f)$_3$•Fe$_2$](ClO$_4$)$_4$**: a) **[4.3a$_3$•Fe$_2$](ClO$_4$)$_4$** (52 μM); b) **[4.3b$_3$•Fe$_2$](ClO$_4$)$_4$** (18 μM); c) **[4.3c$_3$•Fe$_2$](ClO$_4$)$_4$** (8.1 μM); d) **[4.3d$_3$•Fe$_2$](ClO$_4$)$_4$** (13 μM); e) **[(*S*)-4.3f$_3$•Fe$_2$](ClO$_4$)$_4$** (7.6 μM) (MeCN).

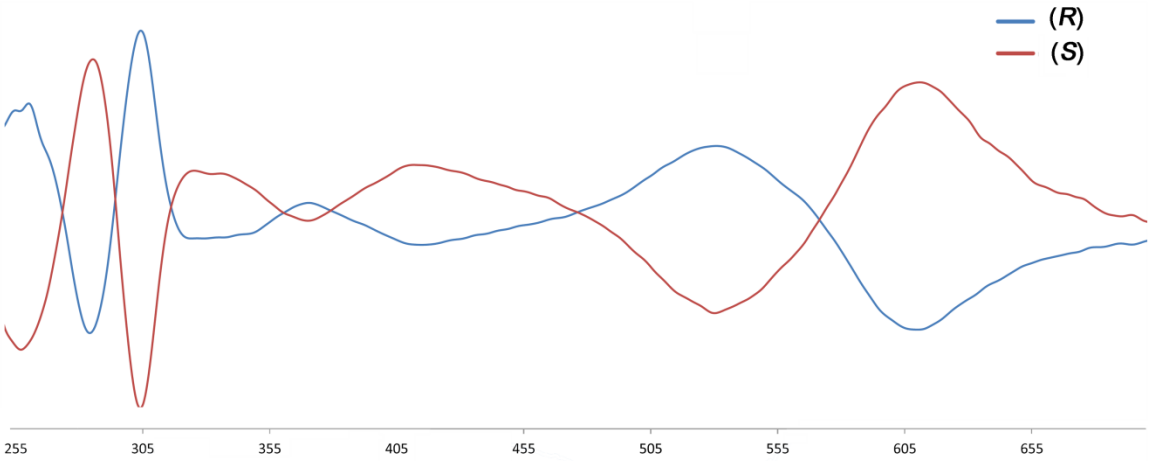

Figure 8.45: CD Spectra of **[(*S*)-4.3f$_3$•Fe$_2$](ClO$_4$)$_4$** and **[(*R*)-4.3f$_3$•Fe$_2$](ClO$_4$)$_4$** (MeCN, 54 μM).

8.12 X-Ray Crystallographic Data

Crystal Structure of [4.3a$_3$•Fe$_2$](ClO$_4$)$_4$ (CCDC # 951758)

A purple fragment of a prism (0.39 x 0.29 x 0.08 mm^3) was used for the single crystal x-ray diffraction study of $[C_{81}H_{60}N_{12}O_3Fe_2][ClO_4]_4$. The crystal was coated with paratone oil and mounted on to a cryo-loop glass fiber. X-ray intensity data were collected at 100(2) K on a Bruker APEX2[2] platform-CCD x-ray diffractometer system (fine focus Mo-radiation, λ = 0.71073 Å, 50KV/30mA power). The CCD detector was placed at a distance of 5.0800 cm from the crystal.

A total of 4800 frames were collected for a sphere of reflections (with scan width of 0.3° in ω, starting ω and 2θ angles of –30°, and Φ angles of 0°, 90°, 120°, 180°, 240°, and 270° for every 600 frames, 20 sec/frame exposure time, and one 360° Φ scan with starting ω and 2θ angles at –45° and 30°, respectively). The frames were integrated using the Bruker SAINT software package[3] and using a narrow-frame integration algorithm. Based on a triclinic crystal system, the integrated frames yielded a total of 117348 reflections at a maximum 2θ angle of 60.14° (0.72 Å resolution), of which 23999 were independent reflections (R_{int} = 0.0283, R_{sig} = 0.0232, redundancy = 4.9, completeness = 99.8%) and 20198 (84.2%) reflections were greater than 2σ(I). The unit cell parameters were, a = 10.9347(3) Å, b = 19.6886(5) Å, c = 22.3960(6) Å, α = 110.010(1)°, β = 96.481(1)°, γ = 104.184(1)°, V = 4288.8(2) Å^3, Z = 2, calculated density D_c = 1.506 g/cm^3. Absorption corrections were applied (absorption coefficient μ = 0.546 mm^{-1}; max/min transmission = 0.9581/0.8156) to the raw intensity data using the SADABS program.[4]

The Bruker SHELXTL software package[5] was used for phase determination and structure refinement. The distribution of intensities (E^2-1 = 0.959) and no systematic absent reflections indicated two possible space groups, P-1 and P1. The space group P-1 (#2) was later determined to be correct. Direct methods of phase determination followed by two Fourier cycles of refinement led to an electron density map from which most of the non-hydrogen atoms were identified in the asymmetric unit of the unit cell. With subsequent isotropic refinement, all of the non-hydrogen atoms were identified. There were one cation of $[C_{81}H_{60}N_{12}O_3Fe_2]^{4+}$ (where one O-atom of the three C=O groups was disordered with disordered site occupancy ratio of 37%/32%/31%), four anions of $[ClO_4]^-$ (where three of the four anions were disordered with site occupancy ratios of 95%/5%, 56%/44%, 51%/49%), five partially occupied (97%, 96%, 90%, 88% and 24% occupied) CH_3CN molecules, two partially occupied (22%, 11% occupied) water molecules, and one partially occupied (43% occupied) benzene (located at the inversion center) present in the asymmetric unit of the unit cell. The 24% occupied CH_3CN molecule was located at the inversion

center. The C and G-level alerts given by checkcif are main due to the disordered anions (ClO_4^-) and partially occupied solvents of crystallization (acetonitrile, water and benzene).

Atomic coordinates, isotropic and anisotropic displacement parameters of all the non-hydrogen atoms were refined by means of a full matrix least-squares procedure on F^2. The H-atoms were included in the refinement in calculated positions riding on the atoms to which they were attached, except the H-atoms of the partial water molecules were restrained as ideal models using DFIX. The refinement converged at R1 = 0.0366, wR2 = 0.0918, with intensity, I>2σ(I). The largest peak/hole in the final difference map was 0.998/-0.416 e/Å^3.

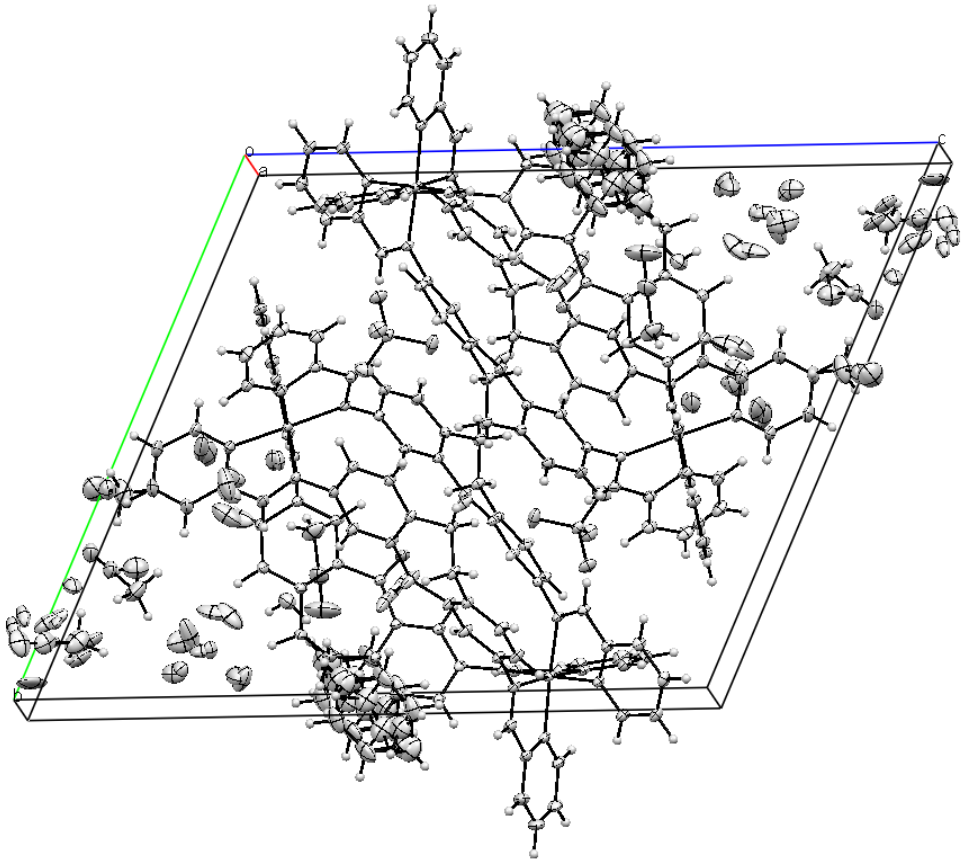

Figure 8.46: Unit cell of **[4.3a$_3$•Fe$_2$](ClO$_4$)$_4$** (Vapor diffusion of benzene into acetonitrile, 100K)

Table 8.1. Crystal data and structure refinement for **[4.3a$_3$•Fe$_2$](ClO$_4$)$_4$**.

Empirical formula	$C_{90.21}H_{73.84}Cl_4Fe_2N_{15.97}O_{19.33}$	
Formula weight	1944.30	
Temperature	100(2) K	
Wavelength	0.71073 Å	
Crystal system	Triclinic	
Space group	P-1	
Unit cell dimensions	*a* = 10.9347(3) Å	α= 110.010(1)°.
	b = 19.6886(5) Å	β= 96.481(1)°.
	c = 22.3960(6) Å	γ = 104.184(1)°.
Volume	4288.8(2) Å^3	
Z	2	
Density (calculated)	1.506 Mg/m^3	
Absorption coefficient	0.546 mm^{-1}	
F(000)	2003	
Crystal size	0.39 x 0.29 x 0.08 mm^3	
Theta range for data collection	1.79 to 29.57°.	
Index ranges	-15<=*h*<=15, -27<=*k*<=27, -31<=*l*<=31	
Reflections collected	117348	
Independent reflections	23999 [*R*(int) = 0.0283]	
Completeness to θ = 29.57°	99.8 %	
Absorption correction	Semi-empirical from equivalents	
Max. and min. transmission	0.9581 and 0.8156	
Refinement method	Full-matrix least-squares on F^2	
Data / restraints / parameters	23999 / 648 / 1403	
Goodness-of-fit on *F*^{2}	1.021	
Final R indices [I>2σ (I)]	*R*1 = 0.0366, *wR*2 = 0.0918	
R indices (all data)	*R*1 = 0.0465, *wR*2 = 0.0976	
Largest diff. peak and hole	0.998 and -0.416 *e*.Å^{-3}	

Crystal Structure of $[4.3b_3 \bullet Fe_2](ClO_4)_4$ (CCDC# 951759)

A purple fragment of a prism (0.51 x 0.28 x 0.02 mm^3) was used for the single crystal x-ray diffraction study of $[C_{81}H_{66}N_{12}O_3Fe_2][ClO_4]_4$. The crystal was coated with paratone oil and mounted on to a cryo-loop glass fiber. X-ray intensity data were collected at 100(2) K on a Bruker APEX2[2] platform-CCD x-ray diffractometer system (fine focus Mo-radiation, λ = 0.71073 Å, 50KV/35mA power). The CCD detector was placed at a distance of 5.0600 cm from the crystal.

A total of 3600 frames were collected for a sphere of reflections (with scan width of 0.3^o in ω, starting ω and 2θ angles of $–30^o$, and Φ angles of 0^o, 90^o, 120^o, 180^o, 240^o, and 270^o for every 600 frames, 120 sec/frame exposure time, and one 360^o Φ scan with starting ω and 2θ angles at $–45^o$ and 30^o, respectively). The frames were integrated using the Bruker SAINT software package[4] and using a narrow-frame integration algorithm. Based on an orthorhomic crystal system, the integrated frames yielded a total of 228675 reflections at a maximum 2θ angle of 46.74^o (0.90 Å resolution), of which 25938 were independent reflections (R_{int} = 0.1099, R_{sig} = 0.0626, redundancy = 8.8, completeness = 99.7%) and 19864 (76.6%) reflections were greater than 2σ(I). The unit cell parameters were, **a** = 20.7761(16) Å, **b** = 40.5163(32) Å, **c** = 41.9666(33) Å, **α** = **β** = **γ** = 90^o, V = 35326(5) $Å^3$, Z = 8, calculated density D_c = 1.290 g/cm^3. Absorption corrections were applied (absorption coefficient μ = 0.503 mm^{-1}; max/min transmission = 0.9905/0.7816) to the raw intensity data using the SADABS program.[4]

The Bruker SHELXTL software package[5] was used for phase determination and structure refinement. The distribution of intensities (E^2-1 = 0.791) and no systematic absent reflections indicated two possible space groups, Cmma and Abm2. The space group Abm2 (#39) was later determined to be correct. Direct methods of phase determination followed by two Fourier cycles of refinement led to an electron density map from which most of the non-hydrogen atoms were identified in the asymmetric unit of the unit cell. With subsequent isotropic refinement, all of the cations and anions atoms were identified but not the solvent atoms. The PLATON-SQUEEZE program[6] was applied to remove possible disordered acetonitrile and diethyl ether solvents

present in the asymmetric unit of the unit cell before final refinement. The potential solvent void volume was calculated to be 7468.1 $Å^3$ [21% of the unit cell volume]. There were one full-cation of $C_{81}H_{66}N_{12}O_3Fe_2$, six full-anions of ClO_4 present in general positions of the asymmetric unit. There were two half-cations of $C_{81}H_{66}N_{12}O_3Fe_2$, and two half-anions of ClO_4 located at the mirror plane perpendicular to the b-axis. There was one anion of ClO_4 located at the two-fold rotation axis parallel to the c-axis. One of the six full-anions was modeled with disorder (disordered ratio 52%/48%). The structure was refined as a racemic twin (with major/minor twin ratio of 77%/23%). The alert levels B, C and G in the checkcif report are mostly due to the poor quality of the crystal and solvent(s) disordered that were squeezed out in the final refinement using PLATON-SQUEEZE.

Atomic coordinates, isotropic and anisotropic displacement parameters of all the non-hydrogen atoms were refined by means of a full matrix least-squares procedure on F^2. The H-atoms were included in the refinement in calculated positions riding on the atoms to which they were attached. The refinement converged at R1 = 0.0579, wR2 = 0.1338, with intensity, $I>2\sigma(I)$. The largest peak/hole in the final difference map was 0.653/-0.340 e/$Å^3$.

Table 8.2. Crystal data and structure refinement for **[4.3b$_3$•Fe$_2$](ClO$_4$)$_4$**.

Empirical formula	$C_{162}\ H_{132}\ Cl_7\ Fe_4\ N_{24}\ O_{34}$	
Formula weight	3430.47	
Temperature	100(2) K	
Wavelength	0.71073 Å	
Crystal system	Orthorhombic	
Space group	Abm2 (#39)	
Unit cell dimensions	*a* = 20.7761(16) Å	α=90°.
	b = 40.516(3) Å	β=90°.
	c = 41.967(3) Å	γ =90°.
Volume	35326(5) Å^3	
Z	8	
Density (calculated)	1.290 Mg/m^3	
Absorption coefficient	0.503 mm^{-1}	
F(000)	14136	
Crystal size	0.51 x 0.28 x 0.02 mm^3	
Theta range for data collection	1.38 to 23.37°.	
Index ranges	-23<=*h*<=23, -45<=*k*<=44, -46<=*l*<=46	
Reflections collected	228675	
Independent reflections	25938 [*R*(int) = 0.1099]	
Completeness to θ = 29.57°	99.7 %	
Absorption correction	Semi-empirical from equivalents	
Max. and min. transmission	0.9905 and 0.7816	
Refinement method	Full-matrix least-squares on F^2	
Data / restraints / parameters	25938 / 497 / 2177	
Goodness-of-fit on F^2	1.001	
Final R indices [I>2σ (I)]	*R*1 = 0.0579, *wR*2 = 0.1338	
R indices (all data)	*R*1 = 0.0777, *wR*2 = 0.1427	
Absolute structure parameter	0.230(12)	
Largest diff. peak and hole	0.653 and -0.340 *e*.Å^{-3}	

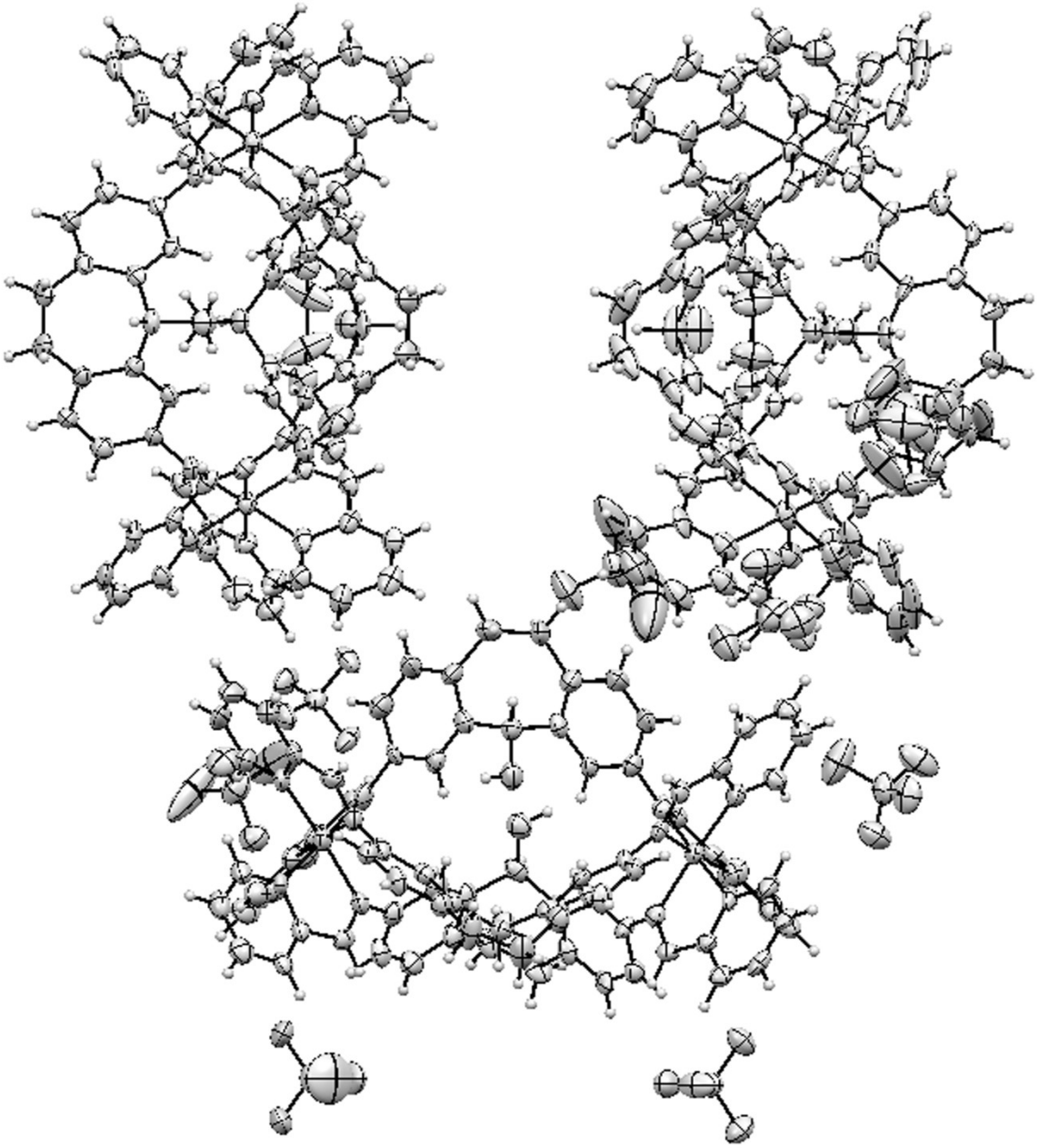

Figure 8.47: Three-unit stacking observed in the crystal of **[4.3b$_3$•Fe$_2$](ClO$_4$)$_4$** (Vapor diffusion of ether into acetonitrile with 1% mesitylene, 100K).

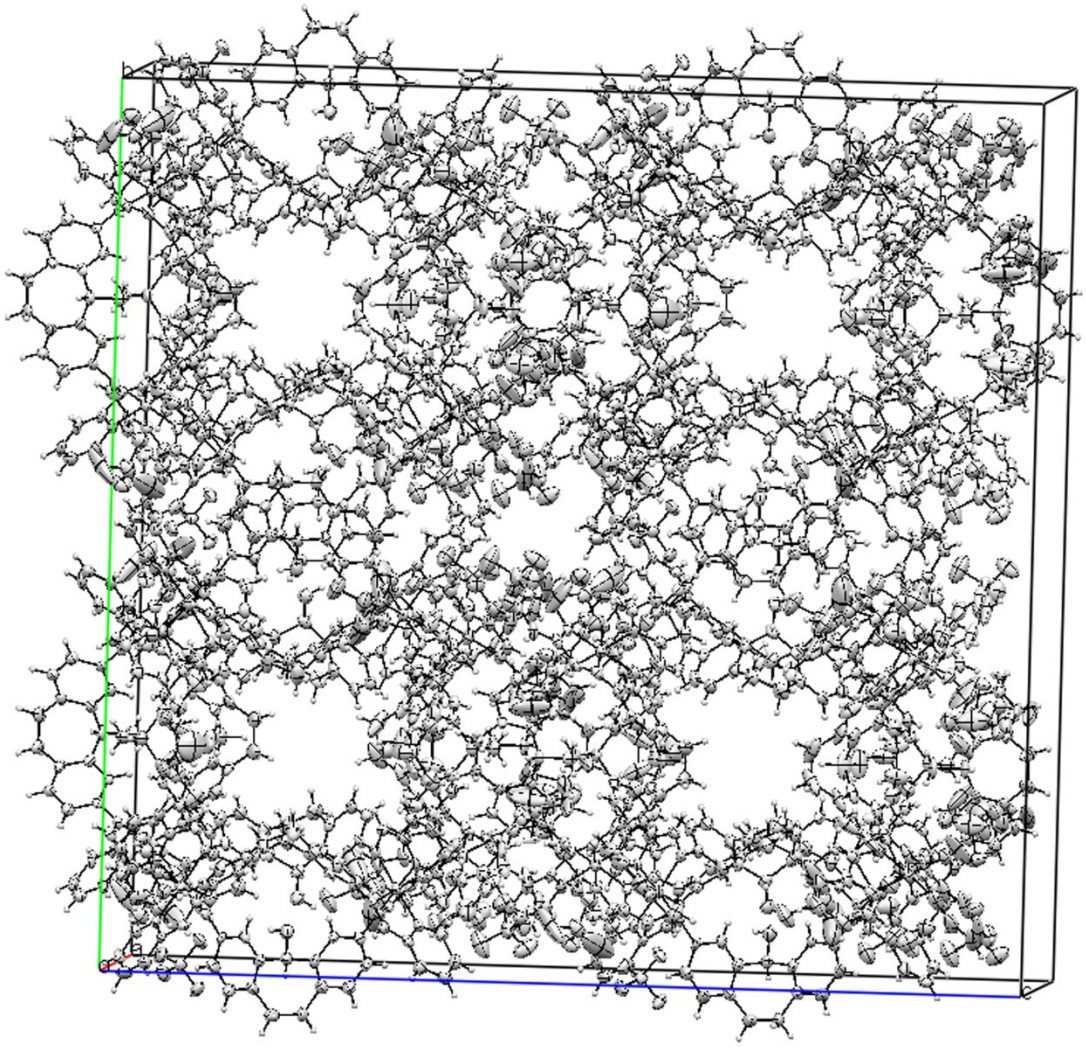

Figure 8.48: Unit cell of **[4.3b$_3$•Fe$_2$](ClO$_4$)$_4$** (Vapor diffusion of ether into acetonitrile with 1% mesitylene, 100K).

Crystal Structure of [(ClO$_4$)⊂4.7b$_6$·Fe$_4$](ClO$_4$)$_7$·MeCN (CCDC# 951759)

A dark purple prism fragment (0.552 x 0.402 x 0.113 mm^3) was used for the single crystal x-ray diffraction study of $[C_{150}H_{108}N_{24}O_6Fe_4][ClO_4]_8$. The crystal was coated with paratone oil and mounted on to a cryo-loop glass fiber. X-ray intensity data were collected at 100(2) K on a Bruker APEX2[2] platform-CCD x-ray diffractometer system (fine focus Mo-radiation, λ = 0.71073 Å, 50KV/35mA power). The CCD detector was placed at a distance of 8.1200 cm from

the crystal.

A total of 6000 frames were collected for a hemisphere of reflections (with scan width of 0.3^o in ω, two sets of starting ω-2θ angles at -21^o and at -30^o and each set had Φ angles of 0^o, 45^o, 90^o, 135^o, and 180^o for every 600 frames, 120 sec/frame exposure time). The Bruker Cell_Now program[7] was used to obtain the two different orientation matrices of the rotational twin components (Twin law is 180^o rotation about the 1 0 0 reciprocal axis). These matrices were imported into the APEX2 program for Bravais lattice determination and initial unit cell refinement. The frames were integrated using the Bruker SAINT software package[3] and using a narrow-frame integration algorithm. Based on a monoclinic crystal system, the integrated frames yielded a total of 52071 unique independent reflections [at maximum $2\theta = 51.05^o$ (0.82 Å resolution), data completeness = 73.9%] and 34126 (65.5%) reflections were greater than $2\sigma(I)$. The unit cell parameters were, **a** = 31.2973(18) Å, **b** = 33.5583(19) Å, **c** = 40.235(2) Å, **β** = $108.896(2)^o$**,** V = 39981(4) $Å^3$, Z = 8, calculated density D_c = 1.211 g/cm^3. Absorption corrections were applied (absorption coefficient μ = 0.449 mm^{-1}; max/min apparent transmission = 0.745210/0.608965) to the raw intensity data using the Bruker TWINABS program.[8] The data quality was poor. The low data completeness were due to the large unit cell where the detector was placed at a long distance of 8.1200 cm from the crystal. Hence certain unique reflections were not collected and missing. No attempt was made to obtain higher data completeness percentage because of the long exposure time of 120 second per frame used and twinning issue. The A, B, C, and G level alerts in the checkcif report are due to the poor quality data collected. Attempts to get higher quality crystals failed.

The Bruker SHELXTL software package[5] was used for phase determination and structure refinement. Using the first twin domain HKL 4 intensity data, the distribution of intensities (E^2-1

= 0.992) and systematic absent reflections indicated one possible space group, P2(1)/c. The space group P2(1)/c (#14) was later determined to be correct. Direct methods of phase determination followed by two Fourier cycles of refinement led to an electron density map from which most of the non-hydrogen cation and anion atoms were identified in the asymmetric unit of the unit cell. With subsequent isotropic refinement, all of the non-hydrogen cation and anion atoms were identified. The combined (major and minor components) HKLF 5 intensity dataset was used in the final structure refinement. There were two cations of $C_{150}H_{108}N_{24}O_6Fe_4$ (the two cations are conformers), 16 fully and partially occupied anions of ClO_4, and 19 fully and partially occupied CH_3CN solvent molecules present in the asymmetric unit of the unit cell. The rotational twin law was 180^o rotation about the 1 0 0 reciprocal axis. The major/minor component twin ratio was 57%/43%. All the ClO_4 anion-atoms and four of the nineteen CH_3CN solvent molecules were refined isotropically. There are large amount of solvent voids where the high difference electron density peaks were located but the solvent molecules cannot be clearly distinguished. PLATON SQUEEZE was not attempted.

Atomic coordinates, isotropic and anisotropic displacement parameters of all the non-hydrogen atoms were refined by means of a full matrix least-squares procedure on F^2. The H-atoms were included in the refinement in calculated positions riding on the atoms to which they were attached. The refinement converged at R_1 = 0.1376, wR_2 = 0.3663, with intensity, I>2σ(I). The largest peak/hole in the final difference map was 2.565/-1.273 e/Å^3.

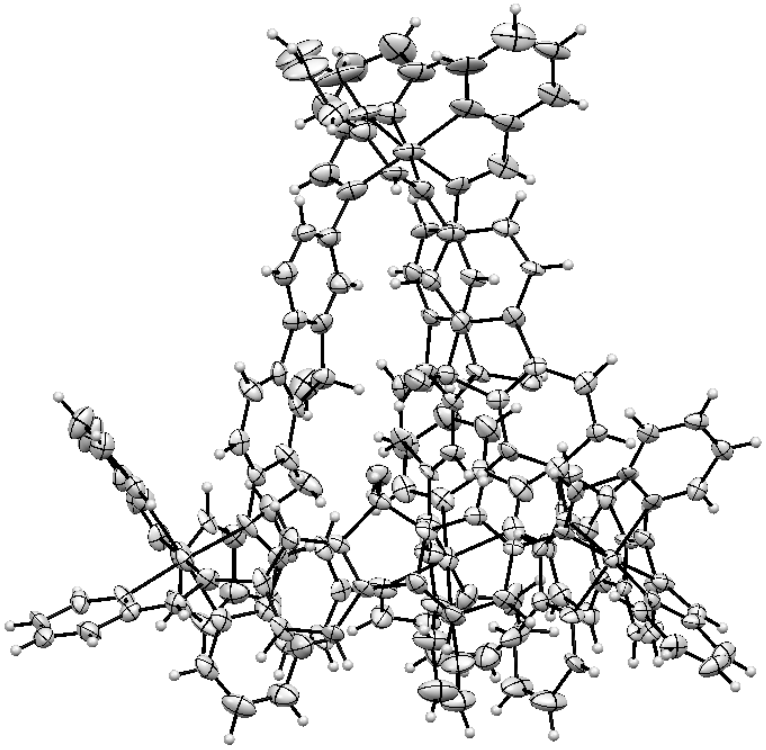

Figure 8.49: ORTEP structure of **[(ClO_4)⊂4.7b_6·Fe_4]$(ClO_4)_7$** (Slow evaporation from acetonitrile, diffracted at 100 °K).

Table 8.3. Crystal data and structure refinement for **$[(ClO_4)\subset 4.7b_6{\cdot}Fe_4](ClO_4)_7{\cdot}MeCN$**

Empirical formula	$C_{169.01}H_{136.52}Cl_{6.93}Fe_4N_{33.51}O_{33.73}$	
Formula weight	3645.66	
Temperature	100(2) K	
Wavelength	0.71073 Å	
Crystal system	Monoclinic	
Space group	P2(1)/c	
Unit cell dimensions	a = 31.2973 (18) Å	α= 90°.
	b = 33.5583 (19) Å	β= 108.896 (2)°.
	c = 40.235 (2) Å	γ = 90°.
Volume	39981 (4) $Å^3$	
Z	8	
Density (calculated)	1.211 g/cm^3	
Absorption coefficient	0.449 mm^{-1}	
F(000)	15014	
Crystal size	0.552 x 0.402 x 0.113 mm^3	
Theta range for data collection	1.326 to 25.525°.	
Index ranges	-37<=h<=33, 0<=k<=40, 0<=l<=47	
Reflections collected	52071	
Independent reflections	52071 [R(int) = 0.0417]	
Completeness to θ = 51.05°	73.9 %	
Absorption correction	Semi-empirical from equivalents	
Max. and min. transmission	0.745210 and 0.608965	
Refinement method	Full-matrix least-squares on F^2	
Data / restraints / parameters	52071 / 4167 / 4133	
Goodness-of-fit on F^2	1.642	
Final R indices [I>2σ (I)]	R_1 = 0.1376, wR_2 = 0.3663	
R indices (all data)	R_1 = 0.2006, wR_2 = 0.4151	
Largest diff. peak and hole	2.565 and -1.273 $e.Å^{-3}$	

Complex $[7.13_2{\bullet}Fe](ClO_4)_2$ (CCDC # 934197)

A black prism fragment (0.46 x 0.33 x 0.06 mm^3) was used for the single crystal X-ray diffraction study of $[C_{13}H_{11}N_7]_2Fe]][ClO_4]_2{\cdot}CH_3CN$. The crystal was coated with paratone oil and mounted on to a cryo-loop glass fiber. X-ray intensity data were collected at 100(2) K on a Bruker APEX2[2] platform-CCD x-ray diffractometer system (fine focus Mo-radiation, λ = 0.71073 Å, 50KV/35mA power). The CCD detector was placed at a distance of 5.0600 cm from the crystal.

A total of 3600 frames were collected for a sphere of reflections (with scan width of 0.3° in ω,

starting ω and 2θ angles at –30°, and φ angles of 0°, 90°, 120°, 180°, 240°, and 270° for every 600 frames, 10 sec/frame exposure time). The frames were integrated using the Bruker SAINT software package[3] and using a narrow-frame integration algorithm. Based on a monoclinic crystal system, the integrated frames yielded a total of 66601 reflections at a maximum 2θ angle of 56.56° (0.75 Å resolution), of which 8277 were independent reflections (R_{int} = 0.0412, R_{sig} = 0.0234, redundancy = 8.0, completeness = 99.9%) and 6905 (83.4%) reflections were greater than 2□(I). The unit cell parameters were, **a** = 21.4191(8) Å, **b** = 10.8147(4) Å, **c** = 15.1758(6) Å, **β** = 108.398(1)°, V = 3335.7(2) Å^3, Z = 4, calculated density D_c = 1.646 g/cm^3. Absorption corrections were applied (absorption coefficient μ = 0.688 mm^{-1}; max/min transmission = 0.9625/0.7426) to the raw intensity data using the SADABS program.[4]

The Bruker SHELXTL software package[5] was used for phase determination and structure refinement. The distribution of intensities (E^2-1 = 0.961) and systematic absent reflections indicated one possible space group, P2(1)/c. The space group P2(1)/c (#14) was later determined to be correct. Direct methods of phase determination followed by two Fourier cycles of refinement led to an electron density map from which most of the non-hydrogen atoms were identified in the asymmetric unit of the unit cell. With subsequent isotropic refinement, all of the non-hydrogen atoms were identified. There were one cation of $[C_{13}H_{11}N_7]_2Fe]^{2+}$, two anions of $[ClO_4]^-$, and one solvent molecule of CH_3CN present in the asymmetric unit of the unit cell. All the NH2-groups H-atoms were involved in intermolecular hydrogen bonding.

Atomic coordinates, isotropic and anisotropic displacement parameters of all the non-hydrogen atoms were refined by means of a full matrix least-squares procedure on F^2. The H-atoms were included in the refinement in calculated positions riding on the atoms to which they were attached, except for the NH_2-group H-atoms were refined unrestrained. The refinement converged at R1 = 0.0358, wR2 = 0.0867, with intensity I>2σ (I). The largest peak/hole in the final difference map was 0.566/-0.616 e/Å^3.

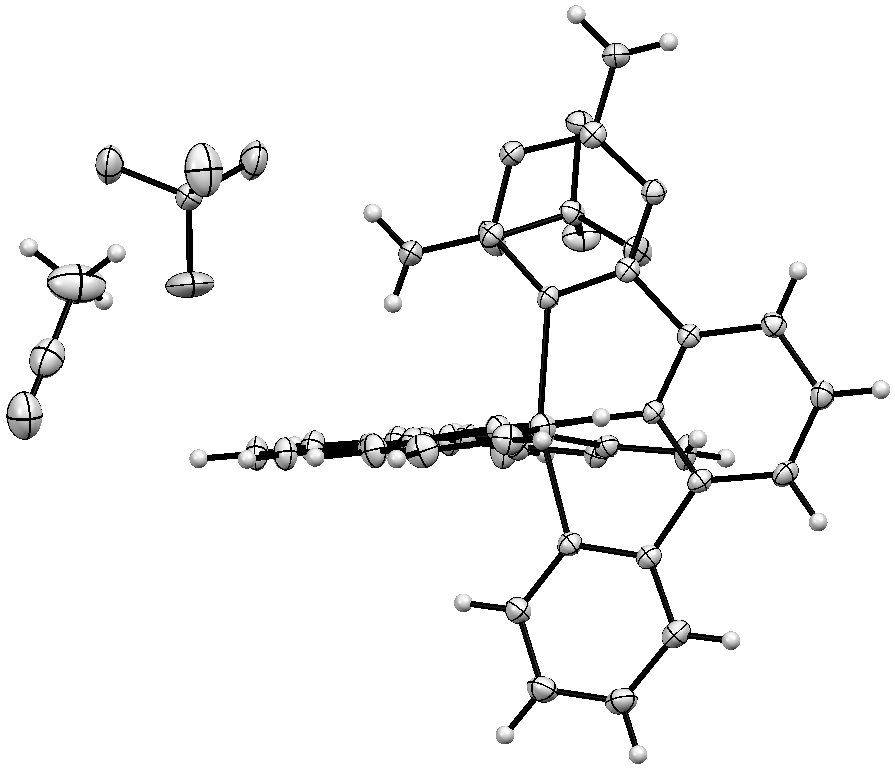

Figure 8.50: Individual molecules of **[7.13$_2$•Fe](ClO$_4$)$_2$**•MeCN from the crystal structure (100 °K).

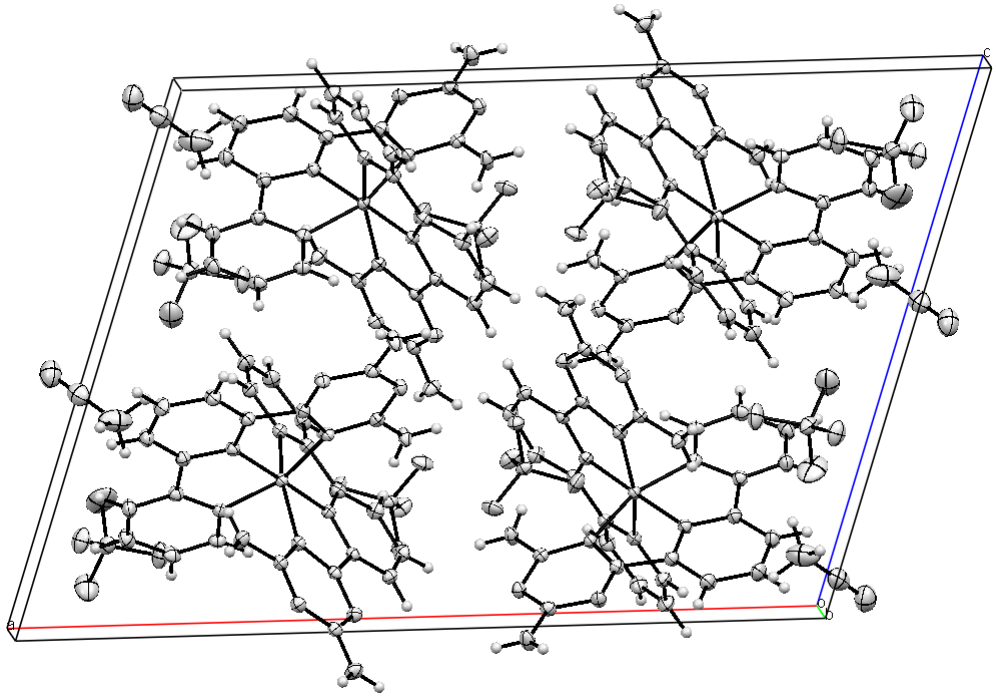

Figure 8.51: Unit cell of **[7.13$_2$•Fe](ClO$_4$)$_2$**•MeCN crystal structure (100 °K).

Table 8.4. Crystal data and structure refinement for **[7.13$_2$•Fe](ClO$_4$)$_2$•MeCN**.

Empirical formula	C_{28} H_{25} Cl_2 Fe N_{15} O_8	
Formula weight	826.38	
Temperature	100(2) K	
Wavelength	0.71073 Å	
Crystal system	Monoclinic	
Space group	P2(1)/c	
Unit cell dimensions	*a* = 21.4191(8) Å	α= 90°.
	b = 10.8147(4) Å	β= 108.3980(10)°.
	c = 15.1758(6) Å	γ = 90°.
Volume	3335.7(2) Å^3	
Z	4	
Density (calculated)	1.646 Mg/m^3	
Absorption coefficient	0.688 mm^{-1}	
F(000)	1688	
Crystal size	0.46 x 0.33 x 0.06 mm^3	
Theta range for data collection	2.00 to 28.28°.	
Index ranges	-28<=*h*<=28, -14<=*k*<=14, -20<=*l*<=20	
Reflections collected	66601	
Independent reflections	8277 [*R*(int) = 0.0412]	
Completeness to θ = 28.28°	99.9 %	
Absorption correction	Semi-empirical from equivalents	
Max. and min. transmission	0.9625 and 0.7426	
Refinement method	Full-matrix least-squares on F^2	
Data / restraints / parameters	8277 / 0 / 512	
Goodness-of-fit on *F*^{2}	1.031	
Final R indices [I>2σ (I)]	*R*1 = 0.0358, *wR*2 = 0.0867	
R indices (all data)	*R*1 = 0.0464, *wR*2 = 0.0926	
Largest diff. peak and hole	0.566 and -0.616 *e*.Å^{-3}	

8.13 Extraneous Data

Parent Cages

fac_4	$fac_3 \cdot mer_1$	$fac_2 \cdot mer_2$	$fac_1 \cdot mer_3$	mer_4
ΔΔΔΔ/ΛΛΛΛ – 7	ΔΔΔ,Λ/ΛΛΛ,Δ – 13	ΔΔ,ΔΔ/ΛΛ,ΛΛ – 13	Δ,ΛΛΛ/Λ,ΔΔΔ – 13	ΔΔΔΔ/ΛΛΛΛ – 7
ΔΔΔΛ/ΛΛΛΔ – 13	ΔΔΔ,Δ/ΛΛΛ,Λ – 13	ΔΔ,ΛΛ/ΛΛ,ΔΔ – 13	Δ,ΔΔΔ/Λ,ΛΛΛ – 13	ΔΔΔΛ/ΛΛΛΔ – 13
ΔΔΛΛ/ΛΛΔΔ – 18	ΔΔΛ,Λ/ΛΛΔ,Δ – 46	ΔΛ,ΔΛ/ΛΔ,ΛΛ – 46	Λ,ΛΔΔ/Δ,ΔΛΛ – 46	ΔΔΛΛ/ΛΛΔΔ – 18
	ΔΔΛ,Δ/ΛΛΔ,Λ – 46	ΔΛ,ΔΛ/ΛΔ,ΛΔ – 64	Δ,ΛΔΔ/Λ,ΔΛΛ – 46	

ΔΔΔΔ/ΛΛΛΛ
in_6, $in_5 \cdot out_1$
$in_4 \cdot out_2$, $in_3 \cdot out_3$
$in_2 \cdot out_4$, $in_1 \cdot out_5$
out_6

ΔΔΔΔ/ΛΛΛΔ
$in_3 \cdot in_3$, $in_2 \cdot in_3 \cdot out_1$
$in_1 \cdot in_3 \cdot out_2$, $in_3 \cdot out_3$
$in_2 \cdot in_2 \cdot out_1 \cdot out_1$
$in_1 \cdot in_2 \cdot out_2 \cdot out_1$
$in_2 \cdot out_3 \cdot out_1$
$in_2 \cdot in_1 \cdot out_1 \cdot out_2$
$in_1 \cdot in_1 \cdot out_2 \cdot out_2$
$in_1 \cdot out_3 \cdot out_2$
$in_2 \cdot out_1 \cdot out_3$
$in_1 \cdot out_2 \cdot out_3$
$out_3 \cdot out_3$

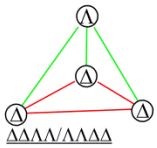

ΔΔΔΔ/ΛΛΔΔ
$in_1 \cdot in_1 \cdot in_4$, $in_1 \cdot in_1 \cdot in_3 \cdot out_1$
$\mathbf{in_1 \cdot in_1 \cdot in_2 \cdot out_2}$, $in_1 \cdot in_1 \cdot in_1 \cdot out_3$
$in_1 \cdot in_1 \cdot out_4$, $out_1 \cdot in_1 \cdot in_4$
$out_1 \cdot in_1 \cdot in_3 \cdot out_1$
$\mathbf{out_1 \cdot in_1 \cdot in_2 \cdot out_2}$
$out_1 \cdot in_1 \cdot in_1 \cdot out_3$
$out_1 \cdot in_1 \cdot out_4$
$out_1 \cdot out_1 \cdot in_4$
$out_1 \cdot out_1 \cdot in_3 \cdot out_1$
$\mathbf{out_1 \cdot out_1 \cdot in_2 \cdot out_2}$
$out_1 \cdot out_1 \cdot in_1 \cdot out_3$, $out_1 \cdot out_1 \cdot out_4$

ΔΔΔ,Λ/ΛΛΛ,Λ
$in_3 \cdot in_3$, $in_2 \cdot in_3 \cdot out_1$
$in_1 \cdot in_3 \cdot out_2$, $in_3 \cdot out_3$
$in_2 \cdot in_2 \cdot out_1 \cdot out_1$
$in_1 \cdot in_2 \cdot out_2 \cdot out_1$, $in_2 \cdot out_3 \cdot out_1$
$in_2 \cdot in_1 \cdot out_1 \cdot out_2$, $in_1 \cdot in_1 \cdot out_2 \cdot out_2$
$in_1 \cdot out_3 \cdot out_2$, $in_2 \cdot out_1 \cdot out_3$
$in_1 \cdot out_2 \cdot out_3$, $out_3 \cdot out_3$

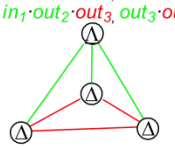

ΔΔΔ,Δ/ΛΛΛ,Λ
Same as ΔΔΔ,Λ/ΛΛΛ,Δ

ΔΔΛ,Λ/ΛΛΔ,Δ
$in_2 \cdot in_1 \cdot in_2 \cdot in_1$, $in_1 \cdot out_1 \cdot in_1 \cdot in_2 \cdot in_1$
$out_2 \cdot in_1 \cdot in_2 \cdot in_1$, $in_2 \cdot out_1 \cdot in_2 \cdot in_1$
$in_1 \cdot out_1 \cdot out_1 \cdot in_2 \cdot in_1$
$out_2 \cdot out_1 \cdot in_2 \cdot in_1$, $in_2 \cdot in_1 \cdot in_1 \cdot out_1 \cdot in_1$
$\mathbf{in_1 \cdot out_1 \cdot in_1 \cdot in_1 \cdot out_1 \cdot in_1}$
$out_2 \cdot in_1 \cdot in_1 \cdot out_1 \cdot in_1$
$in_2 \cdot out_1 \cdot in_1 \cdot out_1 \cdot in_1$
$\mathbf{in_1 \cdot out_1 \cdot out_1 \cdot in_1 \cdot out_1 \cdot in_1}$
$out_2 \cdot out_1 \cdot in_1 \cdot out_1 \cdot in_1$ $in_2 \cdot in_1 \cdot out_2 \cdot in_1$,
$in_1 \cdot out_1 \cdot in_1 \cdot out_2 \cdot in_1$
$out_2 \cdot in_1 \cdot out_2 \cdot in_1$, $in_2 \cdot in_1 \cdot out_2 \cdot in_1$
$in_1 \cdot out_1 \cdot in_1 \cdot out_2 \cdot in_1$
$out_2 \cdot in_1 \cdot out_2 \cdot in_1$, $in_2 \cdot out_1 \cdot out_2 \cdot in_1$
$in_1 \cdot out_1 \cdot out_1 \cdot out_2 \cdot in_1$
$out_2 \cdot out_1 \cdot out_2 \cdot in_1$
$in_2 \cdot in_1 \cdot in_2 \cdot out_1$, $in_1 \cdot out_1 \cdot in_1 \cdot in_2 \cdot out_1$
$out_2 \cdot in_1 \cdot in_2 \cdot out_1$, $in_2 \cdot out_1 \cdot in_2 \cdot out_1$
$in_1 \cdot out_1 \cdot out_1 \cdot in_2 \cdot out_1$
$out_2 \cdot out_1 \cdot in_2 \cdot out_1$, $in_2 \cdot in_1 \cdot in_1 \cdot out_1 \cdot out_1$
$\mathbf{in_1 \cdot out_1 \cdot in_1 \cdot in_1 \cdot out_1 \cdot out_1}$
$out_2 \cdot in_1 \cdot in_1 \cdot out_1 \cdot out_1$
$in_2 \cdot out_1 \cdot in_1 \cdot out_1 \cdot out_1$
$\mathbf{in_1 \cdot out_1 \cdot out_1 \cdot in_1 \cdot out_1 \cdot out_1}$
$out_2 \cdot out_1 \cdot in_1 \cdot out_1 \cdot out_1$
$in_2 \cdot out_1 \cdot in_1 \cdot out_1 \cdot out_1 \cdot in_1$
$out_2 \cdot in_1 \cdot out_2 \cdot out_1$, $in_1 \cdot out_1 \cdot in_1 \cdot out_2 \cdot out_1$
$out_2 \cdot in_1 \cdot out_2 \cdot out_1$, $in_2 \cdot in_1 \cdot out_2 \cdot out_1$
$in_1 \cdot out_1 \cdot in_1 \cdot out_2 \cdot out_1$
$out_2 \cdot in_1 \cdot out_2 \cdot out_1$, $in_2 \cdot out_1 \cdot out_2 \cdot out_1$
$in_1 \cdot out_1 \cdot out_1 \cdot out_2 \cdot out_1$
$out_2 \cdot out_1 \cdot out_2 \cdot out_1$

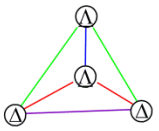

ΔΔΛ,Δ/ΛΛΔ,Λ
Same as ΔΔΛ,Λ/ΛΛΔ,Δ

ΔΔ,ΔΔ/ΛΛ,ΛΛ
Same as ΔΔΛΛ/ΛΛΔΔ

ΔΔ,ΔΛ/ΛΛ,ΔΔ
Same as ΔΔΛΛ/ΛΛΔΔ

ΔΛ,ΔΔ/ΛΔ,ΛΔ
Same as ΔΔΛ,Λ/ΛΛΔ,Δ

ΔΔ,ΔΔ/ΛΔ,ΔΔ
$in_1 \cdot in_1 \cdot in_1 \cdot in_1 \cdot in_1 \cdot in_1$
$out_1 \cdot in_1 \cdot in_1 \cdot in_1 \cdot in_1 \cdot in_1$
$in_1 \cdot out_1 \cdot in_1 \cdot in_1 \cdot in_1 \cdot in_1$
$out_1 \cdot out_1 \cdot in_1 \cdot in_1 \cdot in_1 \cdot in_1$
$in_1 \cdot in_1 \cdot out_1 \cdot in_1 \cdot in_1 \cdot in_1$
$out_1 \cdot in_1 \cdot out_1 \cdot in_1 \cdot in_1 \cdot in_1$
$in_1 \cdot out_1 \cdot out_1 \cdot in_1 \cdot in_1 \cdot in_1$
$out_1 \cdot out_1 \cdot out_1 \cdot in_1 \cdot in_1 \cdot in_1$
$in_1 \cdot in_1 \cdot in_1 \cdot out_1 \cdot in_1 \cdot in_1$
$out_1 \cdot in_1 \cdot in_1 \cdot out_1 \cdot in_1 \cdot in_1$
$in_1 \cdot out_1 \cdot in_1 \cdot out_1 \cdot in_1 \cdot in_1$
$out_1 \cdot out_1 \cdot in_1 \cdot out_1 \cdot in_1 \cdot in_1$
$in_1 \cdot in_1 \cdot out_1 \cdot out_1 \cdot in_1 \cdot in_1$
$out_1 \cdot in_1 \cdot out_1 \cdot out_1 \cdot in_1 \cdot in_1$
$in_1 \cdot out_1 \cdot out_1 \cdot out_1 \cdot in_1 \cdot in_1$
$out_1 \cdot out_1 \cdot out_1 \cdot out_1 \cdot in_1 \cdot in_1$
$in_1 \cdot in_1 \cdot in_1 \cdot in_1 \cdot out_1 \cdot in_1$
$out_1 \cdot in_1 \cdot in_1 \cdot in_1 \cdot out_1 \cdot in_1$
$in_1 \cdot out_1 \cdot in_1 \cdot in_1 \cdot out_1 \cdot in_1$
$out_1 \cdot out_1 \cdot in_1 \cdot in_1 \cdot out_1 \cdot in_1$
$in_1 \cdot in_1 \cdot out_1 \cdot in_1 \cdot out_1 \cdot in_1$
$out_1 \cdot in_1 \cdot out_1 \cdot in_1 \cdot out_1 \cdot in_1$
$in_1 \cdot out_1 \cdot out_1 \cdot in_1 \cdot out_1 \cdot in_1$
$out_1 \cdot out_1 \cdot out_1 \cdot in_1 \cdot out_1 \cdot in_1$
$in_1 \cdot in_1 \cdot in_1 \cdot out_1 \cdot out_1 \cdot in_1$
$out_1 \cdot in_1 \cdot in_1 \cdot out_1 \cdot out_1 \cdot in_1$
$in_1 \cdot out_1 \cdot in_1 \cdot out_1 \cdot out_1 \cdot in_1$
$out_1 \cdot out_1 \cdot in_1 \cdot out_1 \cdot out_1 \cdot in_1$
$in_1 \cdot in_1 \cdot in_1 \cdot in_1 \cdot in_1 \cdot out_1$
$out_1 \cdot in_1 \cdot in_1 \cdot in_1 \cdot in_1 \cdot out_1$
$in_1 \cdot out_1 \cdot in_1 \cdot in_1 \cdot in_1 \cdot out_1$
$out_1 \cdot out_1 \cdot in_1 \cdot in_1 \cdot in_1 \cdot out_1$
$in_1 \cdot in_1 \cdot out_1 \cdot in_1 \cdot in_1 \cdot out_1$
$out_1 \cdot in_1 \cdot out_1 \cdot in_1 \cdot in_1 \cdot out_1$
$in_1 \cdot out_1 \cdot out_1 \cdot in_1 \cdot in_1 \cdot out_1$
$out_1 \cdot out_1 \cdot out_1 \cdot in_1 \cdot in_1 \cdot out_1$
$in_1 \cdot in_1 \cdot in_1 \cdot out_1 \cdot in_1 \cdot out_1$
$out_1 \cdot in_1 \cdot in_1 \cdot out_1 \cdot in_1 \cdot out_1$
$in_1 \cdot in_1 \cdot out_1 \cdot out_1 \cdot in_1 \cdot out_1$
$out_1 \cdot in_1 \cdot out_1 \cdot out_1 \cdot in_1 \cdot out_1$
$in_1 \cdot out_1 \cdot out_1 \cdot out_1 \cdot in_1 \cdot out_1$
$out_1 \cdot out_1 \cdot out_1 \cdot out_1 \cdot in_1 \cdot out_1$
$in_1 \cdot in_1 \cdot in_1 \cdot in_1 \cdot out_1 \cdot out_1$
$out_1 \cdot in_1 \cdot in_1 \cdot in_1 \cdot out_1 \cdot out_1$
$in_1 \cdot out_1 \cdot in_1 \cdot in_1 \cdot out_1 \cdot out_1$
$out_1 \cdot out_1 \cdot in_1 \cdot in_1 \cdot out_1 \cdot out_1$

ΔΔΛ,Λ/ΛΛΔ,Δ (Continued)
$in_1 \cdot in_1 \cdot out_1 \cdot in_1 \cdot out_1 \cdot out_1$
$out_1 \cdot in_1 \cdot out_1 \cdot in_1 \cdot out_1 \cdot out_1$
$in_1 \cdot out_1 \cdot out_1 \cdot in_1 \cdot out_1 \cdot out_1$
$out_1 \cdot out_1 \cdot out_1 \cdot in_1 \cdot out_1 \cdot out_1$
$in_1 \cdot in_1 \cdot in_1 \cdot out_1 \cdot out_1 \cdot out_1$
$out_1 \cdot in_1 \cdot in_1 \cdot out_1 \cdot out_1 \cdot out_1$
$in_1 \cdot out_1 \cdot in_1 \cdot out_1 \cdot out_1 \cdot out_1$
$out_1 \cdot out_1 \cdot in_1 \cdot out_1 \cdot out_1 \cdot out_1$
$in_1 \cdot in_1 \cdot out_1 \cdot out_1 \cdot out_1 \cdot out_1$
$out_1 \cdot in_1 \cdot out_1 \cdot out_1 \cdot out_1 \cdot out_1$
$in_1 \cdot out_1 \cdot out_1 \cdot out_1 \cdot out_1 \cdot out_1$
$out_1 \cdot out_1 \cdot out_1 \cdot out_1 \cdot out_1 \cdot out_1$

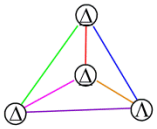

Δ,ΛΛΛ/Λ,ΔΔΔ
Same as ΔΔΔ,Λ/ΛΛΛ,Δ

Δ,ΔΔΔ/Λ,ΛΛΛ
Same as ΔΔΔ,Λ/ΛΛΛ,Δ

Δ,ΛΔΔ/Δ,ΔΛΛ
Same as ΔΔΛ,Λ/ΛΛΔ,Δ

Δ,ΛΔΔ/Λ,ΔΔΛ
Same as ΔΔΛ,Λ/ΛΛΔ,Δ

ΔΔΔΔ/ΛΛΛΛ (All *mer*)
Same as ΔΔΔΔ/ΛΛΛΛ

ΔΔΔΔ/ΛΛΛΔ (All *mer*)
Same as ΔΔΔΛ/ΛΛΛΔ

ΔΔΔΛ/ΛΛΛΔ (All *mer*)
Same as ΔΔΔΛ/ΛΛΛΔ

Figure 8.52: List of structural isomer possibilities of **4.7b** upon assembly with Fe(II) salts.

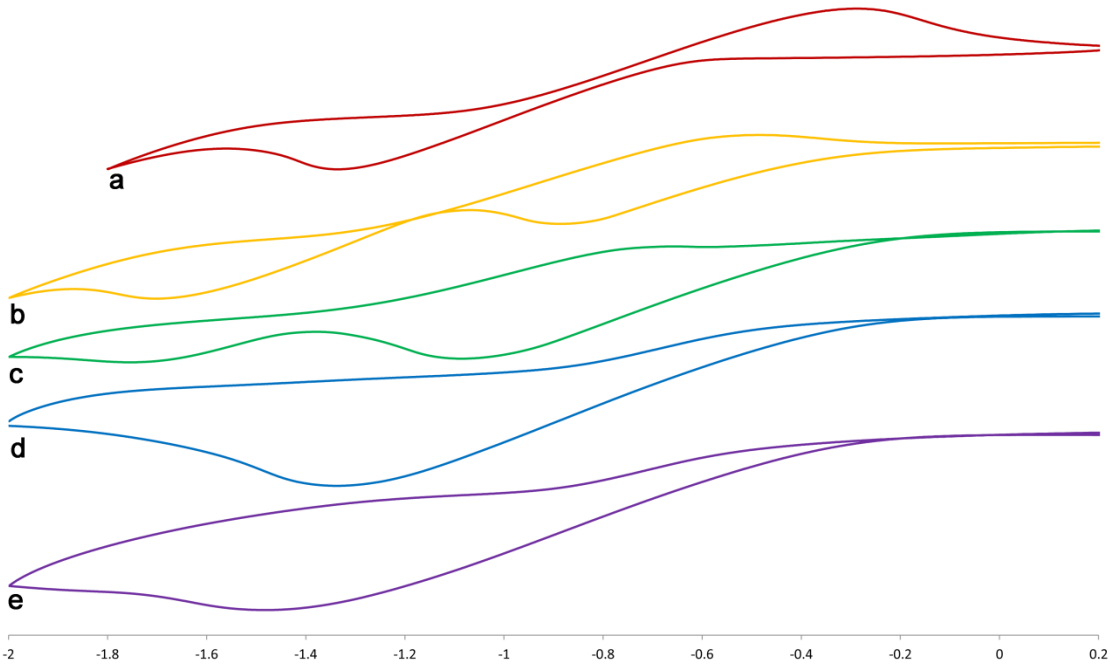

Figure 8.53: Cyclic voltammogram of **[7.13$_2$•Fe](BPh$_4$)$_2$** (MeCN, 500 μM Bu_4NBF_4 Buffer, 48 μM, Scan Rate = 0.05 V/s): a) 0 eq **7.9a**; b) 44 eq **7.9a**; c) 89 eq **7.9a**; d) 133 eq **7.9a**; e) 177 eq **7.9a**.

8.14 References

1) Dewar, M. J. S.; Zoebisch, E. G.; Healy, E. F.; Stewart, J. J. P. "Development and use of quantum mechanical molecular models. 76. AM1: a new general purpose quantum mechanical molecular model." *J. Am. Chem. Soc.*, **1985**, *107*, 3902-3909; calculations performed on SPARTAN 06, Wavefunction Inc.

2) *APEX 2,* version 2012.2-0, Bruker (**2012**), Bruker AXS Inc., Madison, Wisconsin, USA.

3) *SAINT,* version V8.18C, Bruker (**2011**), Bruker AXS Inc., Madison, Wisconsin, USA.

4) *SADABS,* version 2008/1, Bruker (**2008**), Bruker AXS Inc., Madison, Wisconsin, USA.

5) *SHELXTL,* version 2008/4, Bruker (**2008**), Bruker AXS Inc., Madison, Wisconsin, USA.

6) PLATON - SQUEEZE : Spek, A.L. (**2003**). J. Appl. Cryst. 36, 7-13; Spek, A.L. (2009). Acta Cryst. D65, 148-155.

7) *CELL_NOW*, version 2008/4, Bruker (2012), Bruker AXS Inc., Madison, Wisconsin, USA.

8) *TWINABS*, version 2012/1, Bruker (2012), Bruker AXS Inc., Madison, Wisconsin, USA.